POLY(*PARA*PHENYLENEETHYNYLENE)S: PROBING THE BIOLOGICAL INTERFACE WITH BIOMOLECULAR MATERIALS

A Dissertation
Presented to
The Academic Faculty

By

Ronald Lee Phillips II

In Partial Fulfillment
Of the Requirements for the Degree
Doctor of Philosophy in Chemistry

Georgia Institute of Technology

December, 2008

POLY(*PARA*PHENYLENEETHYNYLENE)S:

PROBING THE BIOLOGICAL INTERFACE

WITH BIOMOLECULAR MATERIALS

Dr. Uwe H.F. Bunz, Advisor
School of Chemistry and Biochemistry
Georgia Institute of Technology

Dr. Laren M. Tolbert
School of Chemistry and Biochemistry
Georgia Institute of Technology

Dr. Andrew Lyon
School of Chemistry and Biochemistry
Georgia Institute of Technology

Dr. Nicholas V. Hud
School of Chemistry and Biochemistry
Georgia Institute of Technology

Dr. Sherry M. Owen
Centers for Disease Control

Date Approved: August 13, 2008

Dedicated to Jim Collins (1983-2005)

ACKNOWLEDGEMENTS

I would like to thank my advisor, Dr. Uwe Bunz, for providing me with support, intellectual discussion, personal encouragement, and most importantly friendship. Without him, none of this would have been possible. I would also like to thank colleagues and friends from the Bunz group, past and present, for their personal knowledge and assistance during my time at Georgia Tech. I would like to personally thank Dr. Sandra Shotwell for her patience in training me during my first year in the Bunz group.

Next, I would like to thank the members of my thesis committee (Dr. Laren Tolbert, Dr. Andrew Lyon, Dr. Nicholas Hud, and Dr. Sherry M. Owen) who have been fully supportive and willing to donate their time whenever needed. I would especially like to thank Dr. Laren Tolbert for his incredible help in understanding and interpreting my data. The successful completion of my Ph.D. work has greatly been aided by my committee member's thoughts, suggestions, and generous support. I would also like to thank Dr. Cam Tyson for all of his helpful advice, support, and friendship.

I would like to thank my parents, sister, nephew, and grandmother for their unrelenting love, encouragement, support, and understanding. My family has always stood behind me, despite the decision, and for that I am truly grateful. I have been blessed with such a wonderful family and they have definitely played an integral role in my success.

I would like to thank my friends for their devoted friendships and truly believing in me when I did not believe in myself. It is easy to become discouraged, but it is a

blessing that I have such wonderful friends who continually encourage and lift me up. I have developed friendships while at Georgia Tech which I believe will last a life time.

Lastly, I would like to dedicate my thesis to the memory of my colleague and friend, Jim Collins (1983-2005). His intellect, humor, and friendship definitely made my undergraduate and graduate career more enjoyable and I truly wish Jim could have been here to see me graduate. Jim, you and your family, will always be in my thoughts and I just want to say, Jim I finally made it.

TABLE OF CONTENTS

LIST OF TABLES

LIST OF FIGURES

LIST OF SCHEMES

LIST OF ABBREVIATIONS

Å	Angstrom
A	absorbance
AcOH	acetic acid
ANP	gold nanoparticle
ATP	adenosine triphosphate
Ar	aromatic
BCS	bovine calf serum
ºC	degrees Celsius
cal	calorie
cm^{-1}	wavenumber
Con A	concanavilin A
CP	conjugated polymer
d	days
d	diameter
DCM	dichloromethane
ΔG	Gibbs free energy
ΔH	enthalpy
ΔI	intensity
ΔS	entropy
DI	deionized
DMAB	dimethylaminobenzoic acid

DMEM	Dulbecco's modified eagle's medium
DMF	dimethylformamide
DNA	deoxyribonucleic acid
EA	enzyme activity
ECM	extracellular matrix
EDTA	ethylenediaminetetraacetic acid
ELISA	Enzyme-Linked ImmunoSorbent Assay
ε	molar absorptivity
ESI	electron spray ionization
Et_2O	diethyl ether
EtOAc	ethyl acetate
EtOH	ethanol
eq	equivalents
Eq	equation
F_0	initial fluorescence intensity
$F_{[Q]}$	fluorescence intensity with addition of quencher
FRET	fluorescence resonance energy transfer
g	gram
GPC	gel permeation chromatography
HCSH	Heck-Cassar-Sonogashira-Hagihara
HEPES	(4-(2-hydroxyethyl)-1-piperazineethanesulfonic acid)
IR	infrared
ITC	isothermal titration calorimetry

K	Kelvin
K_a	association constant
K_D	disassociation constant
kDa	kiloDalton
K_{eq}	equilibrium constant
K_{sv}	Stern-Volmer constant
L	liter
LB	liquid broth
LDA	linear discriminant analysis
M	molarity
MA	Monckebergs arteriosclerosis
MeOH	methanol
mg	milligram
MHz	megaHertz
min	minute
mL	milliliter
mmol	millimole
MRSA	Methicillin-resistant Staphylococcus aureus
µL	microliter
µm	micrometer
MS	molecular sieves
MW	molecular weight
MWCO	molecular weight cutoff

N	normality
NC	nanocube
nm	nanometer
NMR	nuclear magnetic resonance
NP	nanoparticle
ns	nanosecond
OD	optical density
P	partition coefficient
$[P]_0$	initial polymer concentration
PB	phosphate buffer
PBS	phosphate buffered saline
P.D.I	polydispersity index
%	percent
PF	poly(fluorene)
Φ_F	quantum yield
Pi	phosphate
pI	isoelectric point
PIPES	piperazine-1,4-bis(2-ethanesulfonic acid)
PNP	polymer nanoparticle
PPEs	poly(*para*phenyleneethynylene)s
PPi	pyrophosphate
ppm	part per million
PPV	poly(phenylenevinylene)

ps	picosecond
[Q]	quencher concentration
R	gas constant
R_f	retention factor
rpm	revolutions per minute
rt	room temperature
SA	streptavidin
SCM	streptavidin coated microspheres
Sw-CO_2	swallowtail carboxylate PPE
T	temperature
TBAF	tetrabutylammonium fluoride
TEA	triethylamine
TEG	triethyleneglycol
TFA	trifluoroacetic acid
Tf_2O	triflic anhydride
THF	tetrahydrofuran
TIPS	triisopropylsilane
TMAD	trimethylammoniumundecanoate
TMS	trimethylsilane
TRIS-HCl	tris (hydroxymethyl) aminomethane hydrochloride
UV	ultra-violet
V_q	quenching volume

SUMMARY

The synthesis and biological sensing applications of novel water soluble poly(*para*phenyleneethynylene)s (PPEs) are presented. The ease of synthesis, synthetic variability, and dramatic chromicity of PPEs makes them well suited for biological and sensing applications. Molecular recognition and signal transduction can be achieved by using PPEs as sensory materials. By incorporating biological functional groups (e.g. sugars), PPEs can efficiently detect the presence of toxic heavy metals, proteins, and bacteria through either fluorescence quenching or enhancement. Rapid, precise, and convenient sensory arrays for the detection of biological analytes are possible through the formation of gold nanoparticle-PPE constructs.

CHAPTER 1

Poly(*para*phenyleneethynylene)s: Synthesis, Properties, and Promise as Biomolecular Materials

1.1 Introduction

Conjugated polymers (CP) have attained significant status in the detection, identification, and quantization of biologically active molecules.[1] Often, they are either utilized in the solid state as sensory coatings for electrodes, or transparently in solution as species that change their absorption and/or emission spectra upon exposure to a specific analyte. They are often superior to non-conjugated, non-fluorescent polymeric scaffolds, as they elegantly combine recognition and transmission elements.[2] If conjugated polymers are functionalized with ionic or highly polar side groups, sensing of biological analytes is possible in aqueous media. Materials with exquisite sensitivity and selectivity for specific analytes can result.

Water soluble poly(*para*phenyleneethynlene)s (PPEs) have received much attention and have shown great promise as highly sensitive fluorescent sensory materials for chemical analytes and biomolecules. However, water soluble PPEs often suffer from low quantum yields, aggregation in aqueous solutions, non-specific interactions with common ions, large polydispersity indices (P.D.I.), and high background fluorescence generated from cells and nutrient media.[3] Therefore, before fluorescence based assays with conjugated polymers can be implemented as a detection method for biological analytes, the synthesis and optimization of water-soluble PPEs must be addressed.

1.2 Synthesis and Properties of Water Soluble PPEs

PPEs are typically synthesized according to Heck-Cassar-Sonogashira-Hagihara (HCSH) reaction conditions which employs a palladium catalyzed process to yield moderate to high molecular weight PPEs (Scheme 1.1).[4-6] This method is advantageous due to its tolerance of monomer functionality, variability of reaction conditions, and simplicity of reaction workup.

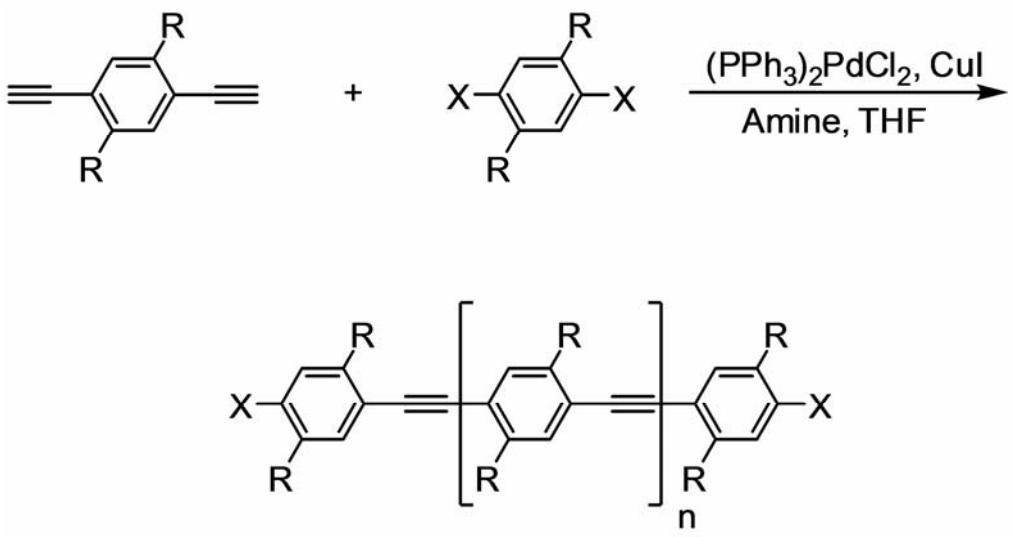

Scheme 1.1. General synthetic scheme for PPEs under HCSH reaction conditions

Commercially available $(Ph_3P)_2PdCl_2$ serves as the catalytic source of Pd. It is first reduced to Pd^0 which is the active form of the catalyst. Typically CuI is used as a co-catalyst. The first step (Scheme 1.2) of the reaction is transmetalation between the catalyst and two molecules of cuprated alkyne. The formed organometallic species is not stable and reductively eliminates a symmetrical butadiyne and generates the active catalyst species. The active catalyst undergoes oxidative addition with an aryl bromide

or iodide. Transmetalation with a cuprated alkyne followed by reductive elimination generates the product and regenerates the catalytic species.

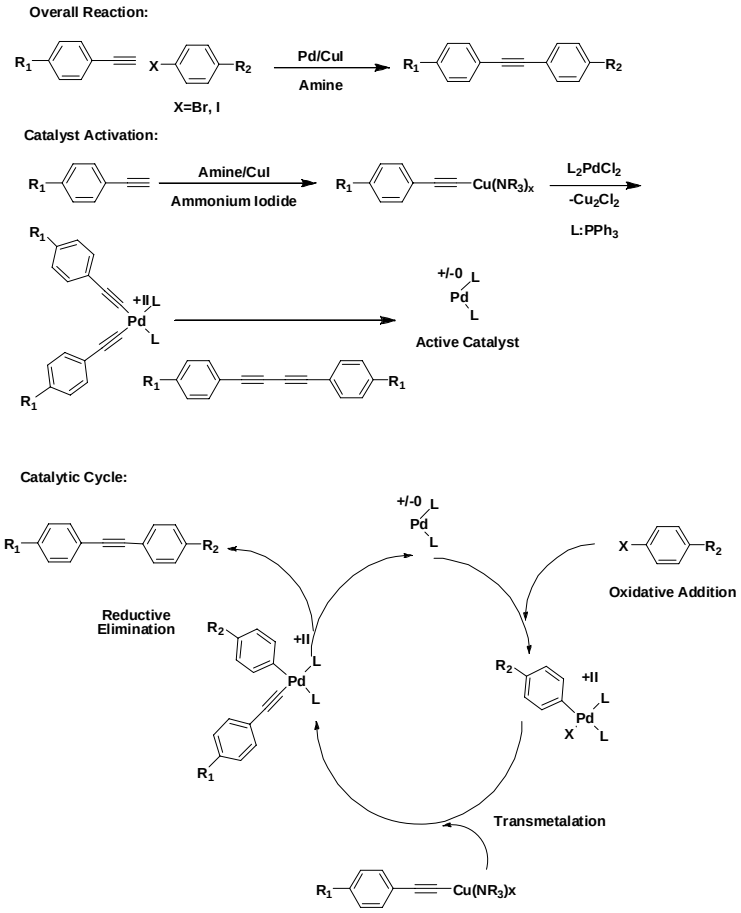

Scheme 1.2. HCSH catalytic cycle for the synthesis of PPEs

Water soluble PPEs are accessible by introducing ionic or polar side groups to solubilize the otherwise hydrophobic polymer backbones (Scheme 1.3). In doing so, a loss in fluorescence quantum yield is usually observed. The decrease in fluorescence results from self quenching of the PPE which is a direct result of polymer aggregation in aqueous media. However, this problem can be minimized by working with low concentrations of PPE or by introducing bulky polar side groups which prevents π-π

stacking of the polymer chains. Also, the large polydispersity indices (P.D.I.) often observed for water soluble PPEs can be greatly reduced by dialyzing a PPE through a dialysis membrane with a narrow molecular weight range.

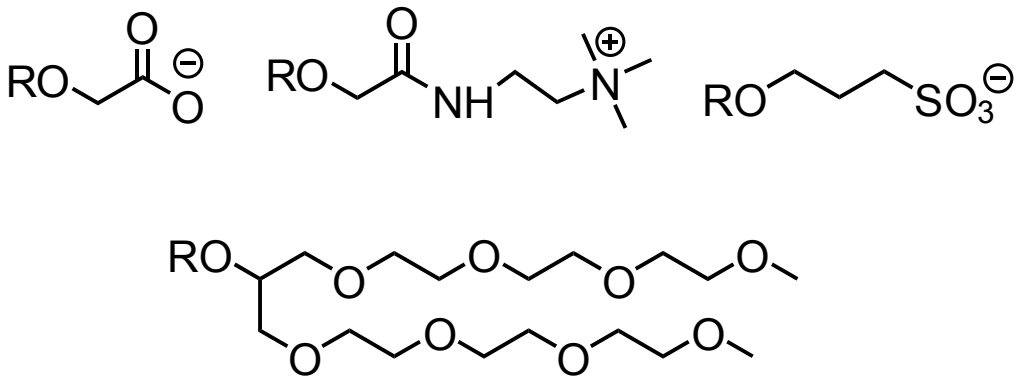

Figure 1.1. Examples of ionic (top) and polar (bottom) functionality for water soluble PPEs

Due to the ease of synthesis, PPEs can be synthesized in large quantities with high purities. Typically, the PPEs are a yellow-orange solid and exhibit a blue-green fluorescence ($\lambda_{emission}$ = 455-465 nm). With the incorporation of heterocyclic monomers such as benzothiadiazole, PPEs with a yellow-orange emission ($\lambda_{emission}$ = 500-550 nm) can be easily achieved.

1.3 Promise as Biomolecular Materials

Conjugated polymers[1,7] have found numerous applications in biosensory processes.[8-9] Grafting of suitable recognition units to the side chains of conjugated polymers (CPs) provides bio- and chemosensory materials. CPs exhibit molecular wire

behavior, multivalent display of recognition units, and superquenching effects all intertwined with spectroscopic properties that stem from conformational changes, excimer/exciplex formation and fluorescence resonance energy transfer (FRET).[10-14] Compared to quenching of the respective monomers, just one recognition element binding to a quencher is enough to quench the fluorescence of the entire polymer chain, creating strong signal amplification. This amplified quenching or superquenching of the CP is useful in monitoring the binding events directly or by displacement assays through removal of the pre-bound quencher and fluorescence turn on of the polymer. Many groups have utilized the intrinsic fluorescence signal amplification properties of CPs and developed sensitivite assays for biologically relevant targets including proteins, DNA, glycopeptides, and carbohydrates. Fluorescent superquenching of CPs by oppositely charged analytes was discovered in 1998 by Whitten *et al*[7,15] and opened a new door to specific sensing applications of CPs.[16] If PPEs are appended with ionic or polar functionalities, sensing of environmentally and biologically important analytes is possible in aqueous solution. Implementation of assay strategies using PPEs will be increasingly useful in the detection of biologically important analytes, toxigenic materials, and a variety of bacteria.

1.4 Conclusion

Optical and fluorescence based detection of biologically important species in aqueous media profits from the endless synthetic variability of PPEs. Different tailored backbones are fitted to the intended purpose by the attachment of suitable recognition elements. To advance fluorescence-based assays with conjugated polymers as a detection

method, one would like to engineer and enhance their sensitivity to such biological analytes. With the above in mind, we shall move through the following steps:

- Synthesis and analysis of anionic water-soluble PPEs
- Sugar substituted PPEs for the detection of lectins and staining of bacteria
- PPE-protein conjugates for the detection of toxic metals
- Molecular recognition based on polyvalent interactions
- Array based protein detection
- Nanosensors for the discrimination of phosphate and pyrophosphate
- Gold nanoparticle-PPE constructs for the detection of pathogens

1.5 References

1. (a) Thomas, S.W.; Joly, G.D.; Swager, T.M. "Chemical Sensors Based on Amplifying Fluorescent Conjugated Polymers" *Chem. Rev.* **2007**, 107, 1339-1386. (b) McQuade, D.T.; Pullen, A.E.; Swager, T.M. "Conjugated Polymer-based Chemical Sensors" *Chem. Rev.* **2000**, 100, 2537-2574.

2. (a) Kiessling, L.L.; Pohl, N.L. "Strength in numbers: Non-natural polyvalent carbohydrate derivatives" *Chem. Biol.* **1996**, 3, 71-77. (b) Kanai, M.; Mortell, K.H.; Kiessling, L.L. "Varying the size of multivalent ligands: The dependence of concanavalin a binding on neoglycopolymer length" *J. Am. Chem. Soc.* **1997**, 119, 9931-9932.

3. Tanhuanpaa, K.; Virtanen, J.; Somerharju, P. "Fluorescence imaging of pyrene-labeled lipids in living cells" *Biochim Biophys Acta*. **2000**, 1497, 308-320.

4. Dieck, H. A.; Heck, R. F. "Palladium Catalyzed Synthesis of Aryl, Heterocyclic and Vinylic Acetylene Derivatives" *J. Organomet. Chem.* **1975**, 93, 259.

5. Cassar, I. "Synthesis of Aryl-Substituted and Vinyl-Substituted Acetylene Derivatives by the Use of Nickel and Palladium Complexes" *J. Organomet. Chem.* **1975**, 93, 253.

6. Sonogashira, K; Tohda, Y.; Hagihara, N. "Convenient Synthesis of Acetylenes – Catalytic Substitutions of Acetylenic Hydrogen with Bromoalkenes, iodoarenes, and bromopyridines" *Tetrahedron Lett.* **1975**, 16, 4467.

7. (a) Pinto, M. R.; Schanze, K. S. "Conjugated polyelectrolytes: Synthesis and applications" *Synthesis* **2002**, 1293-1309. (b) Chen, L. H.; McBranch, D. W.; Wang, H. L.; Helgeson, R.; Wudl, F.; Whitten, D. G."Highly sensitive biological and chemical sensors based on reversible fluorescence quenching in a conjugated polymer" *Proc. Natl. Acad. Sci.* **1999**, 96, 12287-12292.

8. (a) Liu, B.; Bazan, G. C.; "Methods for strand-specific DNA detection with cationic conjugated polymers suitable for incorporation into DNA chips and microarrays" *Proc. Natl. Acad. Sci.* **2005**, 102, 589-593. (b) Dwight, S. J.; Gaylord, B. S.; Hong, J. W.; Bazan, G. C. "Perturbation of fluorescence by nonspecific interactions between anionic poly(phenylenevinylene)s and proteins: Implications for biosensors" *J. Am. Chem. Soc.* **2004**, 126, 16850-16859. Hong, J. W.; Henme, W. L.; Keller, G. E.; Rinke, M. T.; Bazan, G. C. "Conjugated-polymer/DNA interpolyelectrolyte complexes for accurate DNA concentration determination" *Adv.Mater.* **2006**, 18, 878-882

9. Ho, H. A.; Boissinot, M.; Bergeron, M. G.; Corbeil, G.; Dore, K.; Boudreau, D.; Leclerc, M. "Colorimetric and fluorometric detection of nucleic acids using cationic polythiophene derivatives" *Angew. Chem.*

10. (a) Zhou, Q.; Swager, T. M. "Fluorescent chemosensors based on energy migration in conjugated polymers: The molecular wire approach to increased sensitivity" *J. Am. Chem. Soc.* **1995** *117*, 12593-12602. (b) Bunz, U.H.F. "Poly(aryleneethynylene)s: Syntheses, properties, structures, and applications" *Chem. Rev.* **2000**, *100*, 1605-1644. (c) Bunz, U.H.F. "Synthesis and Structures of PAEs" *Adv. Polym. Sci.* **2005**, *177*, 1-52.

11. (a) Kim, I.-B.; Erdogan, B.; Wilson, J. N.; Bunz, U.H.F. "Sugar-poly(para-phenylene ethynylene) conjugates as sensory materials: Efficient quenching by Hg2+ and Pb2+ ions" *Chemistry Eur. J.* **2004**, *10*, 6247-6254. (b) Kim, I.-B.; Dunkhorst, A.; Gilbert, J.; Bunz, U.H.F. "Sensing of lead ions by a carboxylate-substituted PPE: Multivalency effects" *Macromolecules* **2005**, *38*, 4560-4562.

12. Tan, C.Y.; Alas, E.; Müller, J.G.; Pinto, M.R.; Kleiman, V.D.; Schanze, K.S. "Amplified quenching of a conjugated polyelectrolyte by cyanine dyes" *J. Am. Chem. Soc.* **2004**, *126*, 13685-13694

13. (a) Halkyard, C. E.; Rampey, M. E.; Kloppenburg, L.; Studer-Martinez, S. L.; Bunz, U.H.F. "Evidence of aggregate formation for 2,5-dialkylpoly(p-phenyleneethynylenes) in solution and thin films" *Macromolecules* **1998**, *31*, 8655-8659. (b) Kim, J.; Swager, T.M. "Control of conformational and interpolymer effects in conjugated polymers" *Nature* **2001**, *411*, 1030-1034.

14. Bunz, U. H. F.; Imhof, J. M.; Bly, R. K.; Bangcuyo, C. G.; Rozanski, L.; VandenBout, D.A. "Photophysics of poly [p-(2,5-didodecylphenylene) ethynylene] in thin films"*Macromolecules* **2005**, *38*, 5892-5896.

15. Achutyan, K.E.; Bergstedt, T.S.; Jones, R.M.; Chen, L.; Kumaraswamy, S.; Kushon, S.A.; Lu, L.; Ley, K.D.; McBranch, D.; Mukundan, H.; Rininsland, F.; Shi, X.; Xia, W.; Whitten, D.G. "Fluorescence superquenching of conjugated polyelectrolytes: applications for biosensing and drug discovery" *J. Mater. Chem.* **2005**, 15, 2648-2656.

16. (a) Liu, B.; Bazan, G.C.; "Methods for strand-specific DNA detection with cationic conjugated polymers suitable for incorporation into DNA chips and microarrays" *Proc. Natl. Acad. Sci. U.S.A.* **2005**, 102, 589-593. (b) Song, X.; Wang, H.L.; Shi. J.; Park, J.W.; Swanson, B.I. "Conjugated polymers as efficient fluorescence quenchers and their applications for bioassays" *Chem. Mater.* **2002**, 14, 2342-2347. (c) Liu, B.; Bazan, G.C. "Homogeneous fluorescence-based DNA detection with water-soluble conjugated polymers" *Chem. Mater.* **2004**, 16, 4467-4476. (d) Wang, D.; Gong, X.; Heeger, P.S.; Rininsland, F.; Bazan, G.C.; Heeger, A.J. "DNA detection using water-soluble conjugated polymers and peptide nucleic acid probes" *Proc. Natl. Acad. Sci.* **2002**, 99, 49-53.

CHAPTER 2

Synthesis and Characterization of Water Soluble Anionic PPEs

2.1 Introduction

Conjugated polyelectrolytes[1] have found spectacular applications in biosensory processes[2,3] and have also been found useful as hybrid devices, containing both light-emitting electrochemical cells and light-emitting diodes.[4] The main application however is in their promising sensory profiles, allowing for the sensitive detection of metal ions, sugars, DNA, proteins and bacteria.[5-11]

An important issue is the concentration of the ionic groups per repeat unit, which in this case is the carboxylates. Properties of conjugated polyelectrolytes are to a significant extent determined by the electric charges and the resulting electrostatic forces these charges exert. These forces dominate aggregation, excimer formation and analyte binding. To investigate these issues, carboxylate-substituted poly(*para*phenylene-ethynylene)s (PPEs) in which 1-3 carboxylate groups are present per aryleneethynylene unit were prepared.[10,11] The PPEs all feature the same conjugated backbone and are derivatives of dialkoxy-PPEs. However, their pH-dependent absorption and emission spectra, as well as their fluorescence quantum yields, vary dramatically. The difference in behavior should be useful for the construction of biosensory platforms, where multivalent interactions, differential dye replacement and assemblies with charged cofactors are exploited.[12-14] We have recently shown that specifically substituted gold-nanoparticles loaded with negatively charged conjugated polymers unequivocally discern a set of proteins.[15] Assay strategies using conjugated polyelectrolytes will be

increasingly useful in the detection of biologically important species, toxigenic materials and different bacteria. For effective replacement and quenching assays, groups of conjugated polyelectrolytes with tuneable ratios of charge per repeat unit will be useful. We investigated such a materials platform, PPEs with varying ratios of carboxylate functionalities per repeat unit, and investigated their photophysical properties.

2.2 Results and Discussion

2.2.1. Synthesis

With this in mind, we set out to synthesize PPEs which contained varying concentrations of carboxylate functionalities per repeat unit. Synthesis began with

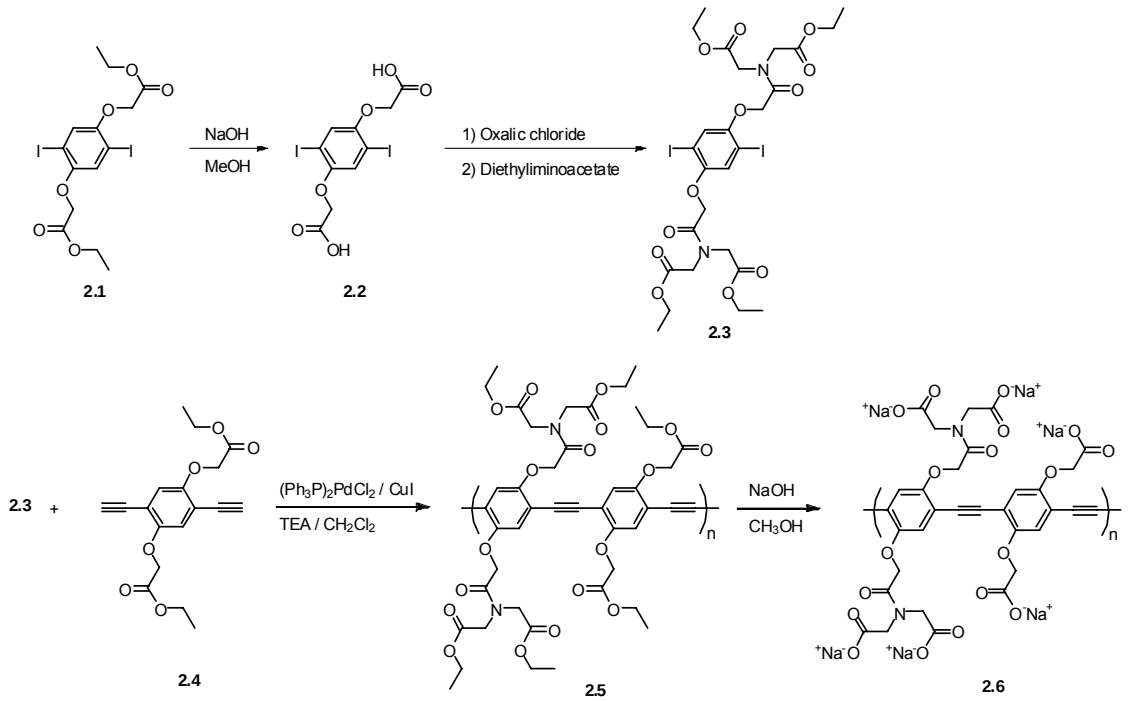

Scheme 2.1. Synthesis of polymer **2.6**

saponification of **2.1**[11], to yield **2.2**, which after exposure to oxalic chloride was transformed into its double acid chloride. Treatment of this intermediate with diethyliminoacetate furnished monomer **2.3** in 46% yield and high purity. Heck-Cassar-Sonogashira-Hagihara[16] coupling of **2.3** to **2.4** afforded PPE **2.5**. Saponification using sodium hydroxide in methanol rendered the desired hexacarboxylated **2.6** as a water soluble, yellow and fluorescent material after precipitation from ethyl ether in almost quantitative yield (Scheme 2.1).

Polymer **2.10** was synthesized using a similar route. Here we started from the literature known diiodide **2.8**, which was coupled to TMS-acetylene and deprotected to afford monomer **2.9**.[17,18] This monomer was coupled to **2.1** under standard Heck-Cassar-Sonogashira-Hagihara conditions[16] using triethylamine as the solvent to yield polymer **2.10** after deprotection with a dilute solution of sodium hydroxide in methanol (Scheme 2.2).

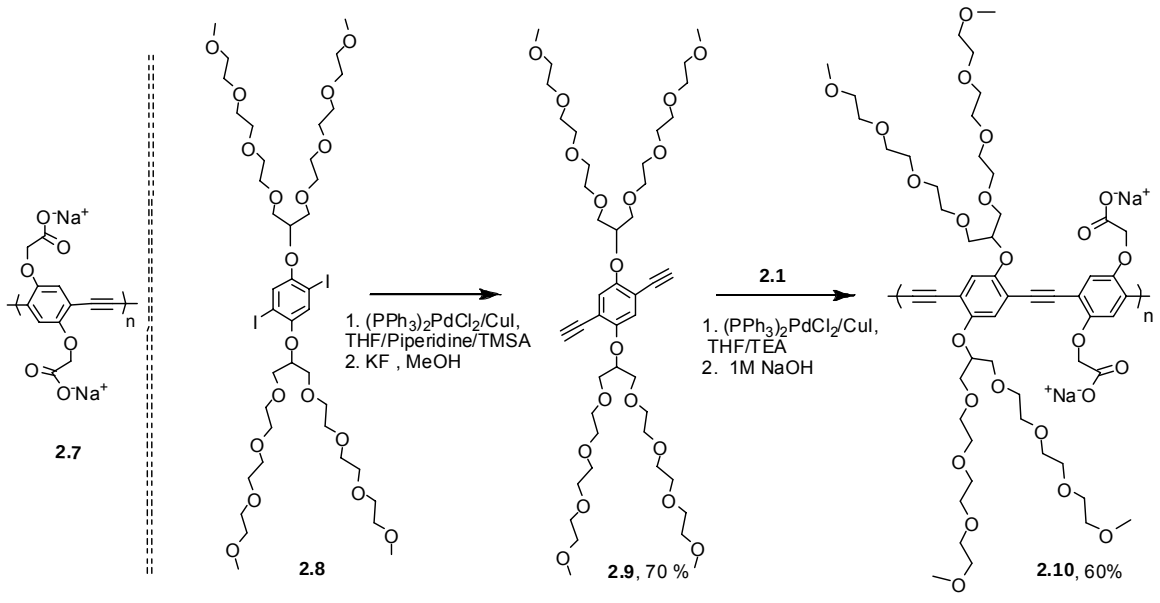

Scheme 2.2. Synthesis of polymer **2.10** and structure of the known dicarboxylate PPE **2.7**

The polymer was isolated in 60% yield after dialysis followed by lyophilization. The use of triethylamine instead of piperidine or morpholine was imperative to avoid transformation of the ester groups into amide functionalities by such secondary amines—a process undesired here. Polymer **2.7** was prepared according to literature.[11] Polymers **2.6**, **2.7**, and **2.10** have M_n's in the range of 1-3 x 10^4 (Table 2.1) and polydispersity indices between 1.8 and 4.3.

2.2.2. Dependence of Absorption and Emission Spectra on the pH.

All three PPEs, **2.6**, **2.7**, and **2.10** are readily soluble in aqueous buffer at pH 7.2. They form yellowish solutions that are blue-turquois fluorescent. These solutions display dramatic effects in their absorption and emission upon change of the pH value (Figures 2.1-2.3, Table 2.1). The introduction of the swallow-tail branched oligoethylene glycol substituent in **2.10** leads to a PPE with a significantly enhanced emission quantum yield in water, an effect reported in PPEs exclusively carrying swallowtail oligoethylene glycol substituents.[16,17] The increase in quantum yield was originally thought to arise from steric shielding of the conjugated backbone by the branched oligoethyleneglycol groups. However, as **2.10** has a quantum yield comparable to that of the swallowtail-PPEs, but is less sterically protected, there must be other, additional operative factors that increase the quantum yield.

The introduction of more carboxylate groups on a per repeat unit basis, as in **2.6**, does not influence the quantum yield when comparing to the quantum yield of PPE **2.7**. When going from pH 7.2 to pH 11, there was neither an effect on the emission wavelength and intensity nor on the absorption spectra in any of the three polymers.

However, when acidifying, the emission intensity of all three PPEs decreases substantially (Figures 2.1-2.3). The emissions of **2.6** and **2.7** are almost completely quenched while that of **2.10** is attenuated and also red shifted due to some excimer/aggregate formation. When the pH is decreased further, **2.6**, **2.7** and **2.10** begin to precipitate out of solution. The spectroscopic properties of the three PPEs at pH < 3, as long as they can be determined, are very similar to those recorded at pH 3. The most dramatic effects are observed in the absorption spectra, when going from a neutral to an acidic solution. Both **2.6** and **2.7** show a red shift in their absorption maxima at a pH < 4. At pH 7.2, the three polymers show absorption maxima at 408-425 nm, *atypical* for dialkoxy-PPEs, as these absorb at around 455 nm when well solubilized in organic solvents.[18a,b] We explain this blue-shift by electrostatic effects inducing maximum twist (90^{o}) between two adjacent aryleneethynylene units to minimize electrostatic repulsion.[19,20] Upon protonation, **2.6** and **2.7** show a significant red shift to 463 nm and 472 nm respectively. This shift mirrors the red shift that is found in hydrophobic dialkoxy-PPEs, which show an absorption at 478 nm in their aggregated state.[20] While **2.7** only develops a shoulder in its absorption upon acidification, the polymer **2.6** has a more pronounced response to pH. At pH 4, the absorption maximum is located at 468 nm and upon going to pH 3 the absorption maximum shifts to 472 nm. We attribute the additional shift to the sequential protonation of the two types of carboxylate groups found in polymer **2.6**. We assume that the carboxylate groups bound to the iminoacetic acid arms are protonated last, as methyliminodiacetic acid has two pK_a values (pK_a2 = 10.2, pK_a1 = 2.81), the first of which is somewhat below that of ethoxyacetic acid. Polymer

2.10 shows the least shift in absorption and upon acidification to pH 3, **2.10** displays an absorption maximum at 455 nm.

The changes in absorption occur when the pH falls below 4, in line with ethoxyacetic acid's pKa of 3.53.[21] At pH 3, most of the carboxylate residues in the three investigated polymers are protonated. Not unexpectedly, the largest changes in absorption are visible around the pH value that corresponds to the pK_a value of the respective acids. Below pH 3, there is only minimal electrostatic repulsion because the polymer chains are now only weakly charged or neutral.

What is the mechanism for the observed red shifts in these PPEs? Conformational effects are known to play a major role.[22] In basic and neutral solutions, neighboring aryleneethynylene groups of **2.6** and **2.7** are maximally twisted to minimize electrostatic repulsion of the negatively charged carboxylate units. When decreasing the pH, planarization and desolvation of the now neutral and hydrophobic PPEs become predominant. The change of optical properties observed here is similar to that observed in the aggregation of hydrophobic PPEs in methanol solution where it is governed by planarization of the main chains.[22,23] The decrease in quantum yields of **2.6**, **2.7** and **2.10** upon protonation is mechanistically more difficult to explain and not well understood; but quite typical for conjugated polyelectrolytes upon charge neutralization in highly polar solvents. We contend that it is a combination of excimer formation and water-alleviated, non-radiative deactivation of the excited state of these polymers.

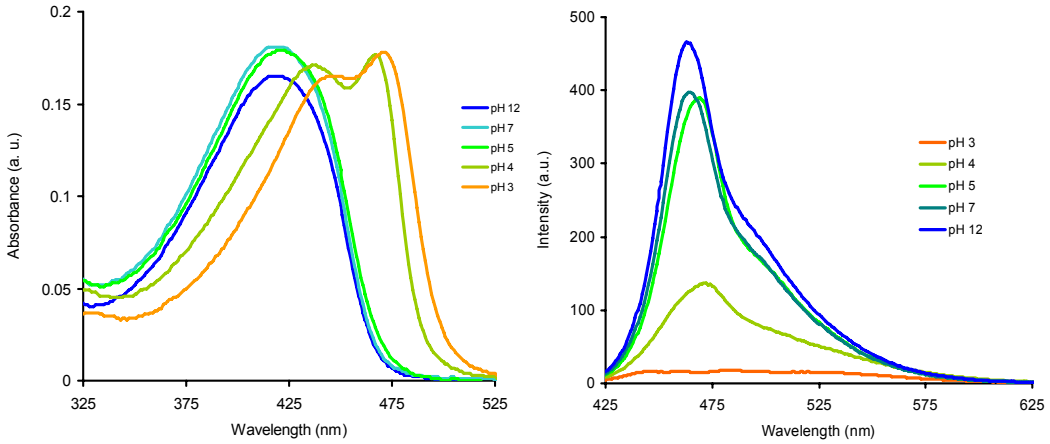

Figure 2.1. Absorption and emission spectra of **2.6** at different pH values

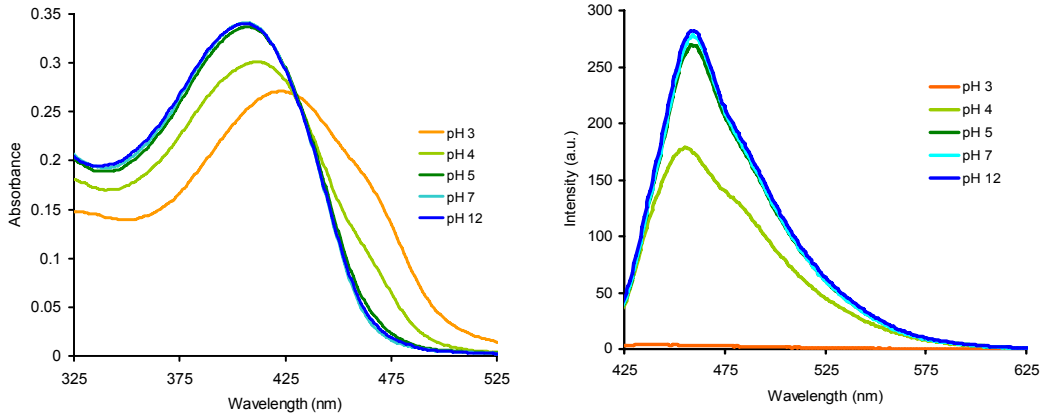

Figure 2.2. Absorption and emission spectra of **2.7** at different pH values

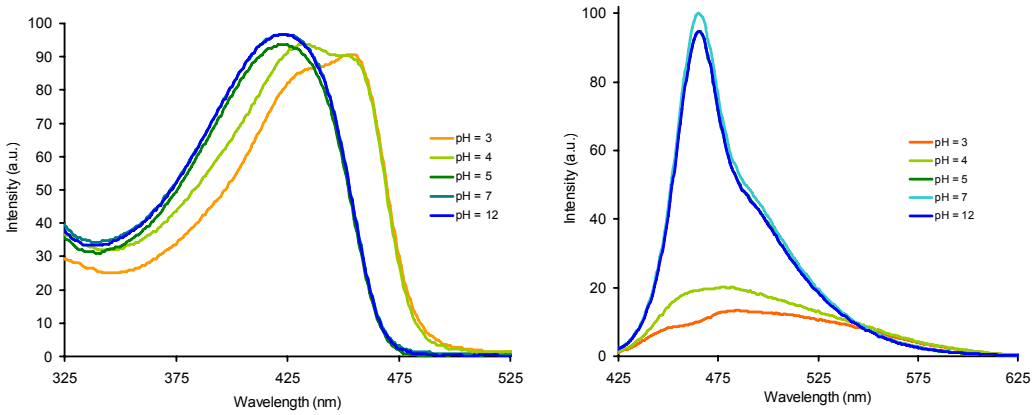

Figure 2.3. Absorption and emission spectra of **2.10** at different pH values.

Table 2.1. Molecular Weight, Optical Properties and Stern-Volmer constants (K_{SV}) for Polymers **2.6, 2.7,** and **2.10** at different pH values

Polymer	***2.6***	***2.7***	***2.10***
$\lambda_{max\ abs.}$ pH 7 (nm)	419	408	425
$\lambda_{max\ abs.}$ pH 4 (nm)	468	414	435
$\lambda_{max\ abs.}$ pH 3 (nm)	472	463 sh	455
$\lambda_{max\ emiss.}$ pH 7 (nm)	465	460	466
$\lambda_{max\ emiss.}$ pH 3 (nm)	483 weak	438 weak	484
Φ pH 7 (nm)	0.08	0.08	0.33
K_{sv} Hg^{2+}	6.4×10^4	1.3×10^4	7.1×10^2
M_n	3.6×10^4	1.2×10^4	2.5×10^4
M_w/M_n	2.1	4.3	1.8

If one is interested in the use of such polymers as a platform in biosensing applications, it is desirable that there be no interference from metal cations. Bunz[14] and Schanze et al.[10] have shown that dicarboxylate-PPE **2.7** is quite sensitive towards the addition of calcium ions, inducing excimer formation with yellow emission; **2.7** is also sensitive towards mercury ions, which are efficient quenchers of fluorescence in **2.6**. Neither **2.6** nor **2.10** are sensitive towards calcium ions in the millimolar range, nor does their emission characteristics change by the addition of other metal ions, with exception of mercury. To quantify the amount of mercury-induced quenching in **2.6, 2.7** and **2.10** we used the Stern-Volmer equation,[24]

$$F_0/F_{[Q]} = K_{SV}[Q] + 1 \qquad \textbf{Eq. 2.1}$$

in which $F_0/F_{[Q]}$ represents the fluorescence intensity of the PPE without (F_0) and at a concentration [Q] ($F_{[Q]}$) of the added quencher. The Stern-Volmer constant, K_{SV}, is obtained as the slope of the plot of $F_0/F_{[Q]}$ vs. the quencher concentration [Q]. We can determine from the short emission lifetime of PPEs (0.3-0.5 ns) that the quenching process is static; i.e. K_{SV} represents an association constant. The Stern-Volmer formalism provides a way to quantify and compare the susceptibility of the three investigated PPEs towards quenching by mercury ions. The K_{SV} values may not be very meaningful as association constants as there are multiple binding sites with different β-values involved upon addition of mercury ions. However, the obtained composite number allows one to compare the sensitivity of the PPEs towards mercury ions. Table 2.1 shows that **2.6** is efficiently quenched by mercury, by a factor of five more than **2.7**, while polymer **2.10** exhibits a Stern-Volmer constant that is very low which suggests that binding of **2.10** to mercury ions is weak due to the low concentration of carboxylate groups. This suggests that an increasing concentration of carboxylate groups makes quenching of these polymers more susceptible towards mercury ions and potentially interesting as metal ion sensors.[25]

2.3 Conclusion

Three anionic water soluble PPEs in which the concentration of the ionic carboxylate units per repeat (two phenyleneethynylene units) unit is six, four and two, respectively have been synthesized. These PPEs show significantly different responses towards decreasing pH and mercury ions. For use as a platform in biosensory applications, the mixed swallowtail carboxylate polymer **2.10** is the most attractive one,

as it shows high emissive quantum yields in water and low interference with metal ions. If metal sensory properties are desired, polymers of the type **2.6** will be more useful. The synthesis of these novel anionic water soluble PPEs allows their use in detection schemes for proteins, metal ions, and pathogens.

2.4 Experimental

Instrumentation and Materials. All chemicals and solvents were used without further purification as received unless otherwise noted. UV-VIS measurements were made with a Shimadzu UV-2401PC recording spectrophotometer. Fluorescence data were obtained with a Shimadzu RF-5301PC spectrofluorophotometer in quartz cuvettes. The fluorescence was recorded at room temperature. Solutions of carboxylate-substituted PPEs were prepared in 0.1 M sodium phosphate buffer (pH = 7.2). Concentrations of PPEs were adjusted to 5×10^{-6} M on the basis of the molecular weight of the repeating unit of PPEs. Solutions of 10 metal compounds are prepared in 0.1 M concentration: They are $Zn(ClO_4)_2$, $CdCl_2$, $Hg(O\text{-}CO\text{-}CF_3)_2$, $Pb(NO_3)_2$, $FeCl_3$, $NiCl_2$, $CoCl_2$, $CuBr_2$, $Ca(NO_3)_2$, and $Mg(OTf)_2$. Quantum yield was measured by using quinine sulfate in 0.1 N sulfuric acid as a reference ($\Phi = 0.54$).

Synthesis of 2.2: Compound **2.1** (2.67 g, 5.00 mmol), sodium hydroxide (4.0 g, 0.1 mol), methanol (60 mL), and water (3 mL) were placed into a 250 mL round-bottom flask and heated to reflux for 48 h. The mixture was allowed to cool down to room temperature and the solvent was removed under reduced pressure. The resulting solid was washed with acetone and dissolved in water. Upon the addition of 1N sulfuric acid,

the precipitate was formed and collected. The colorless solid was obtained in 62 % yield (1.48 g, 3.10 mmol).

Synthesis of 2.3: Compound **2.2** (10.50 g, 21.97 mmol), and oxalyl chloride (20 mL) were placed into a 50 mL round-bottom flask and heated to reflux for 24 h. The mixture was allowed to cool down to room temperature and the solvent was removed under reduced pressure. The resulting product, diethyl iminoacetate (6.23 g, 32.9 mmol), trimethylamine (7.58 g, 74.8 mmol), and dichloromethane (120 mL) were placed in a 250 mL round bottom flask and the reaction mixture was stirred at room temperature for 16 h. The solvent was removed under reduced pressure and water (20 mL) was added to the crude product. The precipitate was collected and washed with water. The colorless solid was obtained in 46 % yield (8.29 g, 10.1 mmol). ^{1}H NMR (300 MHz, $CDCl_3$): δ 7.24 (s, 2H), 4.72 (s, 4H), 4.31 (s, 4H), 4.21-4.17 (m, 12H), 1.25 (t, 12H). ^{13}C NMR (300 MHz, $CDCl_3$): δ 168.90, 168.72, 168.09, 152.89, 123.89, 86.17, 69.55, 62.21, 61.72, 50.04, 48.63, 14.42. IR (cm^{-1}): *v* 3088, 2986, 1725, 1680, 1485, 1466, 1225, 1195, 1022, 873, 757. MS (ESI): $[M+H]^+$ *m/z* 821.0.

Synthesis of polymer 2.5: Monomer **2.3** (820 mg, 1.00 mmol) and monomer **2.4** (347 mg, 1.05 mmol) were dissolved in chloroform (2 mL), THF (2 mL), and triethylamine (1 mL) in an oven dried Schlenk flask. The flask was flushed with nitrogen and frozen and evacuated three times after which $(Ph_3P)_2PdCl_2$ (1.4 mg, 2 μmol), and CuI (0.4 mg, 2 μmol) were added. The mixture was allowed to stir at room temperature for 48 h. The solution was slowly added to ether (200 mL), the precipitate was collected and washed with ether. An orange solid was obtained in 96 % yield (863 mg). The weight average molecular weight was estimated to be 3.6×10^4 with a polydispersity (M_w/M_n) of 2.10**.** ^{1}H

NMR (500 MHz, DMSO-d_6): δ 7.19 (2H), 7.05 (2H), 4.97 (4H), 4.39 (4H), 4.13 (12H), 3.72 (8H), 1.18 (18H). IR (cm^{-1}): ν 3622, 3488, 2985, 2204, 1745, 1680, 1507, 1271, 1189, 1080, 1025, 971, 868, 741. Due to low solubility, ^{13}C NMR spectrum could not be obtained.

Synthesis of polymer 2.6: Polymer **2.5** (200 mg, 0.22 mmol), sodium hydroxide (400 mg, 10 mmol), and methanol (30 mL) were placed into a 100 mL round-bottom flask and heated to reflux for 48 h. The mixture was allowed to cool down to room temperature and the solvent was removed under reduced pressure. The resulting solid was washed with acetone and dissolved in water. The polymer was deprotected in 1M NaOH and EDTA (150 mg) was added to complex any residual copper. The resulting solution was neutralized with 1M HCl, dialyzed against DI H_2O for 3 d, and the solvent was removed resulting in a dark orange solid (179 mg, 0.20 mmol, 91% yield). ^1H NMR (500 MHz, D_2O): δ 4.91 (4H), 4.58 (4H), 3.98 (8H). IR (cm^{-1}): ν 3350, 2894, 2203, 1652, 1593, 1406, 1327, 1208, 1116, 1040, 980, 932, 850, 720. Φ_{water} = 0.08. Due to low solubility, ^{13}C NMR spectrum could not be obtained.

Synthesis of 2.9: Compound **2.8**[17] (4.61 g, 4.11 mmol) was dissolved in dry THF (5 mL) and stirred under N_2 for 15 min. Upon degassing, CuI (0.01 eq., 0.042 mmol, 8.1 mg), $(PPh_3)_2PdCl_2$ (0.01 eq., 0.042 mmol, 29.5 mg), piperidine (5 mL), and TMS-acetylene (4 eq., 16.8 mmol, 2.39 mL) were all added to the reaction. The reaction was stirred at room temperature for 2 d. The reaction mixture was diluted with THF (25 mL) and filtered to remove any excess salts. The solvent was removed and the crude product was purified by silica gel chromatography (9:1 EtOAc / MeOH). The resulting product was an orange oil (3.62 g, 3.40 mmol, 83.0 %). ^1H NMR (500 MHz, $CDCl_3$): δ 7.08 (s, 2H), 4.35 (m, 2H),

3.75-3.41 (m, 56H), 3.30 (s, 12H), 0.2 (s, 18H). ^{13}C NMR (500 MHz, $CDCl_3$): δ 153.69, 121.11, 115.61, 100.85, 99.76, 79.62, 71.68, 70.94, 70.39, 70.33, 70.27, 58.78, 0.00. IR (cm^{-1}): *v* 3018, 2891, 2204, 1489, 1396, 1351, 1216, 1099, 1028, 928, 850, 758. The purified product was dissolved in MeOH (50 mL). KF (4 eq., 1.07 g, 0.0140 mol) was dissolved in MeOH (25 mL) and added to the previous solution. The reaction was stirred overnight at room temperature. The solvent was removed and the crude product was re-dissolved in $CHCl_3$. The solution was extracted with H_2O and the organic fractions were collected and concentrated in vacuo which yielded an orange oil (2.64 g, 2.96 mmol, 87.1 %). ^{1}H NMR (500 MHz, $CDCl_3$): δ 7.05 (s, 2H), 4.30 (m, 2H), 3.68-3.50 (m, 56H), 3.41 (s, 12H), 3.25 (s, 2H). ^{13}C NMR (500 MHz, $CDCl_3$): δ 154.31, 121.67, 115.20, 83.00, 80.18, 79.54, 72.06, 71.30, 70.76, 70.71, 70.64, 59.15. IR (cm^{-1}): *v* 3302, 3019, 2891, 2201, 1489, 1394, 1338, 1217, 1099, 1028, 926, 850, 758. MS (ESI): $[M+H]^+$ *m/z* 891.5.

Synthesis of polymer 2.10: Compound **2.9** (890 mg, 1 mmol), compound **2.1** (534 mg, 1 mmol), THF (3 mL), and TEA (3 mL) were all combined in a 25 mL Schlenk tube. Upon degassing, $(PPh_3)_2PdCl_2$ (0.5 mol%, 3.51 mg), and CuI (1 mol%, 1.91 mg) were added to the mixture under N_2 and allowed to react for 2 d. The polymer was precipitated in hexane (500 mL), collected, and dried which resulted in an orange solid (680 mg, 0.60 mmol, 60%). GPC (vs. polystyrene standards in chloroform): M_n = 25,211, M_w/M_n = 1.837, n = 21. ^{1}H NMR (500 MHz, $CDCl_3$): δ 7.33 (s, 2H), 7.14 (s, 2H), 4.78(s, 4H), 4.54(m, 2H), 4.20 (m, 4H), 3.87-3.38 (m, 56H), 3.11 (s, 12H), 1.28 (t, 6H). ^{13}C NMR (500 MHz, $CDCl_3$): δ 168.03, 154.65, 151.23, 124.65, 120.22, 117.06, 115.31, 92.35, 91.76, 80.34, 72.45, 71.68, 71.02, 70.77, 70.32, 66.87, 61.32, 59.32, 13.74. The protected polymer **2.10** (660 mg, 0.56 mmol) was deprotected in 1M NaOH and EDTA

(250 mg) was added to complex any residual copper. The resulting solution was neutralized with 1M HCl, dialyzed against DI H_2O for 3 d, and the solvent was removed resulting in a dark orange flaky solid. ^{1}H NMR (500 MHz, D_2O): δ 7.12 (s, 2H), 6.97 (s, 2H), 4.61 (s, 4H), 4.43 (m, 2H), 3.79-3.41 (m, 56H), 3.27 (s, 12H). IR (cm^{-1}): ν 3422, 2919, 2204, 1613, 1489, 1405, 1350, 1275, 1208, 1088, 944, 852. Φ_{water} = 0.33. Due to low solubility, ^{13}C NMR spectrum could not be obtained.

2.5 References

1. (a) Pinto, M. R.; Schanze, K. S. "Conjugated polyelectrolytes: Synthesis and applications" *Synthesis* **2002**, 1293-1309. (b) Thomas, S.W.,III; Joly, G.D.; Swager, T.M. "Chemical sensors based on amplifying fluorescent conjugated polymers" *Chem. Rev*. **2007**, 107, ASAP. (c) Chen, L.H.; McBranch, D.W.; Wang, H.L.; Helgeson, R.; Wudl, F.; Whitten, D.G. "Highly sensitive biological and chemical sensors based on reversible fluorescence quenching in a conjugated polymer" *Proc. Natl. Acad. Sci*. **1999**, 96, 12287-12292.

2. (a) Liu, B.; Bazan, G. C.; "Methods for strand-specific DNA detection with cationic conjugated polymers suitable for incorporation into DNA chips and microarrays" *Proc. Natl. Acad. Sci*. **2005**, 102, 589-593. (b) Dwight, S. J.; Gaylord, B. S.; Hong, J. W.; Bazan, G. C. "Pertubation of fluorescence by nonspecific interactions between anionic poly(phenylenevinylene)s and proteins: Implications for biosensors" *J. Am. Chem. Soc*. **2004**, 126, 16850-16859. (c.) Hong, J. W.; Henme, W. L.; Keller, G. E.; Rinke, M. T.; Bazan, G. C. "Conjugated-polymer/DNA interpolyelectrolyte complexes for accurate DNA concentration determination" *Adv. Mater*. **2006**, 18, 878-882.

3. (a) Ho, H.A.; Boissinot, M.; Bergeron, M. G.; Corbeil, G.; Dore, K.; Boudreau, D.; Leclerc, M. "Colorimetric and fluorometric detection of nucleic acids using cationic polythiophene derivatives" *Angew. Chem*. **2002**, 41, 1548-1551. (b) Dore, K; Dubus, S; Ho, HA; Levesque, I; Brunette, M.; Corbeil, G.; Boissinot, M.; Boivin, G.; Bergeron, M. G.; Boudreau, D.; Leclerc, M. "Fluorescent polymeric transducer for the rapid, simple, and specific detection of nucleic acids at the zeptomole level" *J. Am. Chem. Soc*. **2004**, 126, 4240-4244.

4. Shao, Y.; Bazan, G. C.; Heeger, A. J. "Long-lifetime polymer light-emitting electrochemical cells" *Adv. Mater.* **2007**, *19*, 365-370

5. (a) Wang, B.; Wasielewski, M. R. "Design and synthesis of metal ion-recognition-induced conjugated polymers: An approach to metal ion sensory materials" *J. Am. Chem. Soc.* **1997** *119*, 12-21. (b) Fan, L. J.; Jones W. E. "A highly selective and sensitive inorganic/organic hybrid polymer fluorescence "turn-on" chemosensory system for iron cations" *Am. Chem. Soc.* **2006** *128*, 6784-6785. (c) Murphy, C. B.; Zhang, Y.; Troxler, T.; Ferry, V.; Martin, J. J.; Jones W. E. "Probing Forster and dexter energy-transfer mechanisms in fluorescent conjugated polymer chemosensors" *J. Phys. Chem.* B **2004**, *108*, 1537-1543. (d) Zhang, Y.; Murphy, C. B.; Jones W. E. "Poly [p-(phenyleneethynylene)-alt-(thienyleneethynylene)] polymers with oligopyridine pendant groups: Highly sensitive chemosensors for transition metal ions" *Macromolecules* **2002**, *35*, 630-636. (e) Kimura, M.; Horai, T.; Hanabusa, K.; Shirai, H. "Fluorescence chemosensor for metal ions using conjugated polymers" *Adv. Mater*. **1998** *10*, 459-462. (f) Chen, Y.; Fan, Q. L.; Wang, P.; Zhang, B.; Huang, Y.-Q.; Zhang, G-W.; Lu, X-M.; Chan, H.S.O.; Huang, W."A bipyridine-

containing water-soluble conjugated polymer: Highly efficient fluorescence chemosensor for convenient transition metal ion detection in aqueous solution“ *Polymer* **2006**, *47*, 5228-5232.

6. Disney, M. D.; Zheng, J.; Swager, T. M.; Seeberger, P. H.“Detection of bacteria with carbohydrate-functionalized fluorescent polymers“ *J. Am. Chem. Soc*. **2004**, 126, 13343-13346.

7. (a) Kim, I.-B.; Wilson, J. N.; Bunz, U. H. F. “Mannose-substituted PPEs detect lectins: A model for Ricin sensing” *Chem. Commun*. **2005**, 1273-1275. (b) Kim, I.-B.; Dunkhorst, A.; Bunz, U. H. F. “Nonspecific interactions of a carboxylate-substituted PPE with proteins. A cautionary tale for biosensor applications“ *Langmuir* **2005**, 21, 7985-7989. (c) Wilson, J. N.; Wang, Y. Q.; Lavigne, J. J.; Bunz, U. H. F. “A biosensing model system: selective interaction of biotinylated PPEs with streptavidin-coated polystyrene microspheres“ *Chem. Commun*. **2003**, 1626-1627.

8. (a) Tan, C. Y.; Alas, E.; Müller, J. G.; Pinto, M. R.; Kleiman, V. D.; Schanze, K. S. “Amplified quenching of a conjugated polyelectrolyte by cyanine dyes“ *J. Am. Chem. Soc*. **2004**, 126, 13685-13694 (b) Kushon, S. A.; Bradford, K.; Marin, V.; Suhrada, C.; Armitage, B. A.; McBranch, D.; Whitten, D. “Detection of DNA hybridization via fluorescent polymer superquenching“ *Langmuir* **2003**, 19, 6456-6464. (c) Pinto, M. R.; Schanze, K. S. “Amplified fluorescence sensing of protease activity with conjugated polyelectrolytes“ *Proc. Nat. Acad. Sci*. **2004**, 101, 7505-7510.

9. (a) Xue, C. H.; Jog, S. P.; Murthy, P.; Liu, H. Y. “Synthesis of highly water-soluble fluorescent conjugated glycopoly(p-phenylene)s for lectin and Escherichia coli” *Biomacromolecules* **2006**, 7, 2470-2474. (b) Xue, C.; Donuru, V. R. R.; Liu, H. Y. “Facile, versatile prepolymerization and postpolymerization functionalization approaches for well-defined fluorescent conjugated fluorene-based glycopolymers” *Macromolecules* **2006**, 39, 5747-5752. (c) DiCesare, N.; Pinto, M. R.; Schanze, K. S.; Lakowicz, J. R. “Saccharide detection based on the amplified fluorescence quenching of a water-soluble poly(phenylene ethynylene) by a boronic acid functionalized benzyl viologen derivative” *Langmuir* **2002**, 18, 7785-7787.

10. (a) Tan, C. Y.; Pinto, M. R.; Kose, M. E.; Ghiviriga, I.; Schanze, K. S. “Solvent-induced self-assembly of a meta-linked conjugated polyelectrolyte. Helix formation, guest intercalation, and amplified quenching” *Adv. Mater*. **2004**, 16, 1208-1212. (b) Jiang, H.; Zhao, X.; Schanze, K. S. “Amplified fluorescence quenching of a conjugated polyelectrolyte mediated by Ca2+“ *Langmuir* **2006**, 22, 5541.

11. Kim, I.-B.; Dunkhorst, A.; Gilbert, J.; Bunz, U. H. F. “Sensing of lead ions by a carboxylate-substituted PPE: Multivalency effects“*Macromolecules* **2005**, 38, 4560-4562.

12. Kim, I.-B.; Erdogan, B.; Wilson, J. N.; Bunz, U. H. F. “Sugar-poly(para-phenylene ethynylene) conjugates as sensory materials: Efficient quenching by Hg2+ and Pb2+ ions“ *Chemistry Eur. J*. **2004**, 10, 6247-6254.

13. (a) Wiskur, S. L.; Ait-Haddou, H.; Lavigne, J. J.; Anslyn, E. V. “Teaching old indicators new tricks” *Acc. Chem. Res*. **2001**, 34, 963-972. (b) Anslyn, E. V. “Supramolecular analytical chemistry“ *J. Org. Chem*. **2007**, 72, 687-699.

14. Kim, I.-B.; Bunz, U. H. F. “ Modulating the sensory response of a conjugated polymer by proteins: An agglutination assay for mercury ions in water“ *J. Am. Chem. Soc.* **2006**, 128, 2818-2819.

15. You, C.-C.; Miranda, O. R.; Gider, B.; Ghosh, P. S.; Kim, I.-B.; Erdogan, B.; Krovi, S. A.; Bunz, U. H. F.; Rotello V. M. “Detection and identification of proteins using nanoparticle-fluorescent polymer 'chemical nose' sensors“ *Nature Nanotechnology* **2007**, accepted

16. Khan, A.; Müller, S.; Hecht, S. “Practical synthesis of an amphiphilic, non-ionic poly(paraphenyleneethynylene) derivative with a remarkable quantum yield in water” *Chem. Commun*. **2005**, 584-586.

17. Lauter, U.; Meyer, W. H.; Enkelmann, V.; Wegner, G. “Supramolecular structures of poly(p-phenylenes) with oxyethylene side chains and their mixtures with lithium salts“ *Macromol. Chem. Phys*. **1998**, 199, 2129-2140.

18. (a) Bunz, U. H. F. “Poly(aryleneethynylene)s: Syntheses, properties, structures, and applications” *Chem. Rev*. **2000**, 100, 1605-1644. (b) Bunz, U.H.F. “Synthesis and Structures of PAEs” *Adv. Polym. Sci.* **2005**, 177, 1-52. (c) Chinchilla R.; Nájera, C. “The sonogashira reaction: A booming methodology in synthetic organic chemistry” *Chem. Rev*. **2007**, 107, 874 – 922.

19. Kim, J.; Swager, T. M. “Control of conformational and interpolymer effects in conjugated polymers” *Nature* **2001**, 411, 1030-1034.

20. Bunz, U. H. F.; Wilson, J. N.; Bangcuyo, C. *ACS Symp. Series* **2004**, 888, 147-160.

21. http://research.chem.psu.edu/brpgroup/pKa_compilation.pdf

22. Miteva, T.; Palmer, L.; Kloppenburg, L.; Neher, D.; Bunz, U.H.F. “Interplay of thermochromicity and liquid crystalline behavior in poly(p-

phenyleneethynylene)s: pi-pi interactions or planarization of the conjugated backbone?“ *Macromolecules* **2000**, 33, 652-654.

23. (a) Bunz, U. H. F.; Imhof, J. M.; Bly, R. K.; Bangcuyo, C. G.; Rozanski, L.; VandenBout, D. A. “Photophysics of poly [p-(2,5-didodecylphenylene) ethynylene] in thin films” *Macromolecules* **2005**, 38, 5892-5896. (b) Halkyard, C. E.; Rampey, M. E.; Kloppenburg, L.; Studer-Martinez, S. L.; Bunz, U. H. F. “Evidence of aggregate formation for 2,5-dialkylpoly(p-phenyleneethynylenes) in solution and thin films“ *Macromolecules* **1998**, 31, 8655-8659.

24. (a) Zhou, Q.; Swager, T. M. “Fluorescent chemosensors based on energy migration in conjugated polymers: The molecular wire approach to increased sensitivity” *J. Am. Chem. Soc*. **1995** 117, 12593-12602. (b) Lakowicz, J. R. *Principles of Fluorescence Spectroscopy*; Kluwer Academic/Plenum Publishers: New York, **1999**. (c) Stern, O.; Volmer, M. “ The fading time of fluorescence“ *Physikalische Zeitschrift* **1919**, 20, 183-188.

25. Henary, M. M.; Wu, Y. G.; Fahrni, C. J. “Zinc(II)-selective ratiometric fluorescent sensors based on inhibition of excited-state intramolecular proton transfer“ *Chemistry-Eur. J.* **2004**, 10, 3015-3025.

CHAPTER 3

Fluorescence Self Quenching of a Sugar-Substituted PPE Induced by Lectins

3.1 Introduction

Conjugated polymers (CP) have attained considerable status in the detection and quantification of biologically active molecules.[1] CPs have been used as solid state sensory coatings for electrodes and in solution as species that change their absorption and emission spectra upon exposure to a specific analyte. They are often superior to non-conjugated, non-fluorescent polymeric scaffolds,[2] as they elegantly combine recognition and transmission elements.

The optical/fluorescence-based detection of biologically important species in solution profits from the endless synthetic variability of CPs. Different tailored backbones are fitted to the intended purpose by the attachment of suitable recognition elements. The sensing or probing of biomolecular targets by CPs rests on either a) fluorescence resonance energy transfer (FRET), b) ratiometric response or c) quenching of the fluorescence after binding to a specific analyte. All three of these mechanisms are of significant interest and have demonstrated use in the probing of biomolecules. The properties that make CPs so much more powerful than small dyes are a) their facility for acting as molecular antennae, in which one exciton can 'patrol' up to one hundred repeat units, b) their ability for supporting multivalent interactions[3-4] and c) most complex and least well understood, their aggregation phenomena, which can lead to a phenomenally large signal amplification that allows detection of zeptomolar concentrations of DNA.[5]

The quenching of the fluorescence of PPEs by paraquat derivatives was first described by Swager and Zhou in a classic paper.[6] The PPE-analyte interactions could be correctly described by the Stern-Volmer formalism assuming static quenching induced by excited state electron transfer from the PPE to paraquat. The molecular antenna effect led to signal amplification by a factor of up to 100 when compared to similar monomeric fluorophores. Wudl and Whitten[7] later demonstrated superquenching when examining the interaction of paraquat with a sulfonated PPV and explained the observed thousand fold gain in sensitivity by a combination of the antenna effect compounded by paraquat-induced aggregate formation. While quenching with paraquat involves excited state electron transfer, Förster energy transfer can also be employed to quench the fluorescence of a water soluble conjugated polymer by the interaction with the deeply colored cytochrome C, as demonstrated by Heeger et al.[8] A combination of mechanisms is believed to be responsible for the superquenching ability of gold nanoparticles on the fluorescence of conjugated polymers.[9] However, quenching of CP fluorescence can also occur if the analyte does not carry any obvious chromogenic or electron transfer center. This is the case in the interaction of PPEs with proteins such as lysozyme, etc.,[10] or more importantly, Con A as a model protein for biotoxins such as Ricin and E. coli toxin.[11-12]

The classic tool for investigating quenching is the Stern Volmer equation:

$$F_o/F_{[Q]} = 1 + K_{SV}[Q] \qquad \textbf{Eq. 3.1}$$

in which $F_o/F_{[Q]}$ is the ratio of the initial fluorescence intensity F_o and the fluorescence intensity $F_{[Q]}$ in the presence of the quencher Q at a concentration [Q]. K_{SV} is the Stern-Volmer constant, and may refer to static quenching if the complex between fluorophore and quencher is preformed and does not undergo diffusion or to dynamic quenching if

diffusion occurs during the excited state lifetime. In the case of dynamic quenching, K_{SV} represents the equilibrium constant. In the case of static quenching it is assumed that the quencher and the fluorophore form a non-fluorescent ground state complex, and that the slope of $F_o/F_{[Q]}$ for different concentrations of Q provides the binding constant of fluorophore to quencher. In cases of static quenching the fluorescence lifetime of the fluorophore is independent of the concentration of added quencher Q. This is generally the case for PPEs, which have a lifetime of 0.3-0.4 ns.[13] The other necessary prerequisite for a straightforward application of the Stern-Volmer formalism is that a one-to-one complex forms between quencher and fluorophore. It is often argued that at low quencher/ fluorophore concentrations this assumption is valid. One should also note that the concentration of the fluorophore does not show up in this analytical expression of the Stern-Volmer equation.[14] However, for numerous examples of fluorescence quenching of CPs by small molecule quenchers published in the literature the polymer concentration *does* matter.[15] The observed Stern-Volmer 'constants' are inversely dependent upon the concentration of the CP. As a consequence K_{SV} decreases with increasing concentration of CPs.

With this, we decided to probe protein-conjugated polymer interactions using fluorescence quenching of the mannose-substituted poly(*p*-phenyleneethynylene) (PPE) **3.8** by Concanavalin A (Con A), the tetrameric lectin of the jack bean,[3] as Con A displays sensitive quenching of the fluorescence of mannosylated PPEs.[11] As Con A does not contain an easily identifiable electron or charge or charge transfer center we decided to investigate the mechanism of this quenching.

3.2 Results and Discussion

We chose the mannose-substituted PPE **3.8** as a suitable object for our investigation, as it a) carries a negative charge and b) has the mannose residue attached to the PPE chain by a 20-atom tether, suggesting easy interaction of **3.8** with Con A. The structure of PPE **3.8** is displayed in Figure 3.1; in the last step the pre-PPE **3.6** is desilylated and a copper catalyzed 1,3-dipolar cycloaddition to **3.7** is performed to give **3.8** in high yield.[16]

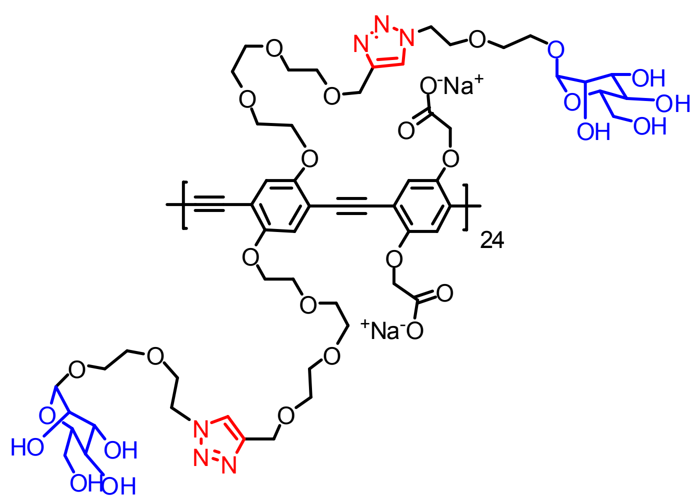

Figure 3.1. Structure of mannose-substituted PPE (**3.8**)

Figure 3.2 displays the dependence of the fluorescence quenching of **3.8** on the concentration of Con A, the classic Stern- Volmer formalism, for different concentrations of the polymer **3.8**. It is immediately noticeable that, at low concentrations of Con A, the S-V plot is linear. At higher concentrations of the quencher Q, the plot is also linear, but with a different slope. Surprisingly, the extracted initial K_{SV} is proportional to the PPE concentration as well, which is contrary to the existence of a 1:1 complex, but

commensurate with a 1:2 complex. If the concentration of PPE **3.8** is below 3 x 10^{-8} M, no quenching whatsoever is observed.

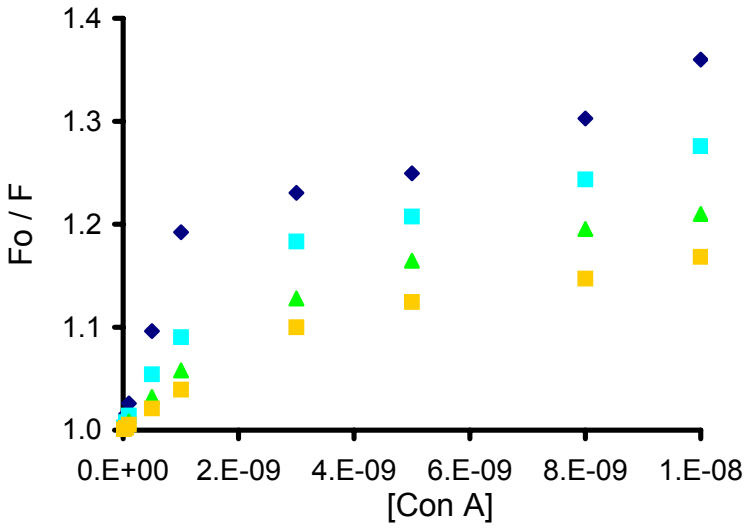

Figure 3.2. Stern-Volmer graph for different PPE concentrations. Dark blue [PPE] = 5 x 10^{-7} M; Turquoise [PPE] = 2.5 x 10^{-7} M; Green [PPE] = 1.25 x 10^{-7} M; Gold [PPE] = 6.25 x 10^{-8} M.

The lifetime of the PPE excited state was measured to be 450 ps and was not dependent on [Con A], in agreement with a purely static quenching mechanism. The presence of a "two-phase" S-V plot, as opposed to a second order plot, suggests the intervention of two such quenching mechanisms. The general treatment of such kinetics is provided by Equation 3.3, where f_1 and f_2 represent the relative fractions of quenching mechanisms ($f_1 + f_2 = 1.0$) and K_{SV1} and K_{SV2} are the respective Stern-Volmer constants. [17]Using the data in Figure 3.2 and Equation 3.2, we determine by least-squares analysis the equilibrium constants shown in Table 3.1 and Figure 3.3.

Table 3.1. Calculated Stern-Volmer constants (K_{sv}) using Equation 3.2 for varying concentrations of **3.8** with Concanavalin A

[PPE], M	$\mathbf{K_{sv1}}$, M^{-1}	$\mathbf{K_{sv2}}$, M^{-1}	$\mathbf{f_1}$	$\mathbf{f_2}$
5.00E-07	5.33E+08	1.03E+05	0.32	0.68
2.50E-07	2.79E+08	7.90E+04	0.31	0.69
1.25E-07	1.91E+08	5.22E+04	0.28	0.72
6.25E-08	1.43E+08	4.42E+04	0.25	0.75

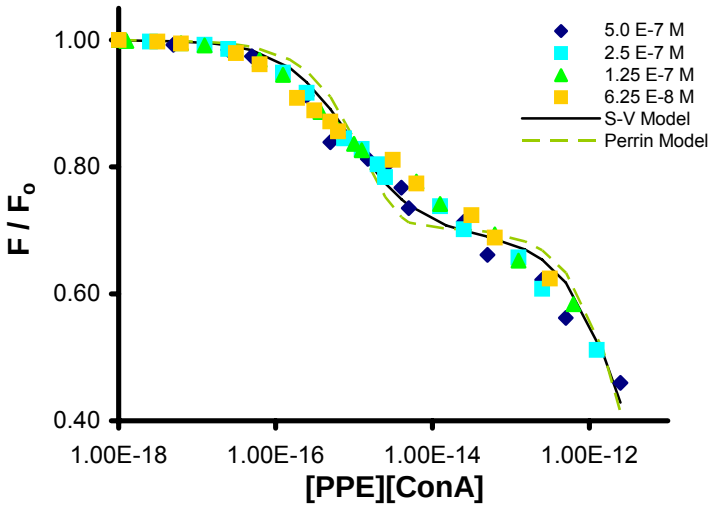

Figure 3.3. Master plot of all quenching data, including fit to Equations 3.3 and 3.4.

Figure 3.4 illustrates that K_{SV1} is linearly dependent on [PPE] and K_{SV2} is partially dependent on [PPE]. We also notice that the two rate constants differ by a factor of 10^4, but that, within experimental error, the contribution of each process to quenching remains nearly constant, i.e., ca. 0.3 for K_{SV1} and 0.7 for K_{SV2}.

$$F_{[Q]}/F_o = f_1/(1 + K_{SV1}[Q]) + f_2/(1 + K_{SV2}[Q]) \qquad \textbf{Eq. 3.2}$$

$$F_{[Q]}/F_o = f_1/(1 + K'_{SV1}[Q][PPE]) + f_2/(1 + K'_{SV2}[Q][PPE]) \qquad \textbf{Eq. 3.3}$$

The near linear dependence of the K_{SV}'s suggests that the quenching involves a complex of two PPE molecules. Indeed, if we assume that $K_{SV}(obs) = K'_{SV}[PPE]$, we can fit all the data in Figure 3.2 to a master equation, Equation 3.3 as shown in Figure 3.3. The RMS error for this least-squares treatment is a factor of two over that for the individual fits. Using this treatment,[18] we obtain a $K'_{SV1} = 1.1 \times 10^{15}$ L^2mol^{-2} (31%) and $K'_{SV2} = 2.5 \times 10^{11}$ L^2 mol^{-2} (69%).

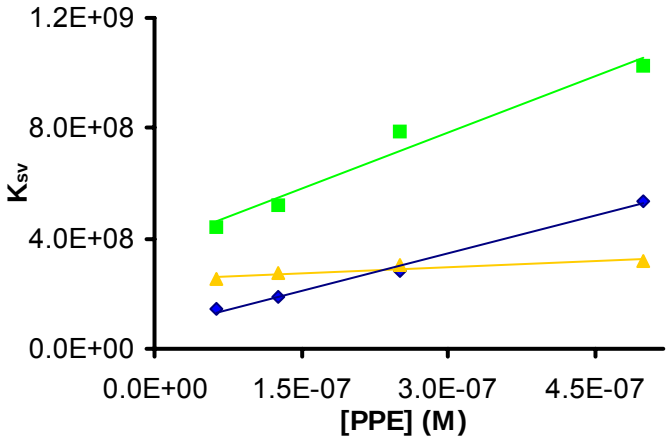

Figure 3.4. Plot of K_{sv1} and K_{sv2} and of f_1 [PPE]. Dark blue = K_{sv1}; Gold = $f_1 * 10^9$; Green = $K_{sv2} * 10^4$.

An alternate fit when static quenching is involved is to use the concept of quenching volume, based upon the Perrin model, in which fluorophores within the quenching volume V_q quench with 100% efficiency and without with 0% efficiency.[19] Again, with the two quenching complexes, this model reduces to equation 3.4:

$$F_{[Q]}/F_o = f_1/(\exp(V_{q1}\,[Q]\,[PPE])) + f_2/(\exp(V_{q2}\,[Q]\,[PPE])) \quad \textbf{Eq. 3.4}$$

Use of a non-linear least-squares fit to this equation provided the fit shown in Figure 3.3 by the dashed line. We note that the total sum of squares for this fit is 4 times

that for equation 3.3. However, since to a first approximation exp(x) = 1+ x, we note that V_q and K_{SV} are almost indistinguishable. The fit to equation 3.4 yields $V_{q1} = 7.6 \times 10^{14}$ and $V_{q2} = 2.1 \times 10^{11}$, which are nearly identical to the K_{SV} values.

To get a better understanding for the association processes that occur, we performed isothermal titration calorimetry (ITC) by adding the polymer solution to a solution of Con A in phosphate buffer at a pH of 7.2 (Figure 3.5). We obtained a binding ratio of N = 3.01 PPE:Con A; ΔG = -7.1 kcal/mol*K, ΔH= -6.4 kcal/mol*K, ΔS = 2.4 cal/mol*K, and a resulting $K_a = 1.6 \times 10^5\ M^{-1}$.

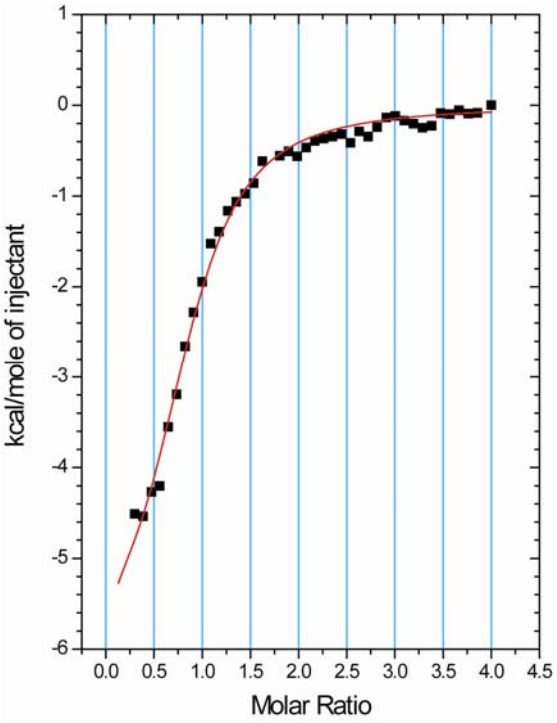

Figure 3.5. Isothermal Titration Calorimetry study of PPE **3.8** with Con A.

We can interpret this data (Figure 3.6) by assuming that in the first step we form a fluorescent 1:1 complex of Con A and **3.8**, with a K_a from ITC data of $1.6 \times 10^5\ M^{-1}$. In

the presence of an excess of **3.8**, a second molecule of **3.8** binds to Con A to form two fluorescence-quenched complexes. We cannot tell from these experiments the exact mechanism of binding, although it may be that one binding mechanism involves 2 mannose units on one PPE and 1 on another, and the other 2 and 2.

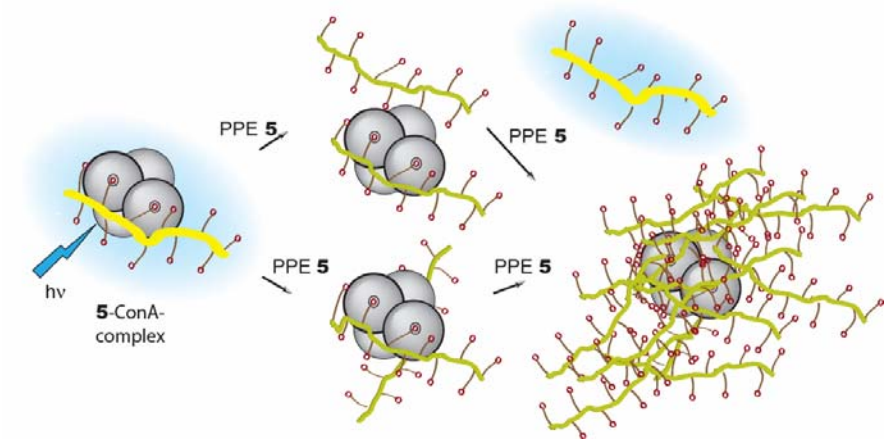

Figure 3.6. Proposed quenching mechanism of mannose-substituted PPE induced by Con A.

Again, taking $V_{q1}(obs) = V_{q1}$ [PPE], we can estimate the quenching volume of the strongest 1:1 complex as $(7.6 \times 10^{14})(5.0 \times 10^{-7}) = 3.8 \times 10^{8}$ L mol^{-1}, or 6.3×10^{8} nm^3 molecule^{-1}, a quenching distance of 430 nm! This extraordinary quenching distance is the direct result, we believe, of the fact that two molecules of PPE are involved, which results in the exciton-coupled amplification even greater than that produced with single molecule quenching,[5] and may indicate the severity of assumptions used by the Perrin model. The large quenching volume may also result from transfer of excitation energy from other molecules of **3.8**, leading to significant signal amplification.

3.3 Conclusion

We have demonstrated that the quenching of the fluorescence of PPE 3.8 is induced by the addition of Con A through the formation of non-fluorescent aggregates. This system is very unusual as it displays increased quenching with increasing fluorophore concentration, approaching the apparent binding constants of streptavidin/biotin. Such aggregation-induced enhancement is not unprecedented and has been seen by Leclerc[20] in the detection of zeptomolar concentrations of DNA. Here as well an energy transfer from an ensemble of conjugated polymer chains to a quencher or a FRET dye gives a sensitivity that is incommensurate with any binding constant. To further enhance the sensitivity of sugar-substituted PPEs towards lectins, additional side chain functionality needs to be employed to increase protein-PPE interactions. The exquisite sensitivity, ease of data collection and data evaluation make the quenching of polymeric fluorophores alluring and, despite the large discrepancies with the ITC derived association constants, uniquely useful and promising for further sensory and probe-type applications.

3.4 Experimental

Instrumentation and Materials. All chemicals and solvents were purchased from commercial sources and were used without further purification unless otherwise specified. Column chromatography was performed using Standard Grade silica gel 60 Å, 32-63 μm (Sorbent Technologies) and the specified eluent. All IR spectra were obtained using a Shimadzu FTIR-8400s spectrometer. ^{1}H NMR spectra were recorded at 298 K on a 300 or 500 MHz spectrometer. Chemical shifts are reported in parts per million (ppm),

using residual solvent (chloroform-*d*) as an internal standard. The data is reported as follows: chemical shift, multiplicity (s = singlet, d = doublet, t = triplet, q = quartet, m = multiplet, br = broad), and integration. ^{13}C HMR spectra were recorded at 300 or 500 MHz, and ^{13}C chemical shifts (δ) are referenced to residual $CHCl_3$ at 77.23 ppm. All absorption spectra were collected using a Shimadzu UV-2401PC spectrophotometer. All emission spectra were acquired using a Shimadzu RF-5301PC spectrofluorophotometer. Quantum yields for the polymers were measured using standard procedures.[21] In all cases, quinine sulfate and 2-aminopyridine were used as standards and all solutions were purged with nitrogen prior to measurement**.**

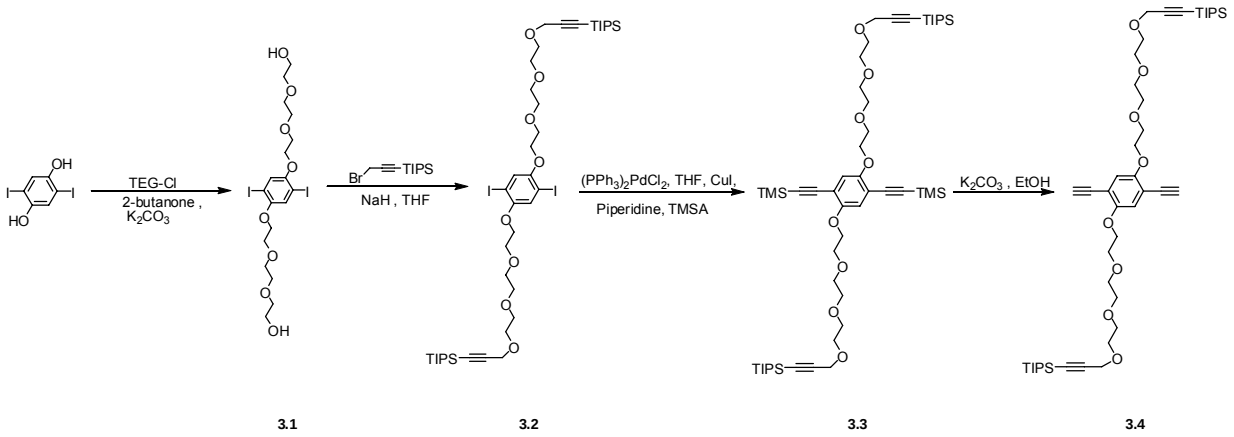

Scheme 3.1. Synthetic scheme for monomer **3.4**

Synthesis of 3.1: 1,4-Dihydroxy-2,5-diiodobenzene (10.1 g, 0.0276 mol) was dissolved in 2-butanone (150 mL) and the resulting solution was added slowly to a stirred suspension of K_2CO_3 (30.6 g, 0.221 mol) in 2-butanone (75mL) under N_2. The reaction mixture was allowed to stir for 5-10 min followed by the slow addition of TEG-Cl (0.111

mol, 16.1 mL). The reaction was heated to 75ºC for 7 days. The solution was cooled to room temperature, the solvent was removed, and the resulting slurry was re-dissolved in CH_2Cl_2. The solution was extracted with water to remove excess K_2CO_3 and the organic fractions were collected and concentrated in vacuo until an oily residue remained. The solution was purified by silica gel chromatography (95:5 EtOAc / MeOH). The product was a flaky colorless solid (13.5 g, 21.6 mmol, 78.8%). ^{1}H NMR (300 MHz, $CDCl_3$): δ 7.21 (s, 2H), 4.11 (t, 4H), 3.85 (t, 4H), 3.79 (t, 4H), 3.72 (t, 4H), 3.66 (t, 4H) 3.57 (t, 4H). ^{13}C NMR (300 MHz, $CDCl_3$): δ 152.94, 123.32, 86.32, 72.44, 71.09, 70.40, 70.14, 69.50, 61.66. IR (KBR, cm^{-1}): ν 3423, 2937, 2892, 1487, 1464, 1353, 1325, 1232, 1215, 1125, 1119, 1084, 1062, 1033, 886, 857, 829, 799.

Synthesis of 3.2: Compound **3.1** (4.50 g, 7.20 mmol) was dissolved in dry THF (200 mL). NaH (3 eq., 0.517 g, 21.6 mmol) was added and the solution was stirred under N_2 for 30 min. After all H_2 had ceased, Tipspropargylbromide (2.1 eq., 4.16 g, 15.1 mmol) was added and the reaction was stirred under N_2 at room temperature overnight. The resulting salts were filtered out, the solvent was removed, and the product was purified using silica gel chromatography (1:3 EtOAc / Hexane). The resulting product was a light yellow oil (4.01 g, 3.90 mmol, 55.0 %). ^{1}H NMR (300 MHz, $CDCl_3$): δ 7.18 (s, 2H), 4.18 (s, 4H), 4.04 (t, 4H), 3.82 (t, 4H), 3.73 (t, 4H), 3.67-3.62 (m, 12H), 1.03 (s, 42H). ^{13}C NMR (300 MHz, $CDCl_3$): δ 152.91, 123.24, 103.13, 87.40, 86.25, 70.98, 70.55, 70.32, 70.11, 69.44, 68.55, 58.98. IR (cm^{-1}): ν 3017.42, 2944.13, 2891.10, 2170.73, 1462.91, 1449.41, 1348.15, 1215.07, 1096.46, 1032.81, 998.09, 927.70, 883.34, 769.54.

Synthesis of 3.3: Compound **3.2** (11.3 g, 11.1 mmol), TMS-acetylene (4 eq, 44.4 mmol, 6.32 ml), CuI (0.01eq, 0.111 mmol, 0.0211 g), $(PPh_3)_2PdCl_2$ (0.01 eq, 0.111 mmol,

0.0778g), THF (75mL), and piperidine (7mL) were all added to a dry 100mL round bottomed flask under N_2. The solution was reacted overnight. Upon completion of the reaction, the solvent was removed, the product was re-dissolved in CH_2Cl_2, and was extracted with water to remove any salts. The organic fractions were collected and the solvent was removed. The crude product was purified by silica gel chromatography (1:3 EtOAc / Hexane). The obtained product was a viscous orange oil (6.52 g, 6.83 mmol, 61.5 %). ^{1}H NMR (300 MHz, $CDCl_3$): δ 6.89 (s, 2H), 4.23 (s, 4H), 4.11 (t, 4H), 3.86 (t, 4H), 3.75 (t, 4H), 3.71-3.62 (m, 12H), 1.03 (s, 42H), 0.213 (s, 18H). ^{13}C NMR (300 MHz, $CDCl_3$): δ 153.79, 117.54, 114.07, 103.17, 100.77, 100.28, 87.48, 71.07, 70.67, 70.37, 69.63, 69.41, 68.62, 59.06, 18.50, 11.03, -0.112. IR (cm^{-1}): ν 3018.39, 2942.21, 2865.06, 2170.73, 1496.66, 1348.15, 1215.07, 1098.39, 1031.85, 928.66, 883.34, 754.12.

Synthesis of 3.4: Compound **3.3** (3.95 g. 4.13 mmol) was dissolved in anhydrous EtOH (200mL). K_2CO_3 (4 eq., 2.29 g) was added to the solution and the reaction was stirred overnight. The solvent was removed and crude product was re-dissolved in CH_2Cl_2. The solution was extracted with water to remove any excess salts. The organic fractions were collected, the solvent was removed, and the product was dried. The resulting product was a dark orange powder (3.20 g, 3.95 mmol, 95.6 %). ^{1}H NMR (500 MHz, $CDCl_3$): δ 6.96 (s, 2H), 4.25 (s, 4H), 4.13 (t, 4H), 3.81 (t, 4H), 3.74 (t, 4H), 3.70-3.59 (m, 12H), 3.31 (s, 2H), 1.01 (s, 42H). ^{13}C NMR (500 MHz, $CDCl_3$): δ 154.51, 118.90, 114.21, 88.34, 83.51, 71.11, 70.84, 70.53, 69.77, 69.53, 69.27, 59.11, 19.48, 12.07. IR (cm^{-1}): ν 3302.84, 3018.39, 2941.54, 2862.06, 2168.32, 1496.66, 1350.25, 1213.65, 1097.49, 1031.85, 927.66, 881.45, 754.23.

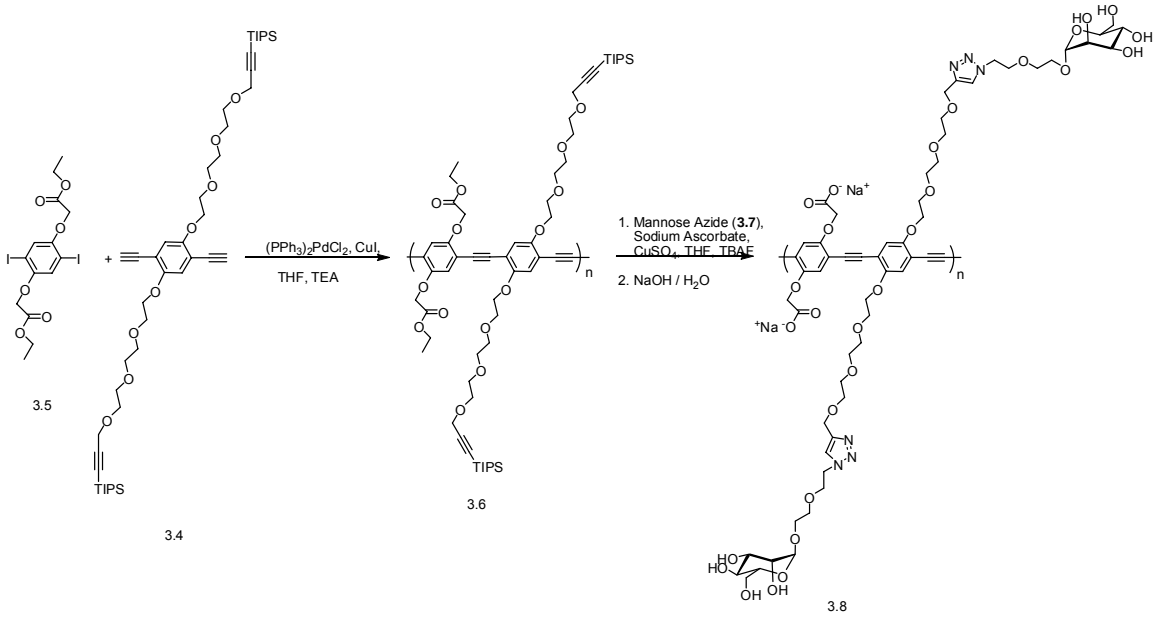

Scheme 3.2. Synthetic scheme for polymer **3.8**

Synthesis of polymer 3.6: Compound **3.5**[22] (534 mg, 1 mmol), **3.4** (809 mg, 1 mmol), TEA (3 mL) and THF (3 mL) were all combined in a 25 mL Schlenk tube and degassed. Upon degassing, $(PPh_3)_2PdCl_2$ (0.5 mol %, 3.51 mg) and CuI (1 mol %, 1.91 mg) were added under N_2 and the solution was reacted at 45 ºC for 3 d. The solution was diluted with THF (25 mL), precipitated into hexane (500 mL), and dried which resulted in an orange flaky solid (1.04g, 0.956 mmol, 96 %). GPC (vs. polystyrene standards in chloroform): M_n = 25,852, M_w/M_n = 2.684, n = 24. ^{1}H NMR (500MHz, $CDCl_3$): δ 7.11 (s, 2H), 7.04 (s, 2H), 4.76 (s, 4H), 4.23 (m, 8H), 3.92-3.68 (m, 24H) 1.30 (t, 6H), 1.06 (s, 42H). ^{13}C NMR (500 MHz, $CDCl_3$): δ 168.52, 153.44, 118.83, 117.69, 114.86, 114.25, 103.17, 92.37, 90.72, 87.42, 70.82, 70.55, 70.28, 69.51, 69.29, 68.57, 67.16, 61.36, 58.97, 17.88, 14.11, 11.23. IR (cm^{-1}): ν 2941.24, 2864.09, 2169.77, 1757.03, 1514.02, 1425.30, 1278.72, 1197.71, 881.41, 678.90.

Synthesis of polymer 3.8: To functionalize the polymer with mannose, compound **3.7**[23] (127 mg, 0.276 mmol) and THF (10 mL) were added to polymer **3.6** (100 mg, 0.0919 mmol) and degassed. Under N_2, $CuSO_4$ (0.44 mg, 0.00276 mmol), sodium ascorbate (2.73 mg, 0.0138 mmol), and TBAF (0.25 mL, 1M solution in THF) were added and the polymer was reacted at 50 ºC for 3 d. The solvent was removed, the polymer was re-dissolved in $CHCl_3$, and extracted with H_2O (3x). The organic fractions were collected, the solvent was removed, and the polymer was deprotected in 1M NaOH at 45 ºC overnight. The resulting solution was neutralized with 1M HCl and dialyzed against DI H_2O for 3 d. The resulting polymer was a dark yellow powder (105 mg, 0.0805 mmol, 88 %). ^{1}H NMR (500MHz, D_2O): δ 8.03 (s, 2H), 7.12 (s, 2H), 7.09 (s, 2H), 4.49 (s, 4H), 4.11-3.03 (br, 58H). IR (cm^{-1}): ν 3320.23, 2879.52, 2192.91, 1585.38, 1437.83, 1409.87, 1328.86, 1262.32, 1117.67, 1031.85, 983.63, 924.80, 855.37. $\Phi_{water} = 0.12$

Monitoring the Concentration Dependence of Sugar Functionalized PPE (3.8) towards Con A. Sugar Functionalized **3.8** was diluted to concentrations of 5 x 10^{-7}, 2.5 x 10^{-7}, 1.25 x 10^{-7}, 6.25 x 10^{-8}, and 3.125 x 10^{-8} M in phosphate buffer at a physiological pH of 7.2. Known concentrations of Con A were titrated into each concentration of polymer solution, which resulted in protein concentrations ranging from the micro to picomolar range. After each titration, the fluorescence quenching was monitored by fluorescence spectroscopy. From the quenching data, Stern-Volmer constants were calculated and it was observed that the Stern-Volmer constant increases upon increasing the polymer concentration. No considerable quenching was observed at 3.125 x 10^{-8} M.

Isothermal Titration Microcalorimetry Study of Sugar Functionalized PPE (3.8) with Con A. In order to determine the binding constant, reaction stoichiometry, and

thermodynamic profile for the interaction of **3.8** with Con A, Isothermal Titration Microcalorimetry (ITC) was used. For each titration, 6 μL of polymer (1 mM in phosphate buffer) was injected from a 300 μL microsyringe at an interval of 5 min into a Con A solution (0.040 mM in PB buffer) while stirring at 310 rpm. As a control, identical injections of each polymer were injected into a PB buffer solution which contained no protein. As expected, the heats of dilution were negligible. The titration data was fitted to a theoretical titration curve (One Site) using software which was provided by Microcal. The binding constant and thermodynamic parameters were calculated using the equation,

$$\Delta G = \Delta H - T\Delta S = -RT\ln K \qquad \textbf{Eq. 3.4}$$

where ΔG, ΔH, and ΔS are the changes in free energy, enthalpy, and entropy, T is the absolute temperature (298 K), R = 1.98 cal/mol*K, and K is the binding constant.

3.5 References

1. (a) Thomas, S. W.; Joly, G. D.; Swager, T. M. "Chemical sensors based on amplifying fluorescent conjugated polymers" *Chem. Rev.* **2007**, *107*, 1339-1386. (b) McQuade, D. T.; Pullen, A. E.; Swager, T. M. "Conjugated polymer-based chemical sensors" *Chem. Rev.* **2000**, *100*, 2537-2574.

2. (a) Kiessling, L. L.; Pohl, N. L. "Strength in numbers: non-natural polyvalent carbohydrate derivatives" *Chem. Biol.* **1996**, *3*, 71-77. (b) Kanai, M.; Mortell, K. H.; Kiessling, L. L. "Varying the Size of Multivalent Ligands: The Dependence of Concanavalin A Binding on Neoglycopolymer Length" *J. Am. Chem. Soc.* **1997**, *119*, 9931-9932.

3. Lis, H.; Sharon, N. "Lectins: Carbohydrate-Specific Proteins that Mediate Cellular Recognition" *Chem. Rev.* **1998**, *98*, 637-674.

4. (a) Kim, I.-B.; Erdogan, Belma.; Wilson, J. N.; Bunz U. H. F. "Sugar-poly(para-phenylene ethynylene) conjugates as sensory materials: Efficient quenching by Hg^{2+} and Pb^{2+} ions" *Chem. Eur. J.* **2004**, *10*, 6247-6254. (b) Mammen, M.; Choi, S. K.; Whitesides G. M. "Polyvalent interactions in biological systems: implications for design and use of multivalent ligands and inhibitors" *Angew. Chem.* **1998**, *37,* 2755-2794.

5. Dore, K.; Leclerc, M.; Boudreau, D. "Investigation of a fluorescence signal amplification mechanism used for the direct molecular detection of nucleic acids" *J. Fluorescence* **2006**, *16*, 259-265.

6. Zhou, Q.; Swager, T. M. "Fluorescent chemosensors Based on energy migration in conjugated polymers: the molecular wire approach to increased sensitivity" *J. Am. Chem. Soc.* **1995**, *117*, 12593-12602.

7. Chen, L.; McBranch, D. W.; Wang, H.-L.; Helgeson, R.; Wudl, F.; Whitten, D. G. "Highly sensitive biological and chemical sensors based on reversible fluorescence quenching in a conjugated polymer" *Proc. Nat. Acad. Sci. (USA)* **1999**, *96*, 12287-12292.

8. Fan, C.; Plaxco K. W.; Heeger, A. J. "High-efficiency fluorescence quenching of conjugated polymers by proteins" *J. Am. Chem. Soc.* **2002**, *124*, 5642-5643.

9. (a) Fan, C.; Wang, S.; Hong, J. W.; Bazan, G. C.; Plaxco, K. W.; Heeger, A. J. "Beyond superquenching: Hyper-efficient energy transfer from conjugated polymers to gold nanoparticles" *Proc. Nat. Acad. Sci. (USA)* **2003**, *100*, 6297-6301. (b) You, C. C.; Miranda, O. R.; Gider, B.; Ghosh, P. S.; Kim, I. B.; Erdogan, B.; Krovi, S. A.; Bunz, U. H. F.; Rotello, V. M. "Detection and identification of proteins using nanoparticle-fluorescent polymer 'chemical nose' sensors" *Nature Nanotech.* **2007**, *2*, 318-323.

10. (a) Kim, I. B.; Dunkhorst, A.; Bunz, U. H. F. "Nonspecific Interactions of a Carboxylate-Substituted PPE with Proteins. A Cautionary Tale for Biosensor Applications" *Langmuir* **2005**, *21*, 7985-7989. (b) Miranda, O. R.; You, C.-C.; Phillips R.; Kim, I.-B.; Ghosh, P. S.; Bunz, U. H. F.; Rotello V. M. "Array-Based Sensing of Proteins Using Conjugated Polymers" *J. Am. Chem. Soc.* **2007,** *129*, 9856-9857. (c) Dwight, S. J.; Gaylord, B. S.; Hong, J. W.; Bazan, G. C. "Perturbation of fluorescence by nonspecific interactions between anionic poly(phenylenevinylene)s and proteins: Implications for biosensors" *J. Am. Chem. Soc.* **2004,** *126*, 16850-16859.

11. (a) Kim, I. B.; Wilson, J. N.; Bunz, U. H. F. "Mannose-substituted PPEs detect lectins: A model for Ricin sensing" *Chem. Commun*. **2005**, 1273-1275. (b) Phillips, R. L.; Kim I.-B.; Carson, B. E.; Tidbeck, B.; Bai, Y., Lowary, T. L.; Bunz, U. H. F. "Sugar-substituted poly(paraphenyleneethynylene)s: sensitivity enhancement towards lectins and bacteria" *Macromolecules.* Accepted. (c) Disney, M. D.; Zheng, J.; Swager, T. M.; Seeberger, P. H. "Detection of Bacteria with Carbohydrate-Functionalized Fluorescent Polymers" *J. Am. Chem. Soc.* **2004,** *126*, 13343-13346.

12. (a) Xue, C.; Jog, S. P.; Murthy, P.; Liu, H. Y. "Synthesis of Highly Water-Soluble Fluorescent Conjugated Glycopoly(p-phenylene)s for Lectin and Escherichia coli" *Biomacromolecules.* **2006**, *7*, 2470-2474. (b) Kaur, P.; Wu, M. Y.; Anzaldi, L.; Waldeck, D. H.; Xue, C. H.; Liu H. Y. *Langmuir* 2007, *23*, 13203-13208. (c) Xue C. H.; Donuru, V. R. R.; Liu, H. Y. "Facile, Versatile Prepolymerization and Postpolymerization Functionalization Approaches for Well-Defined Fluorescent Conjugated Fluorene-Based Glycopolymers" *Macromolecules* **2006,** *39*, 5747-5752.

13. (a) Bunz, U. H. F. "Poly(aryleneethynylene)s: Syntheses, Properties, Structures, and Applications" *Chem. Rev.* **2000**, *100*, 1605-1644. (b) Bourdin, E.; Davey, A.; Blau, W.; Delysse, S.; Nunzi, J. M. "Picosecond excited states in poly(arylene-ethynylene)s" *Chem. Phys. Lett.* **1997**, *275*, 103-107. (c) Bunz, U. H. F.; Imhof, J. M.; Bly, R. K.; Bangcuyo, C. G.; Rozanski, L.; VandenBout, D. A. "Photophysics of Poly[p-(2,5-didodecylphenylene)ethynylene] in Thin Films" *Macromolecules* **2005**, *38*, 5892-5896.

14. Stern, O.; Volmer, M. "Molecular theory of the vapor pressure of solid substances and its significance in the calculation of chemical constants" *Physikalische Zeitschrift* **1919**, *20*, 183-188.

15. Wang, J.; Wang, D. L.; Miller, E. K; Moses, D.; Bazan, G. C.; Heeger, A. J. "Photoluminescence of Water-Soluble Conjugated Polymers: Origin of Enhanced Quenching by Charge Transfer" *Macromolecules* **2000**, *33*, 5153-5158.

16. (a) Englert, B. C.; Bakbak, S.; Bunz, U. H. F. "Click Chemistry as a Powerful Tool for the Construction of Functional Poly(p-phenyleneethynylene)s: Comparison of Pre- and Postfunctionalization Schemes" *Macromolecules* **2005**, *38,* 5868-5877. (b) Huisgen, R.; Szeimies, G.; Möbius, L. "1,3-Dipolar cycloadditions. XXVI. Intramolecular stabilization of an N-(trinitrophenyl)nitrilimine" *Chem. Ber.* **1967**, *100*, 2494-2499. (c) Lewis, W. G.; Green, L. G.; Grynszpan, F.; Radic, Z.; Carlier, P. R.; Taylor, P.; Finn, M. G.; Sharpless, B. K. "Click chemistry in situ: Acetylcholinesterase as a reaction vessel for the selective assembly of a femtomolar inhibitor from an array of building blocks" *Angew. Chem.* **2002**, *41*, 1053-1057. (d) Rostovtsev, V. V.; Green, L. G.; Fokin, V. V.; Sharpless, B. K. "A stepwise Huisgen cycloaddition process: copper(I)-catalyzed regioselective "ligation" of azides and terminal alkynes" *Angew. Chem.* **2002**, *41*, 2596-2599. (e) Helms, B.; Mynar, J. L.; Hawker, C. J.; Frechet, J. M. J. "Dendronized Linear Polymers via "Click Chemistry" *J. Am. Chem. Soc.* **2004**, *126*, 15020-15021.

17. Eftink, M. R. "Fluorescence quenching: theory and applications" *Topics in Fluorescence Spectroscopy,* **1991**, *2*, 53-126. 1998, 199, 2129-2140.

18. In this context, [PPE] refers to repeat unit concentration. The degree of polymerization (DP) is 24, which can be used to correct to polymer concentration.

19. (a) Murphy, C. B.; Zhang Y.; Truxler, T.; Ferry, V.; Martin J. J.; Jones, W. E. "Probing Forster and Dexter Energy-Transfer Mechanisms in Fluorescent Conjugated Polymer Chemosensors" *J. Phys. Chem. B.* **2004,** *108*, 1537-1543. (b) Andre, J. C.; Niclause, M.; Ware, W. R. **"**Kinetics of partly diffusion controlled reactions. I. Transient and apparent transient effect in fluorescence quenching" *Chem. Phys.* **1978**, *28*, 371-377. (c) Lakatos-Lindenberg, K.; Hemenger, R. P.; Pearlstein, R. M. "Solutions of master equations and related random walks on quenched linear chains" *J. Chem. Phys.* **1972**, *56*, 4852-4867.

20. (a) Ho, H. A.; Dore, K.; Boissinot, M.; Bergeron, M. G.; Tanguay, R. M.; Boudreau, D.; Leclerc, M. "Direct Molecular Detection of Nucleic Acids by Fluorescence Signal Amplification" *J. Am. Chem. Soc.* **2005**, *127*, 12673-12676. (b) Dore, K.; Dubus, S.; Ho, H. A.; Levesque, I.; Brunette, M.; Corbeil, G.; Boissinot, M.; Boivin, G.; Bergeron, M. G.; Boudreau, D.; Leclerc, M. "Fluorescent polymeric transducer for the rapid, simple, and specific detection of nucleic acids at the zeptomole level" *J. Am. Chem. Soc.* **2004**, *126*, 4240-4244.

21. "A Guide to Recording Fluorescence Quantum Yields." Horiba Jobin Yvon Ltd. http://www.jobinyvon.co.uk/ukdivisions/Fluorescence/plqy.html

22. Kim, Ik-Bum; Dunkhorst, Anna; Gilbert, James; Bunz, Uwe H.F. "Sensing of Lead Ions by a Carboxylate-Substituted PPE: Multivalency Effects" *Macromolecules* **2005**, 38, 4560-4562.

CHAPTER 4

Sugar-Substituted PPEs: Sensitivity Enhancement Towards Lectins and Bacteria

4.1 Introduction

Lectins, proteins which specifically bind sugars, play a crucial role in cell signaling, cell surface recognition, and pathogen docking.[1-3] While lectins such as Ricin, *Botulinum* toxin and the *E. coli* toxin are pathogenic,[4] Concanavalin A (Con A), the lectin of the jack bean, is much less toxic and used as proof-of-principle for novel methods which detect ligand-protein interactions. Agglutination of erythrocytes,[1] surface plasmon resonance of sugar-containing polynorbene derivatives,[5-6] and colorimetric reactions with sugar-coated polydiacetylene vesicles[7-8] are common methods for studying the interaction of lectins and sugars. We[9] and others[10] have previously reported sugar-substituted conjugated polymers for the potential detection of bioterrorist agents and bacteria.[11] While the reported polymers displayed significant binding, binding constants were clearly not sufficient for trace detection of either proteins or microbes. To advance fluorescence-based assays with conjugated polymers as a detection method, one would like to engineer and enhance their sensitivity to such biological analytes. We investigated increasing linker lengths and the use of more complex sugars. Extending the linker length between the sugar functionality and the conjugated polymer was expected to lead to an increased binding between polymer and analyte, due to enhanced flexibility and decreased entropic cost. The incorporation of more complex sugars such as tri-mannose was attempted to increase the innate sensitivity of these conjugated polymers towards lectins and bacteria. We now disclose the synthesis of two sugar-substituted poly(*para*-

phenyleneethynylene)s, **4.5** and **4.7**, which address these issues by studying their interaction with lectins and their staining and agglutination with two *E. coli* strains.

4.2 Results and Discussion

The synthesis of water soluble sugar-substituted PPEs[12] starts with the preparation of the fundamental building blocks as shown in Schemes **4.3** - **4.5**. Palladium-catalyzed coupling of **4.1** with **4.2** furnished polymer **4.3** which was deprotected *in situ* and subjected to a copper catalyzed 1,3-dipolar cycloaddition with **4.4,** (Scheme 4.1) resulting in polymer **4.5** in 40% yield.[13-14] According to gel permeation chromatography (GPC) vs. polystyrene, M_n was 1.1 x 10^5 and the polydispersity index (PDI) was 2.9. Similarly, the palladium-catalyzed coupling of **4.2** to **4.6,** followed by deacetylation using aqueous sodium hydroxide solution, resulted in **4.7** in a 31% yield after dialysis; **4.7** has an M_n of 6.7 x 10^4 and a PDI of 2.1 respectively (Scheme 4.2). The PPEs **4.5** and **4.7** are water-soluble, yellow materials, that are blue fluorescent in aqueous solution. In both cases the λ_{max} of emission in water is centered at 461 nm. The emission quantum yields in water (Φ_{H2O} for **4.5** and **4.7** are 0.31 and 0.24, respectively.

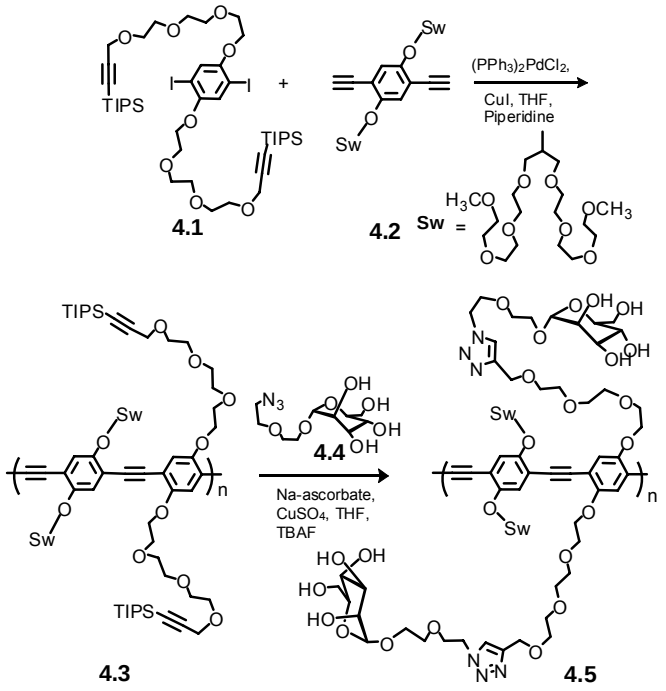

Scheme 4.1. Synthesis of polymer **4.5**

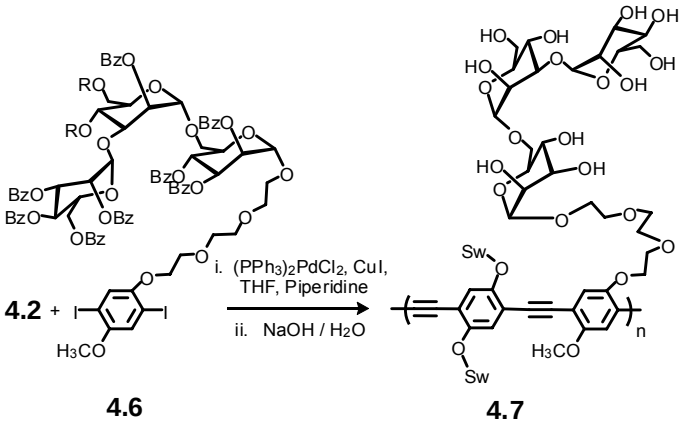

Scheme 4.2. Synthesis of polymer **4.7**

The quantitative aspects of the effect of a quencher Q on the emissive intensity F of a fluorophore with the intrinsic fluorescence intensity F_o is dependent upon the

concentration of the quencher Q, [Q]. In the simplest case, a linear relationship, the Stern-Volmer equation results:[15-16]

$$F_o/F_{[Q]} = 1 + K_{SV}\,[Q] \qquad \textbf{Eq. 4.1}$$

Quenching of the fluorescence can occur in two fundamentally different ways. If a molecule in its excited state has an emissive lifetime that is >10 ns, molecules of the quencher Q encounter the fluorophore in its excited state and lead to collisional or dynamic quenching. If the emissive lifetimes are much shorter, < 1 ns, dynamic quenching is no longer feasible, but static quenching is observed. In static quenching processes, the quencher Q and the fluorophore form a ground state complex, and upon excitation, the preformed complex is efficiently quenched. In the case of PPEs, the emissive lifetimes range from 150-400 ps.[17] *As a consequence, collisional quenching processes are present, but their contribution is negligible in the fluorescence quenching of PPEs.*

The Stern-Volmer formalism furnishes binding constants between fluorophore and quencher in cases that involve only static quenching. The slope of the Stern-Volmer plot, the Stern-Volmer constant, represents the binding constant between quencher and fluorophore. However, if there are multiple quenching mechanisms, the Stern-Volmer formalism is less straightforward and data analysis yields S-V plots that are non-linear in appearance and also dependent upon the concentration of the conjugated polymeric fluorophore. In most cases, upward curves result, and the apparent Stern-Volmer constants plummet upon increase of the concentration of the conjugated polymer.[18-20]

In the case of the interaction of sugar-coated conjugated polymers with Con A an unusual behavior is observed in that the slope of the classic Stern-Volmer plot is very

steep at low [Q] and levels off at higher quencher concentrations, indicating the presence of two binding mechanisms. In addition, we observe that K_{sv} increases upon increasing polymer concentration in the interaction of a negatively charged mannose-substituted PPE with Con A. Such behavior is not reported in the literature; we therefore use a modified version of the Stern-Volmer equation which addresses the issue of multiple quenching pathways.[21]

$$F_{[Q]}/F_o = \Sigma_i f_i/(1 + K_{SVi}[Q]) \qquad \textbf{Eq. 4.2}$$

Such kinetics are provided by Equation 2, where f_i, i = 1,2,3… represents the relative fractions of each quenching mechanism ($\Sigma_i f_i = 1.0$) and K_{SVi}, I = 1,2,3… are the respective Stern-Volmer constants.[22]

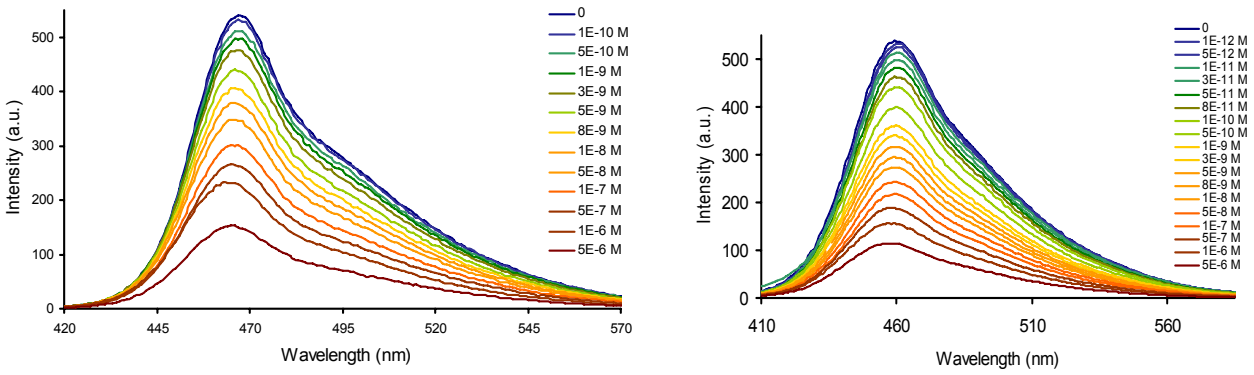

Figure 4.1. Emission spectra of **4.5** (left) and **4.7** (right) with increasing concentrations of Con A.

Known concentrations of Con A were added to solutions of **P5** and **P7** (0.5 μM in phosphate buffered saline) resulting in protein concentrations ranging from the pico- to micromolar range. After each addition of Con A, the fluorescence quenching was

monitored by fluorescence spectroscopy (Figure 4.1) and represented in F/F_o terms (see Figure 2). Using the quenching data from Figure 4.1 and the two-parameter version of Equation 4.2, we determined by least-squares analysis two equilibrium constants.

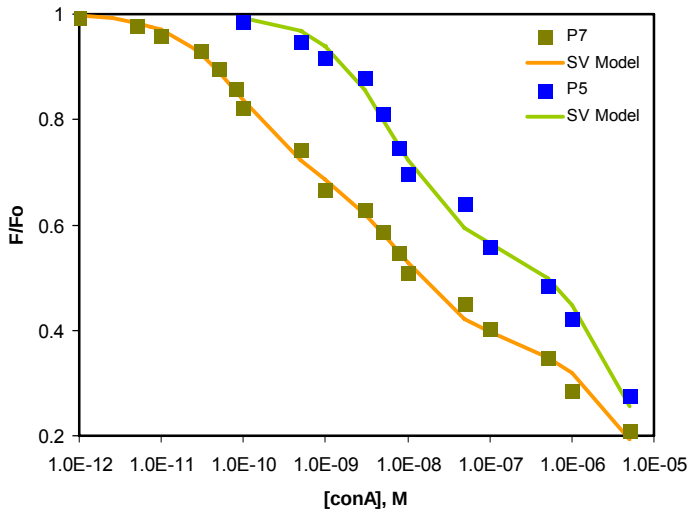

Figure 4.2. Stern-Volmer plot of emission data obtained from quenching experiments of polymers **4.5** and **4.7** with Con A. K_{SV1} and K_{SV2} are obtained from fit of quenching data to Eq. 4.2.

From the analysis, we obtained a K_{SV1} for **4.5** and **4.7** of 1.6 x 10^8 and 3.2 x 10^9 M^{-1} and a K_{SV2} of 2.3 x 10^5 and 6.9 x 10^5 M^{-1} with the contribution of each quenching process remaining constant. A better fit was obtained for **4.5**, however, than for **4.7** (not shown). The tri-mannose functionality of **4.7** may lead to additional quenching mechanisms that may cause it to deviate from this two-complex Stern-Volmer equation (Eq. 4.2). Thus we used the three parameter fit of Equation 4.2 for **4.7**, From this fit, we obtained K_{SV1} of 1.1 x 10^{10} M^{-1}, a K_{SV2} of 1.1 x 10^8 M^{-1} and a K_{SV3} of 1.9 x 10^5. M^{-1}. Polymer **4.7** contains the tri-mannose functionality and exhibits a greater affinity for Con A than the mannose-functionalized **4.5**, which is reflected by its larger K_{SV} constants and

lower limit of detection. This behavior would be expected as the trimannose ligand in **4.7** is specific for lectins that display a mannose binding site.

To get a better understanding for the association processes that occur and to quantitatively determine the binding constant, reaction stoichiometry, and thermodynamic profile for the interaction of **4.5** and **4.7** with Con A, isothermal titration calorimetry (ITC) was used. ITC measures the heat change of a system upon complex formation and provides a thermodynamic profile of the complexation. Since an analyte is titrated into a solution which contains a binding receptor (or receptor into a solution of analyte), K_a and the reaction stoichiometry can be directly obtained.[23] ITC gives a detailed picture of the binding events.

For each titration, the polymer (1 mM in PBS buffer) was injected into a Con A solution (0.040 mM in PBS buffer). As a control, identical samples of each polymer were injected into a PBS buffer solution containing no protein. As expected, the heats of dilution were negligible. The titration data was fitted to a theoretical titration curve using software which was provided by Microcal (One Site Model). The binding constant and thermodynamic parameters were calculated using the equation,

$$\Delta G = \Delta H - T\Delta S = -\mathrm{RT}\ \ln K_a \qquad \textbf{Eq. 3}$$

where ΔG, ΔH, and ΔS are the changes in free energy, enthalpy, and entropy, T is the absolute temperature (298 K), R = 1.98 cal/mol*K, and $K_\mathbf{a}$ is the binding constant.

From the titrations (Figure 4.3), the association constants for **4.5** and **4.7** are 1.0 x 10^5 M^{-1} and 1.6 x 10^6 M^{-1}, respectively. **4.5**, which contained the mannose functionality, exhibited a strong enthalpic contribution (Figure 4.3, left), while **4.7** exhibited a strong entropic contribution (Figure 4.3, right), which is most likely due to desolvation effects.

Desolvation effects are not atypical for rigid ligands and have been observed by Brewer *et al*.[24] As expected, a stronger binding interaction between **4.7** and Con A is observed due to the presence of the tri-mannose functionality.

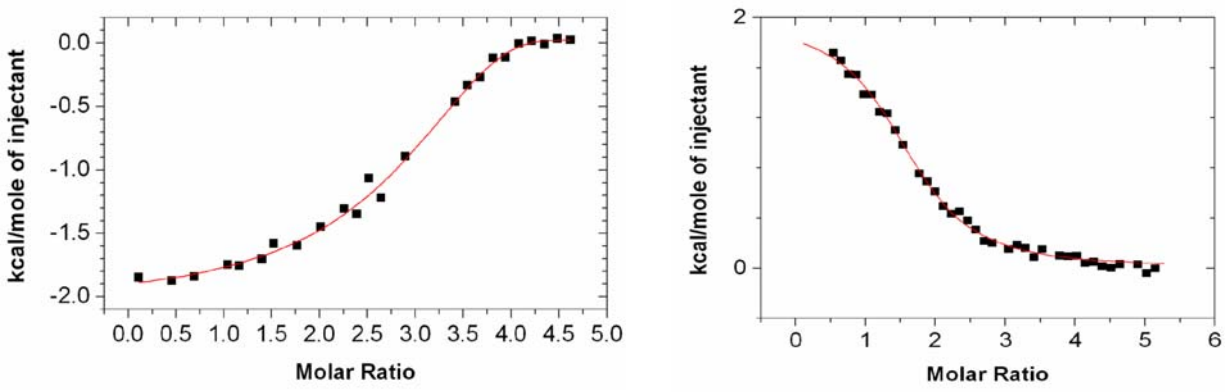

Figure 4.3. Titration study of **4.5** (left) and **4.7** (right) with Con A. For each titration, 6 µL of polymer (1 mM in PBS) was injected from a 300 µL syringe at an interval of 5 min into a ConA solution (0.040 mM in PBS) while stirring at 310 rpm.

Figure 4.4 displays a model that reconciles the large apparent differences between the binding constants obtained from the quenching and the ITC experiments. The quenching experiments are performed in the presence of a large excess of the conjugated polymer. As a consequence, a non-fluorescent, self-quenched 2:1 complex arises. This complex is itself an efficient quencher, extinguishing the fluorescence of further polymer chains that are spatially adjacent to the quencher complex. As a consequence, the K_{SV1} values do not represent binding constants, but are better understood as a quenching volume and represent a colligative property of an ensemble. Leclerc described hyperefficient energy transfer from an ensemble of conjugated polymers to a fluorophore-substituted DNA strand, resulting in a similar occurrence of unexpectedly enhanced sensitivity.[25]

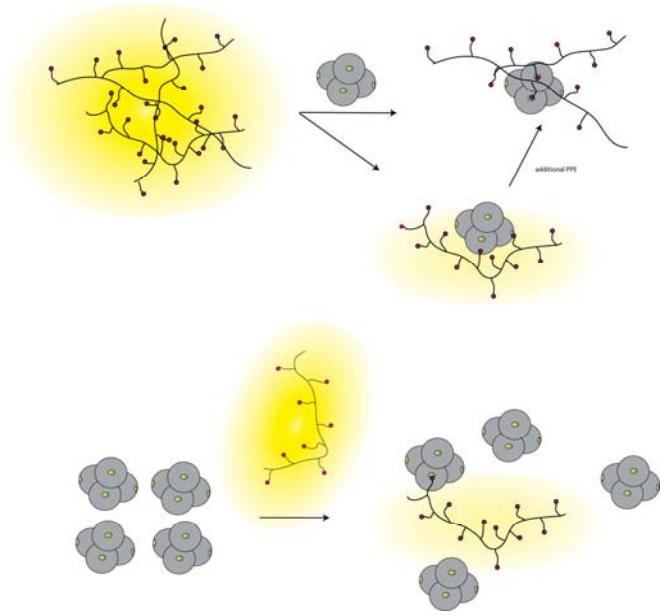

Figure 4.4. Quenching of the fluorescence of **4.5** and **4.7** by Con A in the regimen of high PPE concentration (as observed by the quenching experiments, Top) and at high Con A concentration (as observed in the ITC experiments, Bottom)

On the other hand, the K_{SV2} values are similar to the binding constants K_a obtained by ITC experiments, in which the polymer was added to Con A. In this case, a 1 : 1 complex will form. In this interpretation, K_a and K_{SV2} or K_{SV3} are binding constants, while K_{SV1} indicates a *quenching volume* similar to that obtained by the Perrin[26] model; K_{SV1} therefore would not be a binding constant but an enhancement or amplification factor, describing the ability of the polymer solution to be quenched by a preformed PPE-ConA complex. The increase in the overall K_{sv} with increasing polymer concentration supports this hypothesis. The sensitivity enhancements observed are beyond the association constants obtained from ITC and make functionalized conjugated polymers a powerful tool in potential bioanalytical applications. In conjugated polymers it appears

that not only molecular wire and polyvalency effects operate, but hyper-efficient energy transfer effects can be engineered to increase their sensitivity towards quenching analytes. Having successfully examined the binding of **4.5** and **4.7** with Con A, we decided to investigate their interaction with *E. coli* (strains ORN 178 and ORN 208), which are mannose binding and mutant mannose non-binding strains respectively.[27] We were interested to see if the enhanced binding of **4.7** over **4.5** to Con A would lead to visual differences in their agglutination of the mannose binding *E. coli* strain ORN 178. The strain ORN 208, which has lost its ability to bind to mannose was chosen as a control. Addition of either **4.5** or **4.7** to ORN 208 leads to staining of the bacteria, but not to any agglutination (Figure 4.5). The staining itself is of interest and must be attributed to hydrophobic interactions between the aromatic backbone of the PPE and phenyl rings of aromatic amino acids on the cell wall of the bacteria that are exposed towards the surface. Electrostatic effects are weak or absent, as these polymers are non-charged. However, when **4.5** or **4.7** is exposed to ORN 178 (Figure 4.6) agglutination of the bacteria is observed.

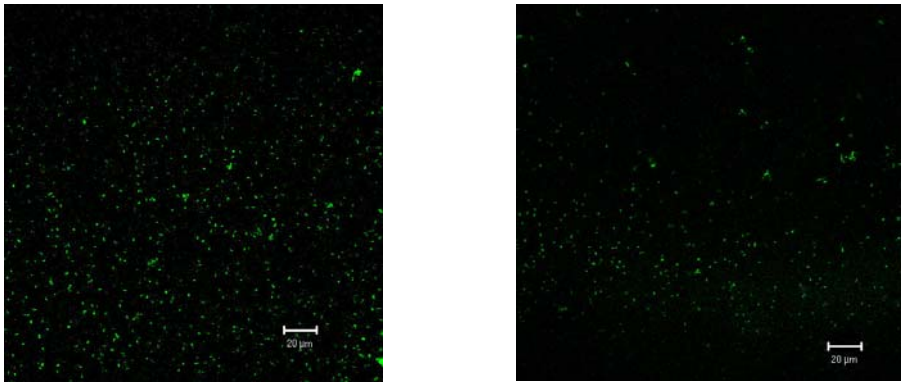

Figure 4.5. Confocal microscopy image of **4.5** with ORN 208 (left) and **4.7** with ORN 208 (right). Bacterial cells were grown in LB medium (10 mL) at 37 ºC for 16 h to an optical density of 1.0 at 600 nm. No considerable binding or aggregation is observed.

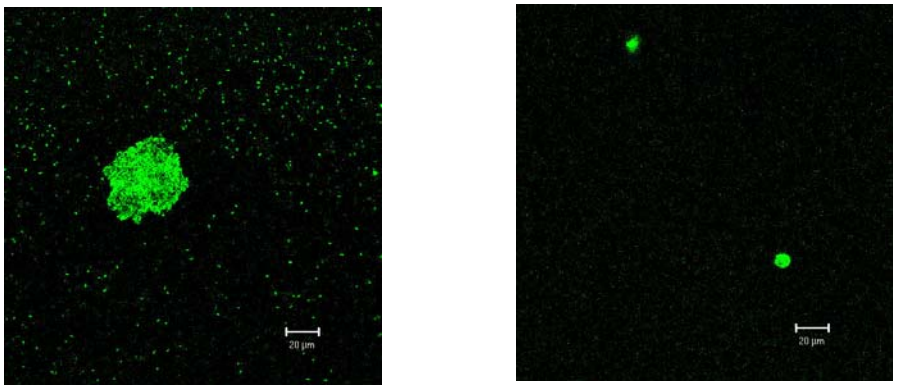

Figure 4.6. Confocal microscopy image of **4.5** with ORN 178 (left) and **4.7** with ORN 178 (right). Bacterial cells were grown in LB medium (10 mL) at 37 ºC for 16 h to an optical density of 1.0 at 600 nm.

In the case of **4.5** loose aggregates interspersed with single, planktonic cells form, while in the case of **4.7** the planktonic bacterial cells have disappeared and instead only dense, fluorescent clusters of bacteria remain. It is remarkable that the increased binding constant of **4.7** to Con A is mirrored in the enhanced agglutination of the mannose-binding *E. coli*. It suggests that the mannose binding epitopes on their pili are similar to the mannose-binding receptors of Con A.

4.3 Conclusion

In conclusion, we report the synthesis of two sugar-substituted PPEs, **4.5** and **4.7**, with high sensitivity towards Con A. Increased sensitivity to sugar binding domains results if either the glyco-substituent is placed further away from the conjugated backbone or if more complex sugars are incorporated into the system, reflected in an increased propensity to induce aggregation in *E. coli* when employing **4.7**. To quantitatively determine the binding constant of the lectin-sugar interactions, we

employed ITC, and a two- or three-component Stern-Volmer equation. Due to the ease of post-functionalization of our PPEs, this fluorescence based detection system, which exhibits excellent sensitivity towards lectins and bacteria, should easily be adapted towards other analytes and pathogens.

4.4 Experimental

Instrumentation and Materials. All chemicals and solvents were purchased from commercial sources and were used without further purification unless otherwise specified. Column chromatography was performed using Standard Grade silica gel 60 Å, 32-63 μm (Sorbent Technologies) and the specified eluent. All IR spectra were obtained using a Shimadzu FTIR-8400s spectrometer. ^{1}H NMR spectra were recorded at 298 K on a 300, 400, 500, or 600 MHz spectrometer. Chemical shifts are reported in parts per million (ppm), using residual solvent (chloroform-*d*) as an internal standard. The data is reported as follows: chemical shift, multiplicity (s = singlet, d = doublet, t = triplet, q = quartet, m = multiplet, dd = doublet of doublets, ddd = doublet of doublet of doublets, br = broad), and integration. For Tri-Mannoside Monomer **4.6**, ^{1}H NMR data are reported as though they are first order, and the peak assignments were made on the basis of 2D-NMR (^{1}H–^{1}H COSY and HMQC) experiments. The α-stereochemistry of the mannopyranosyl residues in **4.20** and **4.6** was established through the measurement of the $^{1}J_{C1,H1}$. ^{13}C HMR spectra were recorded at 100, 125, 300, 400, or 500 MHz, and ^{13}C chemical shifts (δ) are referenced to residual $CHCl_3$ at 77.23 ppm. All absorption spectra were collected using a Shimadzu UV-2401PC spectrophotometer. All emission spectra were acquired using a Shimadzu RF-5301PC spectrofluorophotometer. Quantum yields

for the polymers were measured using standard procedures.[33] In all cases, quinine sulfate and 2-aminopyridine were used as standards and all solutions were purged with nitrogen prior to measurement. Confocal microscopy images were taken with a Zeiss LSM 510 confocal microscope. ESI-MS spectra were recorded on samples suspended in THF or CH_3OH and added NaCl. Optical rotations were measured at 22 ± 2 °C at the sodium D line (589 nm) and are in units of deg·mL(dm·g)$^{-1}$.

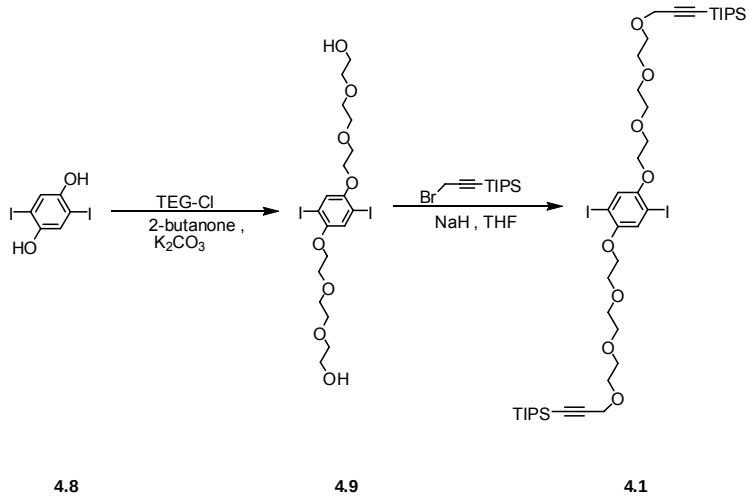

Scheme 4.3. Synthesis of **4.1**

Synthesis of 4.9: 1,4-Dihydroxy-2,5-diiodobenzene (**4.8**) (10.1 g, 0.0276 mol) was dissolved in 2-butanone (150 mL) and the resulting solution was added slowly to a stirred suspension of K_2CO_3 (30.6 g, 0.221 mol) in 2-butanone (75mL) under N_2. The reaction mixture was allowed to stir for 5-10 min followed by the slow addition of TEG-Cl (0.111 mol, 16.1 mL). The reaction was heated to 75ºC for 7 days. The solution was cooled to room temperature, the solvent was removed, and the resulting slurry was re-dissolved in

CH_2Cl_2. The solution was extracted with water to remove excess K_2CO_3 and the organic fractions were collected and concentrated in vacuo until an oily residue remained. The solution was purified by silica gel chromatography (95:5 EtOAc / MeOH). The product was a flaky colorless solid (13.5 g, 21.6 mmol, 78.8%). ^{1}H NMR (300 MHz, $CDCl_3$): δ 7.21 (s, 2H), 4.11 (t, 4H), 3.85 (t, 4H), 3.79 (t, 4H), 3.72 (t, 4H), 3.66 (t, 4H) 3.57 (t, 4H). ^{13}C NMR (300 MHz, $CDCl_3$): δ 152.94, 123.32, 86.32, 72.44, 71.09, 70.40, 70.14, 69.50, 61.66. IR (KBR, cm^{-1}): v 3423, 2937, 2892, 1487, 1464, 1353, 1325, 1232, 1215, 1125, 1119, 1084, 1062, 1033, 886, 857, 829, 799.

Synthesis of 4.1: Compound **4.9** (4.50 g, 7.20 mmol) was dissolved in dry THF (200 mL). NaH (3 eq., 0.517 g, 21.6 mmol) was added and the solution was stirred under N_2 for 30 min. After all H_2 had ceased, Tipspropargylbromide (2.1 eq., 4.16 g, 15.1 mmol) was added and the reaction was stirred under N_2 at room temperature overnight. The resulting salts were filtered out, the solvent was removed, and the product was purified using silica gel chromatography (1:3 EtOAc / Hexane). The resulting product was a light yellow oil (4.01 g, 3.90 mmol, 55.0 %). ^{1}H NMR (300 MHz, $CDCl_3$): δ 7.18 (s, 2H), 4.18 (s, 4H), 4.04 (t, 4H), 3.82 (t, 4H), 3.73 (t, 4H), 3.67-3.62 (m, 12H), 1.03 (s, 42H). ^{13}C NMR (300 MHz, $CDCl_3$): δ 152.91, 123.24, 103.13, 87.40, 86.25, 70.98, 70.55, 70.32, 70.11, 69.44, 68.55, 58.98. IR (cm^{-1}): v 3017.42, 2944.13, 2891.10, 2170.73, 1462.91, 1449.41, 1348.15, 1215.07, 1096.46, 1032.81, 998.09, 927.70, 883.34, 769.54.

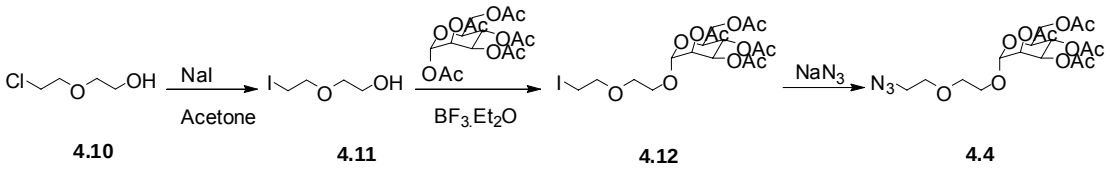

Scheme 4.4. Synthesis of **4.4**

Synthesis of 4.11: 2-(2-chloroethoxy)ethanol (**4.10**) (24.9 g, 0.200 mol), sodium iodide (150 g, 1.0 mol), and acetone (200 mL) were placed in a 500 mL round bottom flask and heated to reflux for 24 h. After cooling, the solvent was evaporated and the slurry was taken up in the minimum amount of water and extracted with Et_2O (3×100 mL). The organic layers were dried ($MgSO_4$), filtered, and evaporated to dryness to give the product (38.4 g, 89 % yield) The product was used in the next step without further purification. ^{1}H NMR (300 MHz, $CDCl_3$): δ 3.76 – 3.51 (m, 6H), 3.21 (t, 2H), 2.63 (s, 1H)

Synthesis of 4.12: 2-(2-iodoethoxy)ethanol (**4.11**) (1.94 g, 9.00 mmol), mannose pentaacetate (1.17 g, 3.00 mmol), and dichloromethane (25 mL) were placed in a 100 mL round bottom flask. BF_3-Et_2O (1.1 mL, 9 mmol) was then added slowly. The reaction mixture was stirred at room temperature for 48 h and then poured into 5% aqueous $NaHCO_3$ (50 mL). The organic layer was separated, washed with 5% aqueous $NaHCO_3$ and water. The organic phase was dried over $MgSO_4$ and evaporated to dryness. The product was isolated by column chromatography (EtOAc/hexane 1:1) as an oil (672 mg, 41 %). ^{1}H NMR (400 MHz, $CDCl_3$): δ 5.35 (dd, 1H), 5.26 (m, 2H), 4.88 (d, 1H), 4.29 (q, 1H), 4.08 (m, 2H), 3.81 (m, 1H), 3.75 (t, 2H), 3.66 (m, 3H), 3.25 (t, 2H), 2.14 (s, 3H), 2.09 (s, 3H), 2.02 (s, 3H), 1.97 (s, 3H). ^{13}C NMR (400 MHz, $CDCl_3$): δ 170.94, 170.31, 170.16, 170.01, 97.89, 72.04, 69.89, 69.78, 69.31, 68.65, 67.33, 66.39, 62.71, 21.18, 20.97, 2.89. IR: *v* 3018.39, 2928.71, 1747.39, 1428.19, 1369.37, 1216.03, 1136.96, 1085.85, 1049.20, 979.77, 757.07.

Synthesis of 4.4: Compound **4.12** (1.17 g, 2.13 mmol), sodium azide (693 mg, 10.7 mmol), and N,N-dimethyl formamide (10 mL) were placed in a 25 mL round bottom

flask and the reaction mixture was stirred at room temperature for 24 h. After cooling, the slurry was taken up in the minimum amount of water and extracted with Et_2O (3×100 mL). The organic layers were dried ($MgSO_4$), filtered, and evaporated to dryness to yield the product. The crude product was purified by column chromatography using EtOAc-Hexane (1:1) mixture which resulted in an oil (747 mg, 76 %). ^{1}H NMR (400 MHz, $CDCl_3$): δ 5.35 – 5.27 (m, 3H), 4.87 (s, 1H), 4.26 (q, 1H), 4.08 (m, 2H), 3.83 (m, 1H), 3.66 (m, 5H), 3.39 (t, 3H), 2.94 (s, 1H), 2.87 (s, 1H), 2.14 (s, 3H), 2.09 (s, 3H), 2.02 (s, 3H), 1.97 (s, 3H). ^{13}C NMR (400 MHz, $CDCl_3$): δ 170.92, 170.30, 170.16, 169.99, 97.96, 70.42, 70.28, 69.74, 69.30, 68.64, 67.53, 66.33, 62.65, 50.96, 21.12, 20.94. IR: *v* 3019.35, 2930.63, 2877.60, 2112.87, 1747.39, 1672.17, 1436.87, 1369.37, 1216.03, 1136.96, 1085.85, 1050.17, 979.77, 752.19.

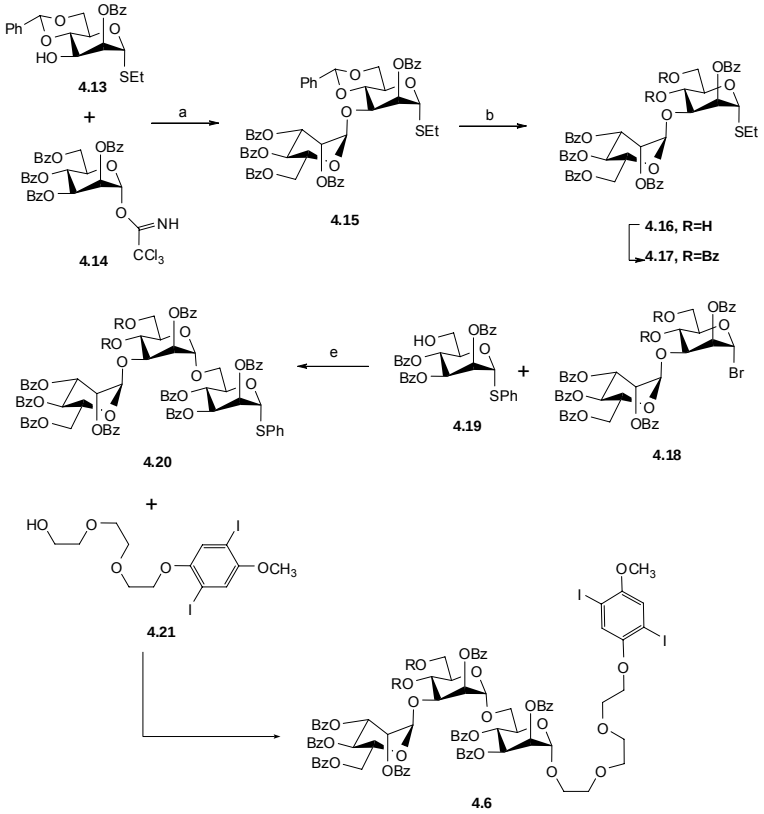

Scheme 4.5. Synthesis of **4.6**

Synthesis of 4.15: Donor **4.13**[28] (1.60 g, 2.15 mmol), acceptor **4.14**[29] (745 mg, 1.79 mmol), and 4 Å MS (0.5 g) were dried for 16 h under vacuum over P_2O_5. To this mixture in CH_2Cl_2 (20 mL) was added TMSOTf (10 μL, 0.54 mmol) at -30 °C. After stirring for 6 h at -30 °C, a few drops of Et_3N was added and the reaction mixture was filtered through Celite and concentrated to give a crude residue that was purified by chromatography (9:1, toluene:EtOAc) to give **4.15** (1.58 g, 89%) as a white foam. R_f 0.32 (9:1, toluene:EtOAc); $[\alpha]_D$ – 47.5 (*c* 0.9, CH_2Cl_2); ^{1}H NMR (400 MHz, $CDCl_3$) δ 8.28-8.25 (m, 2 H, Ar), 8.15-8.11 (m, 2 H, Ar), 8.01-7.97 (m, 2 H, Ar), 7.90-7.86 (m, 2 H, Ar), 7.78-7.75 (m, 2 H, Ar), 7.68-7.63 (m, 1 H, Ar), 7.60-7.46 (m, 7 H, Ar), 7.42-7.20 (m, 12 H, Ar), 6.03 (dd, 1 H, *J* = 10.0, 10.0 Hz, H-4'), 5.80-5.72 (m, 4 H, H-2, H-2', H-3', Benzylidene CH), 5.51 (d, 1 H, *J* = 1.7 Hz, H-1), 5.49 (d, 1 H, *J* = 1.1 Hz, H-1'), 4.66 (dd, 1 H, *J* = 12.2, 2.3 Hz, H-6'a), 4.58 (ddd, 1 H, *J* = 10.0, 4.5, 2.3 Hz, H-5'), 4.51 (dd, 1 H, *J* = 9.4, 3.6 Hz, H-3), 4.45 (dd, 1 H, *J* = 12.2, 4.5 Hz, H-6'b), 4.40–4.29 (m, 3 H, H-5, H-4, H-6a), 3.95 (dd, 1 H, *J* = 9.6, 9.4 Hz, H-6b), 2.75-2.59 (m, 2 H, SCH_2), 1.31 (dd, 3 H, *J* = 7.4, 7.4 Hz, CH_3); ^{13}C NMR (100 MHz, $CDCl_3$) δ 166.09 (C=O), 166.03 (C=O), 165.17 (C=O), 164.97 (C=O), 164.87 (C=O), 136.83 (Ar), 133.44 (Ar), 133.19 (Ar), 133.17 (Ar), 132.85 (Ar), 132.78 (Ar), 129.97 (Ar × 2), 129.82 (Ar × 3), 129.73 (Ar × 2), 129.67 (Ar × 2), 129.53 (Ar × 2), 129.50 (Ar), 129.22 (Ar), 129.11 (Ar), 128.94 (Ar), 128.64 (Ar), 128.59 (Ar × 2), 128.39 (Ar × 2), 128.23 (Ar × 4), 128.09 (Ar × 2), 128.01 (Ar × 2), 125.86 (Ar × 2), 101.29 (benzylidene C), 98.68 (C-1'), 83.34 (C-1), 79.12 (C-4), 73.87 (C-2), 72.95 (C-3), 69.83 (C-2'), 69.68 (C-3'), 69.35 (C-5'), 68.39 (C-6), 66.51 (C-4'), 64.26 (C-5), 62.87 (C-6'), 25.52 (SCH_2), 14.80 (CH_3); HRMS (ESI) calcd. for (M + Na) $C_{56}H_{50}O_{15}SNa$: 1017.2763, found: 1017.2766.

Synthesis of 4.16: A solution of **4.15** (1.72 g, 1.73 mmol) in a mixture of AcOH (60 mL) and H_2O (11 mL) was stirred for 4.5 h at 50 °C. The reaction mixture was then concentrated and purified by chromatography (4:1, toluene:EtOAc) to give **4.16** (1.38 g, 88%) as a white foam. R_f 0.27 (5:1, toluene:EtOAc); $[\alpha]_D$ –17.1 (*c* 2.3, CH_2Cl_2); ^{1}H NMR (400 MHz, $CDCl_3$) δ 8.22-8.19 (m, 2 H, Ar), 8.12-8.09 (m, 2 H, Ar), 8.00-7.96 (m, 2 H, Ar), 7.83-7.79 (m, 2 H, Ar), 7.72-7.68 (m, 2 H, Ar), 7.60-7.23 (m, 15 H, Ar), 6.08 (dd, 1 H, *J* = 10.1, 10.0 Hz, H-4'), 5.81 (dd, 1 H, *J* = 3.2, 2.0 Hz, H-2'), 5.73 (dd, 1 H, *J* = 10.1, 3.2 Hz, H-3'), 5.66 (dd, 1 H, *J* = 3.4, 1.5 Hz, H-2), 5.50 (br s, 2 H, H-1, H-1'), 4.58 (dd, 1 H, *J* = 12.3, 2.5 Hz, H-6'a), 4.46–4.39 (m, 2 H, H-5', H-4), 4.33 (dd, 1 H, *J* = 12.3, 3.8 Hz, H-6'b), 4.26 (dd, 1 H, *J* = 9.4, 3.4 Hz, H-3), 4.18 (ddd, 1 H, *J* = 9.6, 3.6, 3.6 Hz, H-5), 4.08-3.96 (m, 2 H, H-6a, H-6b), 3.63 (br s, 1 H, OH), 2.75-2.59 (m, 2 H, SCH_2), 2.47 (br s, 1 H, OH), 1.31 (dd, 3 H, *J* = 7.4, 7.4 Hz, CH_3); ^{13}C NMR (100 MHz, $CDCl_3$) δ 165.97 (C=O), 165.89 (C=O), 165.53 (C=O), 165.26 (C=O), 164.91 (C=O), 133.39 (Ar), 133.32 (Ar), 133.15 (Ar), 133.07 (Ar), 132.76 (Ar), 129.81 (Ar × 2), 129.80 (Ar), 129.73 (Ar × 2), 129.69 (Ar × 2), 129.60 (Ar × 2), 129.57 (Ar × 2), 129.42 (Ar), 128.98 (Ar), 128.84 (Ar), 128.78 (Ar), 128.60 (Ar × 2), 128.40 (Ar × 2), 128.23 (Ar × 2), 128.17 (Ar × 2), 128.15 (Ar × 2), 99.56 (C-1'), 82.19 (C-1), 79.40 (C-3), 73.92 (C-2), 72.47 (C-5), 70.13 (C-3'), 69.96 (C-2'), 69.47 (C-4), 67.33 (C-5'), 66.05 (C-4'), 62.45 (C-6'), 62.10 (C-6), 25.54 (SCH_2), 14.71 (CH_3); HRMS (ESI) calcd. for (M + Na) $C_{49}H_{46}O_{15}SNa$: 929.2449, found: 929.2451.

Synthesis of 4.17: To a solution of compound **4.16** (1.49 g, 1.65 mmol) in pyridine (25 mL) was added benzoyl chloride (0.83 mL, 6.6 mmol) at 0 °C, and the reaction mixture was stirred at 50 °C for 48 h. The reaction was quenched by the addition of a few drops

of H_2O at 0 °C and then the solution was concentrated. The residue was re-dissolved in CH_2Cl_2 (50 mL) and the resulting solution was washed with a saturated $NaHCO_3$ solution (50 mL) and then brine (30 mL). The organic layer was dried (Na_2SO_4) and concentrated; chromatography of the residue (3:1, hexane:EtOAc) gave **4.17** (1.75 g, 95%) as a white foam. R_f 0.33 (3:1, hexanes:EtOAc); $[\alpha]_D$ – 44.6 (*c* 0.7, CH_2Cl_2); ^{1}H NMR (400 MHz, $CDCl_3$) δ 8.26-8.20 (m, 2 H, Ar), 8.14-8.07 (m, 6 H, Ar), 7.87-7.84 (m, 2 H, Ar), 7.79-7.75 (m, 2 H, Ar), 7.73-7.69 (m, 2 H, Ar), 7.66-7.62 (m, 1 H, Ar), 7.58-7.27 (m, 18 H, Ar), 7.22-7.17 (m, 2 H, Ar), 6.08 (dd, 1 H, *J* = 9.0, 9.0 Hz, H-4), 6.00 (dd, 1 H, *J* = 10.1, 10.1 Hz, H-4'), 5.78 (dd, 1 H, *J* = 3.4, 1.5 Hz, H-2), 5.71 (dd, 1 H, *J* = 10.1, 2.5 Hz, H-3'), 5.57 (d, 1 H, *J* = 1.5 Hz, H-1), 5.36-5.33 (m, 2 H, H-1', H-2'), 4.74-4.67 (m, 2 H, H-5, H-6a), 4.60-4.46 (m, 4 H, H-5', H-6b, H-6'a, H-3), 4.35 (dd, 1 H, *J* = 12.3, 3.4 Hz, H-6'b), 2.77-2.62 (m, 2 H, SCH_2), 1.31 (dd, 3 H, *J* = 7.5, 7.5 Hz, CH_3); ^{13}C NMR (100 MHz, $CDCl_3$) δ 166.07 (C=O), 165.98 (C=O), 165.81 (C=O), 165.29 (C=O), 165.06 (C=O), 164.60 (C=O), 164.56 (C=O), 133.52 (Ar), 133.23 (Ar), 133.19 (Ar × 2), 132.90 (Ar), 132.79 (Ar × 2), 129.94 (Ar × 4), 129.81 (Ar × 2), 129.75 (Ar × 2), 129.65 (Ar × 3), 129.55 (Ar × 2), 129.50 (Ar × 2), 129.21 (Ar), 129.02 (Ar × 2), 128.94 (Ar), 128.80 (Ar), 128.71 (Ar × 2), 128.32 (Ar × 4), 128.30 (Ar × 3), 128.23 (Ar × 2), 128.19 (Ar × 2), 128.03 (Ar × 2), 99.36 (C-1'), 82.20 (C-1), 76.64 (C-3), 73.40 (C-2), 70.06 (C-2'), 69.65 (C-5), 69.27 (C-5'), 69.19 (C-3'), 68.58 (C-4), 66.32 (C-4'), 62.87 (C-6), 62.51 (C-6'), 25.61 (SCH_2), 14.75 (CH_3); HRMS (ESI) calcd. for (M + Na) $C_{63}H_{54}O_{17}SNa$: 1137.2974, found: 1137.2973.

Synthesis of 4.18[30]**:** Compound **4.17** (1.18 g, 1.06 mmol) and 4 Å MS (0.5 g) were dried for 16 h under vacuum over P_2O_5 before being suspended in CH_2Cl_2 (20 mL). The

mixture was stirred for 30 min, followed by the addition of a solution of Br_2 (65 μL, 1.26 mmol) in CH_2Cl_2 (2.5 mL) at r.t. The reaction mixture was stirred for 4.5 h, while being shielded from light. Cyclohexene was then added dropwise until the yellow color disappeared. The crude NMR spectra indicated the full conversion of the thioglycoside to glycosyl bromide **4.18**. R_f 0.38 (2:1, hexanes:EtOAc); $[\alpha]_D$ –31.1 (*c* 0.7, CH_2Cl_2); ^{1}H NMR (600 MHz, $CDCl_3$) δ 8.21-8.19 (m, 2 H, Ar), 8.14-8.11 (m, 4 H, Ar), 8.10-8.07 (m, 2 H, Ar), 7.87-7.84 (m, 2 H, Ar), 7.78-7.75 (m, 2 H, Ar), 7.73-7.70 (m, 2 H, Ar), 7.68-7.65 (m, 1 H, Ar), 7.60-7.53 (m, 3 H, Ar), 7.51-7.47 (m, 4 H, Ar), 7.45-7.36 (m, 7 H, Ar), 7.35-7.29 (m, 4 H, Ar), 7.23-7.19 (m, 2 H, Ar), 6.61 (d, 1 H, *J* = 1.4 Hz, H-1), 6.16 (dd, 1 H, *J* = 10.0, 10.0 Hz, H-4), 5.99 (dd, 1 H, *J* = 10.1, 10.0 Hz, H-4'), 5.88 (dd, 1 H, *J* = 3.3, 1.4 Hz, H-2), 5.69 (dd, 1 H, *J* = 10.1, 3.2 Hz, H-3'), 5.39 (d, 1 H, *J* = 1.8 Hz, H-1'), 5.35 (dd, 1 H, *J* = 3.2, 1.8 Hz, H-2'), 5.06 (dd, 1 H, *J* = 10.0, 3.3 Hz, H-3), 4.76 (dd, 1 H, *J* = 12.4, 2.3 Hz, H-6a), 4.54 (dd, 1 H, *J* = 12.3, 2.5 Hz, H-6'a), 4.55-4.51 (m, 1 H, H-5), 4.49 (dd, 1 H, *J* = 12.4, 3.0 Hz, H-6b), 4.44 (ddd, 1 H, *J* = 10.0, 4.0, 2.5 Hz, H-5'), 4.36 (dd, 1 H, *J* = 12.3, 4.0 Hz, H-6'b); ^{13}C NMR (125 MHz, $CDCl_3$) δ 166.08 (C=O), 165.99 (C=O), 165.56 (C=O), 165.19 (C=O), 165.14 (C=O), 164.72 (C=O), 164.68 (C=O), 133.90 (Ar), 133.51 (Ar), 133.33 (Ar), 133.29 (Ar), 133.12 (Ar), 132.97 (Ar), 132.93 (Ar), 130.09 (Ar × 3), 129.84 (Ar × 3), 129.83 (Ar × 2), 129.77 (Ar × 2), 129.69 (Ar × 2), 129.66 (Ar × 2), 129.62 (Ar × 2), 129.10 (Ar), 129.07 (Ar), 128.91 (Ar × 2), 128.87 (Ar), 128.75 (Ar), 128.71 (Ar), 128.47 (Ar × 3), 128.45 (Ar × 3), 128.38 (Ar × 2), 128.29 (Ar × 2), 128.15 (Ar × 2), 99.58 (C-1', $^1J_{C\text{-}H}$ = 173 Hz), 83.94 (C-1), 75.08 (C-3), 74.31 (C-2), 73.23 (C-5), 70.09 (C-2'), 69.93 (C-5'), 69.19 (C-3'), 67.50 (C-4), 66.38 (C-4'), 62.60

(C-6'), 61.81 (C-6); HRMS (ESI) calcd. for (M + Na) $C_{61}H_{49}O_{17}BrNa$: 1155.2051, found: 1155.2055.

Synthesis of 4.20: The crude reaction solution of **4.18** (above) was diluted by adding CH_2Cl_2 (15 mL) and then **4.19**[31] (741 mg, 1.27 mmol) was added. After the mixture was cooled to -20 °C, AgOTf (656 mg, 2.54 mmol) was added and the reaction was stirred 1.5 h at -20 °C before it was neutralized by the dropwise addition of Et_3N. The resulting solution was diluted with CH_2Cl_2 (15 mL) and filtered through Celite. The filtrate was washed with a sat. aq. $NaHCO_3$ soln. (30 mL), dried (Na_2SO_4), and concentrated to give a crude residue that was purified by chromatography (2:1, hexanes:EtOAc) to give **4.20** (1.40 g, 81% over 2 steps) as a white foam. R_f 0.24 (2:1, hexanes:EtOAc); $[\alpha]_D$ -31.9 (*c* 1.1, CH_2Cl_2). ^{1}H NMR (500 MHz, $CDCl_3$) δ 8.21-8.17 (m, 4 H, Ar), 8.06-8.01 (m, 8 H, Ar), 7.94-7.91 (m, 2 H, Ar), 7.88-7.85 (m, 2 H, Ar), 7.74-7.71 (m, 2 H, Ar), 7.68-7.15 (m, 37 H, Ar), 6.10-6.01 (m, 3 H, H-4', H-4, H-4"), 5.99 (dd, 1 H, *J* = 3.2, 1.2 Hz, H-2), 5.88 (dd, 1 H, *J* = 10.1, 3.2 Hz, H-3), 5.81 (d, 1 H, *J* = 1.2 Hz, H-1), 5.73–5.68 (m, 2 H, H-2', H-3"), 5.40–5.37 (m, 1 H, H-2"), 5.21 (d, 1 H, *J* = 1.6 Hz, H-1"), 5.14 (s, 1 H, H-1'), 4.87 (ddd, 1 H, *J* = 10.0, 5.6, 2.0 Hz, H-5), 4.56 (dd, 1 H, *J* = 9.8, 3.3 Hz, H-3'), 4.51 (dd, 1 H, *J* = 12.2, 2.2 Hz, H-6'a), 4.49 (dd, 1 H, *J* = 12.4, 2.4 Hz, H-6"a), 4.36 (ddd, 1 H, *J* = 10.0, 3.0, 2.4 Hz, H-5"), 4.32 (dd, 1 H, *J* = 12.2, 4.2 Hz, H-6'b), 4.26 (ddd, 1 H, *J* = 10.1, 4.2, 2.2 Hz, H-5'), 4.20 (dd, 1 H, *J* = 12.4, 3.0 Hz, H-6"b), 4.15 (dd, 1 H, *J* = 10.9, 5.6 Hz, H-6a), 3.77 (dd, 1 H, *J* = 10.9, 2.0 Hz, H-6b); ^{13}C NMR (125 MHz, $CDCl_3$) δ 166.04 (C=O), 165.86 (C=O), 165.79 (C=O), 165.55 (C=O), 165.47 (C=O × 2), 165.39 (C=O), 165.03 (C=O), 164.71 (C=O × 2), 133.60 (Ar), 133.50 (Ar), 133.38 (Ar), 133.32 (Ar), 133.25 (Ar), 133.19 (Ar), 133.02 (Ar), 132.93 (Ar), 132.83 (Ar), 131.82 (Ar), 130.12

(Ar), 129.95 (Ar), 129.87 (Ar), 129.78 (Ar), 129.69 (Ar), 129.64 (Ar), 129.32 (Ar), 129.26 (Ar), 129.18 (Ar), 128.91 (Ar), 128.83 (Ar), 128.77 (Ar), 128.53 (Ar), 128.40 (Ar), 128.34 (Ar), 128.23 (Ar), 128.13 (Ar), 128.05 (Ar), 99.75 (C-1", $^1J_{C\text{-}H}$ = 173 Hz), 97.50 (C-1', $^1J_{C\text{-}H}$ = 173 Hz), 86.03 (C-1), 77.58 (C-3'), 72.05 (C-2), 71.71 (C-3"), 70.55 (C-5), 70.49 (C-3), 70.19 (C-2"), 69.69 (C-5"), 69.63 (C-2'), 68.88 (C-5'), 67.60 (C-4), 67.10 (C-4'), 66.98 (C-6), 66.22 (C-4"), 62.58 (C-6'), 62.32 (C-6"); HRMS (ESI) calcd. for (M + Na) $C_{94}H_{76}O_{25}SNa$: 1659.4294, found:1659.4290.

Synthesis of 4.6: Compound **4.20** (1.31 g, 0.80 mmol) and 4 Å MS (0.5 g) were dried for 16 h under vacuum over P_2O_5 before being suspended in CH_2Cl_2 (50mL), together with Ph_2SO (484 mg, 2.39 mmol) and 2,4,6-tri-*tert*-butyl-pyrimidine (729 mg, 2.56 mmol). The mixture was cooled to -60 °C, and Tf_2O (200 μL, 1.2 mmol) was added. The reaction was stirred for 10 min, and a solution of **4.21**[2] (651 mg, 1.28 mmol) in CH_2Cl_2 (10 mL) was added over 5 min. The solution was stirred at -60 °C for 2 h, then warmed to r.t. and stirred for 18 h, before Et_3N was added to neutralize the solution. The resulting mixture was filtered through Celite and the filtrate was washed with a saturated $NaHCO_3$ solution (50 mL) and then brine (30 mL) before being dried (Na_2SO_4) and concentrated. The residue was purified by chromatography (3:2, hexane:EtOAc) to yield **4.6** (1.49 g, 92%) as a white foam. R_f 0.57 (1:1, hexanes: EtOAc); $[\alpha]_D$ -41.6 (*c* 2.1, CH_2Cl_2); ^{1}H NMR (600 MHz, $CDCl_3$) δ 8.21-8.18 (m, 4 H, Ar), 8.07-8.03 (m, 6 H, Ar), 7.99-7.97 (m, 2 H, Ar), 7.91-7.89 (m, 2 H, Ar), 7.83-7.81 (m, 2 H, Ar), 7.73-7.68 (m, 4 H, Ar), 7.65-7.61 (m, 1 H, Ar), 7.58-7.44 (m, 7 H, Ar), 7.43-7.32 (m, 13 H, Ar), 7.30-7.19 (m, 10 H, Ar), 7.14 (s, 1 H, Ar), 6.08 (dd, 1 H, *J* = 9.9, 9.8 Hz, H-4'), 6.05 (dd, 1 H, *J* = 10.1, 10.0 Hz, H-4"), 5.98 (dd, 1 H, *J* = 10.1, 9.9 Hz, H-4), 5.93 (dd, 1 H, *J* = 10.1, 3.3 Hz, H-3),

5.75 (dd, 1 H, *J* = 3.3, 1.7 Hz, H-2), 5.74 (dd, 1 H, *J* = 3.4, 1.8 Hz, H-2'), 5.70 (dd, 1 H, *J* = 10.1, 3.2 Hz, H-3"), 5.37 (dd, 1 H, *J* = 3.2, 1.9 Hz, H-2"), 5.26 (d, 1 H, *J* = 1.9 Hz, H-1"), 5.20 (d, 1 H, *J* = 1.8 Hz, H-1'), 5.17 (d, 1 H, *J* = 1.7 Hz, H-1), 4.66 (dd, 1 H, *J* = 9.8, 3.4 Hz, H-3'), 4.54-4.50 (m, 2 H, H-6'a, H-6"a), 4.42 (ddd, 1 H, *J* = 9.9, 5.2, 2.3 Hz, H-5), 4.39 (ddd, 1 H, *J* = 10.0, 3.0, 2.6 Hz, H-5"), 4.36-4.31 (m, 2 H, H-6'b, H-5'), 4.22 (dd, 1 H, *J* = 12.5, 3.0 Hz, H-6"b), 4.09 (dd, 1 H, *J* = 11.0, 5.2 Hz, H-6a), 4.04 (dd, 2 H, *J* = 5.1, 4.6 Hz, OCH_2), 4.02-3.99 (m, 1 H, H-6b), 3.87-3.76 (m, 11 H, OCH_2 × 4, OCH_3), 3.73 (dd, 2 H, *J* = 4.6, 4.4 Hz, OCH_2); ^{13}C NMR (125 MHz, $CDCl_3$) δ 166.07 (C=O), 165.88 (C=O), 165.77 (C=O), 165.59 (C=O), 165.48 (C=O × 2), 165.47 (C=O), 165.08 (C=O), 164.72 (C=O × 2), 153.53 (Ar), 152.90 (Ar), 133.60 (Ar), 133.52 (Ar), 133.32 (Ar), 133.23 (Ar), 133.09 (Ar), 132.96 (Ar), 132.90 (Ar), 130.11 (Ar), 129.98 (Ar), 129.91 (Ar), 129.71 (Ar), 129.63 (Ar), 129.30 (Ar), 129.20 (Ar), 128.95 (Ar), 128.84 (Ar), 128.50 (Ar), 128.40 (Ar), 128.28 (Ar), 128.14 (Ar), 123.67 (Ar), 121.39 (Ar), 99.75 (C-1", $^1J_{C\text{-}H}$ = 174 Hz), 97.88 (C-1', $^1J_{C\text{-}H}$ = 173 Hz), 97.34 (C-1, $^1J_{C\text{-}H}$ = 172 Hz), 86.58 (Ar-I), 85.41 (Ar-I), 77.36 (C-3'), 71.68 (C-2'), 71.19 (OCH_2), 70.98 (OCH_2), 70.57 (C-2), 70.35 (OCH_2), 70.27 (OCH_2), 70.27 (C-2", C-3), 69.69 (C-3"), 69.64 (OCH_2), 69.62 (C-5), 69.26 (C-5"), 68.96 (C-5'), 67.85 (C-4'), 67.59 (OCH_2), 67.20 (C-4), 66.75 (C-6), 66.26 (C-4"), 62.67 (C-6'), 62.35 (C-6"), 57.11 (OCH_3); HRMS (ESI) calcd. for (M + Na) $C_{101}H_{88}O_{30}I_2Na$: 2058.3381, found: 2058.3. Anal. Calcd for $C_{101}H_{88}O_{30}I_2$: C, 59.59; H, 4.36. Found: C, 59.55; H, 4.40.

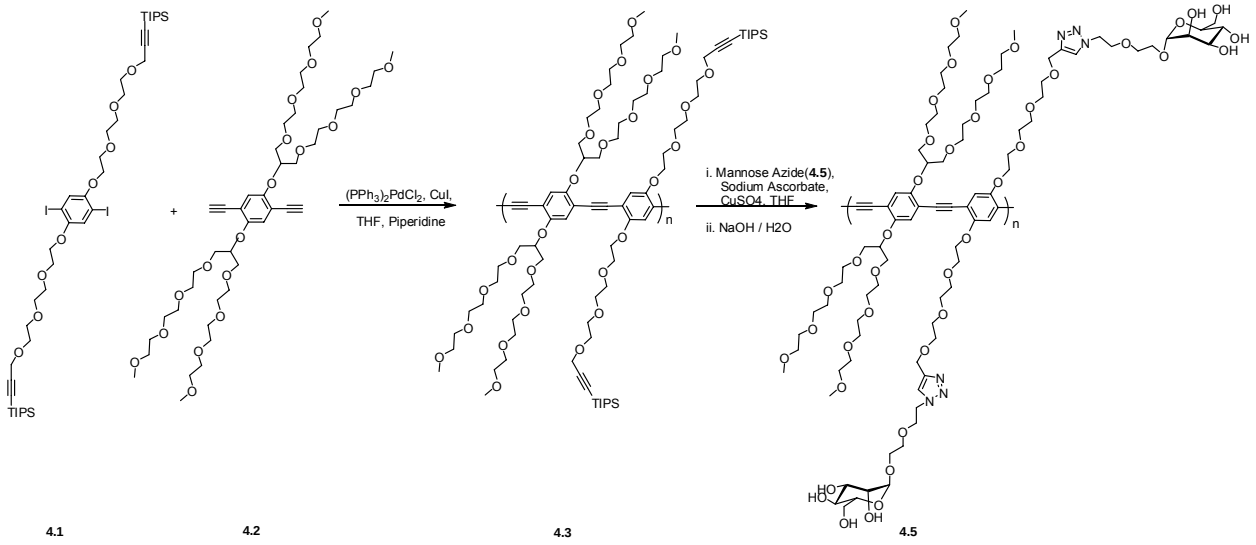

Scheme 4.6. Synthesis of polymer **4.5**

Synthesis of polymer 4.3: Compound **4.1** (1.02 g, 1 mmol), **4.2**[32] (0.891 g, 1 mmol), piperidine (4 mL) and THF (5 mL) were all combined in a 25 mL Schlenk tube and degassed. Upon degassing, $(PPh_3)_2PdCl_2$ (0.5 mol %) and CuI (1 mol %) were added under N_2 and the solution was stirred at room temperature for 2 d. The solution was diluted with THF (25 mL), precipitated into hexane (500 mL), and dried which resulted in a red solid (1.02g, 0.621 mmol, 62 %). GPC (vs. polystyrene standards in chloroform): M_n = 110978, M_w/M_n = 2.879, n = 67. ^{1}H NMR (500MHz, $CDCl_3$): δ 7.21 (s, 2H), 7.11 (s, 2H), 4.59 (m, 2H), 4.35 (s, 4H), 3.91-3.51 (br, 80H), 3.39 (s, 12H), 1.20 (s, 42H). ^{13}C NMR (500 MHz, $CDCl_3$): δ 154.23, 121.62, 119.13, 116.58, 115.42, 104.06, 92.12, 91.69, 87.87, 80.26, 72.39, 71.58, 71.34, 71.05, 70.98, 70.89, 70.15, 69.27, 59.42, 59.20, 18.34, 11.64. IR (cm^{-1}): ν 3018.39, 2950.60, 2207.53, 1514.02, 1423.37, 1215.07, 929.63, 848.62, 763.76, 699.25.

Synthesis of polymer 4.5: To functionalize the polymer with mannose, compound **4.4** (72 mg, 0.156 mmol) and THF (10 mL) were added to **4.3** (100 mg, 0.0607 mmol) and degassed. Under N_2, $CuSO_4$ (0.25 mg, 0.00159 mmol), sodium ascorbate (3.0 mg, 0.0151 mmol), and TBAF (0.20 mL, 1M solution in THF) were added and the polymer was stirred at 50 ºC for 3 d. The solvent was removed, the polymer was re-dissolved in $CHCl_3$, and extracted with H_2O (3x). The organic fractions were collected, the solvent was removed, and the polymer was deprotected in 1M NaOH solution. While deprotecting, EDTA (250 mg) was added to complex residual copper. The polymer solution was neutralized with 1M HCl and dialyzed against DI H_2O for 3 d. The solvent was removed, and the polymer was dried which resulted in a yellow powder (75 mg, 0.0391 mmol, 64 %). ^{1}H NMR (500MHz, $CDCl_3$): δ 8.09 (s, 2H), 7.27 (s, 2H), 7.09 (s, 2H), 4.55 (m, 2H), 4.22 (s, 4H) 3.98-3.42 (br, 110H), 3.37 (s, 12H). IR (cm^{-1}): ν 3402.20, 3018.39, 2920.99, 2849.63, 2399.28, 1599.84, 1474.48, 1422.40, 1215.07, 1106.10, 1019.31, 908.41, 769.54. Φ_{water} = 0.31

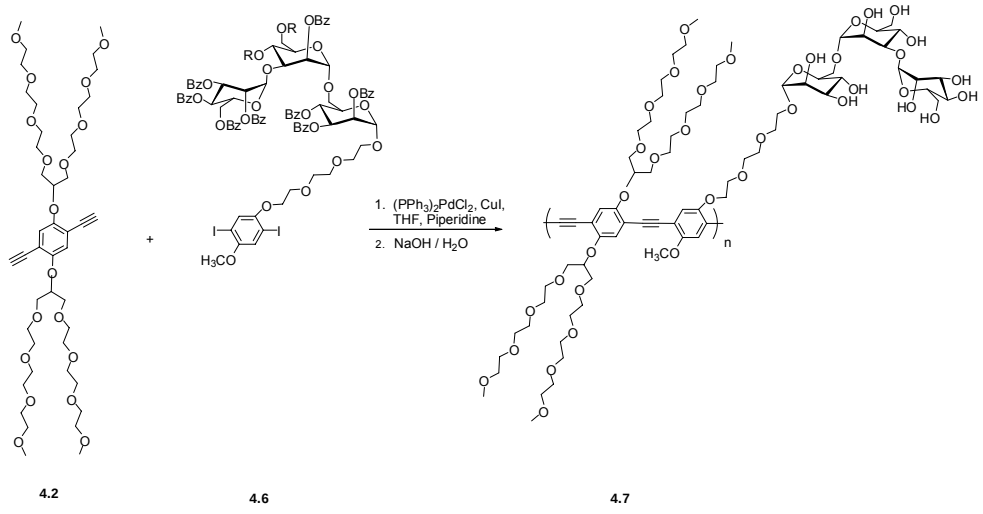

Scheme 4.7. Synthesis of polymer **4.7**

Synthesis of 4.7: Compound **4.2**[32] (168 mg, 0.182 mmol), **4.6** (370 mg, 0.182 mmol), THF (2 mL), MeOH (2 mL), and piperidine (4 mL) were all combined in a 25 mL Schlenk tube. Upon degassing, $(PPh_3)_2PdCl_2$ (0.5 mol%), and CuI (1 mol%) were added to the mixture under N_2 and allowed to react for 2 d. The solvent was removed under vacuum and the polymer was re-dissolved in $CHCl_3$. The polymer solution was extracted with H_2O (3x), the organic fractions were collected, and the solvent was removed. The polymer was deprotected in 1M NaOH and EDTA (250 mg) was added to complex any residual copper. The resulting solution was neutralized with 1M HCl, dialyzed against DI H_2O for 2d, and the solvent was removed resulting in an orange powder (90 mg, 0.056 mmol, 31%). GPC (vs. polystyrene standards in chloroform): M_n = 67,013, M_w/M_n = 2.074, n = 41. ^{1}H NMR (500 MHz, D_2O): δ 7.12 (s, 2H), 7.02 (s, 2H), 4.57 (m, 2H), 3.90-3.32 (br, 88H), 3.22 (s, 3H), 3.07 (s, 12H). IR (cm^{-1}): ν 3329.87, 2921.96, 2863.13, 2210.27, 1585.38, 1444.58, 1415.65, 1330.79, 1259.43, 1208.32, 1096.46, 932.52, 858.23. Φ_{water} = 0.24

Sensitivity of Sugar Functionalized PPEs towards Con A. Each polymer was diluted to a concentration of 5 x 10^{-7} M in PBS buffer at a physiological pH of 7.2. Known concentrations of Concanavalin A were titrated into each polymer solution, which resulted in protein concentrations ranging from the micro to picomolar range. After each titration, the fluorescence quenching was monitored by fluorescence spectroscopy. From the quenching data, Stern-Volmer constants were calculated.

Selectivity of Sugar Functionalized PPEs towards Con A. Each polymer was diluted to a concentration of 5 x 10^{-7} M in PBS buffer at a physiological pH of 7.2. In order to test the selectivity, each polymer solution was incubated for 24 h with a 5 x 10^{-6} M

solution of the following lectins: Artocarpus integrifolia, Arachis hypogaea, Dolichos biflorus, Tetragonolobus purpureas, Ricinus communis, Triticum vulgaris in PBS buffer. After incubation, the fluorescence quenching was monitored by fluorescence spectroscopy. In all cases, only minimal quenching was observed when each polymer was incubated with other lectins. As an example, the selectivity data for **4.7** is shown below.

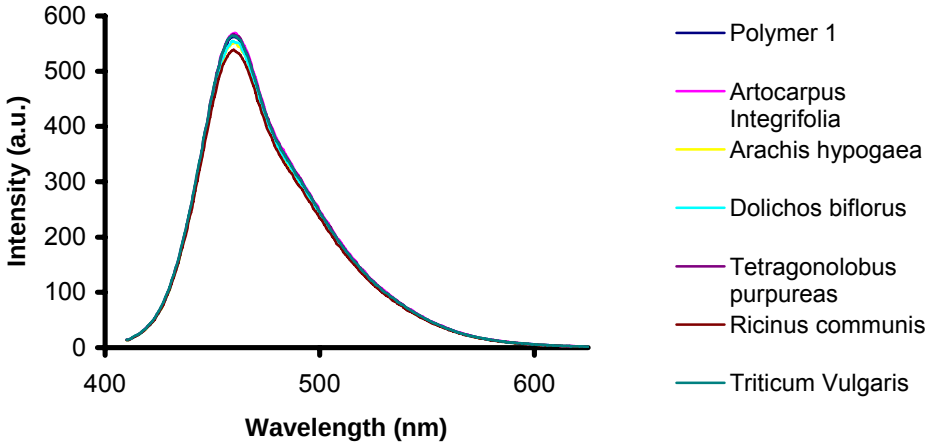

Figure 4.7. Emission Spectra of **4.7** with 5 x 10^{-6} M solutions of various lectins.

Isothermal Titration Microcalorimetry Studies of Sugar Functionalized PPEs with Con A. In order to determine the binding constant, reaction stoichiometry, and thermodynamic profile for the interaction of the sugar functionalized PPEs with Concanavalin A, Isothermal Titration Microcalorimetry (ITC) was used. For each titration, 6 μL of polymer (1 mM in PBS buffer) was injected from a 300 μL microsyringe at an interval of 5 min into a Concanavalin A solution (0.040 mM in PBS buffer) while stirring at 310 rpm. As a control, identical injections of each polymer were

injected into a PBS buffer solution which contained no protein. As expected, the heats of dilution were negligible. The titration data was fitted to a theoretical titration curve using software which was provided by Microcal. The binding constant and thermodynamic parameters were calculated using the equation,

$$\Delta G = \Delta H - T\Delta S = -RT\ln K$$

where ΔG, ΔH, and ΔS are the changes in free energy, enthalpy, and entropy, T is the absolute temperature (298 K), R = 1.98 cal/mol*K, and K is the binding constant.

Table 4.1: ITC data for the interaction of sugar functionalized PPEs with Con A. For the titrations, each polymer (1 mM in PBS buffer) was titrated into a Con A solution (0.040 mM in PBS buffer).

	n (binding ratio)	ΔG (kcal/mol*K)	ΔH (kcal /mol*K)	ΔS (cal /mol*K)	K_a (M^{-1})
4.5	3.05	-6.79	-1.83	16.7	9.97×10^4
4.7	1.66	-8.42	1.98	35.0	1.58×10^6

Bacterial Staining with Sugar Functionalized PPEs. [11] The bacterial strains that were used in this study were kindly provided by Prof. P.E. Orndorff and are labeled as ORN 178 for the mannose binding strain and ORN208 for the mutant mannose non-binding strain.[8] Cells were grown in a LB medium (10 mL) at 37 ºC for 16 h to an optical density of 1.0 at 600 nm. The bacterial culture was centrifuged at 4,000 rpm for 20 min and washed with PBS buffer (3x). A 50 µL aliquot of each polymer (5 uM) was added to a 1 mL aliquot of the bacterial culture in PBS buffer which contained $CaCl_2$ (1 mM) and $MnCl_2$ (1 mM). The solutions were incubated at 25 ºC with mild shaking, centrifuged to pellet the cells, and washed with PBS buffer (3x). The bacteria staining was visualized

using confocal microscopy. An oil immersion 40X objective with excitation at 458 and 488 nm using an Argon laser was used.

4.5 References

1. Lis, H.; Sharon, N. "Lectins: Carbohydrate-Specific Proteins that Mediate Cellular Recognition" *Chem. Rev.* **1998**, *98*, 637-674.

2. (a) Mammen, M.; Choi, S. K.; Whitesides, G. M. "Polyvalent Interaction in Biological Systems: IMplecations for Design and Use of Multivalent Ligands and Inhibitors" *Angew. Chem. Int. Ed*. **1998**, 37, 2755-2794. (b) Kim, I. B.; Erdogan, B.; Wilson, J. N.; Bunz U. H. F. "Sugar-Poly(*paraI*-phenylene ethynylene) Conjugates as Sensory Materials: Efficient Quenching by $Hg^{2+}$and Pb^{2+} ion." *Chem. Eur. J*. **2004**, 10, 6247-6254.

3. Davis, B. G. "Recent Developments in Glycoconjugates" *J. Chem. Soc. Perkin Trans. 1*, **1999**, 2137-2160.

4. Deisingh, A. K.; Thompson, M. "Detection of Infectious and Toxigenic bacteria" *Analyst* **2002**, *127*, 567-581.

5. Kanai, M.; Mortell, K. H.; Kiessling, L. L. "Varying the Size of Multivalent Ligands: The Dependence of Concanavalin A Binding on Neoglycopolymer Length" *J. Am. Chem. Soc.* **1997**, 119, 9931-9932.

6. Smith, E. A.; Thomas W. D.; Kiessling, L. L.; Corn, R. M. "Surface Plasmon Resonance Imaging Studies of Protein-Carbohydrate Interactions" *J. Am. Chem. Soc.* **2003**, 125, 6140-6148.

7. Spevak, W.; Foxall, C.; Charych, D. H.; Dasgupta, F.; Nagy, J.O. "Carbohydrates in an Acidic Multivalent Assembly: Nanomolar P-Selectin Inhibitors" *J. Med. Chem.* **1996**, 39, 1018-1020.

8. Baek, M. G.; Stevens, R. C.; Charych, D. H. "Design and Synthesis of Novel Glycopolythiophene Assemblies for Colorimetric Detection of Influenza Virus and *E.* coli" Bioconjugate *Chem.* **2000**, 11, 777-788.

9. Kim, I. B.; Wilson, J. N.; Bunz, U. H. F. "Mannose-susbstituted PPEs detect lectins: A model for Ricin sensing" *Chem. Commun.* **2005**, *10*, 1273-1275.

10. (a) Xue, C. H.; Luo, F. T.; Liu H. Y. "Post-Polymerization Functionalization Approach for Highly Water-Soluble Well-Defined Regioregular Head-to-Tail Glycopolythiopehenes" *Macromolecules* **2007**, 40, 6863-6870. (b) Xue, C. H.; Jog, S. P.; Murthy, P.; Liu, H. Y. "Synthesis of Highly Water-Soluble Fluorescent Conjugated Glycopoly)p-phenylene)s for Lectin and *Escerichia* coli" Biomacromolecules **2006**, 7, 2470-2474. (c) Xue, C. H.; Donuru, V. R. R.; Liu, H. Y. "Facile, Versatile Prepolymerization and Postpolymerization

Functionalization Approaches for Well-Defined Fluorescent Conjugate Fluorene-Based Glycoploymers" *Macromolecules* **2006**, 39, 5747-5752.

11. (a)Disney, M. D.; Zheng, J.; Swager, T. M.; Seeberger, P. H. "Detection of Bacteria with Carbohyrdate-Functionalized Fluorescent Polymers" *J. Am. Chem. Soc.* **2004**, 126, 13343-13346. (b) McQuade, D. T.; Pullen, A. E.; Swager, T. M. "Conjugated Polymer-Based Chemical Sensors" *Chem. Rev.* **2000**, 100, 2537-2574. (c) Thomas, S. W.; Joly, G. D.; Swager, T. M. "Chemical Sensors Based on Amplifying Fluorescent Conjugated Polymers" *Chem. Rev*. **2007**, 107, 1339-1386.

12. (a) Bunz, U. H. F. "Poly(aryleneethylene)s: Syntheses, Properties, Structures and Applications" *Chem. Rev.* **2000**, 100, 1605-1644. (b) Bunz, U. H. F. "Synthesis and Structure of PAEs" *Adv. Polym. Sci.* **2005**, 177, 1-52.

13. (a) Englert, B. C.; Bakbak, S.; Bunz U. H. F. "Click Chemistry as a Powerful Tool for the Construction of Functional Poly(*p*-phenyleneethynylene)s: Comparison of Pre- and Postfunctionalization Schemes" Macromolecules **2005**, *38*, 5868-5877. (b) Schweinfurth, D.; Hardcastle, K. I.; Bunz, U. H. F. "1,3-Dipolar cycloaddition of alkynes to azides. Construction of operationally functional metal responsive fluorophores" *Chemical Commun.* **2008,** 2203-2205.

14. (a) Huisgen, R.; Szeimies G.; Möbius, L. *Chem. Ber.* **1967**, *100*, 2494-2501. (b) Rostovtsev, V. V.; Green, L. G.; Fokin, V. V.; Sharpless, K. B. "A Stepwise Huisgen Cycloaddition Process: Copper(I)-Catalyzed Regioselective "Ligation" of Azides and Terminal Alkynes" *Angew. Chem. Int Ed.* **2002**, *41*, 2596-2599. (c) Tornoe, C. W.; Christensen, C.; Meldal, M. "Peptidotriazoles on Solid pHase: [1,2,3]-Triazoles by Regiospecific Copper(I)-Catalyzed 1,3-Dipolar Cylcoadditions of Tereminal Alkymes of Azides" *J. Org. Chem.* **2002**, *67*, 3057-3064. (d) Binder, W. H.; Sachsenhofer, R. " 'Click'Chemistry in Polymer and Material Science: the Update" *Macromol. Rapid Commun.* **2007**, *28*, 15-54. (e) Wang, Q.; Chittaboina, S.; Barnhill, H. N. "Highlights in Organic Chemistry Advances in 1,3-Dipolar Cycloaddition Reaction of Azides and Alkynes- A Prototype of "Click" Chemistry"*Lett. Org. Chem.* **2005**, *4*, 293-301. (f) Helms, B.; Mynar, J. L.; Hawker, C. J.; Frechet, J. M. J. "Dendronized Linear Polymers via "Click Chemistry"" *J Am. Chem. Soc.* **2004**, *126*, 15020-15021.

15. (a) Lakowicz, J. R. *Principles of Fluorescence Spectroscopy*; Kluwer Academic/Plenum Publishers: New York, **1999**. (b) Stern, O.; Volmer, M. *Physikalische Zeitschrift* **1919**, *20*, 183-188.

16. Zhou, Q.; Swager, T. M. "Fluorescent Chemosensors Based on Energy Migration in Conjugated Polymers: The Molecular Wire Approach to Increased Sensitvity" *J. Am. Chem. Soc.* **1995**, *117*, 12593-12602.

17. (a) Bourdin, E.; Davey, A.; Blau, W.; Delysse, S.; Nunzi, J. M. "Picosecond Exited States in Poly(arylenethynylene)s "*Chem. Phys. Lett.* **1997**, *275*, 103-105. (b) Bunz, U. H. F.; Imhof, J. M.; Bly, R. K.; Bangcuyo, C. G.; Rozanski, L.; vandenBout, D. A. "Photophysics of Poly[*p*-(2,5-didodecylphenylene)ethynylene] in Thin Films" *Macromolecules* **2005**, *38*, 5892-5896.

18. Chen, L. H.; McBranch, D. W.; Wang, H. L.; Helgeson, R.; Wudl, F.; Whitten, D. G. "Highly Sensitive Biological and Chemical Sensors Based on Reversible Fluorescence Quenching in a Conjugated Polymer " *Proc. Nat. Acad. Sci.* **1999,** *96*, 12287-12292.

19. (a) Fan, C. H.; Wang, S.; Hong, J. W.; Bazan, G. C.; Plaxco, K. W.; Heeger, A. J. "Beyond superquenching: Hyper-Efficient Engery Transfer from Conjugated Polymers to Gold Nanoparticles" *Proc. Nat. Acad. Sci.* **2003**, 100, 6297-6301. (b) Gaylord, B. S.; Wang, S. J.; Heeger, A. J.; Bazan G. C. "Water-Soluble Conjugated Oligomers: Erffect of Chain Length and Aggregation on Photoluminescence-Quenching Efficiencies" *J. Am. Chem. Soc*. **2001**, 123, 6417-6418. (c) Wang, D. L.; Wang, J.; Moses, D.; Bazan, G. C.; Heeger, A. J.; Park, J. H.; Park, Y. W. "Photoluminescence Quenching of Water-Soluble Conjugated Macromolecule by Bipyridinium Derivatives" *Synth. Met.* **2001**, 119, 587-588. (d) Wang, J.; Wang, D. L.; Miller, E. K; Moses, D.; Bazan, G. C.; Heeger, A. J. "Photoluminescence of Water-Soluble Conjugated Polymers:Origin of Enhanced Quenching by Charge Transfer" *Macromolecules* **2000**, 33, 5153-5158.

20. (a) Jiang, H.; Zhao, X. Y.; Schanze, K. S. "Effects of Polymer Agrregation and Quencher Size on Amplified Fluorescence Quenching of Conjugated Polyelectrolytes" *Langmuir* **2007**, *23*, 9481-9486. (b) Muller, J. G.; Atas, E.; Tan, C.; Schanze, K. S.; Kleiman, V. D. "The Role of Exction Hopping and Direct Energy Transafer in teh Efficient Quenching of Conjugated Polymers" *J. Am. Chem. Soc.* **2006,** *128,* 4007-4016. (c) Tan, C. Y.; Atas, E.; Muller, J. G.; Pinto, M. R.; Kleiman, V. D.; Schanze, K. S. "Amplified Quenching of a Conjugated Polyelectrolyte of Cyanine Dyes" *J. Am. Chem. Soc.* **2004,** *126,* 13685-13694. (d) Tan, C. Y.; Pinto, M. R.; Schanze, K. S. "Photophysics, aggregation and amplified quenching of a water-soluble poly(phenylene ethynylene)" *Chem. Commun.* **2002**, 446-447. (e) Harrison, B. S.; Ramey, M. B.; Reynolds, J. R.; Schanze, K. S. "Amplified Fluorescence Quenching in an a Poly(*p*-phenylene)-Based Cationic Polyelectrolyte" *J. Am. Chem. Soc.* **2000**, *122*, 8561-8562.

21. Phillips, R. L.; Kim, I. B.; Tolbert, L. M.; Bunz, U. H. F. "Fluorescence Self-Quenching of a Monnosylated Poly(p-phenyeneeethynylene) Induced by Concanavalin A"J. *Am. Chem. Soc.* **2008**, 130, 6952-6954.

22. Eftink, M. R. *Topics in Fluorescence Spectroscopy*, **1991**, *2*, 53-126

23. Jelesarov, I.; Bosshard, H. R. "Isothermal Titration Calorimetry and Differential Scanning Calorimetry as Complementary Tools to Investigate the Energetics of Bimolecular Recognition" *J. Mol. Recognit.* **1999**, *12*, 3-18.

24. Dam, T.K.; Roy, R.; Page, D.; Brewer, F.C. "Negative Cooperativity Associated with Binding of Multivalent Carbohydrates to Lectins. Thermodynamic Analysis of the "Multivalency Effect""*Biochemistry* **2002**, *41*, 1351-1358.

25. (a) Ho, H. A.; Boissinot, M.; Bergeron, M. G.; Corbeil, G.; Dore, K.; Boudreau, D.; Leclerc, M. "Colorimetric and Fluorometric Detection of Nucleic Acids Using Cationic Polythiophene Derivatives"*Angew. Chem. Int. Ed.* **2002**, *41*, 1548-1551 (b) Dore, K.; Leclerc, M.; Boudreau D. "Investigation of Fluorescence Signal Amplification Mechanism Used for the Direct Molecular Dectection of Nucleic Acids " *J. Fluorescence* **2006** *16*, 259-265

26. Sun, Y. P.; Wallraff, G. M.; Miller, R. D.; Michl, "Models for the Polysilane High Polymers. Room-temperature Solution Fluorescence Quenching lin Linear $Si_{10}Me_{22}$, $Si_{16}Me_{34}$ and Poly(methylp[ropylsilane) by Carbon Tetrachloride" *J.Photochem. Photobiol. A- Chem.* **1992**, *62,* 333-346.

27. Sandra, L.; Spears, P. A.; Havell, E. A.; Hamrick, T. S.; Horton, J. R.; Orndorff, P. E. "Autoregulation of the *dnaA-dnaN* Operon and Effects of DnaA Protein Levels on Replication Initiation in *Bacillus subtilis" J. Bacteriol.* **2001**, *183*, 4099-4102.

28. Garegg, P.J.; Kvarnstroem, I.; Niklasson, A.; Niklasson, G.; Svensson, S.C.T. *J. Carbohydr. Chem.* **1993**, 12, 933–953.

29. Bien, F.; Ziegler, T. "Chemoenzymatic Synthesis of Glycosylated Enantiomarically Pure 4-pentene 1,2- and 1,3-diol Derivatives" *Tetrahedron*:*Asymmetry* **1998**, 9, 781–790.

30. Kihlberg, J.O.; Leigh, D.A.; Bundle, D.R."The in situ Activation of Thioglycosides with Bromine: an Improved Glycosylation Method" *J. Org. Chem.* **1990**, 55, 2860–2863.

31. Christensen, M.K.; Meldal, M.; Bock, K. "Synthesis of Mannose 6-phosphate-containing Disaccharide Threonine Building Blocks and Their Use in Solid-Phase Glycopeptide Synthesis"*J. Chem. Soc.*, *Perkin Trans. 1* **1993**, 1453-1460.

32. Kim, I.B.; Phillips, R.; Bunz, U.H.F. "Carboxylate Group Side-Chain Density Modulates the pH-Dependent Optical Properties of PPEs" *Macromolecules*. **2007**, 40, 5290-5293.

33. "A Guide to Recording Fluorescence Quantum Yields." Horiba Jobin Yvon Ltd. available online: http:/www.jobinyvon.co.uk/ukdivisions/Fluorescence/plqy.html

CHAPTER 5

PPE-Protein Conjugates for the Detection of Toxic Metals

5.1 Introduction

As seen in the previous chapter, grafting of suitable recognition units to the side chains of conjugated polymers (CP) provides bio- and chemosensory materials. CPs exhibit molecular wire behavior, multivalent display of recognition units, and superquenching effects all intertwined with spectroscopic properties that stem from conformational changes, excimer/exciplex formation and fluorescence resonance energy transfer.[1-6] Materials with exquisite sensitivity and selectivity for specific analytes can result. If CPs are appended with ionic or highly polar side groups, sensing of environmentally and biologically important species is possible in aqueous solution. Current applications involving water soluble CPs include DNA-sensing, formation of CP-protein complexes, and the use of sugar-coated poly(*para*phenyleneethynylene)s (PPE)s for the detection of *E. coli*.[7-11]

We have explored water-soluble PPE-protein complexes as agglutination assays for mercury ions, exploiting the sulfhydryl-protease papain as a cofactor, which increased the sensory response of PPE **5.7** by a factor of 20 towards Hg^{2+} ions.[12,13] In this contribution, we investigate the influence of pre-aggregation of a biotinylated PPE, **5.5**, with avidin or streptavidin upon its response to mercuric ions and paraquat (N,N'-dimethyl-4,4'-bipyridinium dichloride).[14] While numerous biotin-functionalized PPEs have been synthesized and examined in their binding ability to (strept)avidin,[10,14] this work goes a step further as it explores the sensory response of the biomolecular

constructs obtained by mixing of a biotin-PPE with (strept)avidin; this concept should allow us to modulate and hone the properties of CPs towards desired ends. We were inspired by Schanze's work, which demonstrated that aggregation of a *meta*-PPE positively influences its sensitivity towards quenching agents, suggesting that aggregated CPs act as coupled electronic entities.[15] We set out to emulate the aggregation by exposing a biotinylated PPE, **5.5**, towards avidin and exploiting the properties of the force-aggregated PPE for sensory applications.

5.2 Results and Discussion

Synthesis of the biotin-functionalized PPE **5.5** was performed by 1-ethyl-3-(3'-(dimethylamino)propyl)carbodiimide (EDC) [16] mediated post-functionalization (Scheme 1) of **5.4** with D-biotin in anhydrous DMF. The water-soluble, biotin-functionalized PPE **5.5** was obtained after hydrolysis of its precursor's ester groups by sodium hydroxide in methanol. The structure of **5.5** was secured by ^{1}H NMR spectroscopy, where the biotin units displayed their specific signals at δ = 1.91-2.85 ppm in addition to the expected signals for the PPE backbone.

The Stern-Volmer equation is useful when measuring the quenching of a conjugated polymer by a quencher Q. The Stern-Volmer constant K_{SV} is defined by:[17,18]

$$F_o/F = K_{SV}[Q] + 1 \qquad \textbf{Eq. 5.1}$$

In this equation, F_o is the fluorescence intensity without added quencher Q, and F is the fluorescence intensity in the presence of Q at a given concentration [Q]. A higher value of K_{SV}, the slope, indicates a greater sensitivity of the system towards Q.

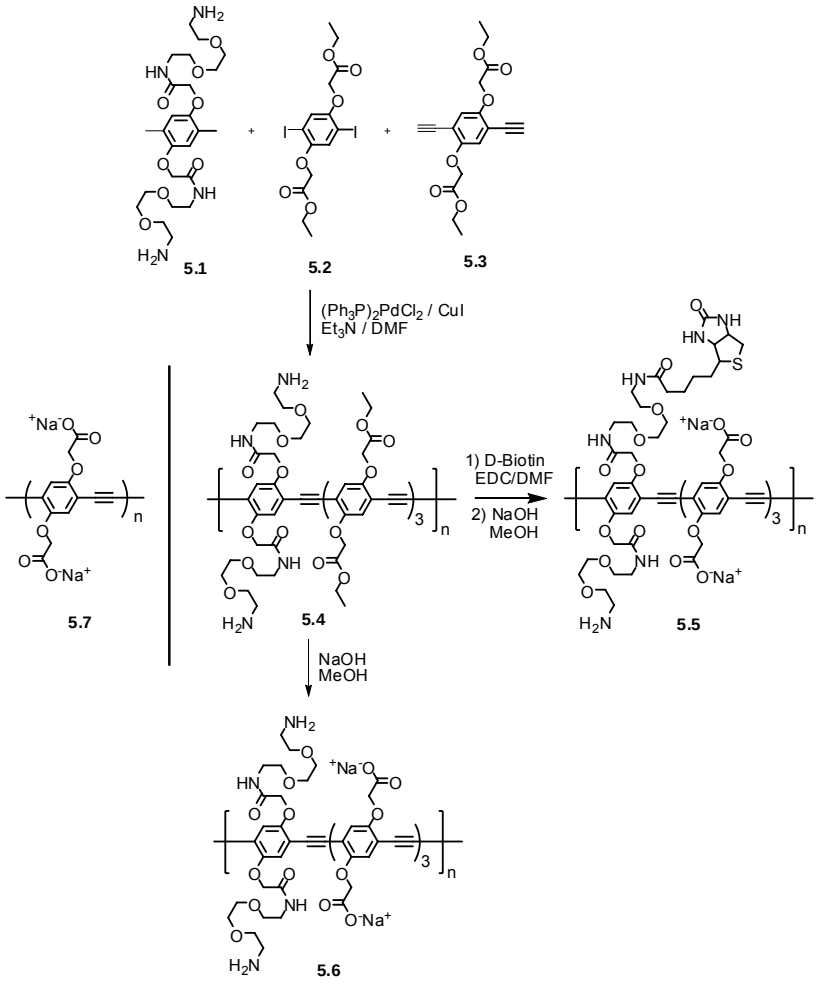

Scheme 5.1. Synthetic scheme of PPEs **5.4**, **5.5**, and **5.6** and structure of carboxylate-substituted PPE **5.7** is shown.

Stern-Volmer quenching is static if Q forms a ground state complex with the fluorophore; K_{SV} represents the binding constant between the quencher and the fluorophore. Alternatively, in dynamic or collisional quenching, Q deactivates the excited state of the fluorophore. Dynamic quenching is unlikely in PPEs, where fluorescence lifetimes of the fluorophore under consideration are short (300-400 ps). Quenching processes for PPEs are generally accepted to be static in nature. The Stern-Volmer constant, K_{SV}, is formally independent of the concentration of the fluorophore;

experimentally, however, it is found that K_{SV} can decrease with increasing concentration of the CP under investigation.[19]

Table 5.1 shows the results of the quenching experiments performed with **5.5**-**5.7**. The first five rows show controls that were performed with **5.7**, which do not promote any specific interaction between polymer and avidin or streptavidin. Yet, nonspecific interactions between avidin and **5.7** are strong, similar to the cases of protein-CP-interactions that have been reported recently.[13] The specific interactions between **5.5** and avidin, streptavidin or dye-labeled streptavidin give K_{SV} values that range from 0.9-3.3 x 10^7 $M^{-1.}$ While these K_{SV} values are quite high, they are only by a factor of 10 higher than those that were found for the non-specific interaction of **5.7** with avidin. They do not reflect the very high (K_{assoc} ~10^{15}) binding constant of (strept)avidin to biotin. A reason for the apparently diminished binding might be the insufficient length of the connecting tether that chains the biotin to the backbone. Control experiments in which **5.5** or its avidin/streptavidin complex were exposed towards paraquat only showed marginal K_{SV} values due to the high ionic strength at which the experiments were performed, using 0.1 M buffer solutions.

The measured K_{SV}, indicating the complex formation between the polymers **5.4**-**5.7** and mercury, are between K_{SV} = 0.8-1.3 x 10^4 M^{-1}. The three polymers surprisingly behave quite similar, showing that the amino-substituted oligoethyleneglycol groups and the carboxylate units must have similar binding affinities towards the mercuric ion.

Table 5.1. Measured Stern-Volmer constants K_{SV} for the quenching of PPEs (**5.5-5.7**)

Substrate	*Cofactor*	*Quencher*	K_{SV} (M^{-1})	*Comment*
5.7	-	Mercuric ion	1.1×10^4	
5.7	-	Avidin	2.3×10^6	Slope obtained from very low [Q]
5.7	-	SA-Rhodamine	No quenching	
5.7	-	SA-Texas-Red	No quenching	
5.7	Avidin	Mercuric ion	4×10^3	
5.6	-	Mercuric ion	8×10^3	
5.5	-	SA-coated microspheres	Qualitiative quenching	
5.5	-	Avidin	3.3×10^7	
5.5	-	SA-Texas-Red	9×10^6	Slope obtained from very low [Q]
5.5	-	SA-Rhodamine	2.8×10^7	
5.5	-	Mercuric ion	1.3×10^4	
5.5	-	Paraquat	1.7×10^3	Low, due to high ionic strength
5.5	SA-coated microspheres	Mercuric ion	7.2×10^4	
5.5	SA	Mercuric ion	5.5×10^4	
5.5	Avidin	Mercuric ion	1.1×10^5	
5.5	Avidin	Paraquat	1.5×10^3	Low, due to high ionic strength
5.5	SA	Paraquat	2.3×10^3	Low, due to high ionic strength

The self-assembled complexes between either **5.7** and avidin or **5.5** and avidin or streptavidin are compared in their sensitivity towards mercury ions. The self-assembled complex of **5.7** and avidin binds less to mercuric ions (K_{SV} = 4 x 10^3 M^{-1}) than **5.7** by itself, while in the case of the biotinylated PPE **5.5**, pre-agglutination with either streptavidin or avidin leads to a significant increase in the binding of the complex to mercuric ions. The highest K_{SV} = 1.1 x 10^5 M^{-1}, resulted when the complex of **5.5**-avidin was exposed to mercuric ions (Table 5.1), representing an almost tenfold increase of K_{SV} compared to the binding of mercuric ions to **5.5**.

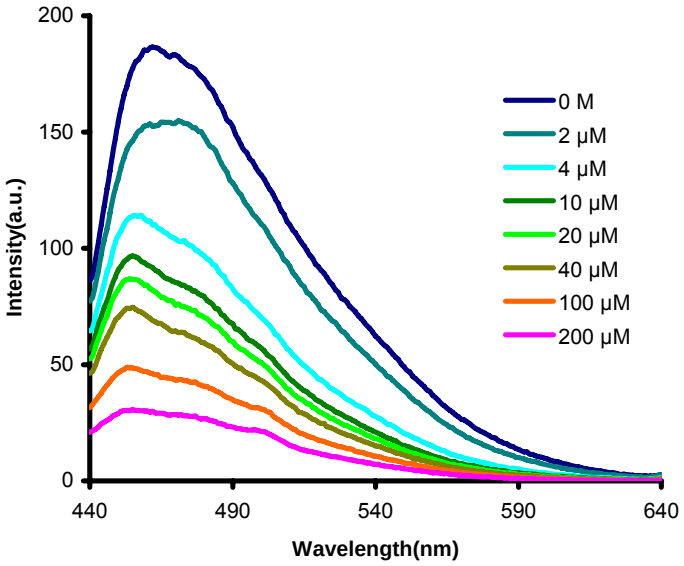

Figure 5.1. Emission spectra of solutions of lightly crosslinked polymer arrays from **5.5** and avidin (60 nM) by addition of increasing concentrations of mercury ions.

We find that PPEs **5.5** and **5.7** are moderately quenched by mercury ions ($K_{SV} \approx 10^4$ M^{-1}) in buffered aqueous solution. Methyl viologen quenches the fluorescence of **5.5**

only weakly with a K_{SV} of 1.7×10^3 M^{-1}. This relatively low K_{SV} is due to the highly ionic environment in which the quenching experiments are performed.

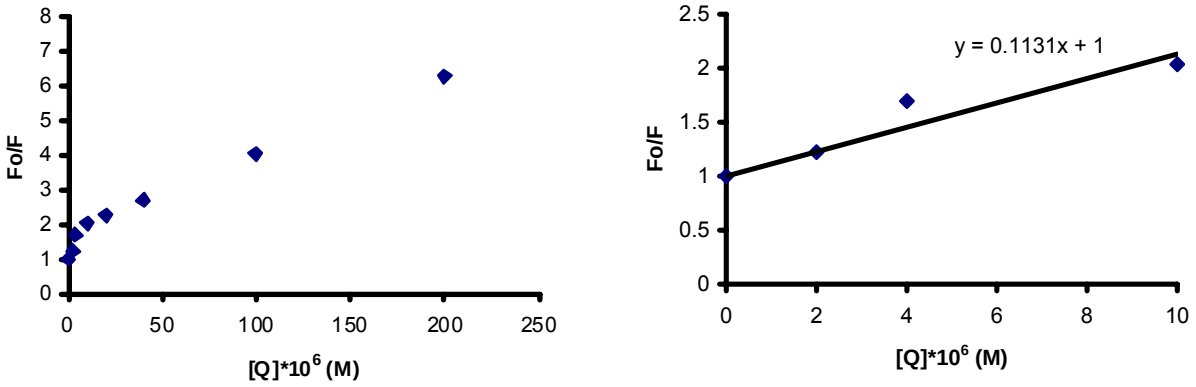

Figure 5.2. Right: F_o/F plots for **5.5**-avidin "armed" polymer with Hg^{2+} ions; Left: Apparent Stern-Volmer constant (K_{SV}) for Hg^{2+} ions based on initial linear parts is 1.1×10^5 M^{-1}.

Upon addition of avidin, streptavidin or streptavidin-coated microspheres, the quenching of **5.5** by methyl viologen is not more efficient, suggesting that the proteins, while agglutinating **5.5**, may screen the polymer chains further from paraquat. In the case of mercuric ions, the situation is different, and here a tenfold increase in sensitivity is observed when we compare the quenching of **5.5** to that of the **5.5**-avidin complex. Interestingly, self-assembled electrostatic complexes formed from **5.7** and avidin show a *decreased* binding to mercury when compared to the binding of mercuric ions to **5.7** alone. We assume that the negative charges of **5.7** are partialy neutralized by the presence of avidin and disallowing for mercuric ions to bind tightly. In the case of the **5.5**-avidin complex, the significant length of the linker, while allowing for an effective interaction of biotin with the avidin and therefore crosslinking, will keep the polymer

chains sufficiently far away from the protein and allow interaction of the carboxylate anions with the mercuric ions.

What is the proposed mechanism for the enhanced quenching of the **5.5**-avidin complex when compared to **5.5**? In the first step, a complex between the biotinylated PPE and avidin (**5.5**-avidin) is formed (Figure 5.3); the fluorescence of this complex decreases. Even very high concentrations of avidin, however, were unable to diminish the fluorescence of **5.5** (or its complex) to less than 40% of the starting value. The **5.5**-avidin complex must enforce a significant degree of interaction between the polymer chains short of an excimer or exciplex. The addition of mercuric ions leads to efficient quenching of the fluorescence of **5.5**-avidin. The concept of using pre-agglutination is of significance as it suggests that the very loose network of CP chains,

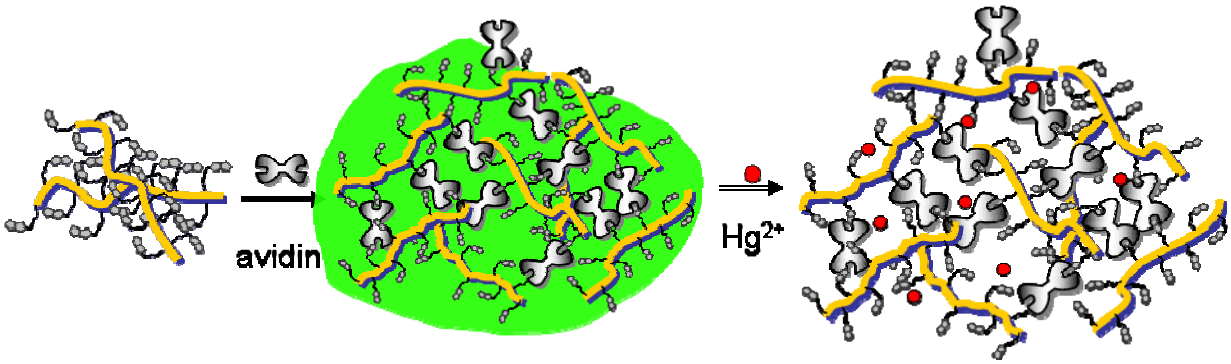

Figure 5.3. Proposed mechanism of the quenching effects shown by the **5.5**-avidin or streptavidin agglutinates upon addition of mercuric ions.

formed by self-assembly, using the biotin-avidin interactions, is primed to be more sensitive to specific analytes than isolated polymer chains are. In the proposed three-dimensional multiplex, the excited state energy transfer is more facile than in only one

dimension (i.e. along one chain). In effect, a '3-d-molecular wire' results, the fluorescence of which is efficiently quenched by the addition of mercuric ions.

There is precedence for this behavior, as in Langmuir Blodgett-films of PPEs, enhanced energy transport was observed in two dimensions.[22] In our case, the loose 3-d network is formed in solution and leads to the desired, enhanced sensory response. While the amplification factor is substantial, manipulation of the side chains to increase the avidin-biotin binding with the use of longer polymers (higher degree of polymerization) and linkers of increased length should lead to further gains in sensitivity.

5.3 Conclusion

We have synthesized the water-soluble biotinylated PPE **5.5** and examined its metal responsive behavior. Upon addition of avidin, **5.5** forms a complex, which displays increased sensitivity towards Hg^{2+} ions when compared to **5.5** alone. We have effectively "armed" **5.5** with avidin to obtain a substantial gain in sensitivity when monitoring for the presence of mercuric ions. While the arming of the biotinylated polymer by (strept)avidin is a non-specific process (with respect to mercuric ions) it increases the *sensitivity* of **5.5** towards Hg^{2+}, a conceptually important process. On the other hand, when the positively charged avidin forms an electrostatic complex with **5.7** it *prevents* the quenching of the fluorescence of **5.7** by Hg^{2+} ions, probably due to the blockage of the carboxylate groups by the positively charged avidin.

The lightly crosslinked **5.5**-avidin complex is proof that CPs display a significantly increased sensitivity towards mercuric ions if self assembly processes are used to form large soluble arrays, here promoted by biotin-(strept)avidin interactions.

The result is an ensemble of electronically coupled polymer chains. We will further study the interactions of conjugated polymers with proteins in live cells to see if we can take advantage of the polyvalent interactions.

5.4 Experimental

Instrumentation and Materials. All chemicals and solvents were used without further purification as received unless otherwise noted. Streptavidin coated microspheres (mean diameter = 0.31 μm) was purchased from Bangs Laboratories, Inc. Streptavidin-tetramethylrhodamine conjugate and streptavidin-Texas Red® conjugate were purchased from Molecular Probes. Avidin (MW = 66,000) was purchased from Sigma-Aldrich Co and streptavidin was purchased from Fluka. Fluorescence data were obtained with a Shimadzu RF-5301PC spectrofluorophotometer in quartz cuvettes. PPE **5.7** was synthesized previously[2] and had the number average molecular weight of 1.2×10^3 with a polydispersity (M_w/M_n) of 4.3. The excitation wavelength was 425 nm (or 405 nm) and the emission was recorded from 440 nm (or 420 nm) to 650 nm. Solutions of PPE **5.5-5.7** were prepared in 0.1 M sodium phosphate buffer (pH = 7.2) with a concentration of 1 mg/L. In each quenching experiment, a small aliquot (20-100 μL) of concentrated quencher solution was added to 5 mL of diluted fluorophore solution by using a calibrated microliter pipet. The fluorescence was recorded at room temperature.

Synthesis of 5.1 – 5.3: Synthesis of **5.1**, **5.2**, and **5.3** were described in our previous reports.[2,23]

Synthesis of polymer 5.4: Monomer **5.1** (222 mg, 0.30 mmol), **5.2** (160 mg, 0.30 mmol), and **5.3** (218 mg, 0.66 mmol) were dissolved in a mixture of triethylamine (1 mL), and

DMF (5 mL) in a Schlenk flask (25 mL) under a flow of nitrogen and with magnetic stirring. $(Ph_3P)_2PdCl_2$ (2.0 mg, 2.8 μmol) and CuI (0.5 mg, 2.8 μmol) were added to the flask. The reaction mixture was stirred at room temperature for 24 h. The solution was slowly added to ether (200 mL). The precipitate was washed with ether and water. A yellow solid was obtained in 99 % yield (421 mg). PPE **5.4** shows an absorption maximum at 436 nm and an emission maximum at 470 nm in chloroform, typical for a dialkoxy-PPE. The number average molecular weight (M_n) of **5.4** is 8.3 x 10^3 (P_n = 6) with a polydispersity index of 1.70 (GPC, polystyrene standard). ^{1}H NMR (DMSO-d_6): δ 7.14, 4.92, 4.19, 3.56, 3.49, 3.09, 1.21.

Synthesis of polymer 5.5: Polymer **5.4** (60 mg, 0.04 mmol) was dissolved in DMF (7 mL) in a flask (25 mL) under a flow of nitrogen and with magnetic stirring. D-biotin (25 mg, 0. 10 mmol), 2,4,6-trimethylpyridine (12 mg, 0.10 mmol), and EDC·HCl (20 mg, 0.10 mmol) were added to the flask in an ice bath. The reaction mixture was stirred at room temperature for 24 h. The solvent was evaporated under a reduced pressure. Methanol (20 mL) and NaOH (200 mg, 5 mmol) were added to the reaction mixture and the temperature was increased to 40 °C. The mixture was stirred for 24 hr. The reaction flask was stored in a refrigerator overnight. The precipitate was collected and washed with methanol and acetone. An orange solid (67 mg) was obtained. ^{1}H NMR (D_2O): δ 6.81, 4.49, 3.35, 3.05, 2.85, 2.71, 2.51, 1.91.

Synthesis of polymer 5.6: Polymer **5.4** (60 mg, 0.04 mmol) and NaOH (200 mg) were dissolved in MeOH/H_2O) (25 mL) in a flask (50 mL) with magnetic stirring. The reaction mixture was stirred at 40 °C for 48 h. The reaction flask was stored in a

refrigerator overnight. The precipitate was collected and washed with methanol and acetone. An orange solid (48 mg, 82%) was obtained. ^{1}H NMR (D_2O): δ 6.70, 4.40, 3.23.

Influence of 10 different metal ions on the optical properties of PPE 5.5 in 0.1 M phosphate buffer solution at pH = 7.2. To investigate the sensory ability of **5.5** toward metal ions, we exposed this polymer to concentrated solutions of metal ions in a 0.1 M phosphate buffer solution (pH = 7.2). The concentration of PPE **5.5** was adjusted to 1 mg/L in a phosphate buffer solution. Solutions of 10 metal salts were prepared at a 0.1 M concentration: They are $Zn(ClO_4)_2$, $CdCl_2$, $Hg(O\text{-}CO\text{-}CF_3)_2$, $Pb(NO_3)_2$, $FeCl_3$, $NiCl_2$, $CoCl_2$, $CuBr_2$, $Ca(NO_3)_2$, and $Mg(OTf)_2$. 20 μL of each metal ion solution was added to 5 mL of a buffered solution of **5.5**. The concentration of each metal ion is 4×10^{-4} M in a buffered solution of **5.5**. Most metal cations showed slight effects while mercury showed a substantial quenching of the fluorescence at a concentration of 4×10^{-4} M. While Pb^{2+} ions showed mild quenching in diluted solution of **5.5**, Hg^{2+} ions showed quenching in **5.5** immediately after the addition of mercury ions.

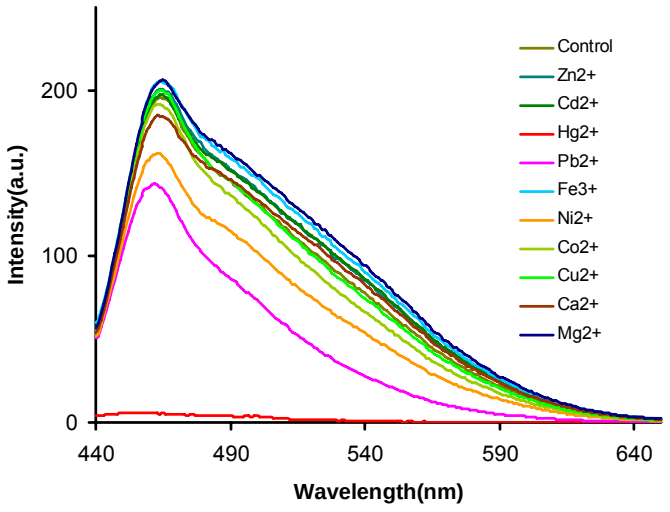

Figure 5.4. Emission spectra of solutions of PPE **5.5** by addition of 20 μL of a 0.4 mM solution of metal ions. Spectra show significant quenching with Hg^{2+} ions.

Concentration dependent quenching of the fluorescence of PPE 5.5 by the addition of mercury ions. A small aliquot (10-100 μL) of concentrated solutions of $Hg(O\text{-}CO\text{-}CF_3)_2$ (1×10^{-3} M and 1×10^{-2} M) was added to each vial containing 5 mL of **5.5**. The concentration of $Hg(O\text{-}CO\text{-}CF_3)_2$ in **5.5** is 2 – 200 μM. In SS**3**, the apparent Stern-Volmer constant (K_{sv}) for Hg^{2+} ions is 1.0×10^4 M^{-1}. Ksv of **5.5** for Hg^{2+} ions is similar to that of **5.7**.

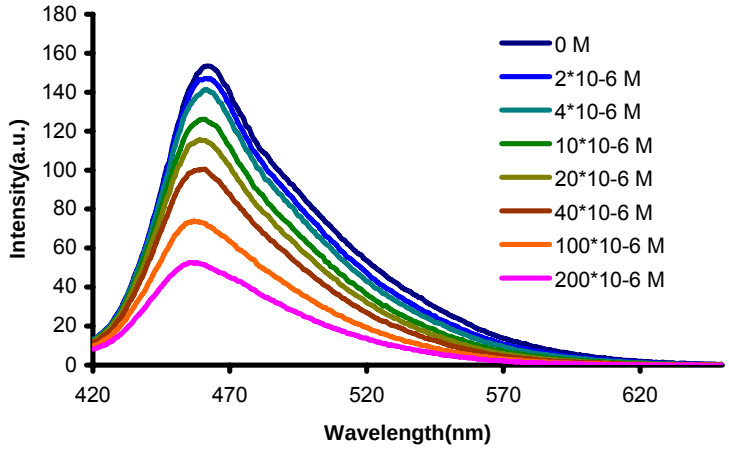

Figure 5.5. Emission spectra of solutions of **5.5** by addition of increasing concentrations of mercury ions.

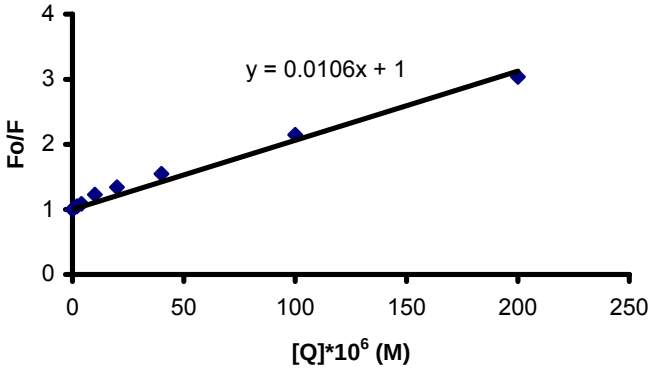

Figure 5.6. F_o/F plots for **5.5** with mercury ions. The apparent Stern-Volmer constant (K_{sv}) for Hg^{2+} ions is 1.0×10^4 M^{-1}.

Influence of streptavidin coated microspheres on the optical properties of PPE 5.5 in 0.1 M phosphate buffer solution at pH = 7.2. 5 – 50 μL of a solution of streptavidin coated microspheres (SCM, Bangs Laboratories catalog code CP01B, mean diameter = 0.31 μm, 1 weight% of spheres) were added to a buffered solution of **5.5**. The fluorescence intensities of **5.5** were decreased by increasing concentration of SCM, indicating the formation of an agglutinate. The standard SCM solutions contain **5.5** (1mg/L), and microspheres (10 mg/L) in 0.1 M buffer solution.

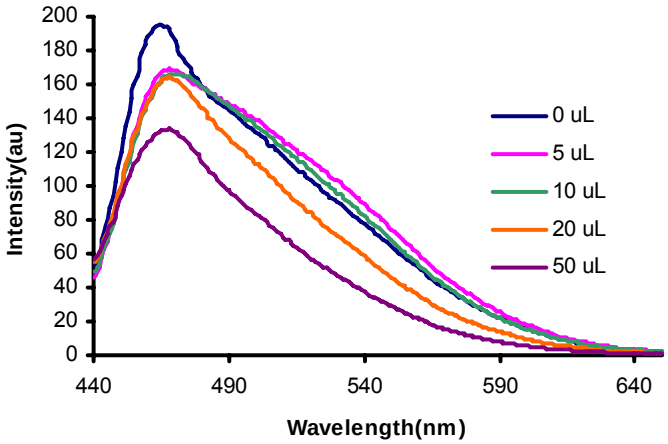

Figure 5.7. Emission spectra of solutions of **5.5** by addition of increasing concentrations of streptavidin coated microspheres (SCM).

Influence of 10 different metal ions on the optical properties of PPE 5.5-streptavidin coated microspheres in 0.1 M phosphate buffer solution at pH = 7.2. 5 uL of SCM was added to 5 mL of **5.5** to form a lightly pre-agglutinated solution of **5.5-SCM**. The pre-agglutinated solutions of **5.5-SCM** were exposed to 10 different metal ions. Solutions of 10 metal salts were prepared at a 0.1 M concentration: They are $Zn(ClO_4)_2$, $CdCl_2$, $Hg(O\text{-}CO\text{-}CF_3)_2$, $Pb(NO_3)_2$, $FeCl_3$, $NiCl_2$, $CoCl_2$, $CuBr_2$, $Ca(NO_3)_2$, and $Mg(OTf)_2$. 20 μL of each metal ion solution was added to 5 mL of a buffered solution of **5.5-SCM**. The concentration of each metal ion is 4×10^{-4} M in a buffered solution of **5.5-SCM**. Most of

the metal ions showed similar quenching effects while Ca ions showed significant quenching unlike **5.5**.

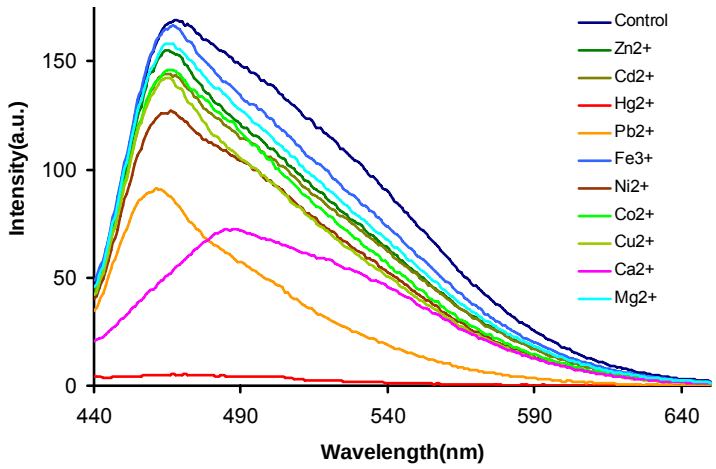

Figure 5.8. Emission spectra of solutions of **5.5-SCM** complexes by addition of 20 µL of a 0.4 mM solution of metal ions. Spectra show significant quenching with Ca^{2+} ions and Hg^{2+} ions.

Concentration dependent quenching of the fluorescence of PPE 5.5-streptavidin coated microspheres complexes by the addition of mercury ions. 100 uL of a SCM solution was added to 100 mL of **5.5**. The solution was centrifuged and the supernatant was decanted. 0.1M phosphate buffer solution was added to the precipitate. This process was repeated three times to remove excess polymer **5.5**. The precipitate was diluted with 0.1M phosphate buffer and the solution was sonicated. In **5.5-SCM** complexes, the apparent Stern-Volmer constant (K_{sv}) based on the linear part of the curve for Hg^{2+} ions is 7.2×10^{4} M^{-1}.

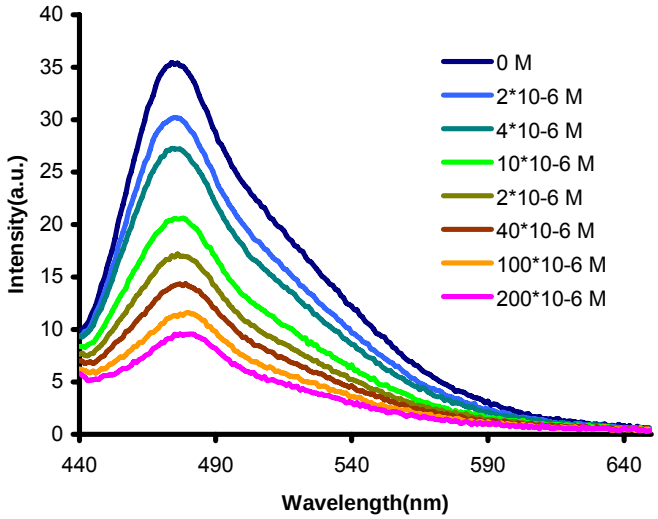

Figure 5.9. Emission spectra of solutions of **5.5-SCM** complexes by the addition of increasing concentrations of mercury ions.

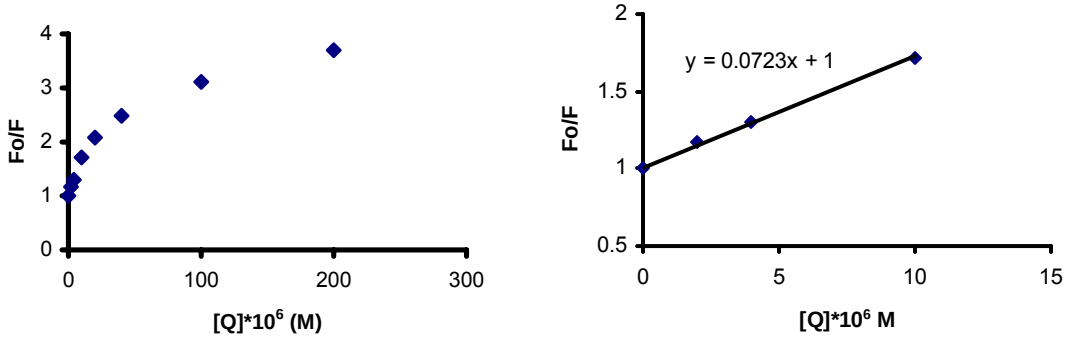

Figure 5.10. F_o/F plots for **5.5-SCM** complexes with mercury ions. The Stern-Volmer constant (K_{sv}) for Hg^{2+} ions based on initial linear parts is 7.2×10^4 M^{-1}.

Quenching of the fluorescence of 5.5 by avidin. A small aliquot (20-500 μL) of concentrated solutions of avidin (1.5×10^{-6} M) was added to each vial containing 5 mL of **5.5**. The concentration of avidin in **5.5** is 6 – 150 nM. The apparent Stern-Volmer constant (K_{sv}) based on the linear part of the curve for avidin is 33×10^6 M^{-1}.

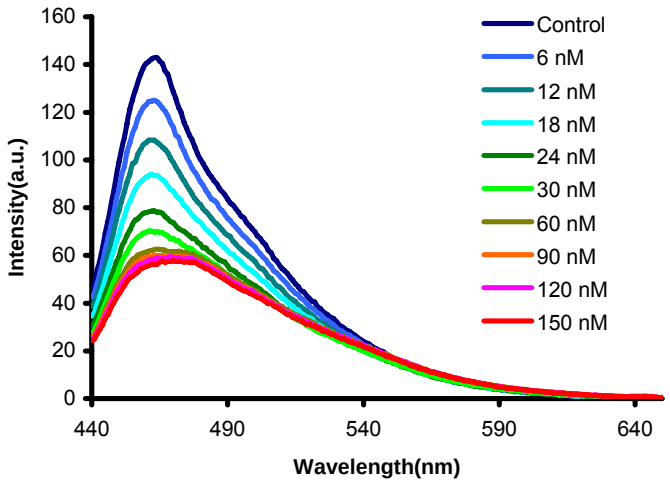

Figure 5.11. Emission spectra of solutions of **3** by addition of increasing concentrations of avidin.

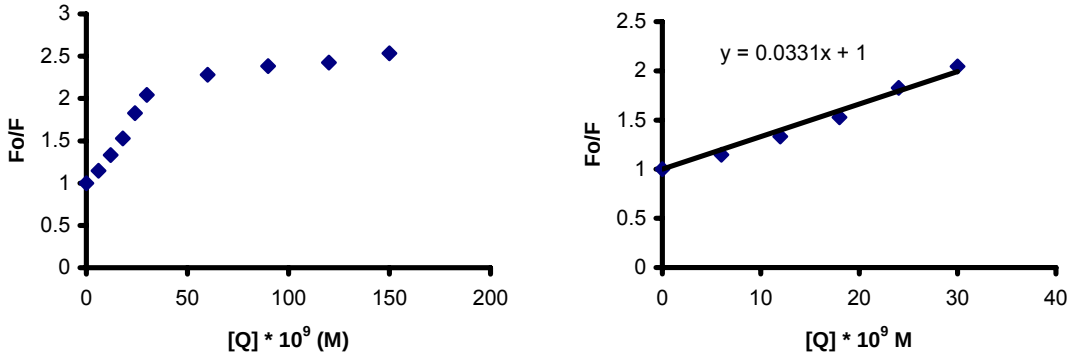

Figure 5.12. F_o/F plots for **5.5** with avidin. The apparent Stern-Volmer constant (K_{sv}) for avidin based on initial linear parts is 33×10^6 M^{-1}.

Quenching of the fluorescence of 5.5 by streptavidin-tetramethylrhodamine conjugate. A small aliquot (20-500 μL) of concentrated solutions of streptavidin-tetramethylrhodamine conjugate (1.5×10^{-6} M) was added to each vial containing 5 mL of **5.5**. The concentration of streptavidin-tetramethylrhodamine conjugate in **5.5** is 6 – 150 nM. The apparent Stern-Volmer constant (K_{sv}) based on the linear part of the curve for the streptavidin-tetramethylrhodamine conjugate is 28×10^6 M^{-1}. We observed a slight

increase of fluorescence due to the fluorescence resonance energy transfer process from PPE to tetramethylrhodamine. Without **5.5**, same concentration of streptavidin-tetramethylrhodamine conjugate showed no distinct emission.

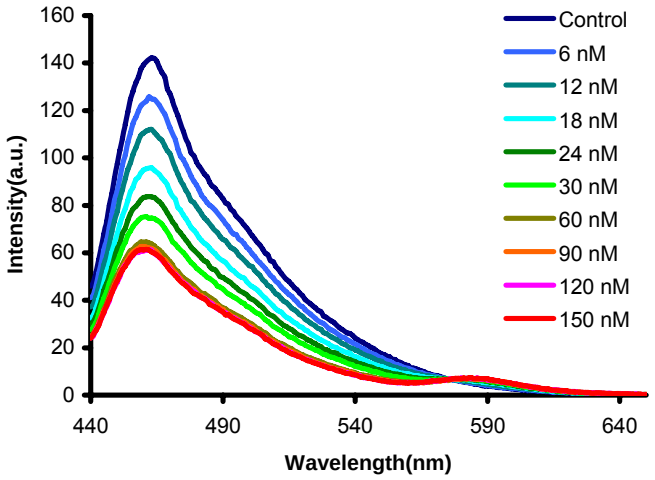

Figure 5.13. Emission spectra of solutions of **5.5** by addition of increasing concentrations of streptavidin-tetramethylrhodamine conjugate.

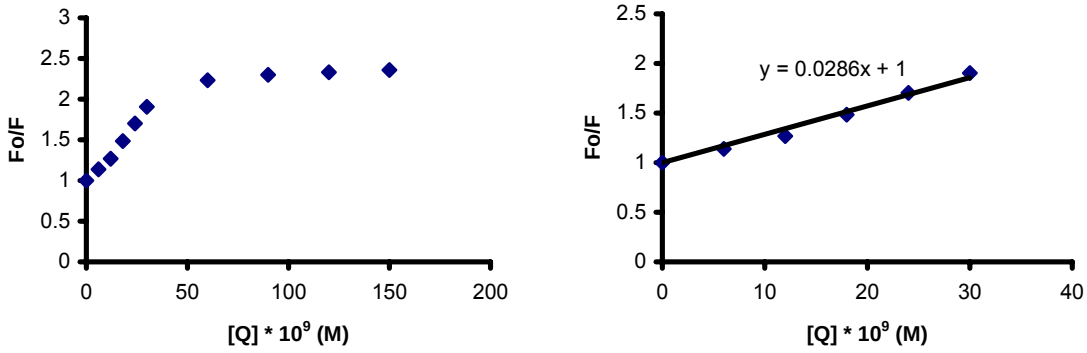

Figure 5.14. F_o/F plots for **5.5** with streptavidin- tetramethylrhodamine conjugate. The apparent Stern-Volmer constant (K_{sv}) for streptavidin-tetramethylrhodamine conjugate based on initial linear parts is 28×10^6 M^{-1}.

Quenching of the fluorescence of 5.5 by streptavidin-Texas Red conjugate. A small aliquot (20-500 μL) of concentrated solutions of streptavidin-Texas Red conjugate (1.5×10^{-6} M) was added to each vial containing 5 mL of **5.5**. The concentration of

streptavidin-Texas Red conjugate in **5.5** is 6 – 150 nM. The apparent Stern-Volmer constant (K_{sv}) based on the linear part of the curve for the streptavidin-Texas Red conjugate is 9×10^6 M^{-1}. We observed a slight increase of fluorescence due to the fluorescence resonance energy transfer process from PPE to Texas Red. The FRET efficiency in streptavidin-Texas Red is greater than that in streptavidin-tetramethylrhodamine conjugate. Without **5.5**, same concentration of streptavidin-Texas Red conjugate showed no distinct emission.

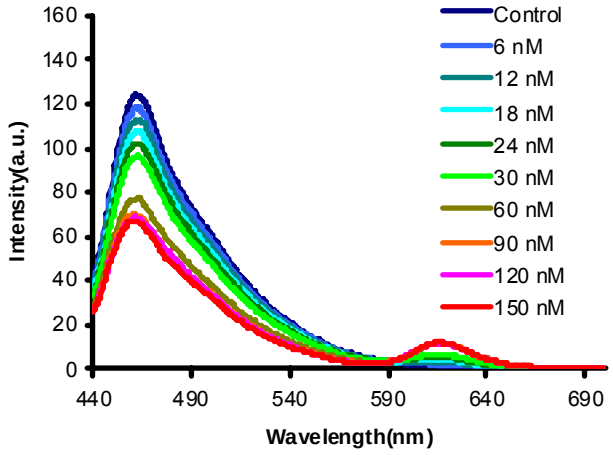

Figure 5.15. Emission spectra of solutions of **5.5** by addition of increasing concentrations of streptavidin-Texas Red conjugate.

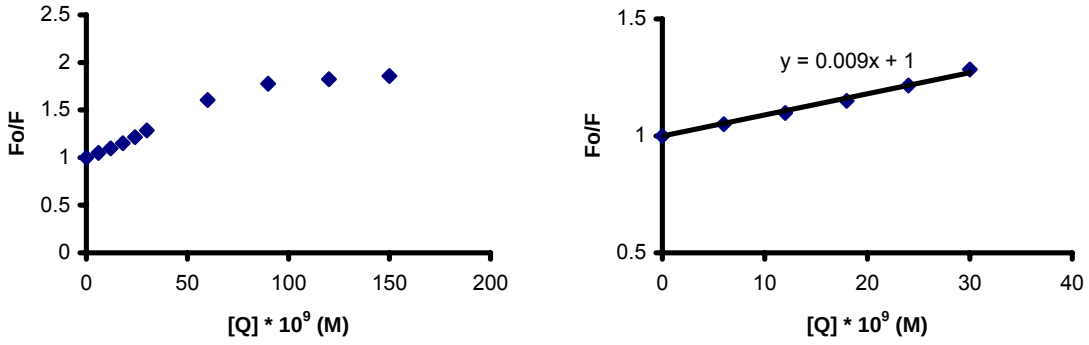

Figure 5.16. F_o/F plots for **3** with streptavidin-Texas Red conjugate. The apparent Stern-Volmer constant (K_{sv}) for streptavidin-Texas Red conjugate based on initial linear parts is 9×10^6 M^{-1}.

Concentration dependent quenching of the fluorescence of 5.5-avidin complexes by added mercury ions. A solution of avidin was added to **5.5** resulting in a 30 mM avidin solution concentration. A small aliquot (10-100 μL) of concentrated solutions of Hg(O-CO-CF_3)$_2$ (1×10^{-3} M and 1×10^{-2} M) was added to each vial containing 5 mL of a **5.5**-avidin solution. The concentration of Hg(O-CO-CF_3)$_2$ in **5.5**-avidin solution is 2 – 200 μM. In **5.5**-avidin complexes, the apparent Stern-Volmer constant (K_{sv}) for Hg^{2+} ions is 1.1×10^5 M^{-1}.

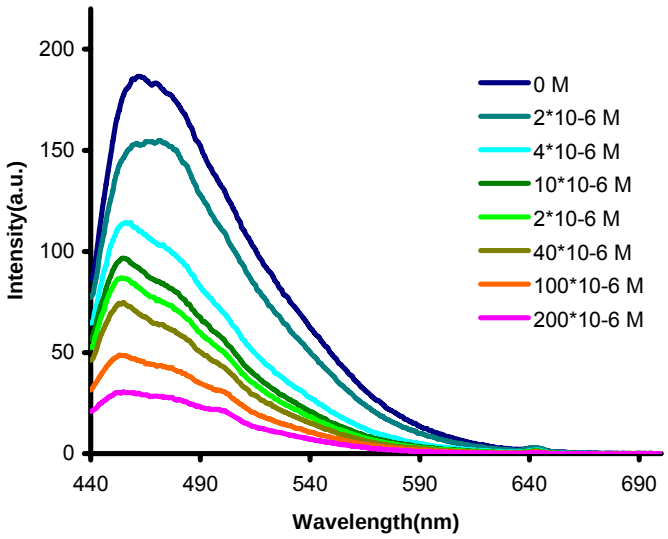

Figure 5.17. Emission spectra of solutions of **5.5-avidin** complexes by addition of increasing concentrations of mercury ions.

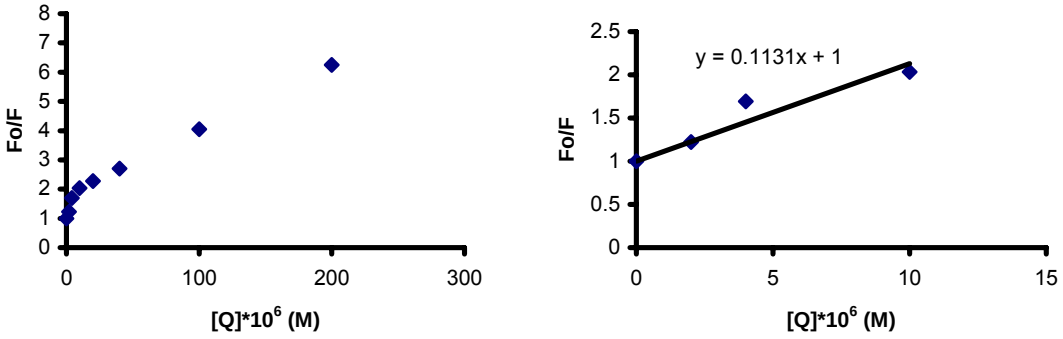

Figure 5.18. F_o/F plots for **5.5-avidin** complexes with Hg^{2+} ions. The apparent Stern-Volmer constant (K_{sv}) for Hg^{2+} ions based on initial linear parts is 1.1×10^5 M^{-1}.

Quenching of the fluorescence of 5.7 by avidin. A small aliquot (20-500 μL) of a concentrated solution of avidin (1.5×10^{-6} M) was added to each vial containing 5 mL of **5.7**. The concentration of avidin in **5.7** is 6 – 150 nM. The apparent Stern-Volmer constant (K_{sv}) based on the linear part of the curve for avidin is 2.3×10^{6} M^{-1}. Positively charged avidin interacts with negatively charged **1** to quench the fluorescence of **5.7**.

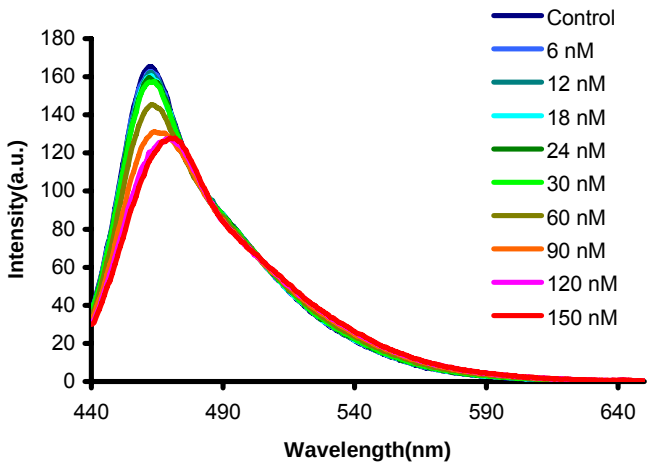

Figure 5.19. Emission spectra of solutions of **5.7** by addition of increasing concentrations of avidin.

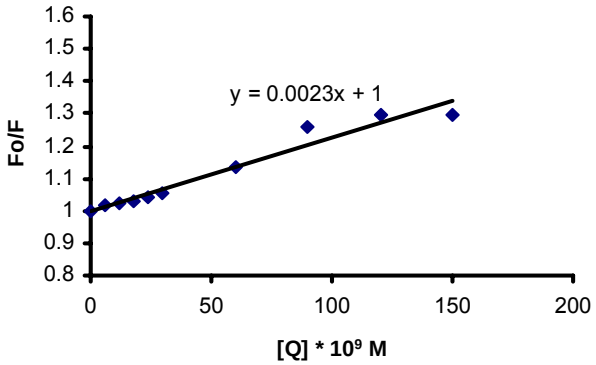

Figure 5.20. F_o/F plots for **5.7** with avidin. The apparent Stern-Volmer constant (K_{sv}) for avidin is 2.3×10^{6} M^{-1}.

Quenching of the fluorescence of PPE 5.7 by streptavidin-Texas Red conjugate. A small aliquot (50-500 μL) of a concentrated solution of streptavidin-Texas Red conjugate (1.5×10^{-6} M) was added to each vial containing 5 mL of **5.7**. The concentration of streptavidin-Texas Red conjugate in **5.7** is 15 – 150 nM.

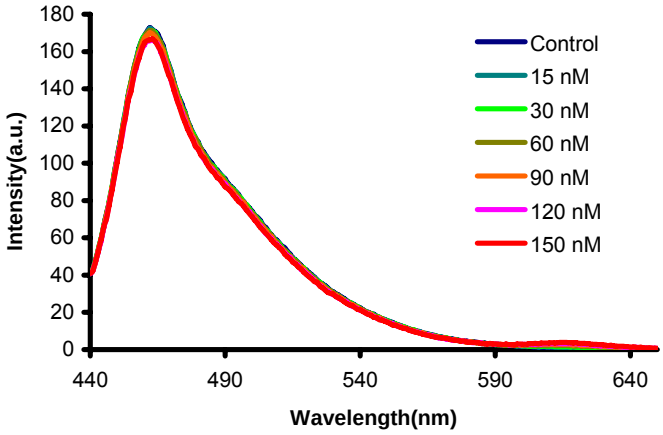

Figure 5.21. Emission spectra of solutions of **5.7** by addition of increasing concentrations of streptavidin-Texas Red conjugate.

Influence of 10 different metal ions on the optical properties of PPE 5.4 in 0.1 M phosphate buffer solution at pH = 7.2. To investigate the sensory ability of **5.4** toward metal ions, we exposed them to concentrated solutions of metal ions in a 0.1 M phosphate buffer solution (pH =7.2). The concentration of PPE **5.4** was adjusted to 1 mg/L in a phosphate buffer solution.. Solutions of 10 metal salts were prepared at a 0.1 M concentration: They are $Zn(ClO_4)_2$, $CdCl_2$, $Hg(O\text{-}CO\text{-}CF_3)_2$, $Pb(NO_3)_2$, $FeCl_3$, $NiCl_2$, $CoCl_2$, $CuBr_2$, $Ca(NO_3)_2$, and $Mg(OTf)_2$. 20 μL of each metal ion solution was added to 5 mL of a buffered solution of **5.4**. The concentration of each metal ion is 4×10^{-4} M in a buffered solution of **5.4**.

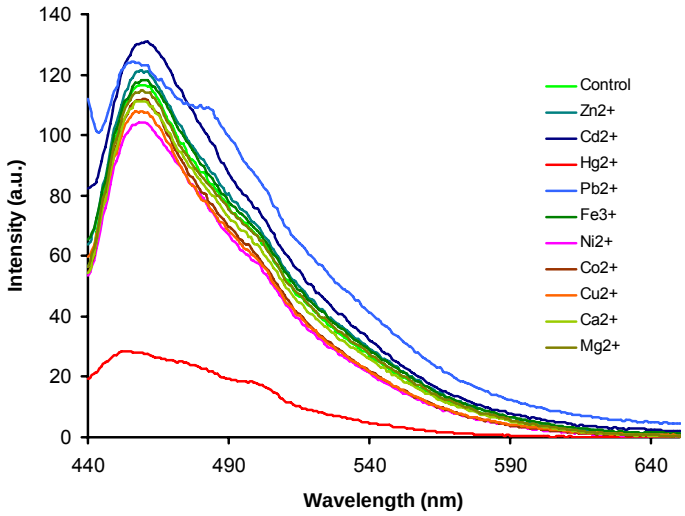

Figure 5.22. Emission spectra of **5.4** by addition of 20 μL of a 0.4 mM solution of metal ions. Spectra show significant quenching with Hg^{2+} ions.

Concentration dependent quenching of the fluorescence of PPE 5.4 by added mercury ions. A small aliquot (10-100 μL) of concentrated solutions of $Hg(O\text{-}CO\text{-}CF_3)_2$ (1×10^{-3} M and 1×10^{-2} M) was added to each vials containing 5 mL of **5.4**. The concentration of $Hg(O\text{-}CO\text{-}CF_3)_2$ in **5.4** is 2 – 200 μM. In **5.4**, the apparent Stern-Volmer constant (K_{sv}) for Hg^{2+} ions is 8×10^3. K_{sv} of **5.4** is similar to those of **5.7** and **5.5**.

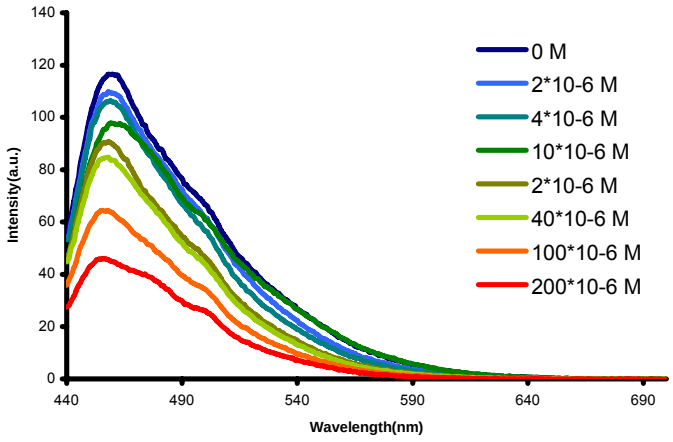

Figure 5.23. Emission spectra of solutions of **4** by addition of increasing concentrations of mercury ions.

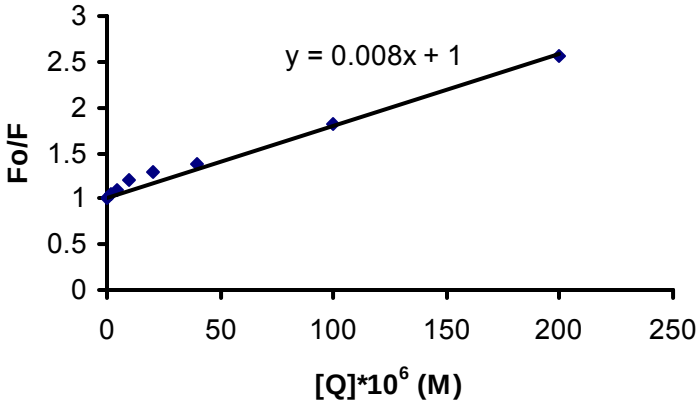

Figure 5.24. F_o/F plots for **5.4** with mercury ions. The apparent Stern-Volmer constant (K_{sv}) for Hg^{2+} ions is 8×10^3 M^{-1}.

Concentration dependent quenching of the fluorescence of PPE 5.5 by the addition of methyl viologen. A small aliquot (10-100 μL) of concentrated solutions of methyl viologen (1×10^{-3} M and 1×10^{-2} M) was added to each vial containing 5 mL of **5.5**. The concentration of methyl viologen in **5.5** is 2 – 200 μM.

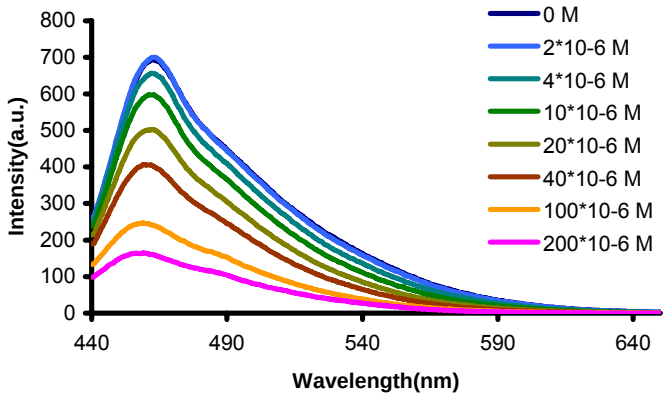

Figure 5.25. Emission spectra of solutions of **5.5** by addition of increasing concentrations of methyl viologen.

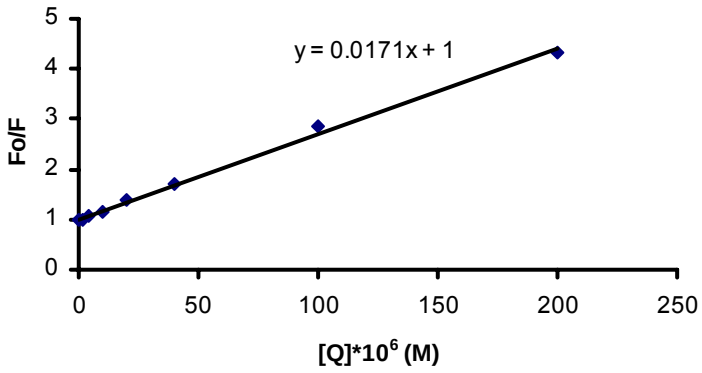

Figure 5.26. F_o/F plots for **5.5** with methyl viologen. The apparent Stern-Volmer constant (K_{sv}) for methyl viologen is 1.7×10^3 M^{-1}.

Concentration dependent quenching of the fluorescence of 5.5-avidin complexes by the addition of methyl viologen. A solution of avidin was added to **5.5** resulting in a 30 mM avidin solution concentration. A small aliquot (10-100 μL) of concentrated solutions of methyl viologen (1×10^{-3} M and 1×10^{-2} M) was added to each vial containing 5 mL of **5.5**-avidin solution. The concentration of methyl viologen in **5.5**-avidin solution is 2 – 200 μM.

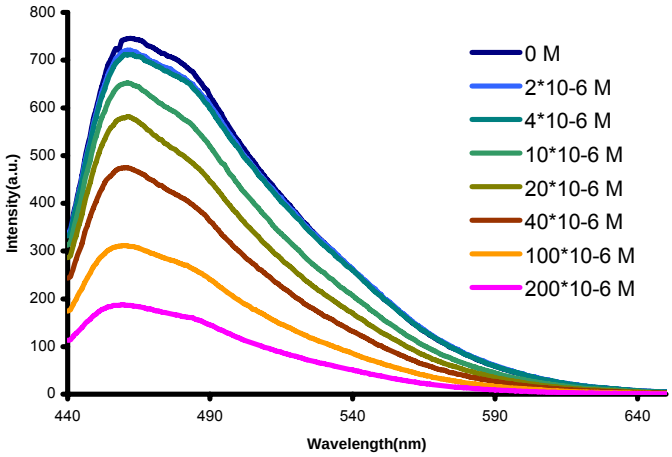

Figure 5.27. Emission spectra of solutions of **5.5-avidin** complexes by addition of increasing concentrations of methyl viologen.

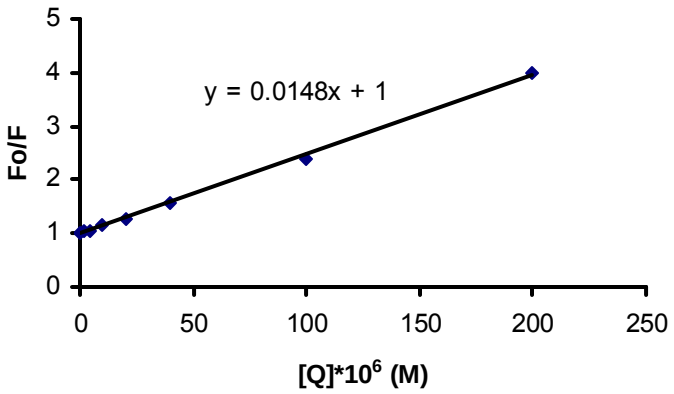

Figure 5.28. F_o/F plots for **5.5-avidin** complexes with methyl viologen. The apparent Stern-Volmer constant (K_{sv}) for methyl viologen is 1.5×10^3 M^{-1}.

Quenching of the fluorescence of PPE 5.5 by streptavidin. A small aliquot (20-500 μL) of a concentrated solution of streptavidin (1.5×10^{-6} M) was added to each vial containing 5 mL of **5.5**. The concentration of streptavidin in **5.5** is 6 – 150 nM. The apparent Stern-Volmer constant (K_{sv}) based on the linear part of the curve for streptavidin is 6.6×10^6 M^{-1}.

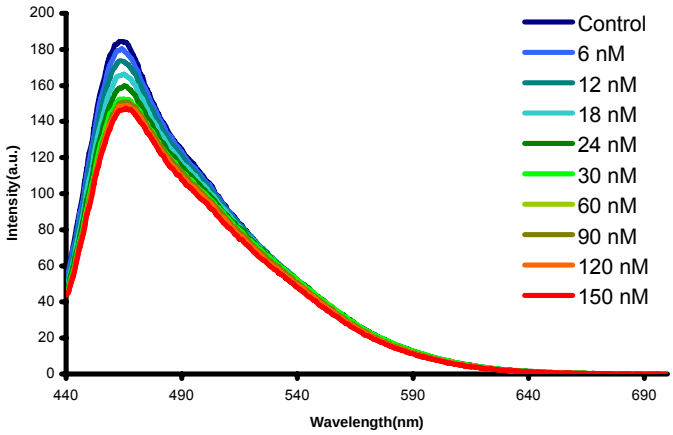

Figure 5.29. Emission spectra of solutions of **5.5** by addition of increasing concentrations of streptavidin.

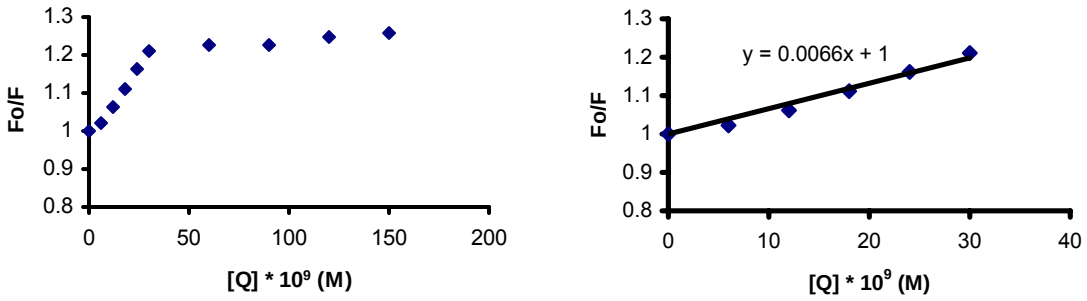

Figure 5.30. F_o/F plots for **5.5** with streptavidin. The apparent Stern-Volmer constant (K_{sv}) for streptavidin based on initial linear parts is 6.6×10^6 M^{-1}.

Quenching of the fluorescence of 5.5-streptavidin complexes by the addition of mercury ions. A solution of streptavidin was added to **5.5** resulting in a 30 mM streptavidin solution concentration. A small aliquot (10-100 μL) of concentrated solutions of $Hg(O\text{-}CO\text{-}CF_3)_2$ (1×10^{-3} M and 1×10^{-2} M) was added to each vials containing 5 mL of a **5.5**-streptavidin solution. The concentration of $Hg(O\text{-}CO\text{-}CF_3)_2$ in **5.5**-streptavidin solution is 2 – 200 μM. In **5.5**-avidin complexes, the apparent Stern-Volmer constant (K_{sv}) for Hg^{2+} ions based on initial linear parts is 5.5×10^4 M^{-1}.

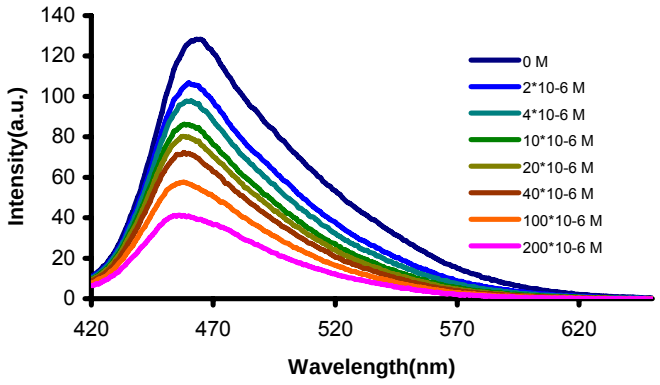

Figure 5.31. Emission spectra of solutions of **5.5**-streptavidin complexes by the addition of increasing concentrations of mercury ions.

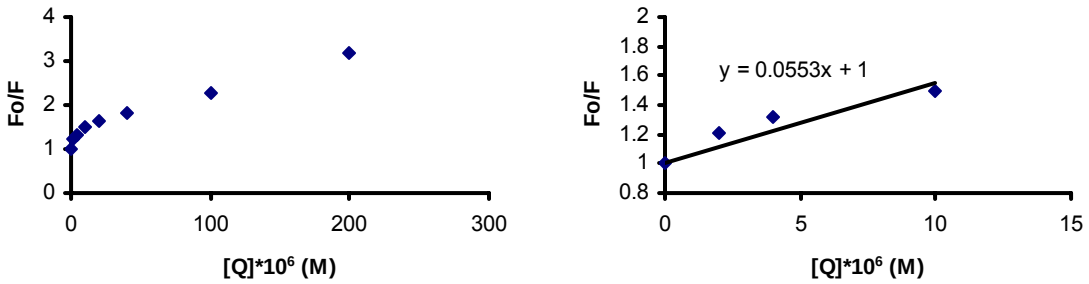

Figure 5.32. F_o/F plots for **5.5**-streptavidin complexes with mercury ions. The apparent Stern-Volmer constant (K_{sv}) for mercury ions based on initial linear parts is 5.5×10^4 M^{-1}.

Quenching of the fluorescence of 5.5-streptavidin complexes by added methyl viologen. A solution of streptavidin was added to **5.5** resulting in a 30 mM streptavidin solution concentration. A small aliquot (10-100 μL) of concentrated solutions of methyl viologen (1×10^{-3} M and 1×10^{-2} M) was added to each vial containing 5 mL of **5.5**-streptavidin solution. The concentration of methyl viologen in **5.5**-streptavidin solution is 2 – 200 μM. In **5.5**-streptavidin complexes, the apparent Stern-Volmer constant (K_{sv}) for methyl viologen is 2.3×10^3 M^{-1}.

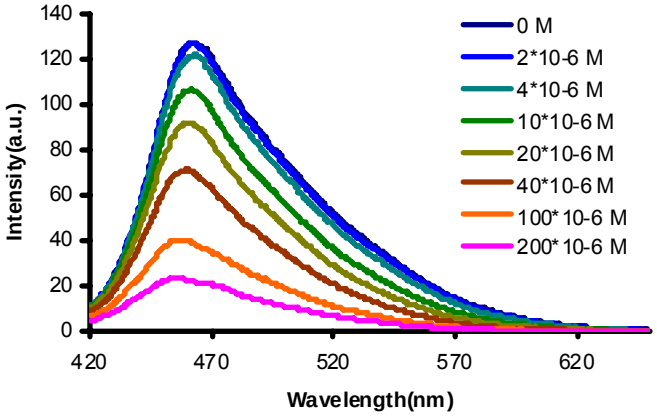

Figure 5.33. Emission spectra of solutions of **5.5**-streptavidin complexes by addition of increasing concentrations of methyl viologen.

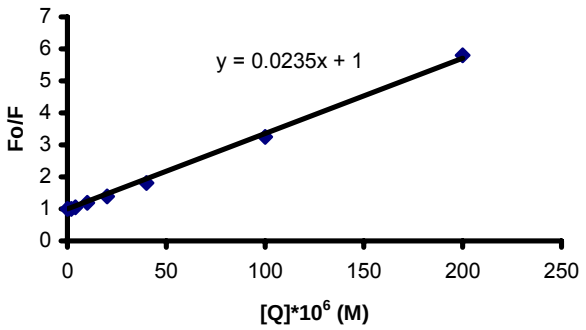

Figure 5.34. F_o/F plots for **5.5-avidin** complexes with methyl viologen. The apparent Stern-Volmer constant (K_{sv}) for methyl viologen is 2.3×10^3 M^{-1}.

5.5 References

1. (a) Zhou, Q.; Swager, T. M. "Fluorescent chemosensors based on energy migration in conjugated polymers: The molecular wire approach to increased sensitivity" *J. Am. Chem. Soc.* **1995** *117*, 12593-12602. (b) Bunz, U. H. F. "Poly(aryleneethynylene)s: Syntheses, properties, structures, and applications" *Chem. Rev.* **2000**, *100*, 1605-1644.

2. (a) Kim, I.-B.; Erdogan, B.; Wilson, J. N.; Bunz, U. H. F. "Sugar-poly(para-phenylene ethynylene) conjugates as sensory materials: Efficient quenching by Hg^{2+} and Pb^{2+} ions" *Chemistry Eur. J.* **2004**, *10*, 6247-6254. (b) Kim, I.-B.; Dunkhorst, A.; Gilbert, J.; Bunz, U. H. F. "Sensing of lead ions by a carboxylate-substituted PPE: Multivalency effects" *Macromolecules* **2005**, *38*, 4560-4562.

3. Tan, C. Y.; Alas, E.; Müller, J. G.; Pinto, M. R.; Kleiman, V. D.; Schanze, K. S. "Amplified quenching of a conjugated polyelectrolyte by cyanine dyes" *J. Am. Chem. Soc.* **2004**, *126*, 13685-13694

4. (a) Halkyard, C. E.; Rampey, M. E.; Kloppenburg, L.; Studer-Martinez, S. L.; Bunz, U. H. F. "Evidence of aggregate formation for 2,5-dialkylpoly(p-phenyleneethynylenes) in solution and thin films" *Macromolecules* **1998**, *31*, 8655-8659. (b) Kim, J.; Swager, T. M. "Control of conformational and interpolymer effects in conjugated polymers" *Nature* **2001**, *411*, 1030-1034.

5. Bunz, U. H. F.; Imhof, J. M.; Bly, R. K.; Bangcuyo, C. G.; Rozanski, L.; VandenBout, D. A. "Photophysics of poly [p-(2,5-didodecylphenylene) ethynylene] in thin films" *Macromolecules* **2005**, *38*, 5892-5896.

6. Pinto, M. R.; Schanze, K. S. "Conjugated polyelectrolytes: Synthesis and applications" *Synthesis* **2002**, 1293-1309.

7. (a) Liu, B.; Bazan, G. C. "Biosensors from conjugated polyelectrolyte complexes" *Proc. Natl. Acad. Sci.* **2002**, *99*, 49-53. (b) Dwight, S. J.; Gaylord, B. S.; Hong, J. W.; Bazan, G. C. "Perturbation of fluorescence by nonspecific interactions between anionic poly(phenylenevinylene)s and proteins: Implications for biosensors" *J. Am. Chem. Soc.* **2004**, *126*, 16850-16859.

8. (a) Ho, H. A.; Boissinot, M.; Bergeron, M. G.; Corbeil, G.; Dore, K.; Boudreau, D.; Leclerc, M. "Colorimetric and fluorometric detection of nucleic acids using cationic polythiophene derivatives" *Angew. Chem.* **2002**, *41*, 1548-1551 2002. (b) Dore, K.; Dubus, S.; Ho, H.A.; Levesque, I.; Brunette, M.; Corbeil, G.; Boissinot, M.; Boivin, G.; Bergeron, M. G.; Boudreau, D.; Leclerc, M. "Fluorescent polymeric transducer for the rapid, simple, and specific detection of Nucleic acids at the zeptomole level" *J. Am. Chem. Soc.* **2004**, *126*, 4240-4244.

9. Chen, L. H.; McBranch, D. W.; Wang, H. L.; Helgeson, R; Wudl, F; Whitten, D. G. "Highly sensitive biological and chemical sensors based on reversible fluorescence quenching in a conjugated polymer" *Proc. Natl. Acad. Sci.* **1999**, *96*, 12287-12292.

10. (a) DiCesare, N.; Pinto, M. R.; Schanze, K. S.; Lakowicz, J. R. "Saccharide detection based on the amplified fluorescence quenching of a water-soluble poly(phenylene ethynylene) by a boronic acid functionalized benzyl viologen derivative" *Langmuir* **2002**, *18*, 7785-7787 (b) Kushon, S. A.; Bradford, K.; Marin, V.; Suhrada, C.; Armitage, B. A.; McBranch, D.; Whitten, D. "Detection of single nucleotide mismatches via fluorescent polymer superquenching" *Langmuir* **2003**, *19*, 6456-6464

11. (a) Disney, M. D.; Zheng, J.; Swager, T. M.; Seeberger, P.H. "Detection of bacteria with carbohydrate-functionalized fluorescent polymers" *J. Am. Chem. Soc.* **2004**, *126*, 13343-13346. (b) Kim, I.-B.; Wilson, J. N.; Bunz, U. H. F. "Mannose-substituted PPEs detect lectins: A model for Ricin sensing" *Chem. Commun.* **2005**, 1273-1275.

12. Kim, I.-B.; Bunz, U. H. F. "Modulating the sensory response of a conjugated polymer by proteins: An agglutination assay for mercury ions in water" *J. Am. Chem. Soc.* **2006**, *128*, 2818-2819.

13. Kim, I.-B.; Dunkhorst, A.; Bunz, U. H. F. "Nonspecific interactions of a carboxylate-substituted PPE with proteins. A cautionary tale for biosensor applications" *Langmuir* **2005**, *21*, 7985-7989.

14. (a) Wilson, J. N.; Wang, Y. Q.; Lavigne, J. J.; Bunz, U. H. F. "Cruciform pi-systems: hybrid phenylene-ethynylene/phenylene-vinylene oligomers" *Chem. Commun.* **2003**, 1626-1627. (b) Dwight, S. J.; Gaylord, B. S.; Hong, J. W.; Bazan, G. C. "Perturbation of fluorescence by nonspecific interactions between anionic poly(phenylenevinylene)s and proteins: Implications for biosensors" *J. Am. Chem. Soc.* **2004**, *126*, 16850-16859.

15. (a) Tan, C. Y.; Pinto, M. R.; Kose, M. E.; Ghiviriga, I.; Schanze, K. S. "Solvent-induced self-assembly of a meta-linked conjugated polyelectrolyte. Helix formation, guest intercalation, and amplified quenching" *Adv.Mater.* **2004**, *16*, 1208-1212. (b) Jiang, H.; Zhao, X.; Schanze, K. S. "Amplified fluorescence quenching of a conjugated polyelectrolyte mediated by Ca^{2+}" *Langmuir* **2006**, *22*, 5541.

16. Carpino, L. A.; El-Faham, A.; Alberico, F. "Efficiency in peptide coupling-1-hydroxy-7-azabenzotriazle vs. 3,4-dihydro-3-hydroxy-4-oxo-1,2,3-benzotriazine" *J. Org. Chem.* **1995**, *60*, 3561-3564.

17. Stern, O.; Volmer, M. “The fading time of fluorescence” *Physikalische Zeitschrift* **1919**, *20*, 183-188.

18. Lakowicz, J. R. *Principles of Fluorescence Spectroscopy*; Kluwer Academic/Plenum Publishers: New York, 1999.

19. Tan, C. Y.; Pinto, M. R.; Schanze, K. S. “Photophysics, aggregation and amplified quenching of a water-soluble poly(phenylene ethynylene)” *Chem. Commun.* **2002**, 446-447.

20. Zheng, J.; Swager, T. M. “Biotinylated poly(p-phenylene ethynylene): unexpected energy transfer results in the detection of biological analytes” *Chem. Commun.* **2004**, 2798-2799.

21. Haskins-Glusac, K.; Pinto, M.; Tan, C.; Schanze, K. S. “Luminescence quenching of a phosphorescent conjugated polyelectrolyte” *J. Am. Chem. Soc.* **2004**, 1*26*, 14964.

22. Levitsky, I. A.; Kim, J. S.; Swager, T. M. “Energy migration in a poly(phenylene ethynylene): Determination of interpolymer transport in anisotropic Langmuir-Blodgett films” *J. Am. Chem. Soc.* **1999**, *121*, 1466.

23. Kim, I. B.; Bunz, U. H. F. “Modulating the sensory response of a conjugated polymer by proteins: An agglutination assay for mercury ions in water” *J. Am. Chem. Soc.* **2006**, 128, 2818-2819.

CHAPTER 6

Molecular Recognition Based on Polyvalent Interactioons

6.1 Introduction

Polyvalent interactions are prevalent throughout nature and play a critical role in maintaining many biological functions, including cell-cell recognition, cell adhesion, cell proliferation, signal transduction, and gene regulation.[1] Synthetic ligands containing multivalent recognition elements may selectively bind to cell-surface receptors and other components of the extracellular matrix, and thus harbor the potential to act as selective inhibitors or effectors of these processes.[2] Compared to their monovalent counter parts, the selectivity and affinity of polyvalent ligands is often superior,[3] therefore offering promising opportunities for the development of new target-specific drugs. For example, multivalent ligands have been developed to inhibit binding of pathogens to host cells,[4] to selectively target tumor cells,[5] and to stimulate immune responses.[6] Polyvalent interactions have also been exploited for designing sensitive analytical reagents. In particular, multifunctionalized synthetic polymers have demonstrated great versatility for the detection of a wide range of analytes, including DNA, metal ions, nitric oxide, lectins, proteins, and bacteria.[7]

The majority of polyvalent synthetic ligands are composed of recognition elements that display already significant selectivity towards the target site as single isolated moieties. The goal of this work was to explore whether a ligand offering multiple *non-specific* interactions might lead to selective recognition of components in the extracellular matrix (ECM) of live cells.

6.2 Results and Discussion

To assemble the individual binding elements in an organized fashion, we utilized a linear, conjugated polymer (CP) as a scaffold. CPs such as poly(*p*-phenylene-ethynylene)s (PPEs), polyfluorenes, or poly(*p*-phenylenevinylene)s are intrinsically fluorescent[8,9] and can be readily visualized by means of fluorescence microscopy. Furthermore, the addition of polar groups render CPs water-soluble without compromising their fluorescence properties.

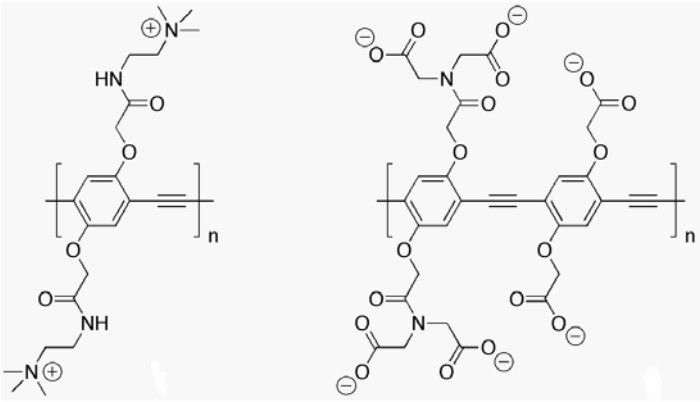

Figure 6.1. Structure of cationic functionalized PPE **6.1** (left) and anionic functionalized PPE **6.2** (right)

We utilized poly(*p*-phenyleneethynylene) as the backbone, which was either functionalized with positively charged tetra-alkyl ammonium groups (PPE **6.1**)[7j] or with negatively charged carboxylates (PPE **6.2**)[7j,9] as non-specific low-affinity binding elements.

As evidenced by Figure 6.2, the two polymers behaved distinctly different when added to live NIH 3T3 fibroblast cells in growth medium (DMEM) at 37°C for 4 hours. While the cationic PPE **6.1** yielded a punctate staining pattern reminiscent of endocytic

vesicles, the anionic PPE **6.2** showed a characteristic filamentous extracellular staining pattern.

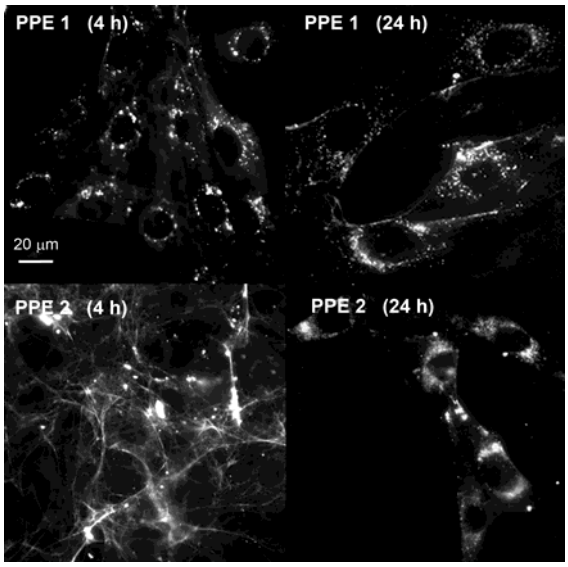

Figure 6.2. Time dependence of the interaction of PPEs with live mouse fibroblast cells (NIH 3T3). Fluorescence micrographs upon incubation with PPE **6.1** (top row) or PPE **6.2** (bottom row) at 37°C for 4 and 24 hours (25 μM polymer in DMEM).

The endocytosis of polycationic molecules, in particular derivatives of the cell penetrating peptides HIV-Tat or poly-arginine, is well documented.[10] Depending on the cargo, different uptake mechanisms might be involved; however, internalization of the cationic molecules is most likely initiated through interaction with negatively charged proteoglycans located within the extracellular matrix. Interestingly, uptake of PPE **6.1** was only partially complete within 30 min and required at least 4 h incubation time for full internalization (Figure 6.3), suggesting a mechanism that is different from receptor mediated endocytosis. Prolonged incubation for 24 h did not lead to additional changes (Figure 6.2, right).

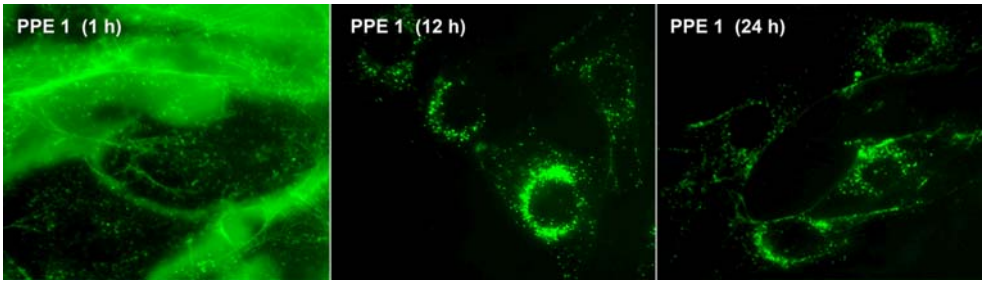

Figure 6.3. . Time dependence of fluorescence distribution of PPE **6.1** in mouse 3T3 fibroblast cells after 1 h (left), 12 h (middle), or 24 h (right) incubation in growth media (DMEM, 10% BCS).

Furthermore, the punctate staining pattern of **6.1** did not co-localize with the subcellular distribution of common endocytic markers such as the transferrin receptor, mannose-6-phosphate receptor (recycling and late endosomes), or lamp1 and lysotracker red (Figures 6.4-6.7).

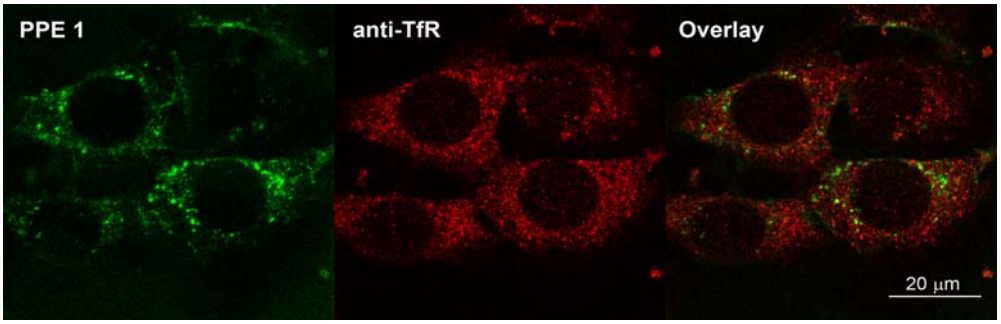

Figure 6.4. Immunofluorescence co-localization of **6.1** with anti-TfR, an antibody specific for the transferrin receptor, which is internalized via clathrin-mediated endocytosis.[20] From left to right: **a)** Fluorescence micrograph of PPE **6.1** (green). **b)** Fluorescence micrograph of anti-TfR (red). **c)** Overlay of **6.1** and anti-TfR.

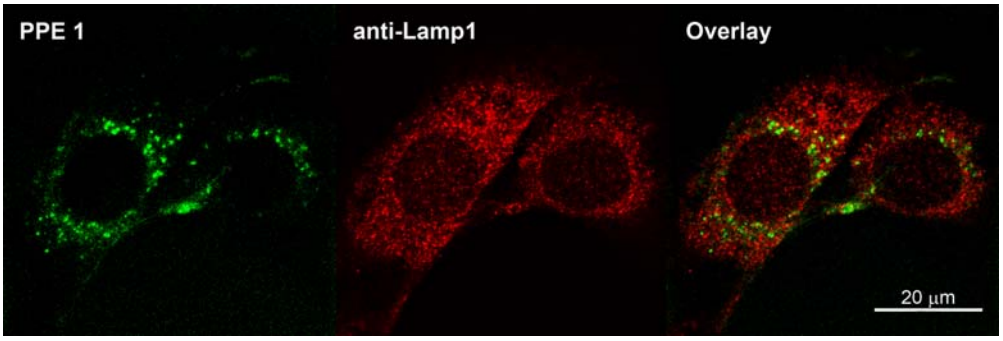

Figure 6.5. Immunofluorescence co-localization of **6.1** with anti-Lamp1, an antibody for a lysosomal glycoprotein.[18] From left to right: **a)** Fluorescence micrograph of PPE **6.1** (green). **b)** Fluorescence micrograph of anti-Lamp1 (red). **c)** Overlay of **6.1** and Lamp1.

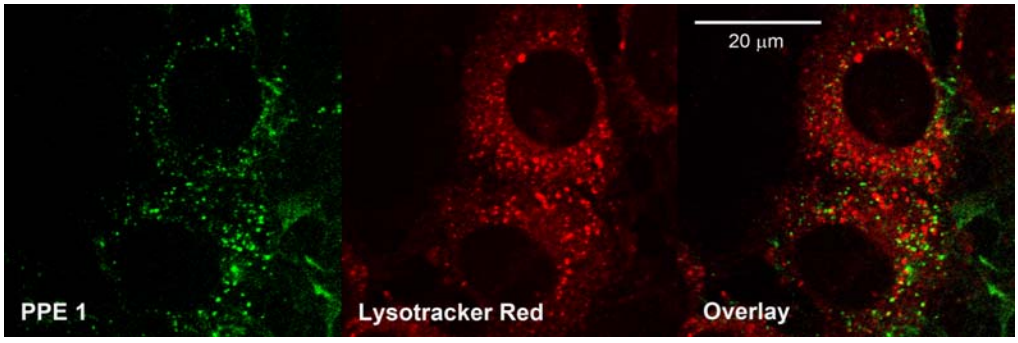

Figure 6.6. Co-localization of **6.1** with Lysotracker Red, a fluorescent probe specific for acidic vacuoles. From left to right: **a)** Fluorescence micrograph of PPE **6.1** (green). **b)** Fluorescence micrograph of Lysotracker Red (red). **c)** Overlay of **6.1** and Lysotracker Red.

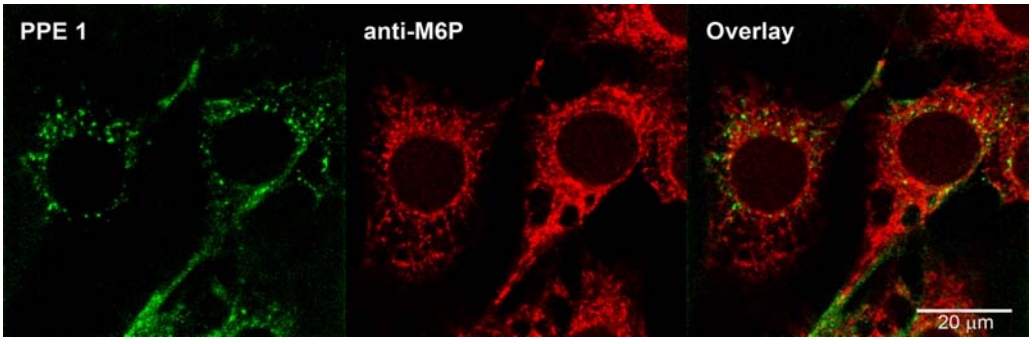

Figure 6.7. Immunofluorescence co-localization of **6.1** with anti-M6P, an antibody specific for the mannose-6-phosphate protein,[17] which is a marker for recycling and late endosomes. From left to right: **a)** Fluorescence micrograph of PPE **6.1** (green). **b)** Fluorescence micrograph of anti-M6P (red). **c)** Overlay of **6.1** and M6P.

In contrast, extracellular staining with PPE **6.2** occurred within minutes, while prolonged incubation over a period of 24 h led to almost complete internalization with a punctate staining pattern similar to that of PPE **6.1** (Figure 6.2, right).

To elucidate the nature of the interaction partner of the anionic PPE **6.2**, we performed a series of histochemical and immunofluorescence studies. In a first experiment we co-incubated live 3T3 cells with PPE **6.2** and phalloidin-546, a specific histochemical reagent for visualizing the distribution of filamentous actin (F-actin). As shown in Figure 6.8, only few areas of overlap were observed; however, a closer inspection of the dual-fluorescence micrograph showed that the PPE staining pattern appeared to some degree aligned with F-actin.

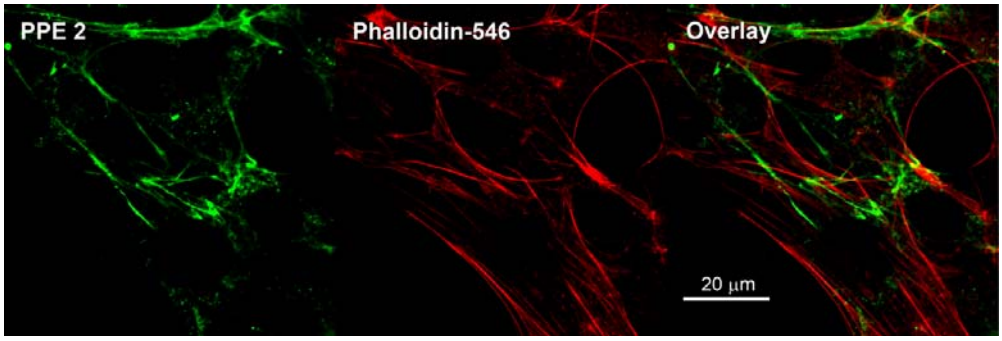

Figure 6.8. Immunofluorescence co-localization of **6.2** with phalloidin-546, a Histochemical reagent for F-actin. From left to right: Fluorescence Micrograph of NIH 3T3 cells stained with PPE **6.2** (green), phalloidin-546 (red), and false color overlay of **6.2** and phalloidin-546.

We thus hypothesized that **6.2** might bind to fibronectin, an extracellular matrix protein, which is known to interact with actin filaments at specific locations within the ECM. Immunofluorescence staining using a commercially available antibody against

fibronectin revealed an almost perfect co-localization with PPE **6.2**, as demonstrated by the yellow areas in the false-color confocal micrograph (Figure 6.9).

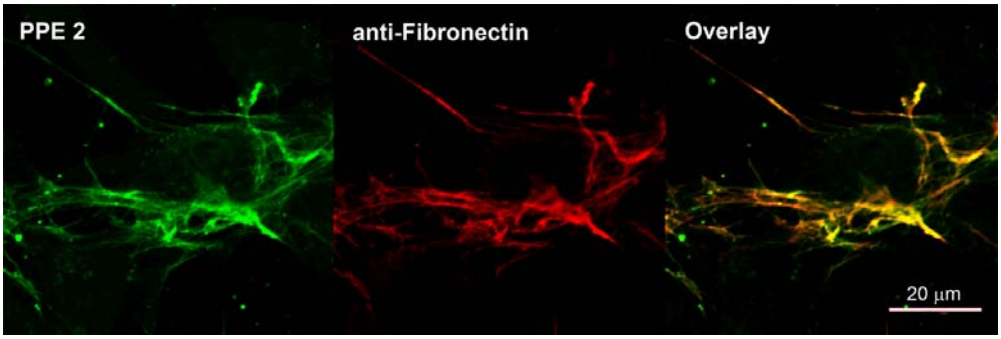

Figure 6.9. Immunofluorescence co-localization of **6.2** with an antibody specific for fibronectin. From left to right: Fluorescence micrograph of NIH 3T3 cells stained with PPE **6.2** (green), anti-fibronectin (red), and false color overlay (areas of co-localization are revealed in orange/yellow).

While the immunofluorescence experiments demonstrate microscopic co-localization of PPE **6.2** with anti-fibronectin, the spatial resolution is insufficient to demonstrate binding on a molecular level. It is conceivable that the polymer might associate only indirectly through another protein with the fibrils. To directly probe the interaction of PPE **6.2** with fibronectin, we performed an *in vitro* binding assay. Fibronectin was adsorbed at different densities on the glass surface of a 96-well plate, then exposed to increasing concentrations of PPE **6.2**, and upon equilibration for 1 h washed to remove unbound polymer. The degree of complex formation was then directly assessed with a microplate reader on basis of the fluorescence intensity of fibronectin-bound polymer. As illustrated in Figure 6.10, the fluorescence increased not only with increasing polymer concentration, but also as a function of the fibronectin surface

density. In absence of fibronectin, PPE **6.2** showed only little adsorption on the glass surface (control).

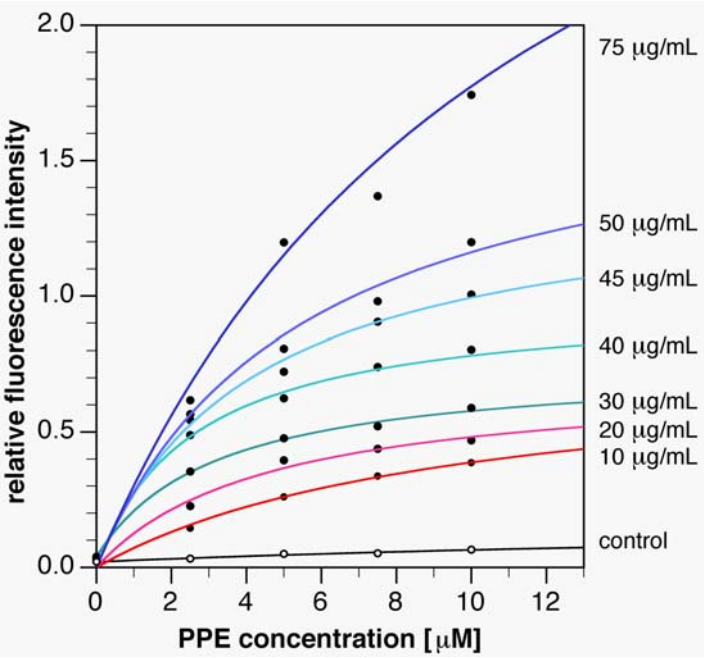

Figure 6.10. Binding assay of PPE **6.2** with surface adsorbed fibronectin. The glass surface of a 96-well plate was incubated with different concentrations of fibronectin as indicated on the right side of the graph. Changes in fluorescence intensities (λ_{ex} = 410 nm, λ_{em} = 460 nm) with varying concentrations of **6.2** (based on monomer Mw) were measured with a plate reader, and the resulting binding isotherms were fitted with Eq. 6.1. Control: fluorescence change in absence of fibronectin.

To test for non-specific binding to a protein other than fibronectin, we adsorbed bovine serum albumin (BSA) on the glass surface. Titration with increasing concentrations of PPE **6.2** showed no interactions beyond the level of the control in absence of a protein (Figure 6.11).

Assuming full equilibration and a slow dissociation rate of polyvalently bound polymer,[11] the changes in fluorescence intensity F can be interpreted as Langmuir isotherms according to equation 6.1,[12]

$$F = \frac{F_{max}[P]_0}{K_D + [P]_0} \qquad \textbf{Eq. 6.1}$$

where F_{max} is the maximum fluorescence intensity (a measure of the binding capacity), $[P]_0$ is the total polymer concentration, and K_D is the equilibrium dissociation constant of the polymer-fibronectin complex adsorbed on the glass surface.

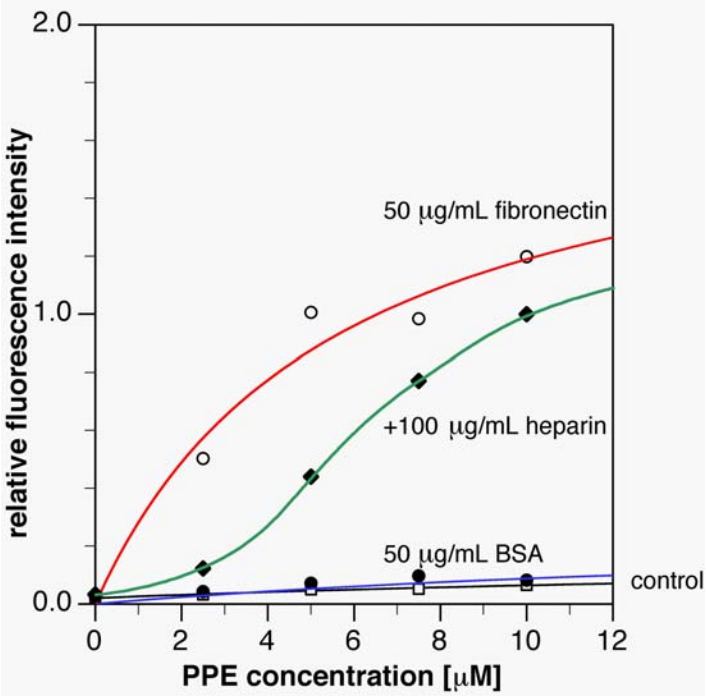

Figure 6.11. Binding assay of PPE **6.2** with surface adsorbed fibronectin (red trace) or bovine serum albumin (BSA, blue trace). The glass surface of a 96-well plate was incubated with 50 µg/mL of fibronectin or BSA. Changes in fluorescence intensities with increasing concentration of **6.2** were measured with a plate reader (λ_{ex} = 410 nm, λ_{em} = 460 nm) and fitted as Langmuir isotherms using Eq. 6.1. In the presence of 100 µg/mL heparin sulfate, binding of PPE **6.2** to fibronectin adsorbed at 50 µg/mL was markedly reduced (green trace). The control trace (black) corresponds to nonspecific binding of the polymer to the glass surface in absence of any surface adsorbed proteins.

A comparison of the dissociation constants K_D obtained from analysis of each binding isotherm revealed a rather narrow distribution (Table 6.1). At a fibronectin coating concentration of 100 μM the surface density reached saturation as reflected by the converging F_{max} values. Averaging over the intermediate fibronectin coating concentration range of 20-50 μM, an apparent dissociation constant of 3.8 ± 1.3 μM was calculated (based on monomer molecular weight). Considering the average molecular weight M_n = 36 kDa of polymer **6.2**,[9] the apparent dissociation constant of the fibronectin-polymer complex is approximately 100 nM, a value that is in agreement with the polyvalent nature of the interaction. It is noteworthy that the avidity of the polymer-fibronectin complex lies in a similar range compared to the multivalent carbohydrate-lectin interactions.[13]

Table 6.1. Dissociation constants for the interaction of PPE **6.2** with fibronectin adsorbed to a glass surface[a]

fibronectin[b] [μg/mL]	KD[c] [μM]	stdev[d] [μM]	Fmax
10	7.4	2.1	66 (±12)
20	4.5	0.3	67 (±10)
30	2.3	0.2	68 (±1)
40	2.6	0.1	98 (±1)
45	4.2	0.3	141 (±4)
50	5.4	0.1	179 (±2)
75	11.8	0.6	387 (±13)
100	11.5	0.5	389 (±12)

[a]pH 7.2, 10 mM PIPES buffer, 25°C. [b]concentration of surface coating solution. [c]dissociation constant based on monomer Mw. [d]standard deviation of KD obtained from nonlinear least-squares fit with Eq.6.1.

While we can only speculate about the nature of the fibronectin binding sites that interact with PPE **6.2**, recent structural data of several fibronectin domains revealed an

extended area of positive charge within FN repeats 12-14, a location that is involved in binding of polyanionic heparin.[14] Repeating the above *in vitro* assay in the presence of 100 μg/mL heparin sulfate yielded a marked reduction of PPE **6.2** binding to fibronectin (Figure 6.11), thus supporting this hypothesis.

Encouraged by these results, we tested next the performance of the PPEs as fluorescent dyes for two-photon excitation microscopy (TPEM). Improved depth penetration in tissue samples, significantly reduced background excitation of endogenous molecules, as well as reduced phototoxicity combined with a small excitation volume suitable for 3D-imaging have rendered TPEM the preferred imaging modality over conventional confocal laser scanning microscopy. The brightness of each PPE was evaluated over a range of wavelengths in chemically fixed cells revealing the optimum excitation wavelength of 710 nm for PPE **6.1**, and a longer wavelength of 760 nm for the negatively charged PPE **6.2**. Both polymers showed bright fluorescence emission combined with good photostability that renders them well suited for TPEM (Figure 6.12).

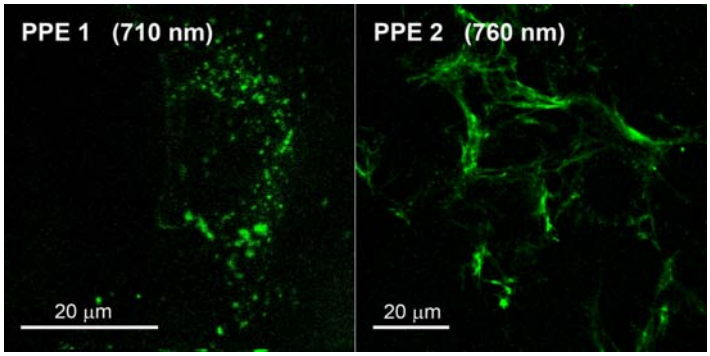

Figure 6.12. Two-photon excitation microscopy of PPEs interacting with live mouse fibroblast cells. Cells were incubated with PPE **6.1** (left, λ_{ex} = 710 nm) or PPE **6.2** (right, λ_{ex} = 760 nm) in DMEM at 37°C for 4 h.

To further evaluate the applicability of PPE **6.1** and **6.2** in live cell studies, we assessed their acute toxicity as a function of PPE concentration and incubation time using the trypan blue exclusion assay. According to these studies, the cell viability remained unchanged within 6-8% of untreated cells up to a concentration of 50 μM and for as long as 24 h. Only when incubated at a concentration of 100 μM PPE over 24 h, the viability decreased by approximately 10% compared to untreated cells (Figure 6.13).[5b]

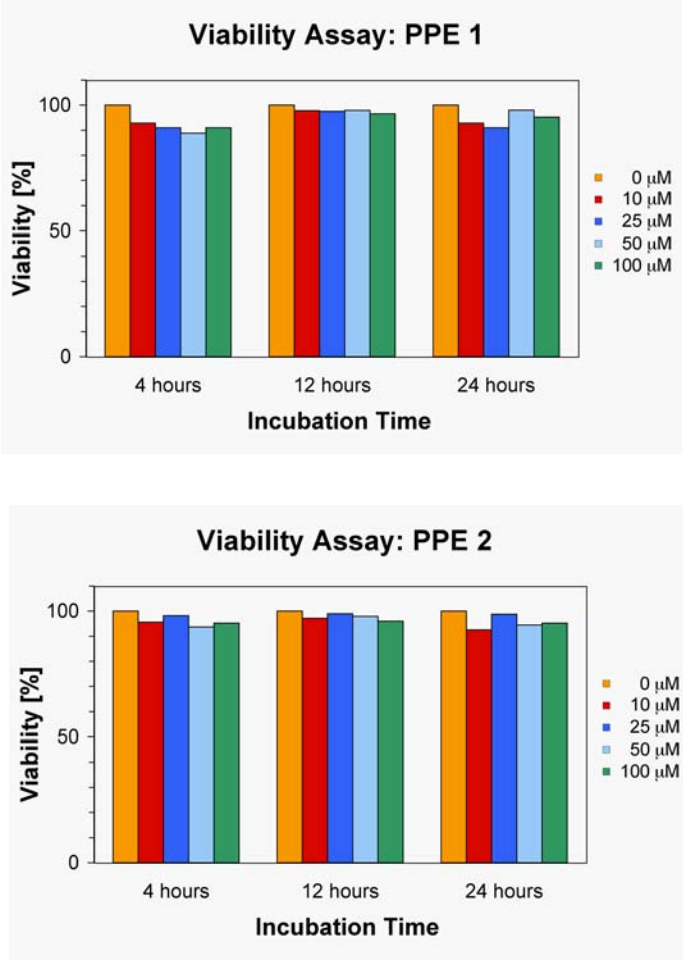

Figure 6.13. Cell viability based on trypan blue exclusion assays.[5] Percentage of viable cells after incubations in growth media (DMEM, 10% BCS) with a range of concentrations of PPE **6.1** (top) or PPE **6.2** (bottom) for 4, 12, or 24 h.

6.3 Conclusion

In conclusion, the polyvalent nature of carboxylated PPE **6.2** leads to selective recognition of the extracellular matrix protein fibronectin. This observation is particularly intriguing considering the intrinsically low affinity of a single carboxylic acid moiety towards a potential target site and the simple topology of the non-chiral, linear polymer backbone. Furthermore, the internalization of the anionic polymer **6.2** upon prolonged incubation is noteworthy, since negatively charged molecules are typically not readily transported into live cells.

Fibronectin participates in an array of essential biological processes, and is also vital for the progress of numerous diseases, including cancer cell survival as well as bacterial or viral infections. This relevance has sparked interest in elucidating the nature and role of its many binding partners and the mechanism of fibronectin fibril assembly.[15] Given the biological importance of fibronectin, its specific recognition by a structurally uniform polymer underscores the utility of weak non-specific polyvalent interactions for the design of new synthetic ligands.

These non-specific interactions between conjugated polymers and proteins could be quite useful for the design and implementation of fluorescence based detection assays for the identification and quantification of proteins.

6.4 Experimental

Reagents. The conjugated polymers PPE **6.1** and **6.2** were synthesized according to previously published procedures.[7] Phalloidin-546 was purchased from Invitrogen. Goat

anti-mouse IgG Alexa Fluor 546 and goat anti-rabbit IgG Alexa Fluor 633 secondary antibodies were purchased from Invitrogen, rabbit anti-fibronectin (human)[16] was obtained from Sigma-Aldrich. Mouse anti-mannose-6-phosphate receptor (bovine calf liver)[17] and mouse anti-LAMP-1[18] (human) were obtained from the Developmental Studies Hybridoma Bank (University of Iowa).

Cell Culture. NIH 3T3 mouse cells were cultured at 37°C (5% CO_2) in Dulbecco's modified Eagle's medium (DMEM) containing 10% bovine serum supplemented with 4 mM L-glutamine.

Fluorescence Microscopy and Image Analysis. For PPE incubation experiments, cells were grown on coverslips to 50-70% confluency, incubated with 25 μM PPE in growth media for 1 h at 37°C in a 5% CO_2 atmosphere, washed with PBS, and either fixed with 3.7% PFA for 30 min prior to mounting the coverslips onto slides with ProLong (Molecular Probes) or directly mounted onto slides with Fluoromount-G (SouthernBiotech).

For immunofluorescence analysis, cells were fixed at room temperature for 30 min with pre-warmed (37°C) 3.7% paraformaldehyde (PFA) freshly prepared in PBS (pH 7.2). The cells were subsequently permeabilized with 0.2% Triton X-100 in PBS (pH 7.2) for 5 min and incubated for 1 h in blocking buffer (Pierce Superblock). Cells were then incubated with either anti-fibronectin (1:100 dilution) or Phalloidin-546 (1.5 U/mL) for 1 h or 20 min respectively. Samples were washed thoroughly with 0.05% Tween20 in PBS, and anti-fibronectin samples were incubated with the secondary antibody anti-rabbit Alexa Fluor 633 (1:1000 dilution) for 1 h. Cells were again washed with Tween20 to

remove any unbound antibodies. The coverslips were then mounted onto slides using ProLong Antifade (Invitrogen) mounting medium.

Images were acquired using a 100X oil immersion objective on a Zeiss LSM Confocal/NLO 510 microscope equipped with Argon 488, Krypton 568, HeNe 633, and NLO/UV 800 lasers. For multicolor imaging, fluorescent dyes were imaged sequentially to eliminate crosstalk between channels. Gray-scale images (12 bit) were subsequently processed to give red/green pseudo-color panels using Adobe Photoshop.

The suitability of the PPE to be visualized by two-photon excitation was investigated using the NLO/UV laser of the confocal microscope. A range of wavelengths extending above and below the absorption maximum (425 nm) doubled were tested initially in cells pre-fixed with 3.7% PFA followed by incubation with 25 μM PPE for 45 min at room temperature. Although fixing the cells prior to incubating with the PPE alters the PPE distribution with respect to that of live cells, this incubation results in a rather homogenous PPE distribution thus providing optimal conditions for determining the optimum wavelength for two-photon excitation. Two-photon excitation at the optimized excitation wavelength of 760 nm was subsequently used to image the PPE distribution in live cells.

Cell Viability Assay. The toxicity of PPE incubations was monitored using the Trypan Blue Exclusion assay.[19] This assay provides viability information in terms of whether or not the integrity of a cell's plasma membrane has or has not been altered by incubations with exogenous molecules. Cells were plated on 48-well plates and incubated with a range of PPE concentrations (0 μM, 10 μM, 25 μM, 50 μM, or 100 μM) over varying periods (4 h, 12 h, and 24 h). A hemacytometer was used to assess cell viability

determined by counting the number of nonviable cells (stained blue) present relative to the total number of cells. Viability was measured as a percentage of the control sample for each time point (control = 0 μM PPE). These studies as well as individual sample counts were performed in triplicate.

PPE 6.2/Fibronectin *In Vitro* Binding Assay. Human plasma fibronectin was purchased from Invitrogen and stored at –20°C in sterile dH_2O. Sterile 96-well plates (Greiner Bio-One flat glass bottom plates) were coated with 50 μL of freshly prepared fibronectin solution at the concentrations indicated in Figure 6.10 and incubated at 4°C overnight. After removing the incubation solution, the plates were carefully washed with 150 μL of PBS buffer solution and blocked against non-specific binding with 125 μL of Pierce SuperBlock solution for 1 h at 4°C. The plates were then incubated with 75 μL of PPE **6.2** solution for 1 h at room temperature. After removal of the PPE, the plates were quickly washed 4 times with 125 μL of PBS buffer solution. Finally, each well was rehydrated with 50 μL of PBS solution and the fluorescence intensity was monitored with a microplate reader (SpectraMax, Molecular Devices; λ_{ex} = 410 nm, λ_{em} = 460 nm). Changes in fluorescence intensity were analyzed as Langmuir isotherms assuming a 1:1 binding interaction between immobilized fibronectin and polymer PPE **6.2** (P) according to equation (Eq. 6.1). To test for non-specific binding to proteins other than fibronectin, the glass surface of a 96-well plate was coated with bovine serum albumin (BSA) at a concentration of 50 μg/mL. The binding assay with PPE **6.2** was carried out as described above for fibronectin. To test for competitive binding of heparin sulfate to fibronectin, fibronectin adsorbed to the glass surface was preincubated with a freshly prepared solution of heparin sulfate (100 μg/mL) prior to addition of the polymer solution

6.5 References

1. Mammen, M.; Choi, S. K.; Whitesides, G. M. "Polyvalent interactions in biological systems: implications for design and use of multivalent ligands and inhibitors" *Angew. Chem., Int. Ed. Engl.* **1998**, 37, 2755-2794.

2. Kiessling, L. L.; Gestwicki, J. E.; Strong, L. E. "Synthetic multivalent ligands in the exploration of cell-surface interactions" *Curr. Opin. Chem. Biol.* **2000**, 4, 696-703.

3. Kitov, P. I.; Bundle, D. R. "On the nature of the multivalency effect: a thermodynamic model" *J. Am. Chem. Soc*. **2003**, 125, 16271-16284.

4. a) Kitov, P. I.; Sadowska, J. M.; Mulvey, G.; Armstrong, G. D.; Ling, H.; Pannu, N. S.; Read, R. J.; Bundle, D. R. "Shiga-like toxins are neutralized by tailored multivalent carbohydrate ligands" *Nature* **2000**, 403, 669-672; b) Mourez, M.; Kane, R. S.; Mogridge, J.; Metallo, S.; Deschatelets, P.; Sellman, B. R.; Whitesides, G. M.; Collier, R. J. "Designing a polyvalent inhibitor of anthrax toxin" *Nat. Biotechnol.* **2001**, 19, 958-961; c) Fan, E. K.; Zhang, Z. S.; Minke, W. E.; Hou, Z.; Verlinde, C.; Hol, W. G. J. "High-affinity pentavalent ligands of escherichia coli heat-labile enterotoxin by modular structure-based design" *J. Am.Chem. Soc*. **2000**, 122, 2663-2664; d) Reuter, J. D.; Myc, A.; Hayes, M. M.; Gan, Z. H.; Roy, R.; Qin, D. J.; Yin, R.; Piehler, L. T.; Esfand, R.; Tomalia, D. A.; Baker, J. R. "Inhibition of viral adhesion and infection by sialic-acid-conjugated dendritic polymers" *Bioconjugate Chem*. **1999**, 10, 271-278.

5. a) Carlson, C. B.; Mowery, P.; Owen, R. M.; Dykhuizen, E. C.; Kiessling, L. L. "Selective tumor cell targeting using low-affinity, multivalent interactions" *ACS Chem. Biol.* **2007**, 2, 119-127. b) Kim I. B.; Shin H.; Garcia A. J.; Bunz U. H. F. "Use of a folate-PPE conjugate to image cancer cells in vitro" *Bioconjugate Chem.* ***2007***, 18, 815-820.

6. Puffer, E. B.; Pontrello, J. K.; Hollenbeck, J. J.; Kink, J. A.; Kiessling, L. L. "Activating B cell signaling with defined multivalent ligands" *ACS Chem. Biol.* **2007**, 2, 252-262.

7. a) Disney, M. D.; Zheng, J.; Swager, T. M.; Seeberger, P. H. "Detection of bacteria with carbohydrate-functionalized fluorescent polymers" *J. Am. Chem. Soc*. **2004**, 126, 13343-13346; b) Fan, C. H.; Plaxco, K. W.; Heeger, A. J. "High-efficiency fluorescence quenching of conjugated polymers by proteins" *J. Am. Chem. Soc.* **2002**, 124, 5642-5643; c) Kim, I. B.; Dunkhorst, A.; Gilbert, J.; Bunz, U. H. F. "Sensing of lead ions by a carboxylate-substituted PPE: multivalency effects" *Macromolecules* **2005**, 38, 4560-4562; d) Kim, I. B.; Phillips, R.; Bunz, U. H. F. "Forced agglutination as a tool to improve the sensory response of a carboxylated poly(p-phenyleneethynylene)" *Macromolecules* **2007**, 40, 814-817; e) Kim, I. B.; Wilson, J. N.; Bunz, U. H. F. "Mannose-substituted PPEs detect

lectins: A model for Ricin sensing" *Chem. Commun.* **2005**, 1273-1275; f) Pieters, R. J. "Interference with lectin binding and bacterial adhesion by multivalent carbohydrates and peptidic carbohydrate mimics" T*rends Glycosci. Glycotechnol*. **2004**, 16, 243-254; g) Smith, R. C.; Tennyson, A. G.; Lim, M. H.; Lippard, S. "Conjugated polymer-based fluorescence turn-on sensor for nitric oxide" *J. Org. Lett.* **2005**, 7, 3573-3575; h) You, C. C.; Miranda, O. R.; Gider, B.; Ghosh, P. S.; Kim, I. B.; Erdogan, B.; Krovi, S. A.; Bunz, U. H. F.; Rotello, V. M. "Detection and identification of proteins using nanoparticle-fluorescent polymer 'chemical nose' sensors" *Nat. Nanotechnol* **2007**, 2, 318-323; i) Xue, C. H.,; Jog, S. P.; Murthy, P.; Liu H. Y. "Synthesis of highly water-soluble fluorescent conjugated glycopoly(p-phenylene)s for lectin and escherichia coli" *Biomacromolecules* **2006**, 7, 2470-2474. j) Miranda, O. R.; You, C. C.; Phillips, R.; Kim, I. B.; Ghosh, P. S.; Bunz, U. H. F.; Rotello, V. M. "Array-based sensing of proteins using conjugated polymers" *J. Am. Chem. Soc.* **2007**, 129, 9856-9857.

8. a) Bunz, U. H. F. "Poly(aryleneethynylene)s: syntheses, properties, structures, and applications" *Chem. Rev.* **2000**, 100, 1605-1644; b) Gaylord, B. S.; Heeger, A. J.; Bazan, G. C. "DNA detection using water-soluble conjugated polymers and peptide nucleic acid probes" *Proc. Natl. Acad. Sci. U. S. A.* **2002**, 99, 10954-10957; c) Ho, H. A.; Boissinot, M.; Bergeron, M. G.; Corbeil, G.; Dore, K.; Boudreau, D.; Leclerc, M. "Colorimetric and fluorometric detection of nucleic acids using cationic polythiophene derivatives" *Angew. Chem., Int. Ed. Engl.* **2002**, 41, 1548-1551; d) Thomas, S. W.; Joly, G. D.; Swager, T. M. "Chemical sensors based on amplifying fluorescent conjugated polymers" *Chem. Rev.* **2007**, 107, 1339-1386.

9. Kim, I. B.; Phillips, R.; Bunz, U. H. F. "Carboxylate group side-chain density modulates the pH-dependent optical properties of PPEs" *Macromolecules* **2007**, 40, 5290-5293.

10. Joliot, A.; Prochiantz, A. "Transduction peptides: from technology to physiology" *Nat. Cell Biol*. **2004**, 6, 189-196.

11. Horan, N.; Yan, L.; Isobe, H.; Whitesides, G. M.; Kahne, D. "Nonstatistical binding of a protein to clustered carbohydrates" *Proc. Natl. Acad. Sci. U. S. A.* **1999**, 96, 11782-11786.

12. a) Langmuir, I. "Constitution and fundamental properties of solids and liquids. I. Solids" *J. Am. Chem. Soc*. **1916**, 38, 2221-2295; b) Ekins, R. P. "Ligand assays: from electrophoresis to miniaturized microarrays" *Clinical Chem.* **1998**, 44, 2015-2030.

13. a) Liang, P. H.; Wang, S. K.; Wong, C. H. "Quantitative analysis of carbohydrate-protein interactions using glycan microarrays: determination of surface and solution dissociation constants" *J. Am. Chem. Soc*. **2007**, 129,

11177-11184; b) Duverger, E.; Frison, N.; Roche, A. C.; Monsigny, M. "Carbohydrate-lectin interactions assessed by surface plasmon resonance" *Biochimie* **2003**, 85, 167-179.

14. Sharma, A.; Askari, J. A.; Humphries, M. J.; Jones, E. Y.; Stuart, D. I. "Crystal structure of a heparin- and integrin-binding segment of human fibronectin" EMBO J. 1999, 18, 1468-1479.

15. Mao, Y.; Schwarzbauer, J. E. "Fibronectin fibrillogenesis, a cell-mediated matrix assembly process" *Matrix Biol.* **2005**, 24, 389-399.

16. Garbarsch, C.; Matthiessen, M. E.; Olsen, B. E.; Moe, D.; Kirkeby, S. "Immunohistochemistry of the intercellular matrix components and the epithelio-mesenchymal junction of the human tooth germ" *Histochem. J.* **1994**, *26*, 110-118.

17. Messner, D. J. "The mannose receptor and the cation-dependent form of mannose 6-phosphate receptor have overlapping cellular and subcellular distributions in liver" *Arch. Biochem. Biophys.* **1993**, *306*, 391-401.

18. Chen, J. W.; Murphy, T. L.; Willingham, M. C.; Pastan, I.; August, J. T. "Identification of two lysosomal membrane glycoproteins" *J. Cell Biol.***1985**, *101*, 85-95.

19. Phillips, H. J.; Terryberry, J. E. "Counting actively metabolizing tissue cultured cells" *Exp. Cell Res.* **1957**, *13*, 341-347.

20. Presley, J. F.; Mayor, S.; McGraw, T. E.; Dunn, K. W.; Maxfield, F. R. "Bafilomycin A1 treatment retards transferrin receptor recycling more than bulk membrane recycling" *J. Biol.Chem.* **1997**, *272*, 13929-13936.

CHAPTER 7

Array Based Protein Detection

7.1 Introduction

Convenient, precise and rapid protein sensing methods are of great importance in medical diagnostics and proteomics.[1] Widely used specific interaction-based sensing protocols (e.g. ELISA) require protein receptors of high affinity and specificity necessitating the generation of pertinent protein receptors/ligands for multi-protein detection. In this regard, sensor array approaches are attractive, using 'differential' binding where the receptors bind to their analytes by different binding characteristics that are selective rather than specific.[2] This technique, namely 'electronic nose/tongue' has provided highly versatile sensors.[3-4] This principle has recently been used to attain protein detection through either fluorescence quenching[5] or indicator-displacement.[6] While these sensors have been shown effective, they feature high limits of detection and/or relatively small sets of proteins were studied.

Effective protein sensing requires efficient protein receptors and competent signal transducers. Water-soluble conjugated polymers with pendant charged residues provide an excellent scaffold for sensor design.[7-8] These materials are suited to bind protein surfaces due to their multivalent binding features. Particularly, their optical properties are sensitive to minor conformational or environmental changes,[7,9] enabling efficient signal transduction of the binding events. Moreover, the homogeneous sensor systems have appealing attributes in high-throughput screening.

7.2 Results and Discussion

In this work we used six functionalized poly(*p*-phenyleneethynylene)s (PPEs)[10] to build a protein sensor array (Figure 7.1). These highly fluorescent polymers possess various charge characteristics and molecular scales. Such structural features provide tremendous binding diversity upon interaction with protein analytes, generating distinct fluorescence response patterns for protein discrimination.

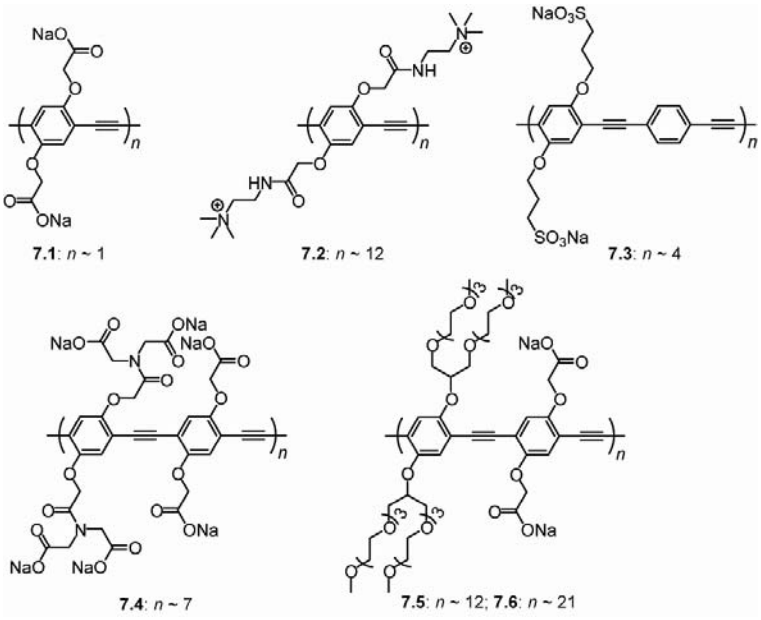

Figure 7.1. Chemical structures of PPEs, **7.1**-**7.6**.

We have chosen 17 proteins as sensing targets (Table 7.1). These proteins possess diverse structural characteristics including metal/nonmetal-containing, molecular weight (M_w), isoelectric point (pI), and UV absorbance values. Notably, many protein targets

have comparable M_w and pI values, thereby providing excellent objects for examining the differentiation ability of the PPE-based sensor array.

Table 7.1. Basic properties of the proteins used as sensing targets.

Protein	Metal	Mw / kDa	pI	ε_{280} / M^{-1} cm^{-1}
α-Amylase (α-Am)	Y	50	5.0	130000
Bovine serum albumin (BSA)	N	66.3	4.8	46860
α-Chymotrypsin (ChT)	N	25	8.7	51000
Cytochrome *c* (CytC)	Y	12.3	10.7	23200
Ferritin (Fer)	Y	750	4.5	950000
β-Galactosidase (β-Gal)	N	540	4.6	1128600
Hemoglobin (Hem)	Y	64.5	6.8	125000
Histone (His)	N	21.5	10.8	3840
Human serum albumin (HSA)	N	69.4	5.2	37800
Lipase (Lip)	N	58	5.6	54350
Lysozyme (Lys)	N	14.4	11.0	38000
Myoglobin (Myo)	Y	17.0	7.2	13940
Papain (Pap)	N	23.0	9.6	57500
Acid phosphatase (PhosA)	N	110	5.2	257980
Alkaline phosphatase (PhosB)	N	140	5.7	62780
Ribonuclease A (RibA)	N	13.7	9.4	10000
Subtilisin A (SubA)	N	30.3	9.4	26030

In the sensing studies, the fluorescence of the polymer solution (100 nM, on the basis of number-averaged molecular weight) in phosphate buffered saline (PBS) was recorded before and after addition of protein analytes. The fluorescence intensity changes are regarded as the fluorescent response in the presence of proteins. The six polymers display substantial overlap in their absorption and emission spectra, allowing the same excitation wavelength (430 nm) and emission wavelength (465 nm) to be used for all

polymers to expedite their analysis on the microplate reader. To facilitate the quantitative detection of proteins, we generated patterns at protein concentrations at a standard UV absorbance (A_{280}=0.005), the lowest concentration for all proteins to induce substantial emission changes of the polymers. With this as the detection limit of the system, protein identification was readily achieved in combination of UV measurements (*vide post*). Besides metalloproteins e.g. CytC, Fer, Hem and Myo, non-metalloproteins also generally quench the polymer emission (Figure 7.2), indicating that the electronic states of the polymers are modulated by protein binding.

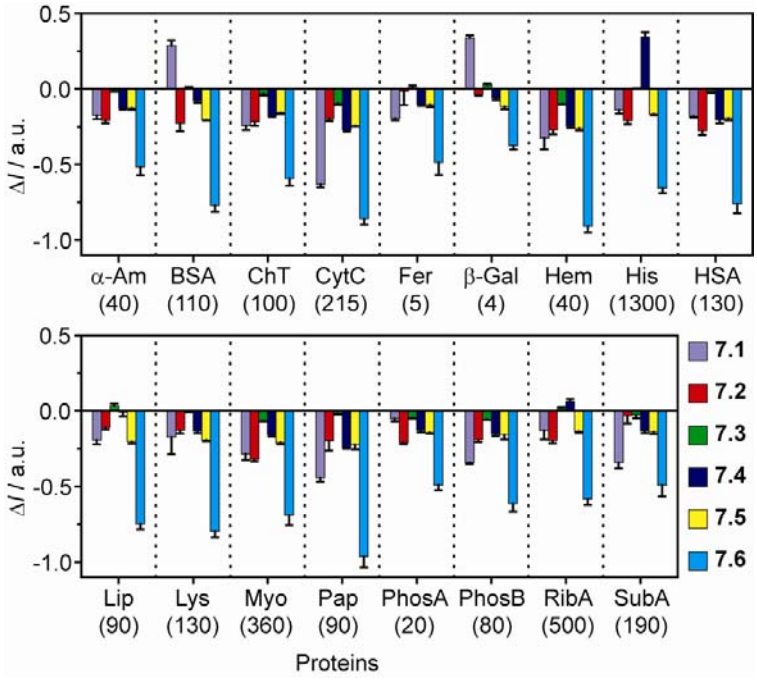

Figure 7.2. Fluorescence response (ΔI) patterns of the PPE polymer array (**7.1-7.6**) against various protein analytes (A_{280} = 0.005). Each value is an average of six parallel measurements. The values in the parentheses below the protein ID indicate the protein concentrations in nM.

In comparison with polymers in the absence of proteins, the fluorescence quenching extent ranges from 5% to 50%. These fluorescence responses are not

correlated with the pI and M_w of the proteins. Significantly, the fluorescence response patterns are characteristic and highly reproducible for particular proteins, indicating the possibility of protein discrimination.

The fluorescence response patterns were subjected to Linear Discriminant Analysis (LDA), a statistical method which can separate classes of objects by formulating componential boundaries or assigning new objects to appropriate classes.[11] LDA converts the patterns of the training matrix (6 polymers × 17 proteins × 6 replicates) to canonical scores. The first three canonical factors contain 65.0%, 20.8%, and 7.3% of the variation, respectively, occupying 93.1% of total variation. Figure 7.3 illustrates a 3-D plot of simplified emission response patterns.

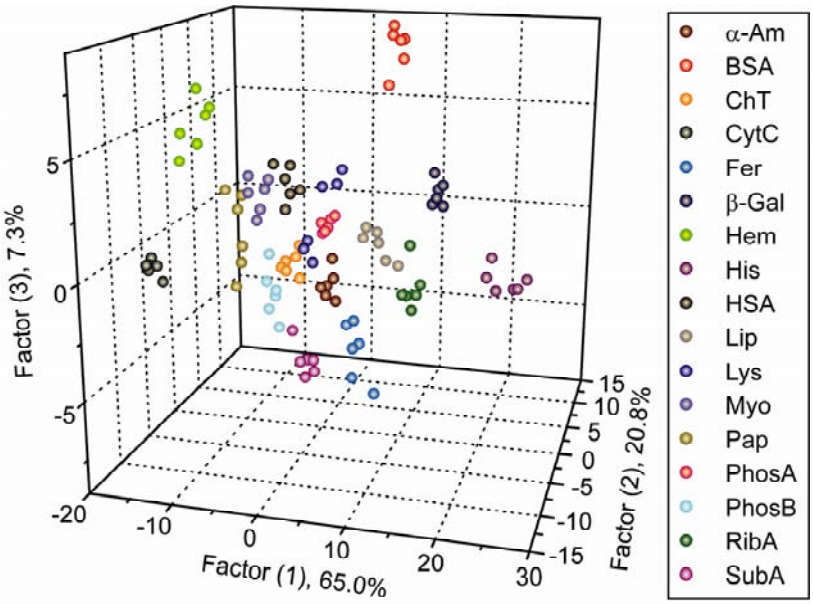

Figure 7.3. Canonical score plot for the first three factors of simplified fluorescence response patterns obtained with PPE polymer array against 17 protein analytes (A_{280} = 0.005).

The canonical patterns are clustered into 17 different groups correlating to the protein identities, confirming that LDA can properly discriminate the complex emission response patterns. Furthermore, the jackknifed matrix with cross-validation reveals a classification accuracy of 100%. For a single polymer, however, the classification accuracies range from 26% to 56% (Table 7.2), indicating that an array of different sensors is essential for protein discrimination.

Table 7.2. LDA classification accuracy of protein analytes (A_{280} = 0.005) by using individual fluorescent polymers and the array of the fluorescent polymers as sensors. The values are taken from the jackknifed classification matrix based on LDA analysis of the raw data (6 replicates)

Protein	**7.1**	**7.2**	**7.3**	**7.4**	**7.5**	**7.6**	**7.1-7.6**
α-Am	0%	0%	0%	33%	50%	50%	100%
BSA	83%	0%	17%	67%	17%	17%	100%
ChT	50%	0%	17%	83%	0%	33%	100%
CytC	100%	0%	0%	100%	100%	67%	100%
Fer	50%	17%	0%	83%	67%	0%	100%
β-Gal	83%	67%	33%	50%	33%	100%	100%
Hem	0	67%	17%	33%	67%	50%	100%
His	50%	0%	67%	100%	50%	33%	100%
HSA	33%	17%	17%	67%	17%	0%	100%
Lip	33%	67%	50%	50%	17%	33%	100%
Lys	0%	67%	50%	0%	50%	33%	100%
Myo	17%	100%	100%	50%	33%	67%	100%
Pap	100%	0%	33%	67%	0%	83%	100%
PhosA	100%	0%	50%	0%	33%	0%	100%
PhosB	33%	33%	67%	50%	0%	67%	100%
RibA	0%	0%	83%	100%	17%	33%	100%
SubA	0%	17%	33%	17%	33%	0%	100%
Average	43%	26%	37%	56%	34%	39%	100%

We next focused on detection and identification of protein samples with both unknown concentration and identity. The unknowns from the training set were submitted to an analysis protocol that included determination of UV absorbance at 280 nm, dilution

of solution to A_{280} = 0.005, generation of fluorescence response patterns against the sensor array, and LDA (Scheme 7.1).

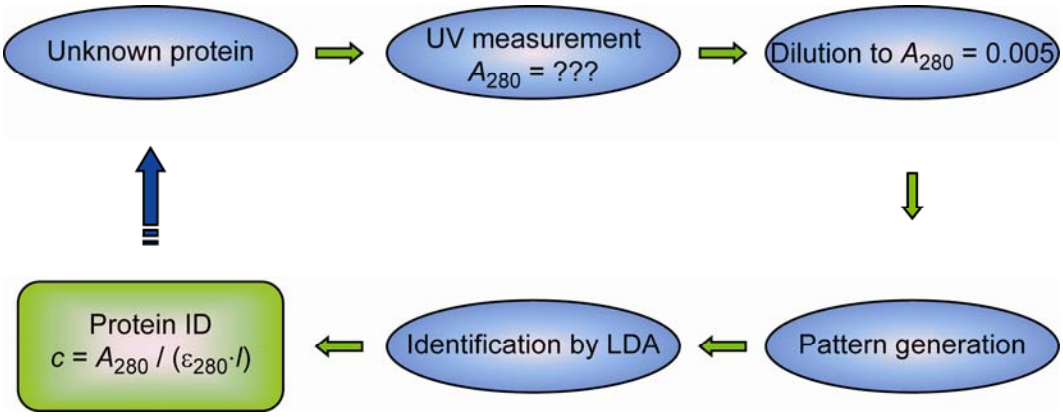

Scheme 7.1. Schematic representation for the detection procedure of unknown proteins using array-based sensors.

During LDA, the new cases were classified to the groups generated through the training matrix according to their shortest Mahal distances to respective groups. Once the protein was identified, the initial protein concentration was obtained through the Beer-Lambert Law using the ε_{280} values listed in Table 7.1. Out of 68 protein samples that were randomly selected from the 17 protein species, only 2 samples were misclassified, affording an identification accuracy of 97%. Moreover, the protein concentrations were generally determined within ±5% deviation.

7.3 Conclusion

We have demonstrated that a PPE-based sensor array can effectively detect and identify proteins. Benefiting from their high fluorescence sensitivity as well as inherent

amplification effects, this array of six conjugated polyelectrolytes displays an unprecedented discrimination ability towards 17 protein analytes. Taking its convenience, accuracy, and versatility into account, this protocol holds great promise for applications in medical diagnostics. With the introduction of functionalized nanoparticles into our polymeric detection method, we should be able to utilize these constructs to greatly enhance the sensitivity and flexibility of our sensor arrays towards protein and pathogen detection.

7.4 Experimental

Instrumentation and Materials. α-Amylase (α-Am, from *Bacillus licheniformis*), bovine serum albumin (BSA), α-chymotrypsin (ChT, from bovine pancreas, type I-S), cytochrome *c* (CytC, from equine heart), ferritin (Fer, from equine spleen), β-galactosidase (β-Gal, from *Escherichia coli*), hemoglobin (Hem, from human), histone (His, from calf thymus, type III-S), human serum albumin (HSA), lipase (Lip, from *candida rugosa*, type VII), lysozyme (Lys, from chicken egg white), myoglobin (Myo, from equine heart), papain (Pap, from papaya latex), acid phosphatase (PhosA, from potato), alkaline phosphatase (PhosB, from bovine intestinal mucosa), ribonuclease A (RibA, from bovine pancreas, type I-A), and subtilisin A (SubA, from *Bacillus licheniformis*) were purchased from Sigma and used as received. Phosphate buffered saline (PBS, pH 7.4, 1×) was purchased from Invitrogen and used as the solvent throughout the fluorescence assays. UV-vis spectra were measured in a rectangular quartz cuvette (light path = 10 mm) on a Hewlett Packard 8452A diode array spectrophotometer. Fluorescence spectra were recorded in a conventional quartz cuvette

(10 × 10 × 40 mm) on a Jasco FP-6500 fluorimeter. The polymers were dissolved in phosphate buffered saline (1 ×) to make 100 nM of stock solutions on the basis of their molecular weights. Polymers **7.1** and **7.3**-**7.6** were synthesized according to the reported procedures.[10] Polymer **7.2** was prepared according to a procedure described below.

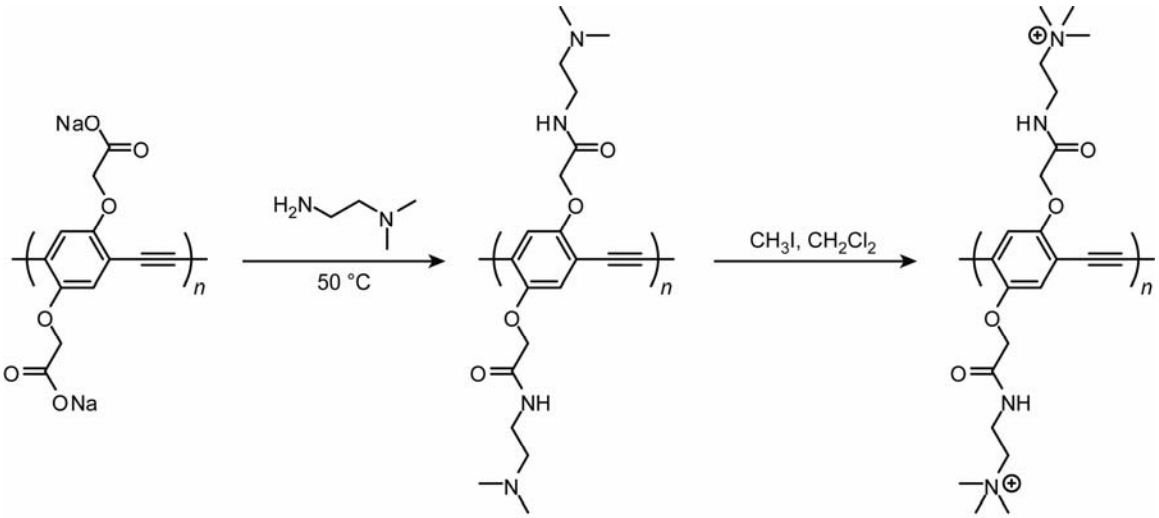

Pre-7.2 **7.2**

Scheme 7.2. Synthesis of cationic polymer **7.2**

Synthesis of pre-7.2: The mixture of dicarboxylate PPE (25 mg, 0.082 mmol) and *N*,*N*-dimethylethylenediamine (25 mL) was stirred at 50 ºC for 24 h. After removal of the solvent, the residue was washed thoroughly with hexane. After being dried under vacuum, **pre-7.2** was obtained as a dark orange solid (52 mg, 0.077 mmol, 94 %). ^{1}H NMR (300 MHz, $CDCl_3$): δ 7.14 (s, 2H), 4.52 (s, 4H), 3.31 (s, 4H), 2.81 (s, 4H), 2.17 (s, 12H). ^{13}C NMR (300 MHz, $CDCl_3$): δ 168.97, 157.57, 118.45, 113.49, 92.94, 90.67, 68.57, 58.10, 44.97, 36.44.

Synthesis of polymer 7.2: **Pre-7.2** (40 mg, 0.1 mmol) was dissolved in dichloromethane (25 mL) and iodomethane (15 mL) was added for methylation. The reaction mixture was stirred at room temperature overnight. After removal of the solvent, the polymer was washed with hexane and dried under vacuum. The product is a dark orange powder (63 mg, 0.094 mmol, 94%). ^{1}H NMR (300 MHz, D_2O): δ 7.09 (s, 2H), 4.50 (s, 4H), 3.74 (s, 4H), 3.52 (s, 4H), 3.27 (s, 18H). ^{13}C NMR (300 MHz, D_2O): δ 167.51, 156.13, 118.10, 113.54, 93.03, 90.86, 66.21, 65.33, 54.16, 36.38.

Protein sensing study. Each polymer solution (100 nM, 200 μL) in PBS was respectively loaded into a well on a 96-well plate (300 μL Whatman® Glass Bottom microplate) and the fluorescence intensity values at 465 nm were recorded on a Molecular Devices SpectraMax M5 microplate reader with excitation at 430 nm. Subsequently, 10 μL of protein solution was added to each well and the final protein concentrations in the wells were A = 0.005 at 280 nm, which was initially calibrated using UV/vis spectroscopy. The fluorescence intensity values at 465 nm were recorded again. The difference between the two measurements before and after addition of proteins was treated as the fluorescence response. This process was repeated for 17 protein targets to generate six replicates of each. Thus, the 17 proteins were tested against the six-polymer array (**7.1**-**7.6**) six times, to afford a training data matrix of 6 polymers × 17 proteins × 6 replicates. The raw data matrix was processed using classical linear discriminant analysis (LDA) in SYSTAT (version 11.0). In LDA, all variables were used in the model (complete mode) and the tolerance was set as 0.001. The raw fluorescence response patterns were transformed to canonical patterns where the ratio of between-class variance to the within-class variance was maximized according to the

preassigned grouping. The Mahalanobis distances of each individual pattern to the centroid of each group in a multidimensional space were calculated and the assignment of the case was based on the shortest Mahalonobis distance.

Protein concentration determination. In the studies featuring unknown analyte protein concentrations, sixty-eight unknown protein solutions were randomly selected from the 17 protein species and subjected to an analysis procedure as illustrated in Scheme 7.1. The protocol included UV absorption measurement of protein samples at 280 nm, dilution to A_{280} = 0.005, fluorescence response pattern recording against the sensor array (**7.1**~**7.6**, 100 nM), and LDA. The new cases were classified to the groups generated through the training matrix (6 polymers × 17 proteins × 6 replicates) according to their shortest Mahalanobis distances. After the protein identity was recognized by LDA, the initial protein concentration (c) was deduced from the A_{280} value and corresponding molar extinction coefficient (ε_{280}) according to the Beer-Lambert law: $c = A_{280}/(\varepsilon_{280} \cdot l)$ In the experimental setup, the protein sample preparation, data collection and LDA analysis were performed by different persons.

7.5 References

1. Kodadek, T. "Protein microarrays: prospects and problems" *Chem. Biol.* **2001**, 8, 105-115.

2. Albert, K. J.; Lewis, N. S.; Schauer, C. L.; Sotzing, G. A.; Stitzel, S. E.; Vaid, T. P.; Walt, D. R. "Cross-reactive chemical sensor arrays" *Chem. Rev.* **2000**, 100, 2595-2626.

3. Wright, A. T.; Anslyn, E. V. "Differential receptor arrays and assays for solution-based molecular recognition" *Chem. Soc. Rev.* **2006**, 35, 14-28.

4. (a) Leonard, J. P.; dos Santos, C. M. G.; Plush, S. E.; McCabe, T.; Gunnlaugsson, T. "pH driven self-assembly of a ternary lanthanide luminescence complex: the sensing of anions using a β-diketonate-Eu(III) displacement assay" *Chem. Commun*. **2007**, 129-131. (b) Folmer-Andersen, J. F.; Kitamura, M.; Anslyn, E. V. "Pattern-based discrimination of enantiomeric and structurally similar amino acids: an optical mimic of the mammalian taste response" *J. Am. Chem. Soc*. **2006**, 128, 5652-5653. (c) Lee, J. W.; Lee, J. S.; Kang, M.; Su, A. I.; Chang, Y. T. "Visual artificial tongue for quantitative metal-cation analysis by an off-the-shelf dye array" *Chem. Eur. J*. **2006**, 12, 5691-5696. (d) Buryak, A.; Severin, K. A. "A chemosensor array for the colorimetric identification of 20 natural amino acids" *J. Am. Chem. Soc*. **2005**, 127, 3700-3701. (e) Greene, N. T.; Shimizu, K. D. "Colorimetric molecularly imprinted polymer sensor array using dye displacement" *J. Am. Chem. Soc*. **2005**, 127, 5695-5700. (f) Rakow, N. A.; Suslick, K. S. A. "A colorimetric sensor array for odor visualization" *Nature* **2000**, 406, 710-713.

5. (a) Sandanaraj, B. S.; Demont, R.; Thayumanavan, S. "Generating patterns for sensing using a single receptor scaffold" *J. Am. Chem. Soc*. **2007**, 129, 3506-3507. (b) Zhou, H.; Baldini, L.; Hong, J.; Wilson, A. J.; Hamilton, A. D. "Pattern recognition of proteins based on an array of functionalized porphyrins" *J. Am. Chem. Soc*. **2006**, 128, 2421-2425. (c) Baldini, L.; Wilson, A. J.; Hong, J.; Hamilton, A. D. "Pattern-based detection of different proteins using an array of fluorescent protein surface receptors" *J. Am. Chem. Soc*. **2004**, 126, 5656-5657. (d) Kim, I.-B.; Dunkhorst, A.; Bunz, U. H. F. "Nonspecific interactions of a carboxylate-substituted PPE with proteins. A cautionary tale for biosensor applications" *Langmuir* **2005**, 21, 7985-7989.

6. (a) You, C.-C.; Miranda, O. R.; Gider, B.; Ghosh, P. S.; Kim, I.-B.; Erdogan, B.; Krovi, S. A.; Bunz, U. H. F.; Rotello, V. M. "Detection and identification of proteins using nanoparticle-fluorescent polymer 'chemical nose' sensors" *Nat. Nanotech*. **2007**, 2, 318-323. (b) Wright, A. T.; Griffin, M. J.; Zhong, Z.; McCleskey, S. C.; Anslyn, E. V.; McDevitt, J. T. "Differential receptors create

patterns that distinguish various proteins" *Angew. Chem. Int. Ed.* **2005**, 44, 6375-6378.

7. (a) Thomas, S. W. III; Joly, G. D.; Swager, T. M. "Chemical sensors based on amplifying fluorescent conjugated polymers" *Chem. Rev*. **2007**, 107, 1339-1386. (b) Ambade, A. V.; Sandanaraj, B. S.; Klaikherd, A.; Thayumanavan, S. "Fluorescent polyelectrolytes as protein sensors" *Polym. Int*. **2007**, 56, 474-481.

8. (a) Kim, I.-B.; Wilson, J. N.; Bunz, U. H. F. "Mannose-substituted PPEs detect lectins: a model for Ricin sensing" *Chem. Commun*. **2005**, 1273-1275. (b) Disney, M. D.; Zheng, J.; Swager, T. M.; Seeberger, P. H. "Detection of bacteria with carbohydrate-functionalized fluorescent polymers" *J. Am. Chem. Soc*. **2004**, 126, 13343-13346.

9. (a) Dwight, S. J.; Gaylord, B. S.; Hong, J. W.; Bazan, G. C. "Perturbation of fluorescence by nonspecific interactions between anionic poly(phenylenevinylene)s and proteins: Implications for biosensors" *J. Am. Chem. Soc*. **2004**, 126, 16850-16859. (b) Fan, C.; Plaxco, K. W.; Heeger, A. J. "High-efficiency fluorescence quenching of conjugated polymers by proteins" *J. Am. Chem*. Soc. **2002**, 124, 5642-5643.

10. (a) Kim, I.-B.; Phillips, R. L.; Bunz, U. H. F. "Carboxylate group side-chain density modulates the pH-dependent optical properties of PPEs" *Macromolecules* **2007**, 40, 5290-5293. (b) Kim, I.-B.; Dunkhorst, A.; Gilbert, J.; Bunz, U. H. F. "Sensing of lead ions by a carboxylate-substituted PPE: multivalency effects" *Macromolecules* **2005**, 38, 4560-4562. (c) Tan, C.-Y.; Pinto, M. R.; Schanze, K. S. "Photophysics, aggregation and amplified quenching of a water-soluble poly(phenylene ethynylene)" *Chem. Commun*. **2002**, 446-447.

11. (a) Jurs, P. C.; Bakken, G. A.; McClelland, H. E. "Computational methods for the analysis of chemical sensor array data from volatile analytes" *Chem. Rev*. **2000**, 100, 2649-2678. (b) Brereton, R. G. *Chemometrics: Data Analysis for the Laboratory and Chemical Plant*, John Wiley & Sons, **2003**, pp 183-255.

CHAPTER 8

Nanosensors for the Detection of Phosphate and Pyrophosphate

8.1 Introduction

Mönckeberg's arteriosclerosis[1-3] (MA) is a form of vascular calcification that affects the arteries in the lower limbs but can, in rare cases, also afflict other soft tissues, including the pharynx.[4] MA is quite common in patients with renal failure undergoing hemodialysis[5] but is also observed in diabetic patients suffering from neuropathies.[6] The calcification in MA is caused by the unwanted deposit of hydroxyapatite into blood vessels.[7] It is contended that MA is one factor for the enhanced cardiac mortality in diabetic and end stage renal dialysis patients.

Interestingly enough, the primary reason for the vascular calcification observed in MA is *not* the excess concentration of calcium and/or phosphate (Pi) ions *but the relative lack of inorganic pyrophosphate (PPi) in these patients, as evidenced by their lowered PPi serum levels.* In healthy individuals, the level of serum Pi (1:1 HPO_4^{2-} and $H_2PO_4^-$ at pH7.2) is 0.8-1.5 $mmolL^{-1}$,[8] but that of PPi is only 3.3 (± 0.2) µmol/L. In MA-patients this level is decreased to 2.3 (± 0.2) µmol/L.[5] However, an excess of PPi can lead to crystalline calcium-PPi deposits, leading to a form of arthritis. Therefore, the facile detection of the PPi level in serum would be of great interest. The classic analytical determination of Pi is based on colorimetric molybdate and related assays,[9,10] however, PPi can not be quantitated by this method. Instead, enzymatic assays are deployed in clinical settings[11,12] to obtain PPi concentrations in blood serum. While these assays are sensitive and reliable, they are also elaborate and involve radioactively labeled reagents.

A direct and fast fluorescence-based assay for PPi would be attractive for the expeditious chemical quantification of this ion in serum.

The determination of phosphate-type anions including PPi has been pursued with small fluorescent dyes in water.[13-22] Often, such PPi sensors working in water exploit the complexation of a multiply amine or pyridine-appended fluorophore with a zinc salt into a composite probe. These probes bind PPi quite nicely, particularly if the fluorophores are doubly zinc complexed: PPi is chelated by the zinc ions held in place by suitable binding appendages. While the competition between PPi and Pi binding has not been carefully examined in these systems, it seems that Pi/PPi ratios of up to 100 can be tolerated and micromolar amounts of PPi are detected in 0.01 M HEPES buffer. However, the zinc-based sensors might be less efficient when sensing Pi/PPi under more realistic conditions: The concentration of Mg^{2+} and Ca^{2+} is significant in serum and could lead to problems, as both bind tightly to any phosphate-type anions and may also de-complex the probes. The masking of serum-Ca^{2+} or serum-Mg^{2+} with either cyclen or fluoride anions would also be a problem, as one could expect that the metallofluorophores might also suffer from decomplexation or metal (ligand) exchange.

We felt that for successful serum Pi/PPi analyses, an alternative, simple, variable, modular, sensitive, robust and easily modifiable approach was desirable. Our suggested solution to the Pi/PPi problem employs a self-assembled poly(*para*phenyleneethynylene) nanoparticle hybrid (PNP) that works specific and sensitively for phosphate- and phosphate-related anions but is insensitive to *all* other anions and functions in water. The concept expands our earlier notion that the addition of a suitable cofactor to a conjugated polymer is valuable to detect and discern transition metals, different proteins or

bacteria.[23,24] Using conjugated polymers with suitable cofactors in the form of matching-mismatching single-stranded DNA is a concept that was successfully implemented by Bazan[25] and by Leclerc[26] and also exploited by Schanze[27] to detect and quantify DNA.

In this work we describe the self-assembly of spinel nanocubes $(CoFe_2O_4)_x$[28] with the conjugated polymer **8.1**[29,30] and the use of this simple non-fluorescent material as a turn-on displacement probe for phosphate type anions.[31] The electrostatically bound PPE is efficiently replaced from the spinel surface forming a fluorescent solution upon addition of phosphate anions. The PNPs detect PPi in the presence of a more than 1000-fold excess of Pi. The herein described experiments are a proof of concept as we have neither optimized the structure, charge density or the size of the used PPE nor have we manipulated the surface properties of the spinel nanocubes (NC) to achieve more sensitive detection of PPi in serum.

8.2 Results and Discussion

Upon mixing PPE **8.1** (5 μM) with 10-nm cobalt ferrite spinel NCs $(CoFe_2O_4)_x$ in PIPES-buffered solutions (50 mM, pH 7.2, 0.1 M $KClO_4$) the fluorescence of **8.1** (degree of polymerization, P_n = 16) was quenched to 10% of its original intensity in the presence of 20 pM of the NC. A probable quenching mechanism is Förster resonance energy transfer (FRET) from the excited state of **8.1** to the NC, but other mechanisms such as electron transfer can not be excluded either.[32] The NCs have a strong absorption at 463 nm, the emission maximum of **8.1**. Quenching is not unexpected as gold nanoparticles extinguish the fluorescence of conjugated polymers with high efficiency in assemblies produced via electrostatic interactions.[33-35] The multivalent display of the carboxylic acid

in **8.1** plays a critical role to stabilize the NP-PPE assemblies (Figure 8.1) as one NC quenches the fluorescence of approximately 10^4 PPE chains. To support the claim of multivalency between **8.1** and the NCs we investigated the interaction of the NPs with trimer **8.2.** Even at NC concentrations above 1 $nmolL^{-1}$ the fluorescence of **8.2** was not appreciably quenched and the constructs formed from **8.2** and the NCs were not further investigated.

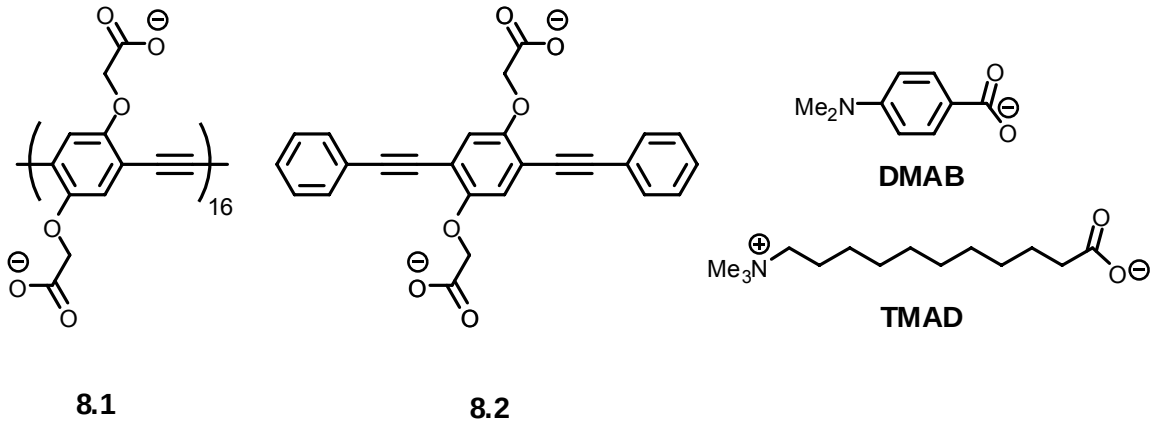

Figure 8.1. Structure of carboxylate substituted PPE (**8.1**), carboxylate substituted trimer (**8.2**), dimethylaminobenzoic acid (**DMAB**), and trimethylammonium-undecanoate (**TMAD**)

To understand the interactions between **8.1** and the NCs, we examined the fluorescence quenching of PPE **8.1** not only by the dimethylaminobenzoic acid (DMAB) functionalized NCs but also with propionate-modified, unmodified and trimethyl-ammoniumundecanoate (TMAD) modified NCs (Schemes 8.1-8.2). In Figure 8.2, the Stern Volmer plots of quenching of **8.1** by DMAB and TMAD-coated NCs are shown.

The DMAD-NCs give the most efficient quenching, while the TMAD-protected nanocubes were comparatively inefficient in quenching the fluorescence of the PPE **8.1**.

NC concentrations at which the fluorescence drops to 10% of original value ($[Q]_{90}$) of **8.1** (5 μM) is 20 pM for the DMAB-NCs, while a concentration of approximately 2 μM of the TMAD-NCs is necessary to reach the same $[Q]_{90}$.

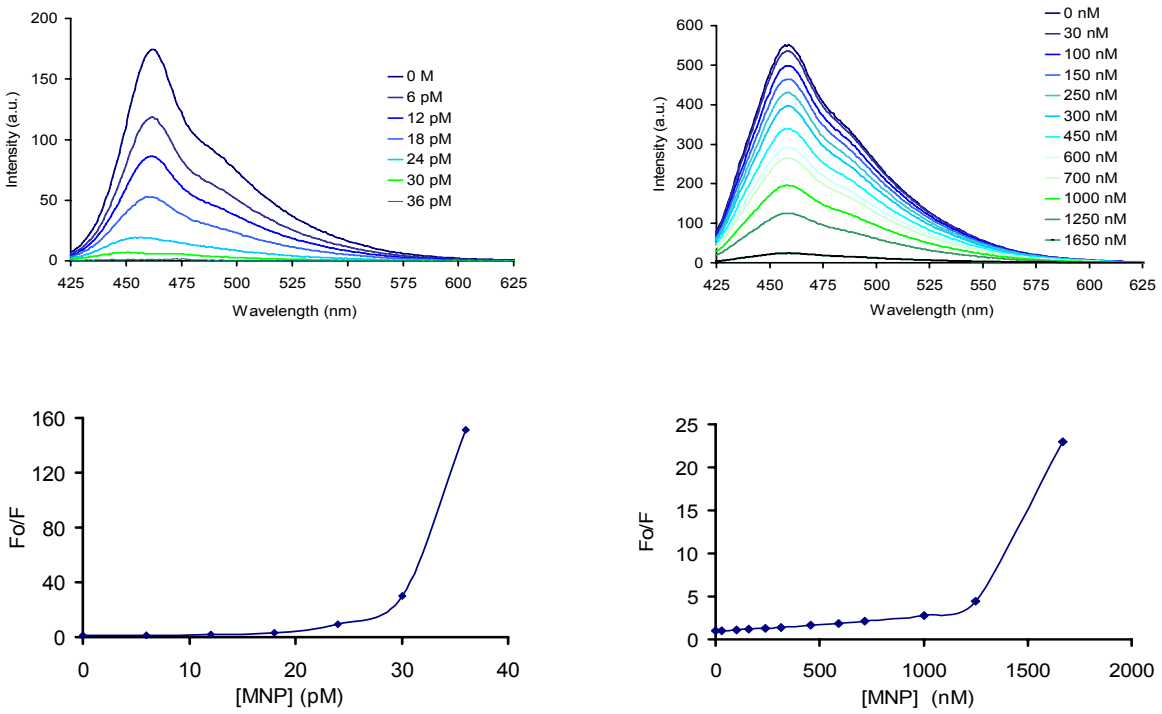

Figure 8.2. Fluorescence quenching (top) and Stern-Volmer plot (bottom) of PPE **8.1** by 10-nm NC $(CoFe_2O_4)_x$ stabilized by DMAB (left) or TMAD (right).

The concentration of **8.1** was μM based on the molecular weight of the repeating unit and all experiments were performed in a PIPES buffered solution. Scheme 8.1 displays the interpretation of our results. In the case of the DMAB-functionalized nanocubes, the DMAB is uncharged as its pK_a values are 2.6 and 5.0 respectively in water.

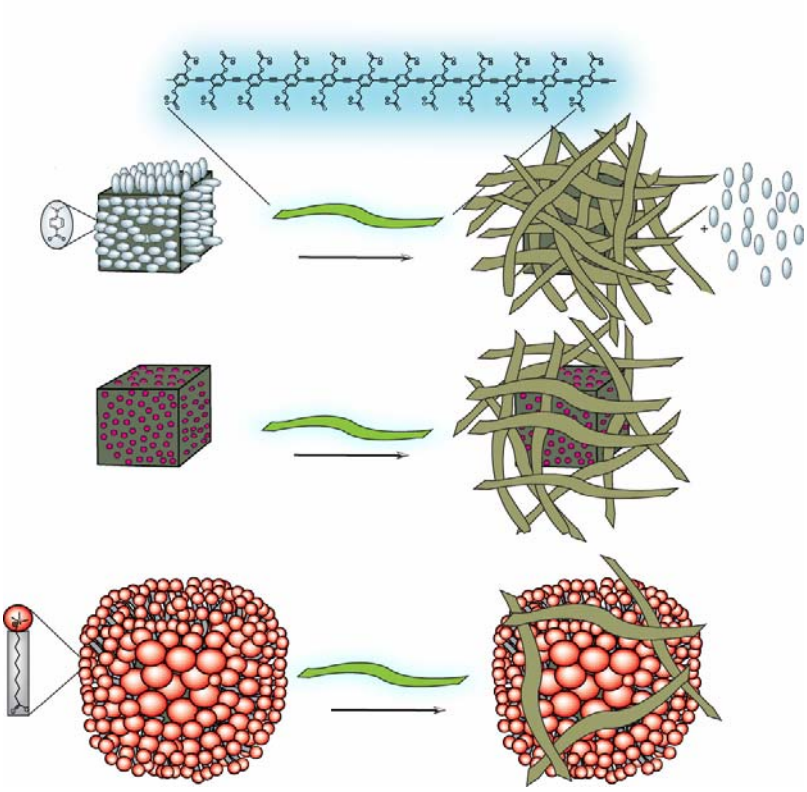

Scheme 8.1. Schematic representation for the PNP self-assembly and fluorescence quenching with conjugated polymers. Top: Displacement of the DMAB by **8.1**. Middle: Coordination of **1** to an unprotected NC (red dots are small inorganic counter-anions that are not replaced efficiently). Bottom: Addition of **8.1** to TMAD functionalized NCs. In this case the TMAD is not released but **8.1** complexes with the cationic ammonium head group.

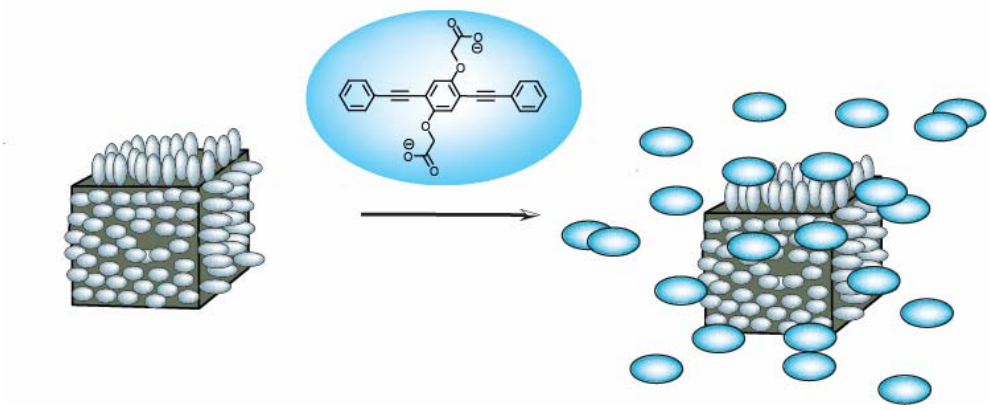

Scheme 8.2. Inefficiency of small fluorophores (**8.2**) in replacing DMAB from the NC.

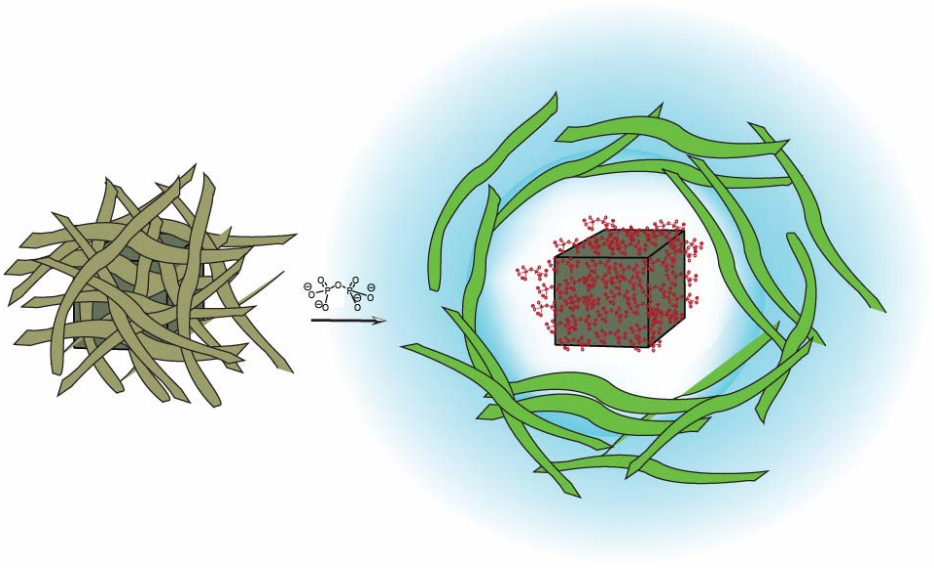

Scheme 8.3. Working principle of the nanocube based displacement assay. On the left hand side is the quenched nanocube PPE-construct, on the right hand side is the now PPi-decorated cube and the displaced and now fluorescent PPE.

When coordinated to the NCs, the apparent pK_a of the DMAB may be different and better estimated as the pK_a of the hypothetical zwitterion, which was calculated/estimated to be 4.3 according to Wepster et al.[36] As a consequence, even coordinated to the NC, we do not assume that the coordinated DMAB-amine is protonated at pH 7.2, conditions under which all of the experiments were performed. We interpret the very large differences in the $[Q]_{90}$ values between DMAB and TMAD-stabilized NCs that in the first case the ligand DMAB is displaced, and **8.1** is complexed to a "naked" NC, while in the latter case, the interaction of the NC to **8.1** is attenuated by the interspersed, positively charged TMAD, which is not removed by added **8.1**; instead a weak complex forms between the complexed NC and **8.1** (Scheme 8.1).

In the case of the unfunctionalized NCs the $[Q]_{90}$ is 4 nM and for the unfunctionalized spherical NPs $[Q]_{90}$ it is 2 nM respectively, demonstrating that surface

chemistry plays a significant role in the complex formation. In the case of the "unfunctionalized" nanocubes and nanospheres, the surface of the nanoparticles must be "studded" with small inorganic counterions such as chloride or hydroxide, which are bound tightly to the nanoparticles, which attenuate the positive charge available for the interaction of the NC with the PPE **8.1**.

To get a further insight into these processes, we investigated the DMAB and the TMAD functionalized cubes by IR spectroscopy before and after the addition of the PPE **8.1**. Photoacoustic IR experiments demonstrate that the addition of the PPE **8.1** to the DMAB-coated NCs leads to displacement of a significant fraction of the bound DMAB from the NCs, while according to the same surface IR-measurements the NCs coated with TMAD do not experience any change. The PPE **8.1** therefore does not displace the TMAD from the NCs but is electrostatically bound to the outer sphere of the still fully TMAD-coated NCs.

Fluorescence quenching of **8.1** by the low concentrations of the DMAB-coated NCs suggested that the PNPs could be used as turn-on nanosensors for negatively charged analytes by displacement of the PPE from the NCs. Scheme 8.3 shows the proposed concept of our nanosensor. The PNPs, formed by the combination of the DMAB-NCs and **8.1** are non-fluoresecent. If the negatively charged conjugated polymer is displaced from the nanocube *selectively* by an analyte through strong binding of the analyte to the NC, specific fluorescence recovery should be observed, and the PNPs would act as nano-displacement sensors. As the functionalization of both the spinel nanocubes and the conjugated polymer are facile, constructs with a variety of binding characteristics and strengths will be available by simple combination of aqueous

solutions of nanoparticle and conjugated polymers. Such PNPs should have potential in bioanalytical applications and a limitless range of properties (Scheme 8.1). Figure 8.3 shows the exposure of DMAB-NC to 2 mM of different anions in 50 mM piperazine-1,4-bis-(2-ethanesulfonic acid) (PIPES) buffered solutions (pH 7.2). Only Pi anions disassemble **8.1** from the nanocubes, probably due to their high charge density and affinity towards the exposed cobalt and iron sites on the cubes, giving significant fluorescence recovery from the PNPs. The addition of biologically relevant cations (K^+, Na^+, Zn^{2+}, Mg^{2+}, Ca^{2+}) in mM concentrations did not disassemble the PNPs

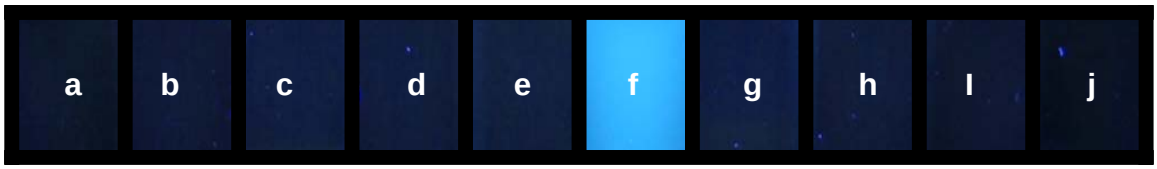

Figure 8.3. Fluorescence recovery of the PNPs in PIPES upon the addition of different anions viewed under a hand-held UV-lamp (λmax 366 nm). Concentration of the DMAB-NCs was 30 pmol; concentration of **8.1** was 5 μM a: Control, b: NaF, c: NaCl, d: NaBr, e: NaI, f: HNa_2PO_4, g: Na_2SO_4, h: CH_3COONa, i: $NaNO_3$, j: $NaNO_2$. The concentration of each anion is 2 mM.

Because the PNPs were uniquely responsive to phosphate ions, we suspected that other, more highly charged phosphate species such as adenosine triphosphate (ATP) and PPi ions would also disassemble the PNPs (Figure 8.4). A remarkable fluorescence increase was indeed found upon the addition of nM concentrations of PPi or ATP to the PNPs. Biological fluids contain metal cations for which ATP and PPi have a high binding affinity (Mg^{2+}, Ca^{2+}).

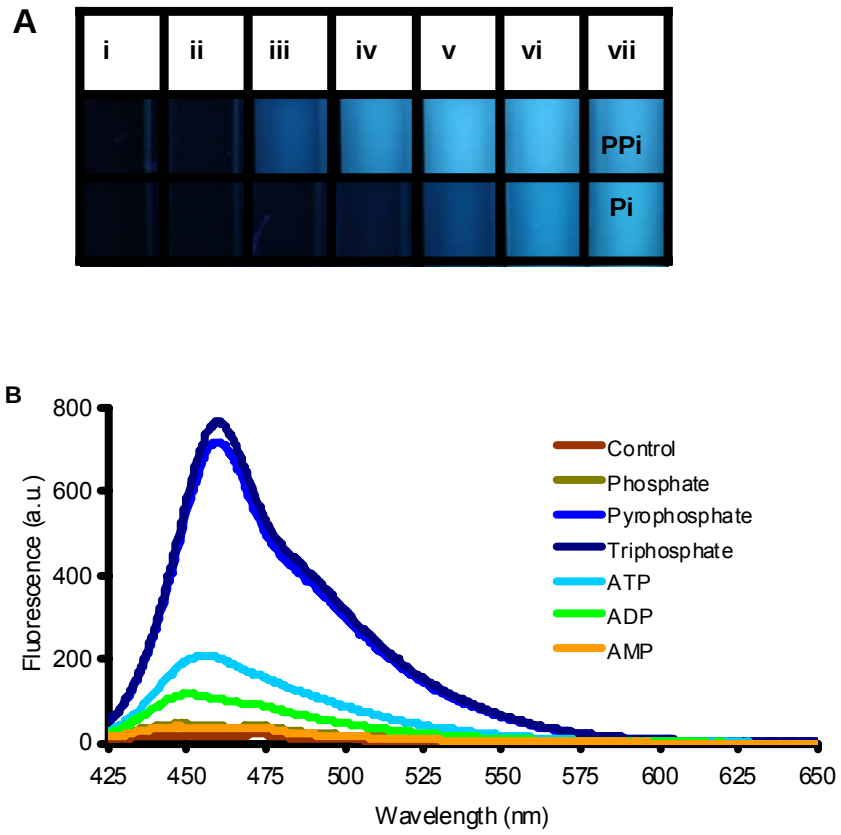

Figure 8.4. (A) Fluorescence recovery of the DMAB-NP-PPE(**8.1**) assemblies in PIPES buffer (pH 7.2) upon the addition of $P_2O_7^{4-}$ (PPi) and PO_4^{3-} (Pi) ions i) Control, ii) 2×10^{-7} M, iii) 2×10^{-6} M, iv) 2×10^{-5} M, v) 2×10^{-4} M, vi) 2×10^{-3} M, vii) 2×10^{-2} M, (B) Fluorescence spectra of the solutions of the NP-PPE(**8.1**) assembly in PIPES buffered solutions (pH 7.2) upon the addition of phosphate type anions. Concentrations of the phosphate and related anions are 4 μM. Concentration of the NCs was 30 pmol; concentration of **8.1** was 5 μM.

In the presence of Mg^{2+} and Ca^{2+} ions (2 mM), the fluorescence recovery of PNP by ATP and PPi was diminished, but still sufficiently high to detect either anion at micromolar concentration. Neither K^+ nor Na^+ ions interfere with the detection of PPi, however, Mg^{2+} and Ca^{2+} ions were easily masked by the addition of fluoride anions. The

fluorescence recovery for added PPi is much greater than that for ATP, yet the *detection limit* is similar.

In biodiagnostic applications for the determination of PPi one would first determine the cumulative phosphate response by the PNP constructs, then hydrolyze the PPi to phosphate by addition of alkaline phosphatase, and then re-determine the fluorescence enhancement using the solution in which the PPi had been hydrolyzed into phosphate. The difference in fluorescence recovery would be attributable to PPi. As a proof of concept we checked the suitability of the PNPs to monitor the activity of pyrophosphatase (Figure 8.5), hydrolyzing PPi to Pi in the presence of Mg^{2+} ions.[37] Our approach was designed to measure the fluorescence modulation from the PNPs responding to the decrease in the concentration of PPi in the enzymatic assay.[38] To determine the pyrophosphatase activity we measured the time dependent decrease of PPi by addition of small aliquots of the pyrophosphatase solution to the PNPs. We recorded the kinetics using PPi solutions, adding 2 – 0.4 "units" of pyrophosphatase (Figure 8.5). The enzyme activity of each set was monitored upon the change of the fluorescence in the PPi-PNP mix.[39]

Depending on the amount of the enzyme units, the saturation time in which full hydrolysis of PPi to Pi is achieved, was variable, indicating that quantification of the enzyme and its activity were easily achieved by the PNPs. Figure 8.5 shows the experimental design and the results, demonstrating that PNPs measure the enzymatic activity of pyrophosphatase due to their high sensitivity for PPi ions.

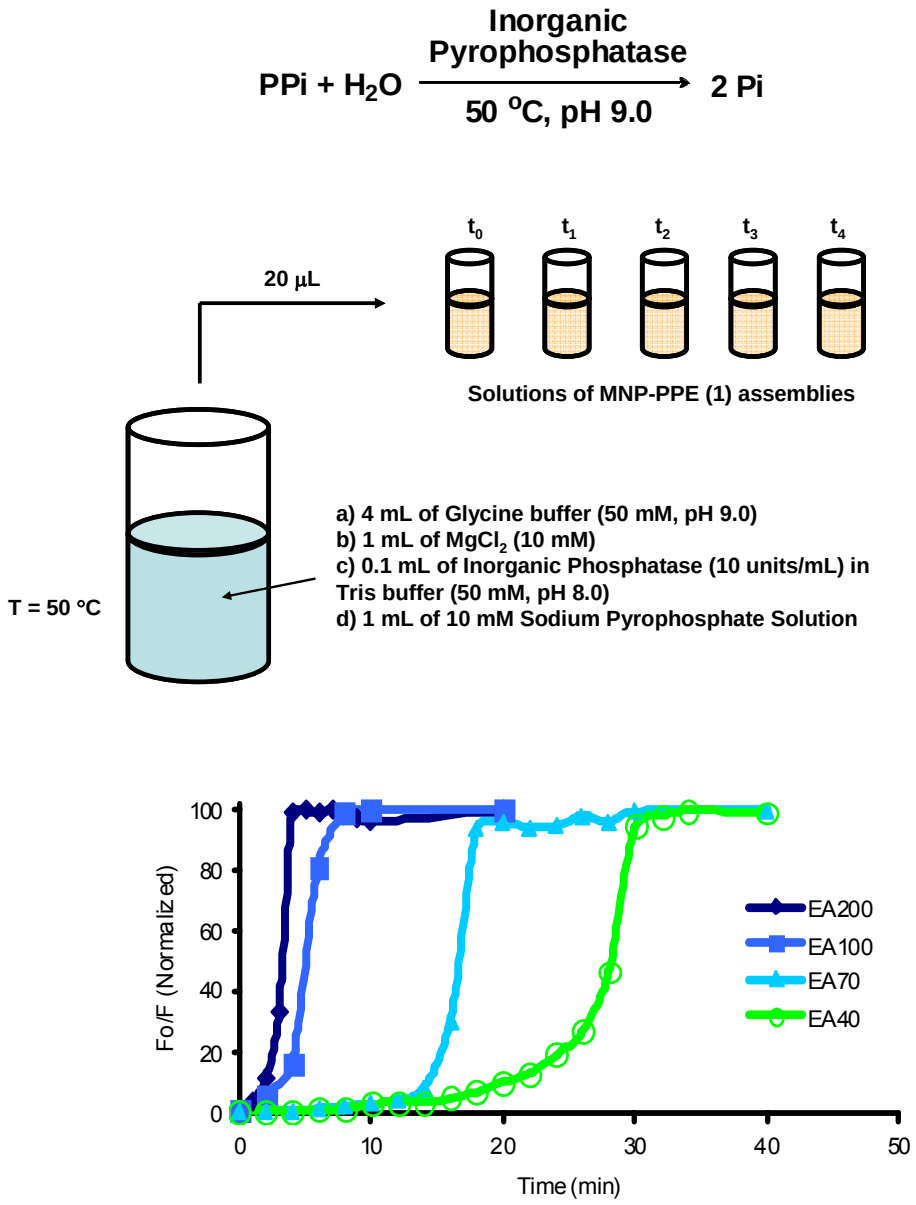

Figure 8.5. Kinetics of the enzymatic assay of pyrophosphatase monitored by the PNP. Concentration of the DMAB-NC s was 30 pmol; concentration of **8.1** was 5 µM. F_o is the fluorescence intensity from the solution of the assemblies, where 20 µL of the assay solution at $t_o = 0$ was transferred to the assembly solution, and F is the fluorescence intensity from the solution of the assemblies where 20 µL of the assay solution at time t was transferred to the assembly solution. EA200-EA40 indicates units of pyrophosphatase used in the enzymatic assays. EA200 = 2 units, EA100 = 1 unit, EA70 = 0.7 unit, and EA40 = 0.4 unit. If only enzyme is added, there is no change in fluorescence intensity.

A critical question for MA (Figure 8.6) is the determination of small amounts of PPi in the presence of a large excess of Pi as found in blood serum. Solutions 0.1 mM in Pi were spiked with increasing amounts of PPi at physiological pH. At a concentration of 0.1 mM, Pi does not disrupt the PNPs under release of the fluorescent PPE. Only a slight increase in fluorescence is visible. If solutions that contain 0.1 mM Pi and 400 nM of PPi are investigated, a sufficient amount of PPE is released to give rise to a strong signal. As the ratio of Pi/PPi is > 250 in blood serum, any proposed sensing scheme must show a selectivity of PPi/Pi significantly above 500. *The herein presented PNPs can detect PPi in a solution that is 40 nM in PPi and 0.1 mM in Pi, demonstrating that their selectivity against PPi/Pi is in the range of 2500, i.e. PPi can be detected in the presence of a 2500-fold excess of Pi* using a simple self-assembled PNP.

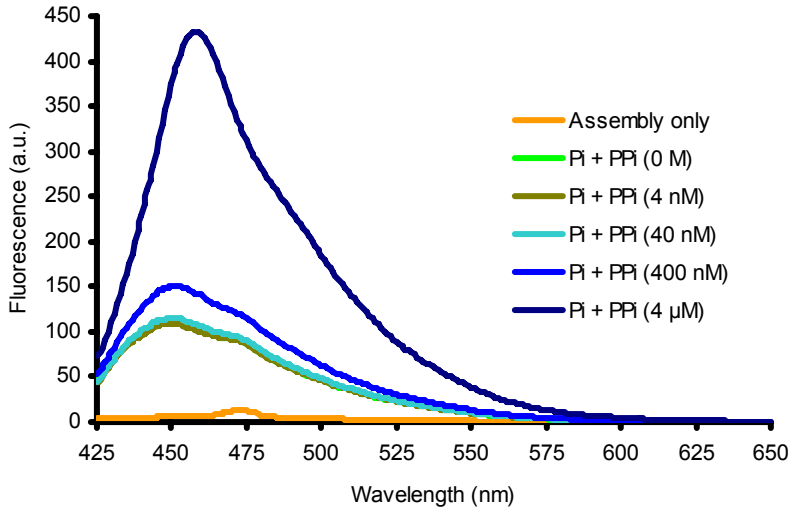

Figure 8.6. Fluorescence spectra of the solutions of the PNPs upon the addition of PPi ions in the presence of 0.1 mM of $HPO_4^{2-}/H_2PO_4^-$ ions at pH 7.2. Concentration of the NPs was 30 pmol; concentration of **8.1** was 5 µM.

8.3 Conclusion

DMAB-coated $(CoFe_2O_4)_x$-NCs combine with **8.1** to furnish non-fluorescent PNPs, acting as simple, self-assembled, convenient fluorescence turn-on probes for PPi at nanomolar concentrations. An imminent application of this scheme is the successful monitoring of phosphatase activity in vitro. The assay is robust as it can be performed in the presence of 0.1 mM Pi under physiological conditions and shows excellent selectivity for PPi. The combination of conjugated polymers with different surface-coated nanoparticles should provide PNPs of related structure with greatly varying analytical capabilities for the detection of Pi and related anions. Using a small ensemble of PNPs as "chemical tongues" or "chemical noses"[40] might help to discriminate biologically important species in serum, saliva and other biological fluids. The trivial ease of the assembly process combined with the broad array of nanoparticles and conjugated polymers available, should make PNPs and their assemblies powerful, yet simple, versatile biodiagnostic tools, in which the recognition element (nanoparticle) is separated from the transmission element (conjugated polymer) and therefore, independently addressable. As next step we will examine PNPs as nanomaterial-based[41-45] PPi and Pi sensors in clinical settings, and while the direct sensing of PPi is not possible, a suitable strategy would be to use a difference method (vide supra) to determine the concentration of PPi. This should be possible as the both the concentration ranges and the differences in sensitivity of our PNPs towards different phosphate-type anions in the concentrations that they are found in biological fluids are just correct for this approach.

8.4 Experimental

Instrumentation and Materials. All chemicals and solvents were used without further purification as received unless otherwise noted. Cobalt ferrite spinel NPs $(CoFe_2O_4)_x$[28] and 12-(trimethyl-ammonium)dodecanoate (TMAD)[46] were synthesized according to published procedure. Polymer **8.1** was synthesized according to a previous report[30] and had a number average molecular weight of 4,800 g/mol with a polydispersity index of 1.77. UV-VIS measurements were made with a Shimadzu UV-2401PC recording spectrophotometer. Fluorescence data were obtained with a Shimadzu RF-5301PC spectrofluorophotometer in quartz cuvettes. The fluorescence was recorded at room temperature. FTIR measurements were performed using a BIO-RAD FTS-6000 spectrometer. The samples were measured using a MTEC Model 300 photoacoustic cell. An average of 30 scans with a resolution setting of $4cm^{-1}$ was used to produce each spectrum. Concentrations of PPE (**1**) were adjusted to 5×10^{-6} M on the basis of the molecular weight of the repeating unit of PPEs.

8.5 References

1. Shanahan, C. M.; Cary, N.R.B.; Salisbury, J. R.; Proudfoot, D.; Weissberg, P.L.; Edmonds, M.E. "Medial localization of mineralization-regulating proteins in association with Monckeberg's sclerosis: evidence for smooth muscle cell-mediated vascular calcification" *Circulation* **1999**, 100, 2168.

2. Proudfoot, D.; Shanahan, C.M.; Weissberg, P.L. "Vascular calcification: new insights into an old problem" *J. Pathology* **1998**, *185*, 1.

3. Al-Absi, A.I.; Wall, B.M.; Cooke, C.R. "Medial arterial calcification mimicking temporal arteritis" *Am. J. Kidney Diseases* **2004**, *44*, 73.

4. Couri, C.E.B.;da Silva, G.A.; Martinez, J.A.B.; Pereira, F.D.A.; de Paula, F.J.A. "Monckeberg's sclerosis - is the artery the only target of calcification?" *Cardiovascular Disorders* **2005**, 5, 34.

5. Lomashvili, K.A.; Khawandi, W.; O'Neill, W.C. "Reduced plasma pyrophosphate levels in hemodialysis patients" *J. Am. Soc. Nephrol.* **2005**, 16, 2495.

6. Chantelau, E. *VASA-J. Vascular Diseases* **2001**, *30*, 15.

7. Fleisch, H.; Russell, R.G.; Straumann, F. "Effect of pyrophosphate on hydroxyapatite and its implications in calcium homeostasis" *Nature* **1966**, *212*, 901.

8. Biomaterials Science (Ed. B. Ratner, A. S. Hoffman, F. J.Schoen, J. E. Lemons,) Academic Press: London, **1996**.

9. Eibl, H.; Lands, W.E. "A new, sensitive determination of phosphate" *Anal. Biochem.* **1969**, *30*, 51.

10. Leiboff, S.L. "A colorimetric method for the determination of inorganic phosphate in blood serum" *J. Biol. Chem.* **1928**, *79*, 611.

11. Lust, G.; Seegmiller, J.E. "A rapid, enzymatic assay for measurement of inorganic pyrophosphate in biological samples" *Clin. Chim. Acta* **1976**, *66*, 241.

12. Cheung, C.P.; Suhadolnik, R. *J. Anal. Biochem.* **1977**, *83*, 61.

13. (a) Lee, H.N.; Xu, Z.; Kim, S.K.; Swamy, K.M.K.; Kim, Y.; Kim S.J.; Yoon, J. "Pyrophosphate-selective fluorescent chemosensor at physiological pH: formation

of a unique excimer upon addition of pyrophosphate" *J. Am. Chem. Soc.* **2007**, 129, 3828. (b) Jang, Y.J.; Jun, E.J.; Lee, Y.J.; Kim, Y.S.; Kim, J.S.; Yoon, J. "Highly effective fluorescent and colorimetric sensors for pyrophosphate over H_2PO_4- in 100% aqueous solution" *J. Org. Chem*. **2005**, 70, 9603.

14. a) Lee, D.H.; Kim, S.Y.; Hong, J.-I. "Fluorescent sensors: A fluorescent pyrophosphate sensor with high selectivity over ATP in water" *Angew. Chem. Int. Ed.* **2004**, 43, 4777. (b) Lee, D.H.; Kim, J.H; Son, S.U.; Chung, Y.K.; Hong, J.-I. "An azophenol-based chromogenic pyrophosphate sensor in water" *J. Am. Chem. Soc.* **2003**, 125, 7752.

15. Hanshaw, R.G.; Hilkert, S.M.; Jiang, H.; Smith, B.D. "An indicator displacement system for fluorescent detection of phosphate oxyanions under physiological conditions" *Tetrahedron Lett.* **2004**, 45, 8721.

16. Fabbrizzi, L.; Marcotte, N.; Stomeo, F.; Taglietti, A. "Pyrophosphate detection in water by fluorescence competition assays: inducing selectivity through the choice of the indicator" *Angew. Chem. Int. Ed.* **2002**, 41, 3811.

17. Mizukami, S.; Nagano, T.; Urano, Y.; Odani, A.; Kikuchi, K. "A fluorescent anion sensor that works in neutral aqueous solution for bioanalytical application" *J. Am. Chem. Soc.* **2002**, 124, 3920.

18. Vance, D.H.; Czarnik, A.W. "Real-time assay of inorganic pyrophosphatase using a high-affinity chelation-enhanced fluorescence chemosensor" *J. Am. Chem. Soc.* **1994**, *116*, 9397.

19. Beer, P.D.; Gale, P.A. "Anion recognition and sensing: the state of the art and future perspectives" *Angew. Chem. Int. Ed.* **2001**, *40*, 486.

20. Gunnlaugsson, T.; Glynn, M.; Tocci, G.M.; Kruger, P.E.; Pfeffer, F.M. "Anion recognition and sensing in organic and aqueous media using luminescent and colorimetric sensors" *Coord. Chem. Rev.* **2006,** 250, 3094.

21. For the sensing of PPi in non-aqueous solution see (a) Aldakov, D.; Anzenbacher, P. "Dipyrrolyl quinoxalines with extended chromophores are efficient fluorimetric sensors for pyrophosphate" *Chem. Commun.* **2003**, 1394. (b) Anzenbacher, P.; Palacios, M.A.; Kursikova, J.; Marquez, M. "Simple electrooptical sensors for inorganic anions" *Org. Lett.* **2005**, 7, 5027.

22. (a) Zhang, X.; Guo, L.; Wu, F.Y.; Jiang, Y.B. "Development of Fluorescent Sensing of Anions under Excited-State Intermolecular Proton Transfer Signaling Mechanism" *Org. Lett.* **2003**, 5, 2667-2670. (b) Kubo, Y.; Kato, M.; Misawa, Y.; Tokita, S. "A fluorescence-active 1,3-bis(isothiouronium)-derived naphthalene

exhibiting versatile binding modes toward oxoanions in aqueous MeCN solution: new methodology for sensing oxoanions" *Tetrahedron Lett*. **2004**, 45, 3769.

23. (a) Kim, I.B.; Bunz, U.H.F. "Modulating the sensory response of a conjugated polymer by proteins: an agglutination assay for mercury ions in water" *J. Am. Chem. Soc.* **2006**, 128, 2818. (b) You, C.C.; Miranda, O.R.; Gider, B.; Ghosh, P.S.; Kim, I.B.; Erdogan, B.; Krovi, S.A.; Bunz, U.H.F.; Rotello, V.M. "Detection and identification of proteins using nanoparticle-fluorescent polymer 'chemical nose' sensors" *Nature Nanotech.* **2007**, 2, 318. (d) Phillips, R.L.; Miranda, O.R.; You, C.C.; Rotello, V.M.; Bunz, U.H.F. "Rapid and efficient identification of bacteria using gold-nanoparticle-poly(para-phenyleneethynylene) constructs" *Angew. Chem. Int. Ed.* **2008**, 47, 2590.

24. For general reviews see: (a) Thomas, S.W.; Joly, G.D.; Swager, T.M. "Chemical sensors based on amplifying fluorescent conjugated polymers" *Chem. Rev.* **2007**, 107, 1339. (b) McQuade, D.T.; Pullen, A.E.; Swager, T.M. "Conjugated polymer-based chemical sensors" *Chem. Rev.* **2000**, 100, 2537. (c) Bunz, U.H.F. "Poly(aryleneethynylene)s: syntheses, properties, structures, and applications" *Chem. Rev*. **2000**, 100, 1605.

25. Liu, B.; Bazan, G.C. "Methods for strand-specific DNA detection with cationic conjugated polymers suitable for incorporation into DNA chips and microarrays" *Proc. Natl Acad. Sci. USA* **2005**, 102, 589.

26. Ho, H.A.; Leclerc, M. "Optical sensors based on hybrid aptamer/conjugated polymer complexes" *J. Am. Chem. Soc.* **2004**, 126, 1384.

27. Pinto, M.R.; Schanze, K.S. "Amplified fluorescence sensing of protease activity with conjugated polyelectrolytes" *Proc. Natl Acad. Sci. USA* **2004**, 101, 7505.

28. Song, Q.; Zhang, Z.J. "Shape control and associated magnetic properties of spinel cobalt ferrite nanocrystals" *J. Am. Chem. Soc.* **2004**, 126, 6164.

29. Kim, I.B.; Dunkhorst, A.; Bunz, U.H.F. "Nonspecific interactions of a carboxylate-substituted PPE with proteins. A cautionary tale for biosensor applications" *Langmuir* **2005***,* 21, 7985.

30. Kim, I.B.; Dunkhorst, A.; Gilbert, J.; Bunz, U.H.F. *"*Sensing of lead ions by a carboxylate-substituted PPE: multivalency effects" *Macromolecules* **2005**, 38, 4560.

31. Metzger, A.; Anslyn, E.V. "A chemosensor for citrate in beverages" *Angew. Chem. Int. Ed.* **1998**, 37, 649.

32. Lakowicz, J. R. *Principles of Fluorescence Spectroscopy*, 2nd Ed, Springer Verlag, New York, **2004**.

33. Fan, C.; Wang, S.; Hong, J.W.; Bazan, G.C.; Plaxco, K.W.; Heeger, A.J. "Beyond superquenching: Hyper-efficient energy transfer from conjugated polymers to gold nanoparticles" *Proc. Natl Acad. Sci. USA* **2003**, 100, 6297.

34. Since the quenching of the fluorescence of 1 by the NP could be due to internal filter effect as a consequence of the absorption of the NP, we measured the emission spectra of the solutions of the NP-1 assemblies after precipitation using a magnet. Under a magnetic field, free NPs and PPE 1 bound NPs were removed. The supernatant was effectively non-fluorescent after addition of NPs [40 pM], indicating the formation of the NP-PPE assemblies. The NP-PPE assemblies are easily re-dispersed into the solution by shaking in the absence of a magnetic field. The model compound 2 was not quenched by the NPs. The electrostatic interaction between 2 and NPs is insufficient to form a stable complex in the presence of buffer.

35. Yavuz Cafer, T.; Mayo, J.T.; Yu, W.W.; Prakash, A.; Falkner, J.C.; Yean, S.; Cong, L.; Shipley, H.J.; Kan, A.; Tomson, M.; Natelson, D.; Colvin, V.L. "Low-field magnetic separation of monodisperse Fe3O4 nanocrystals" *Science* **2006**, 314, 964.

36. Graaf, B.V.D.; Hoefnagel, A.J.; Wepster, B.M. "Substituent effects. 7. Microscopic dissociation constants of 4-amino- and 4-(dimethylamino)benzoic acid" *J. Org. Chem.* **1981**, 46, 653-657.

37. The Sigma quality control test procedure for the enzymatic assay of inorganic pyrophosphatase was employed.

38. A small aliquot of the assay was transferred to the solution of the assemblies at set time intervals. The fluorescence of the solution is measured after 20 min of incubation time. The initial concentration of sodium PPi in the assay was 1.6 mM [10 mmole]. One "unit" of pyrophosphatase will liberate 1.0 μmole of inorganic Pi per minute at pH 9.0 at 50 ^{o}C. The fluorescence recovery from the solution was gradually decreased with increasing incubation time. Beyond a certain incubation time of the assay, the fluorescence intensity of the solution remained constant, indicating that all of the PPi had been hydrolyzed by the enzyme. No further fluorescence recovery was observed.

39. Where a small aliquot of the assay solution was transferred to the test solution of the assemblies. Note that the addition of the enzyme in the solution of the assemblies does not change any fluorescence. The fluorescence intensity was measured until the intensity did not change further. Once the enzyme hydrolyzes all of pyrophosphate ions in the assay (or at very low concentration of PPi ions), the fluorescence of the solution of the assemblies remains unchanged. The normalized Fo/F was plotted as a function of incubation time in each experiment.

40. Albert, K.J.; Lewis, N.S.; Schauer, C.L.; Sotzing, G.A.; Stitzel, S.E.; Vaid, T.P.; Walt, D.R. “Cross-reactive chemical sensor arrays” *Chem. Rev.* **2000**, 100, 2595.

41. Rosi, N.L.; Mirkin, C.A. “Nanostructures in biodiagnostics” *Chem. Rev.* **2005**, 105, 1547.

42. Alivisatos, P. “The use of nanocrystals in biological detection” *Nature Biotechnol.* **2004**, 22, 47.

43. Chan, W.C.W.; Nile, S. “Quantum dot bioconjugates for ultrasensitive nonisotopic detection” *Science* **1998**, 281, 2016.

44. Zhang, C.Y.; Yeh, H.C.; Kuroki, M.T.; Wang, T.H. “Single-quantum-dot-based DNA nanosensor” *Nature Mater.* **2005**, 4, 826.

45. Medintz, I.L.; Clapp, A.R.; Mattoussi, H.; Goldman, E.R.; Fisher, B.; Mauro, J. M. “Self-assembled nanoscale biosensors based on quantum dot FRET donors” *Nature Mater.* **2003**, 2, 630.

46. Srivastava, S.; Samanta, B.; Jordan, B.J.; Hong, R.; Xiao, Q.; Tuominen, M.T.; Rotello, V.M. “Integrated Magnetic Bionanocomposites through Nanoparticle-Mediated Assembly of Ferritin” *J. Am. Chem. Soc.* **2007**, 129, 11776-11780.

CHAPTER 9

Gold Nanoparticle-PPE Constructs for the Detection of Pathogens

9.1 Introduction

Fast and efficient identification of pathogens in water and biological fluids is an important issue in medical, forensic and environmental sciences.[1-2] We demonstrate herein that non-covalent conjugates of gold nanoparticles[3] and a fluorescent polymer[4-8] identify bacteria effectively within minutes. Nanoparticle-bacteria interactions release the bound fluorescent polymer from the gold nanoparticle quencher, resulting in a "turn-on" of the polymer's fluorescence. The fluorescence responses generated by the bacterial surfaces provide an efficient means of their discrimination.[5] We have differentiated 12 bacteria by this method. Both species of bacteria as well as strains of a single species were discerned, without the use of antibodies[6-7] or radioactive markers.[8]

Conventional plating and culturing[9] is generally used to identify causative bacterial pathogens in clinical environments. While technologically advanced systems have been developed for specific microorganisms,[10] these methods are complex or require sophisticated instrumentation. Plating and culturing is accurate, but requires >24 h. Point-of-care treatment decisions are therefore made *without* access to microbiological information, potentially leading to the prescription of a sub-optimal antibiotic. An example is the treatment of keflex- or methicillin-resistant *S. aureus* strains (MRSA) in community-acquired infections that require treatment with either sulfa drugs or vancomycin.[11] Reisner et al. have investigated >9000 cases of clinically reported bacterial infections[9] and found that 85-90% were due to only seven pathogens with *S.*

aureus and *E. coli* being responsible for half of all infections. A simple and rapid test that could discern clinically prevalent pathogens would be of great value, increasing the efficacy of therapy, and reducing the occurrence of drug-resistant bacteria arising from inefficient antibiotic prescription.

The detection of bacteria and pathogens plays a crucial role in food safety.[12] For example, *E. coli* O157:H7 is a world-wide cause of foodborne illness, responsible for more than 2000 hospitalizations and 60 deaths directly related to bacterial infection each year in the United States.[7,13] Major outbreaks were associated with the contamination of unpasteurized juice, vegetables, water, etc.[14] However, testing food for contamination is difficult due to the complex and/or lengthy analysis protocols.

To address the issue of rapid identification of bacteria, we developed a protocol for bacterial sensing using an array of gold nanoparticle-conjugated polymer constructs.[15-16]This 'chemical nose' combines a series of analyte receptors to differentiate targets according to their unique response diagrams. An anionic conjugated polymer (Figure 9.1) is initially associated with cationic gold nanoparticles to afford fluorescence-quenched complexes. In the presence of bacteria, the negatively-charged bacterial surface[17] competitively interacts with the nanoparticles to release the semiconducting polymer, restoring fluorescence; 1.6 nm gold nanoparticles[18] seem to recognize patches of hydrophobic/functional surfaces on microorganisms and poly(L-lysine)-coated gold nano-particles self-assemble with live bacteria through complementary electrostatic interactions.[19-21] The π-conjugated polymer used in this study provides both multivalency[20] and the molecular wire effect[21] to facilitate efficient signal generation in the sensing process. As functional "patches" (*e.g.* the charged residues and hydrophobic

"hot spots") are prevalent on cell and microbial exteriors,[21] this strategy has potential applications in the identification of a wide variety of microorganisms.

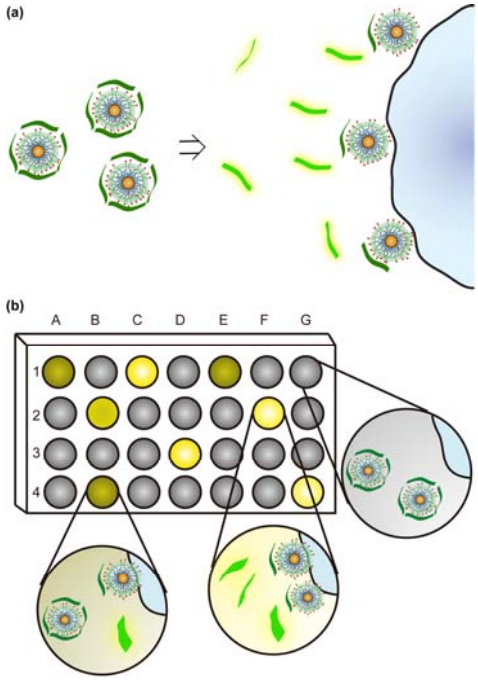

Figure 9.1. Design of the nanoparticle-conjugated polymer sensor array. a) Schematic representation of the displacement of anionic conjugated polymers from cationic nanoparticles by negatively charged bacterial surfaces. b) Schematic illustration of fluorescence pattern generation on a microplate.

9.2 Results and Discussion

For the fluorophore displacement strategy we chose **Sw-CO$_2$**[22] and three hydrophobic ammonium-functionalized gold nanoparticles (**NP$_1$-NP$_3$**)[16] as sensor elements (Figure 9.2). Fluorescence titration studies revealed that the cationic gold nanoparticles (**NP$_1$-NP$_3$**) quench the fluorescence of **Sw-CO$_2$** through formation of supramolecular complexes (Figure 9.3 and Table 9.1).[15]

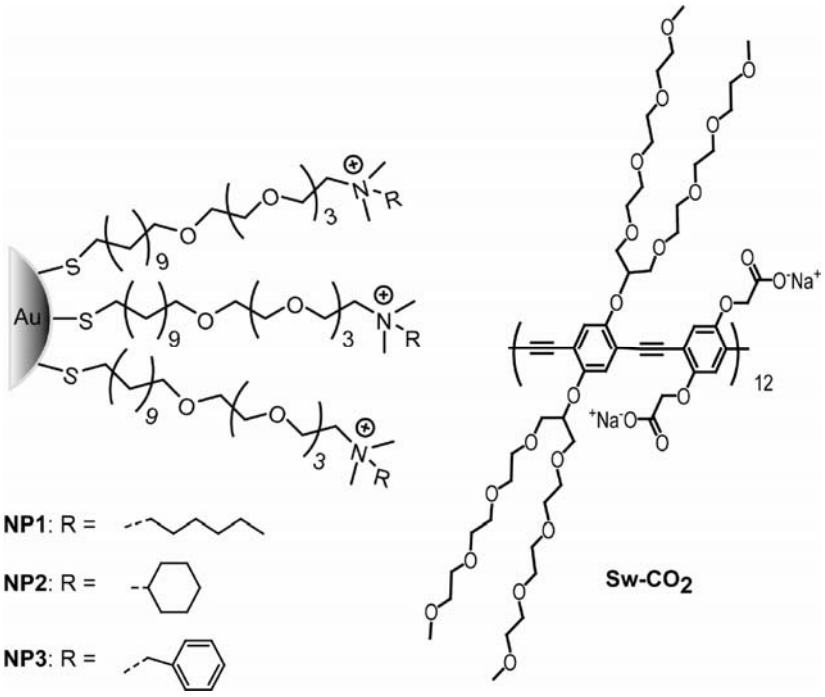

Figure 9.2. Receptor and transducer components of the bacterial sensors. a) Structural representation of three cationic gold nanoparticles (**NP_1-NP_3**) with various hydrophobic tails. b) Chemical structure of the conjugated polymer (**Sw-CO_2**) featuring a branched oligo(ethylene glycol) side chain to suppress non-specific polymer-microorganism interactions.

Quenching by the nanoparticle is efficient: typically, an aqueous solution of the polymer (100 nM, based on 12 repeat units/polymer) with a stoichiometric amount of nanoparticle displays approximately 20% of the initial fluorescence of **Sw-CO_2** (Φ = 0.33). The polymer and a stoichiometric amount of nanoparticles (**NP_1-NP_3**) were mixed in 5 mM phosphate buffer (pH 7.4) to yield nanoparticle-**Sw-CO_2** constructs with final polymer and nanoparticle concentrations of 100 nM and 10-40 nM, respectively.

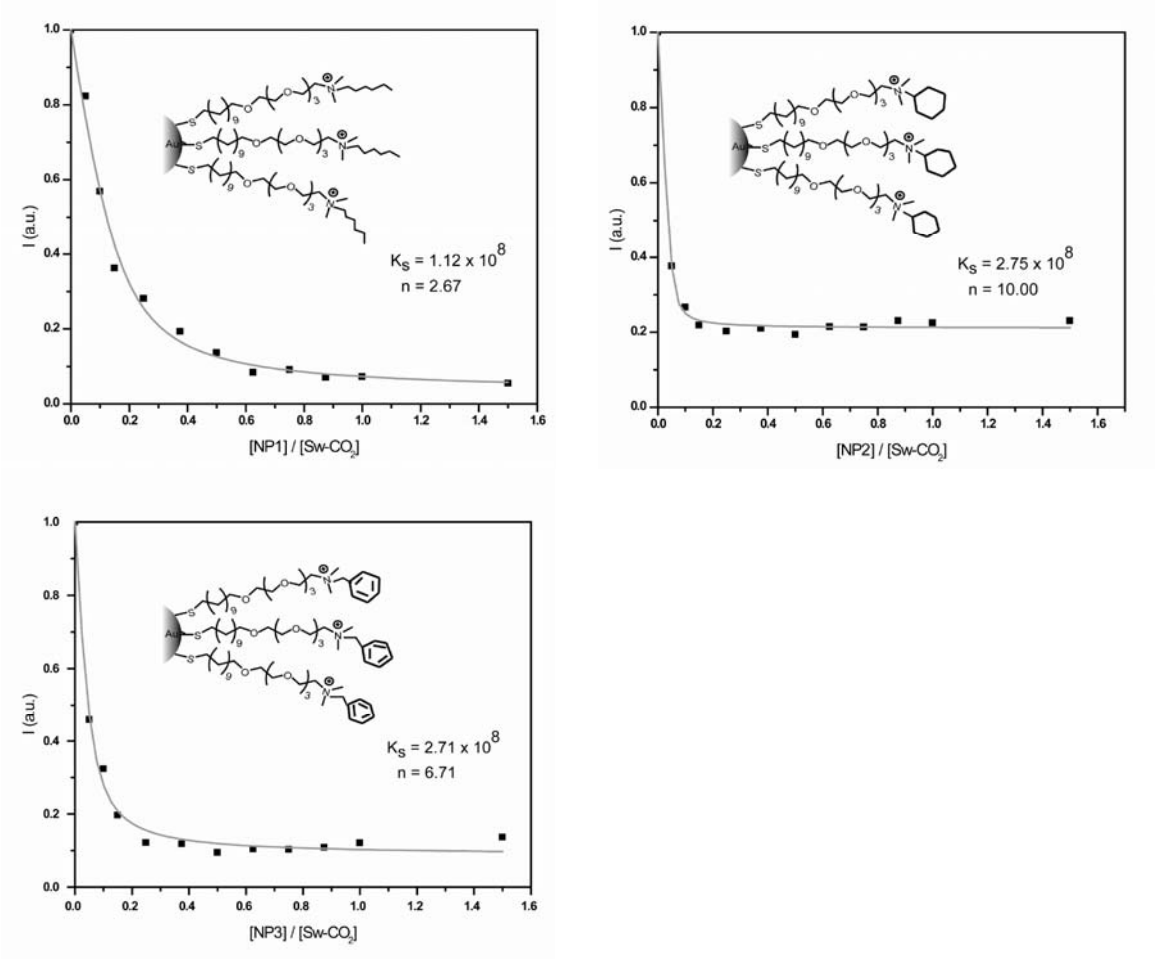

Figure 9.3. Fluorescence titration curves for the complexation of **Sw-CO$_2$** (100 nM) with cationic gold nanoparticles (**NP$_1$-NP$_3$**). The changes in fluorescence intensity at 463 nm were measured following the addition of cationic nanoparticles (0-150 nM) with an excitation wavelength of 400 nm. The solid lines represent the best curve-fitting using a calculation model of a single set of identical binding sites.

Table 9.1. Binding constants (K_S) and binding stoichiometries (n) between anionic polymer (**Sw-CO$_2$**) and three cationic nanoparticles (**NP$_1$-NP$_3$**) as determined from fluorescence titration.

Nanoparticle	K_S / 10^8 M^{-1}	$-\Delta G$ / kJ mol^{-1}	n
NP$_1$	1.12	45.9	2.67
NP$_2$	2.75	48.1	10.0
NP$_3$	2.71	48.1	6.71

The exposure of these three nanoparticle-**Sw-CO_2** constructs towards bacteria (OD_{600} = 0.05) induced different levels of fluorescence changes (Figure 9.4). In most cases, the fluorescence of the solution increases upon addition of the microorganisms. Significantly, the fluorescence changes exhibit reproducible patterns that depend upon the strains and classes of bacteria, indicating differentiation in the fluorophore displacement.

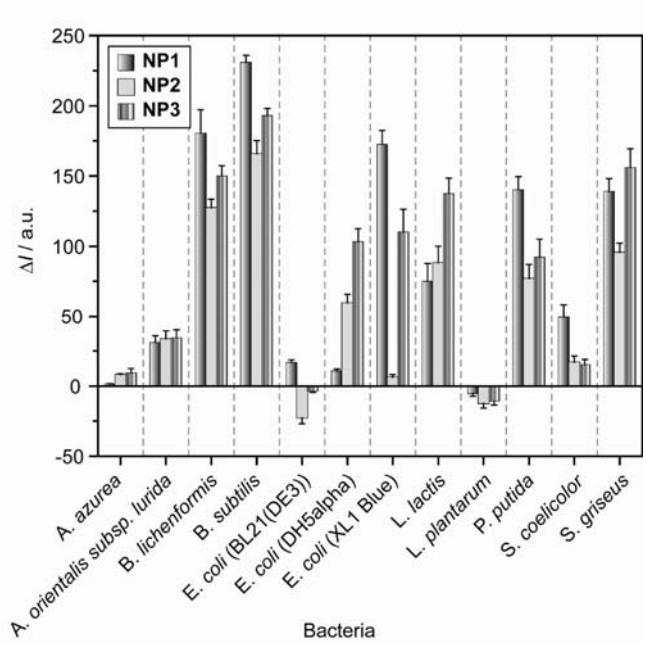

Figure 9.4. Fluorescence response patterns of nanoparticle-polymer constructs in the presence of various bacteria (OD_{600} = 0.05). Each value is an average of six parallel measurements and the error bars are shown.

The 12 different bacteria display excellent separation when the fluorescence changes were plotted in a three-dimensional graph with the fluorescence change of the three nanoparticles (**NP_1-NP_3**) as the respective axes (Figure 9.5), explicitly demonstrating the ability of these particles to discriminate between bacteria.

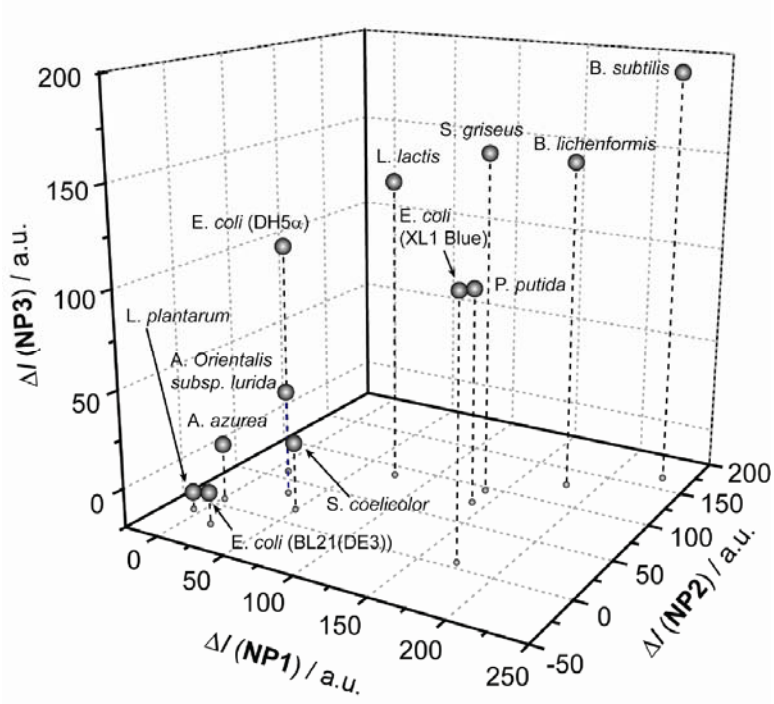

Figure 9.5. Fluorescence response patterns of nanoparticle-polymer constructs in the presence of various bacteria (OD_{600} = 0.05). Three-dimensional representation of the fluorescence intensity changes against the three nanoparticle-polymer constructs.

Initially both hydrophilic and hydrophobic nanoparticles were tested for the array. Upon incubation with bacteria, however, only the hydrophobic ones (**NP_1-NP_3**) produced significant fluorescence recovery. Since hydrophobic and hydrophilic nanoparticles exhibit comparable binding affinities to **Sw-CO_2**, the difference in the fluorescence recovery indicates that the former strongly interact with bacteria. A plausible explanation is that the hydrophobic parts of the nanoparticles interact with hydrophobic regions on the surface of the bacteria (*e.g.* the alkyl chains in teichoic acid), enhancing the electrostatic nanoparticle-bacteria interaction and, thereby, the fluorescence regeneration. Both electrostatic and hydrophobic interactions seem to play important roles in the complexation of these particles with bacteria. We plan to engineer nanoparticles with

varying size, shape and hydrophobicity to augment the diversity in the fluorescence response.

The fluorescence response patterns were analyzed through linear discriminant analysis (LDA), a quantitative statistical method extensively used in pattern recognition.[23-24] Discriminant functions were deduced by maximizing the separation between classes relative to the variation within classes; LDA (Figure 9.6) transformed the raw patterns to canonical scores which are clustered into 12 groups according to the individual bacteria.

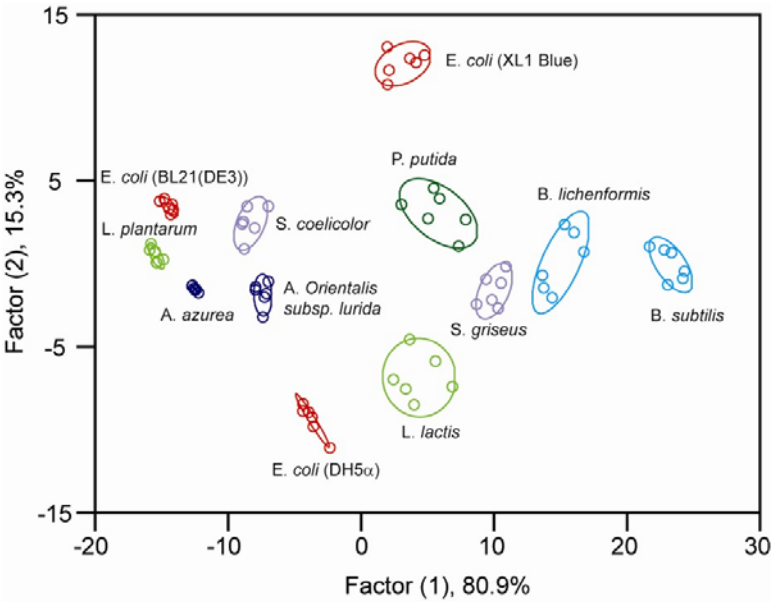

Figure 9.6. Canonical score plot for the fluorescence response patterns as determined with LDA. The first two factors consist of 96.2% variance and the 95% confidence ellipses for the individual bacteria are depicted.

The jackknifed matrix (with cross-validation) in LDA reveals a 100% classification accuracy. We can discern all 12 microorganisms, which contain both Gram-positive (e.g. *A. azurea*, *B. subtilis*) and Gram-negative (e.g. *E. coli, P. putida*) species.

The LDA plot does not place the Gram-negative bacteria into an identifiable part of the graph, suggesting that other effects are also involved in the discrimination process. Different strains of *E. coli* can be easily discerned with the current sensor array but the three *E. coli* strains are not grouped particularly close in the LDA plot, indicating that subtle differences in the bacteria generate marked changes in response. While the herein introduced concept is useful, it should be noted that the present system can merely differentiate bacteria in a clean buffered solution. Although, it is suitable to analyze many biological samples (e.g. water), pre-separation is required for most biological fluids as the concomitant proteins may affect the analytical results. In this regard, the introduction of recognition elements specific for a bacterial surface on the nanoparticles would greatly address this problem.

With the patterns shown in Figure 9.4 as the training matrix (3 constructs × 12 bacteria × 6 replicates), we can identify unknown solutions of bacteria, randomly selected from the 12 bacterial species grown in different batches. Fluorescence response patterns generated from the three nanoparticle-polymer constructs were analyzed by LDA. After transformation of the patterns to the canonical scores using the discriminant functions established on the training samples, the Mahalanobis distances of the new case to the respective centroids of 12 groups were calculated. The closer a specific data set is to the center of one group, the more likely it belongs to that group. This assignment is based on the shortest Mahalanobis distance to the 12 bacteria in a three-dimensional space (canonical factors 1 to 3). For the 64 samples studied, 61 were correctly identified; a detection accuracy of >95% demonstrates expediency and reliability. The differentiation

of the three strains of *E. coli* suggests suitable identification of pathogenic strains of normally harmless bacteria.

9.3 Conclusion

The integration of cationic gold nanoparticles with conjugated polymers provides an easily accessible yet potentially powerful biodiagnostic tool, in which the functional nanoparticles and the fluorescent polymer serve as the recognition elements and the transducer, respectively. The efficient quenching ability of gold nanoparticles coupled with the 'molecular wire' effect of conjugated polymers compound the pronounced fluorescence response, which is dictated by the binding strength of the bacterium to the gold nanoparticle. Therefore, manipulating the surface chemistry of gold nanoparticles and the constitution of the conjugated polymer will result in constructs with expanded binding capabilities. By investigating the mechanism of binding which occurs between the hydrophobic nanoparticles and the conjugated polymer, we should be able to gain an understanding of the specific factors which govern fluorescence recovery. Based on our ability to readily differentiate 12 different bacteria using only three systems, we speculate that the detection of *any* microorganism including the differentiation of pathogenic and resistant strains will be possible with this approach.

9.4 Experimental

Instrumentation and Materials. The number average molecular weight (M_n = 25 kDa), polydispersity index (PDI = 1.8) and degree of polymerization (P_n = 12) of **Sw-CO$_2$** were determined by gel permeation chromatography. The cationic gold nanoparticles (**NP$_1$-**

NP_3, $d \sim 2$ nm)[16] were synthesized according to published procedures. The bacteria, including *Amycolatopsis azurea* (*A. azurea*), *Amycolatopsis orientalis subsp. lurida* (*A. orientalis subsp. lurida*), *Bacillus lichenformis* (*B. lichenformis*), *Bacillus subtilis* (*B. subtilis*), *Escherichia coli (BL21(DE3))* (E.*coli (BL21(DE3*)), *Escherichia coli (DH5α)* (*E.coli (DH5α)), Escherichia coli* (*XL1 Blue*) (*E.coli* (*XL1 Blue*)), *Lactococcus lactis* (*L. lactis*), *Lactococcus plantarum* (*L. plantarum*), *Pseudomonas putida* (*P. putida*), *Streptomyces coelicolor* (*S. coelicolor*), and *Streptomyces griseus* (*S. griseus*), were graciously donated by Dr. A. Bommarius (Georgia Institute of Technology) and Dr. J. Hardy (University of Massachusetts Amherst). Fluorescence intensity changes at 463 nm were recorded in 96-well plates (300 μL Whatman® Glass Bottom microplate) on a Molecular Devices SpectraMax M5 micro plate reader with an excitation wavelength of 400 nm

Bacterial Stock Preparation. Bacterial cells were grown in LB medium (3 mL) at 37 ºC to an optical density of 1.0 at 600 nm. The cultures were centrifuged (4000 rpm, 15 min) and washed with phosphate buffer (5 mM, pH 7.4) three times, resuspended in phosphate buffer and diluted to an absorbance of 1.0 at 600 nm.

Fluorescence Titrations. Fluorescence titration experiments determined the complexation between nanoparticles and **Sw-CO_2**. Fluorescence intensity changes at 463 nm were recorded with an excitation wavelength of 400 nm.

Fluorophore Displacement. **Sw-CO_2** and stoichiometric amounts of **NP_1-NP_3**, as determined by the fluorescence titration study were diluted with phosphate buffer (5 mM, pH 7.4) to solutions with a final **Sw-CO_2** concentration of 100 nM. Each solution (200 μL) was placed into a well on the microplate. After incubation for 15 min, the

fluorescence intensity at 463 nm was recorded with an excitation wavelength of 400 nm. Next, 10 μL of a bacterial solution (OD_{600} = 1.0) was added to each well. After incubation for another 15 min, the fluorescence intensity at 463 nm was measured again.

LDA Analysis. The fluorescence intensity before addition of the bacteria was subtracted from that obtained after addition of the bacteria to record the overall fluorescence response (ΔI). This process was completed for 12 bacteria to generate six replicates of each, leading to a training data matrix of 3 constructs × 12 bacteria × 6 replicates that was subjected to a classical linear discriminant analysis (LDA) using SYSTAT (version 11.0). The Mahalanobis distances of each individual pattern to the centroid of each group in a multidimensional space were calculated and the case was assigned to the group with the shortest Mahalanobis distance. A similar procedure was also performed to identify 64 randomly selected bacterial samples based on their fluorescence response patterns. The classification of new cases was achieved by computing their shortest Mahalanobis distances to the groups generated through the training matrix (3 constructs ($\mathbf{NP_1}$-$\mathbf{NP_3}$) × 12 bacteria × 6 replicates). During the identification of unknown bacteria, the bacterial samples were randomly selected from the 12 respective bacteria and the solution preparation, data collection, and LDA analysis were each performed by different researchers, resulting in a double-blind process.

9.5 References

1. Deisingh, A.K.; Thompson, M. “Detection of infectious and toxigenic bacteria.” *Analyst* **2002**, 127, 567-581.

2. Berry, V.; Gole, A.; Kundu, S.; Murphy, C.J.; Saraf, R.F. “Deposition of CTAB-terminated nanorods on bacteria to form highly conducting hybrid systems.” *J. Am. Chem. Soc*. **2005**, 127, 17600-17601.

3. Daniel, M.C.; Astruc, D. “Gold nanoparticles: Assembly, supramolecular chemistry, quantum-size-related properties, and applications toward biology, catalysis, and nanotechnology.” *Chem. Rev.* **2004**, 104, 293-346.

4. Thomas, S.W.; Joly, G.D.; Swager, T.M. “Chemical sensors based on amplifying fluorescent conjugated polymers.” *Chem. Rev*. **2007**, 107, 1339-1386.

5. Rosi, N.L.; Mirkin, C.A. “Nanostructures in biodiagnostics.” *Chem. Rev*. **2005**, 105, 1547-1562.

6. Zhao, X.; Hilliard, L.R.; Mechery, S.J.; Wang, Y.; Bagwe, R.P.; Jin, S.; Tan, W. “A rapid bioassay for single bacterial cell quantitation using bioconjugated nanoparticles.” *Proc. Natl. Acad. Sci. U.S.A*. **2004**, 101, 15027-15032.

7. Bertozzi, C.R.; Bednarski, M.D. “Antibody targeting to bacterial-cells using receptor-specific ligands.” *J. Am. Chem. Soc*. **1992**, 114, 2242-2245.

8. Amann, R.I.; Ludwig, W.; Schleifer, K.H. “Phylogenetic identification and in-situ detection of individual microbial-cells without cultivation.” *Microbiol. Rev*. **1995**, 59, 143-169.

9. Reisner, B.S.; Woods, G.L. Reisner, B.S.; Woods, G.L. *J. Clin. Microbiol*. **1999**, 37, 2024-2026. “Times to detection of bacteria and yeasts in BACTEC 9240 blood culture bottles.” *J. Clin. Microbiol*. **1999**, 37, 2024-2026.

10. See Table S5 in Supporting Information and extra citations in the SI.

11. Edmond, M.B.; Wallace, S.E.; McClish, D.K.; Pfaller, M.A.; Jones, R.N.; Wenzel, R.P. "Nosocomial bloodstream infections in United States hospitals: A three-year analysis.” *Clin. Infect. Dis*. **1999**, 29, 239-244.

12. Batt, C.A. “Materials science - Food pathogen detection.” *Science* **2007**, 316, 1579-1580.

13. Frenzen, P.D.; Drake, A.; Angulo, F.J. “Economic cost of illness due to Escherichia coli O157 infections in the United States.” *J. Food Prot*. **2005**, 68, 2623-2630.

14. Mead, P.S.; Slutsker, L.; Dietz, V.; McCaig, L.F.; Bresee, J.S.; Shapiro, C.; Griffin, P.M.; Tauxe, R.V. "Food-related illness and death in the United States." *Emerg. Infect. Dis*. **1999**, 5, 607-625.

15. Fan, C.; Plaxco, K.W.; Heeger, A.J. "High-efficiency fluorescence quenching of conjugated polymers by proteins." *J. Am. Chem. Soc*. **2002**, 124, 5642-5643.

16. You, C.C.; Miranda, O.R.; Gider, B.; Ghosh, P.S.; Kim, I.B.; Erdogan, B.; Krovi, S.A.; Bunz, U.H.F.; Rotello, V.M. "Detection and identification of proteins using nanoparticle-fluorescent polymer 'chemical nose' sensors" *Nat. Nanotechnol*. **2007**, 2, 318-323.

17. (a.)Teichoic acids and lipoteichoic acids are present on the surface of Gram-positive bacteria, while the outer membranes of Gram-negative bacteria are composed of lipopolysaccharides (LPSs). Furthermore, the membranes of most bacteria contain a large amount of anionic phospholipids (e.g. phosphatidylgylcerol), making the bacterial surface negatively charged; (b) M. Kates in Handbook of Lipid Reseach: Glycolipids, Phosphoglycolipids and Sulfoglycopids, ed. M. Kates, Plenum Publishing Corporation, Springer; 1st edition, 1990, pp. 123-234; (c) Dmitriev, B.; Toukach, F.; Ehlers, S. "Towards a comprehensive view of the bacterial cell wall" *TRENDS in Microbiology*, **2005**, 13, 569-574; (d) Koch, A.L. "Bacterial walls as target for attack" *Clinical Microbiology Reviews*, **2003**, 16, 673-687; (e) Schaffer, C.; Messner, P. " The structure of secondary cell wall polymers: how Gram-positive bacteria stick their cell walls together" *Microbiology*, **2005**, 151, 643-651; (f) Bos, M.P.; Tefsen, B.; Geurtsen, J.; Tommassen, J. "Identification of an outer membrane protein required for the transport of lipopolysaccharide to the bacterial cell surface" *PNAS*, **2004**, 101, 9417-9422.

17. Dynamic light scattering (DLS) investigation revealed that the gold nanoparticles used in this study have a hydrodynamic diameter of 8~9 nm.

18. Niemeyer, C.M. *Angew. Chem*. **2001**, 113, 4254-4287; "Nanoparticles, proteins, and nucleic acids: Biotechnology meets materials science"*Angew. Chem. Int. Ed*. **2001**, 40, 4128-4158.

19. Kim, I.B.; Erdogan, B.; Wilson, J.N.; Bunz, U.H.F. "Sugar-poly(para-phenylene ethynylene) conjugates as sensory materials: Efficiency quenching by Hg2+ and Pb2+ ions." *Chem. Eur. J*. **2004**, 10, 6247-6254.

20. Zhou, Q.; Swager, T.M. "Fluorescent chemosensors based on energy migration in conjugated polymers: The molecular wire approach to increased sensitivity" *J. Am. Chem. Soc*. **1995**, 117, 12593-12602.

21. Kim, I.B.; Phillips, R.; Bunz, U.H.F. “Carboxylate group side-chain density modulates the pH-dependent optical properties of PPEs” *Macromolecules* **2007**, 40, 5290-5293.

22. R. G. Brereton in Chemometrics: Data Analysis for the Laboratory and Chemical Plant, John Wiley & Sons, Ltd. 2003.

23. Jurs, P.C.; Bakken, G.A.; McClelland, H.E. “Computational methods for the analysis of chemical sensor array data from volatile analytes” *Chem. Rev*. **2000**, 100, 2649-2678.

CHAPTER 10

Gold Nanoparticle-PPE Constructs as Biomolecular Material Mimics: Understanding the Electrostatic and Hydrophobic Interactions

10.1 Introduction

The combination of CPs with ANPs is a powerful one that has lead to novel biomolecular and bio-inspired materials with hierarchical structures.[1] This alliance is attractive not only from a structural standpoint, as the properties of both components are easily modified, but from an electronic one as well: ANPs and CPs interact by energy transfer and both have transitions in the visible or in the UV range. These interactions are examplified by reported combinations of poly(*p*-phenylenevinylene)s (PPV), polyfluorenes (PF) and poly(p-phenyleneethynylene)s (PPE) with ANPs.[2-3] A seminal study on the interaction of CPs and ANPs was published by Heeger and Bazan.[2] They observed that electrostatic interactions between a negatively charged ANP and positively charged conjugated polymers of the PPV and the PF types lead to efficient binding between the ANP and the CP as indicated by the ANPs' ability to quench the fluorescence of the CP.

We have recently employed hydrophobically functionalized ANPs in combination with the CP **Sw-CO_2** as powerful constructs to discern proteins and bacteria through fluorescence recovery via displacement assays. In the course of these investigations we noted significant variance in the binding of the positively charged ANPs to negatively charged CPs depending on the structural features of the ANP.

It is not clear how the hydrophobicity of a monolayer protected ANP influences the magnitude of the interaction between ANP and CP (in this case the highly fluorescent **Sw-CO$_2$** with a quantum yield (Φ_F greater than 0.3). As such, we were interested in preparing a series of nanoparticles (**NP$_1$-NP$_{11}$**) that differed only in the size and structure of their exterior ammonium group (Fig. 10.1). Though there has been a thorough study on the quenching of ANPs by CPs by Bazan and Heeger, these authors used citrate-coated ANPs that interacted with positively charged CPs; modulation of the binding between ANP and CP by changing the exposed end of the protective monolayer has not been reported. A technical issue we have found necessary to address is how to perform the data analysis pertaining to the quenching experiments between ANPs and CPs. Results of quenching experiments involving CPs are analyzed using a simple Stern-Volmer formalism,[4] by which, if static quenching can be assumed,[5] the binding constant between an ANP and a fluorophore is extracted from the following equation (Eq. 10.1):

$$\frac{I_0}{I_{[Q]}} = 1 + K_{SV}[Q]$$

$I_0/I_{[Q]}$ is the quotient of the fluorescence intensity in the absence (I_0) and the presence of a specific concentration [Q] of the quencher Q ($I_{[Q]}$). K_{sv} represents the binding constant between ANP and CP. From this simple equation Heeger and Bazancalculated binding constants between ANP and conjugated polymer that were in excess of $K_{SV} = 10^{10}$ M^{-1}. While this data workup is simple, it is not without problems (vide infra). The highly efficient quenching process brought on by complexation of the ANP and the CP is of unusually large magnitude and may be a consequence of both the molecular wire effect and the efficient Förster type energy

transfer from the excited state of the conjugated polymer to the plasmon band of the ANP. Polyvalency[6-7] is probably also involved, as it can be reasonably assumed that multiple electrostatic interactions occur between polymer chain and a single ANP. Despite the strength of the interaction between CP and ANP, their affinity for one another can be modulated by varying the structure of the positively charged monolayer ensheathing the ANP.

ANPs are easily synthesized[8-10] and monolayer functionalized with different and suitably substituted thiols or disulfides that chemisorb and oxidatively add to the gold surface after ANP formation. As the number of potential disulfide and thiol ligands is essentially unlimited, different ligand coating can give ANP unique physical and chemical properties; ANP-conjugated polymer constructs form when the two components are mixed. Upon addition of a sufficient amount of nanoparticle to the system, the fluorescence of the conjugated polymer is fully quenched.[11] These ANP-PPE complexes can be disrupted by the introduction of a suitable, charged analyte, which leads to free PPE chains in solution and a subsequent fluorescence turn-on.

We have exploited this principle for the successful sensing of both proteins[11] and bacteria.[12] As we have created libraries of nanoparticles, we can influence both the binding of the employed PPE as well as its decomplexation from the ANP by an analyte.

Our recently published bacterial sensor[12] employing three simple ANP-PPE constructs showed impressive selectivity; however, it is also helped to illustrate the effect of increasing salt concentration on the binding between ANP and conjugated polymers,

as well as to demonstrate the influence of the hydrophobic character of the monolayer protected ANPs on the binding constant K_B between ANP and CP. Herein we investigate the influence of increasing hydrophobic character on the ANP/CP binding and examine its dependence upon ionic strength.

10.2 Results and Discussion

The Ligands **L_1-L_{11}** were synthesized according to Scheme 10.1 through quaternization of the tertiary amines **1-11** by the mesylate **L_0**. Deprotection with trifluoroacetic acid in the presence of triisopropylsilane as a reducing agent gave **L_1-L_{11}** as yellowish oils.

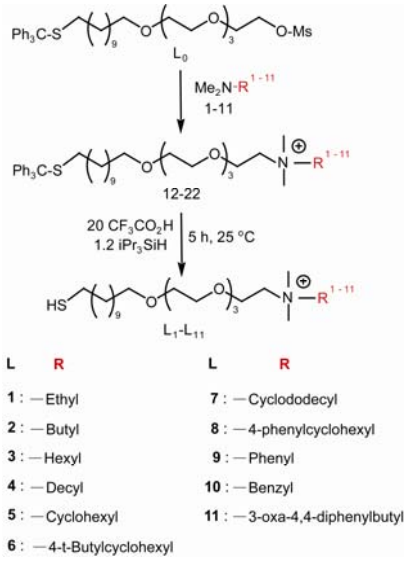

Scheme 10.1. Synthesis of the thiols **L_1-L_{11}**. Yields of **L_1-L_{11}** are above 95% in all cases starting from **L_0**.

The **NP_1-NP_{11}** were synthesized by dissolving pentanethiol-protected ANPs generated from a literature procedure[13] in dried dichloromethane (DCM) and subsequently adding thiols **L_1-L_{11}** respectively. Removal of solvent, dialysis in water and

lyophilization afforded **NP_1-NP_{11}** as brownish-red powders, which freely re-dispersed in water.

The PPE **Sw-CO_2** was prepared according to a literature procedure[14] and used as a 5 micromolar solution in buffer. The polymer had a degree of polymerization (P_n) of 12 and a molecular weight (M_n) of 14 KDa with a polydispersity index (PDI) of 1.8.

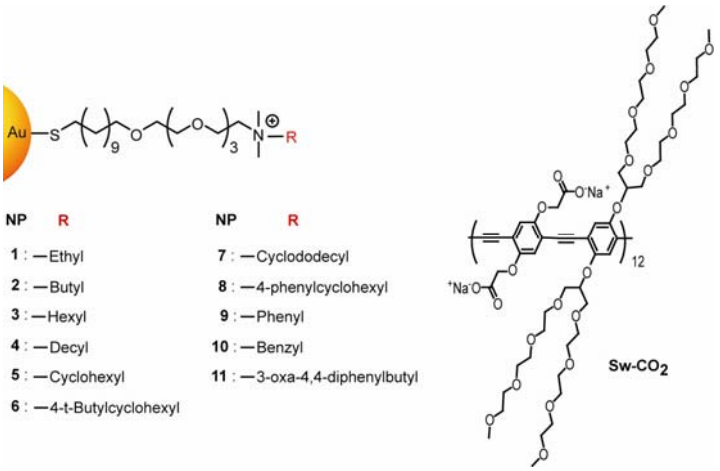

Figure 10.1. Monolayer protected gold nanoparticles (ANP) and structure of PPE (**Sw-CO_2**) investigated in this study.

The quenching of **Sw-CO_2** by the ANP is a static process in terms of the Stern-Volmer formalism, as the emission lifetimes of the PPEs are generally between 150 and 450 ps.[15] Hence, any dynamic quenching effects, while present, have only a minute influence. We have recently developed the following binding model, which we exploit to investigate the quenching processes of the PPE by the ANPs (Eq. 10.2).[16]

$$I_{[Q]} = I_0 + \frac{\alpha}{2}\left([F]_0 + n[Q]_{tot} + \frac{1}{K_{SV}}\right) - \left\{\left([F]_0 + n[Q]_{tot} + \frac{1}{K_{SV}}\right)^2 - 4n[F]_0[Q]_{tot}\right\}^{0.5}$$

I_0 is the fluorescence intensity of the PPE at a concentration $[F]_0$ in the absence of quencher [Q] (in this case nanoparticles), $I_{[Q]}$ is the fluorescence intensity of the PPE in the presence of a concentration [Q] of gold nanoparticle, $[Q]_{tot}$ is the total concentration of the added quencher, and n denotes the valency of the ANP, i.e. how many sites the ANP has to quench multiple PPE chains. The term α is used to correlate the fluorescence intensities and concentrations of the two species. This factor is constant if the instrumental variables (e.g. slit width, excitation wavelength, sensitivity, etc.) and the nanoparticle and polymer identities are fixed.

In obtaining the Stern-Volmer binding constant, the current form of the equation (Eq. 10.2) allows us to approximate K_{sv} by performing a curve fitting analysis using ten different concentrations of nanoparticle quencher.

The formula in Eq. 10.2 is considerably more complex than Eq. 10.1, as the Stern-Volmer formalism makes assumptions that do not hold well in the high binding regimen we are investigating. In these cases, the SV-plots curve upward and are not linear as would be expected. One of the reasons for the non-linear behvior is the expression of the term [Q] in Eq. 10.1, as it refers to the concentration of free quencher and *not* to the easily measured total concentration of quencher $[Q]_{tot}$. If $[F]_0/K_{sv} < 1$ the assumption that $[Q]_{free} \approx [Q]_{tot}$ is justified and the Stern-Volmer approximation provides a simple and convenient but powerful tool for extracting binding constants in an analytical way. If $[F]_0/K_{sv} > 1$, the assumption that $[Q]_{free} \approx [Q]_{tot}$ breaks down and the observed Stern-Volmer plots are invariably upwardly sloped. An analytical expression for the concentration of free quencher is unfortunately not available and most literature studies make use of $[Q]_{total}$ instead of

$[Q]_{free}$. Consequently, one finds an innate upward curvature to the Stern-Volmer plot if $[F]_0/K_{sv} > 1$. While this upward curvature is often attributed to superquenching or other effects such as Dexter energy transfer, we suspect that it is due, at least in part, to the incorrect use of $[Q]_{total}$ instead of $[Q]_{free}$.[17] There is a second minor issue with the Stern-Volmer formalism in that it assumes the formation of a 1:1 complex that is fully quenched and does not display any residual fluorescence. Use of Eq. 10.2 resolves all of these issues.

In our first experiments we explored the influence of different buffers on the binding strengths between ANP and **Sw-CO_2**. As shown in Figure 10.2 the binding curves are nearly superimposable in PB, PIPES, HEPES and TRIS-HCl buffers at a 5 mmol concentration. In the case of phosphate buffered saline (PBS) the binding constant is lower and there is a significant final residual fluorescence at high ANP concentration. As **Sw-CO_2** has a P_n of 12 and a PDI of 1.8, there is expected to be a fraction of short oligomers in such polymer solutions. Since shorter polymer chains do not support polyvalent interactions to the ANP as well, their binding will be considerably less efficient, and addition of salt will screen the electrostatic attractions between polymer and ANP more so for short polymer chains than for longer ones.

In another series of experiments we investigated the influence of PPE concentration on K_{sv}. Figure 10.3 shows the dependence of the binding constant upon the concentration of the PPE. Binding constants obtained from a 10 nM solution of PPE are identical to those obtained from a 1 μM solution of PPE as predicted by Eq. 10.2, because they are not affected by the Stern-Volmer equation.

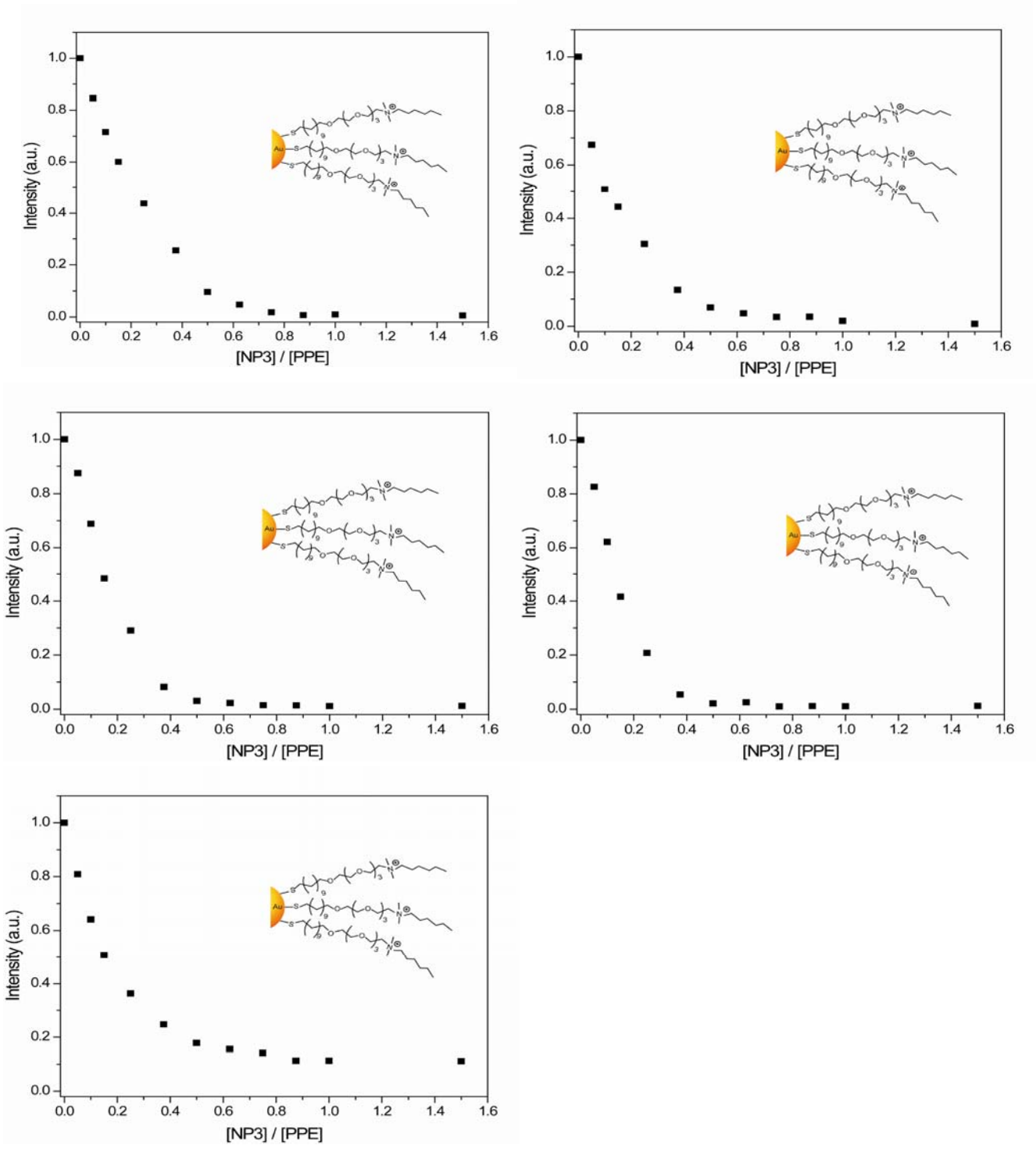

Figure 10.2. Fluorescence titration curves for the complexation of $\mathbf{NP_3}$ with $\mathbf{Sw\text{-}CO_2}$ in PB (top left), PIPES (top right), HEPES (middle left), Tris-HCl (middle right), and PBS (bottom left)

After performing these preliminary studies, we investigated the eleven nanoparticles **NP_1-NP_{11}** (Fig. 10.1) for their ability to quench the fluorescence of **Sw-CO_2** in the presence of 0, 100, 250, 500 and 1000 mM of NaCl to determine and evaluate the relationship between electrostatic and hydrophobic effects. Figure 10.1 shows that **NP_1-NP_4** display increasingly long hydrocarbon tails while **NP_5-NP_7** feature cyclic hydrophobic substituents on the ammonium functionality. The **NP_8-NP_{11}** contain aromatic residues and are therefore grouped together.

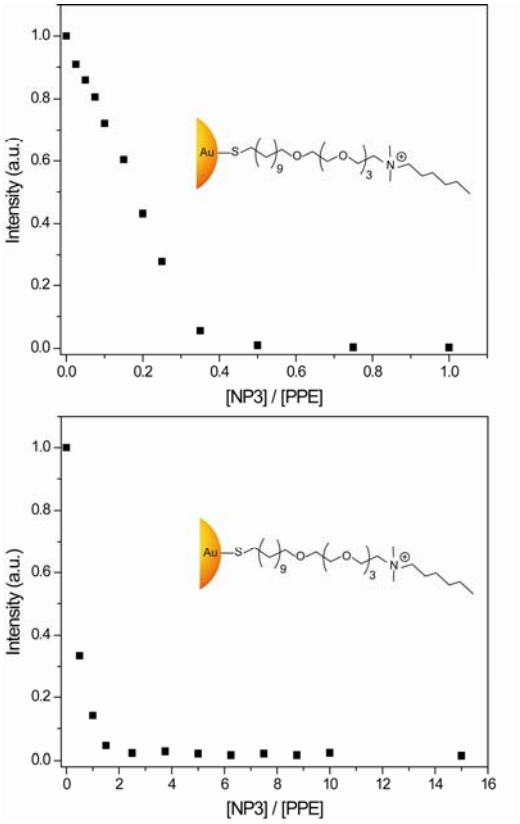

Figure 10.3. Quenching of PPE by **NP_3** for a PPE concentration of 1 μm (top; 8.5 x 10^7 M^{-1}) and 10 nm (bottom; 8.6 x 10^7 M^{-1}). Experimental values for Ksv's are nearly concentration independent.

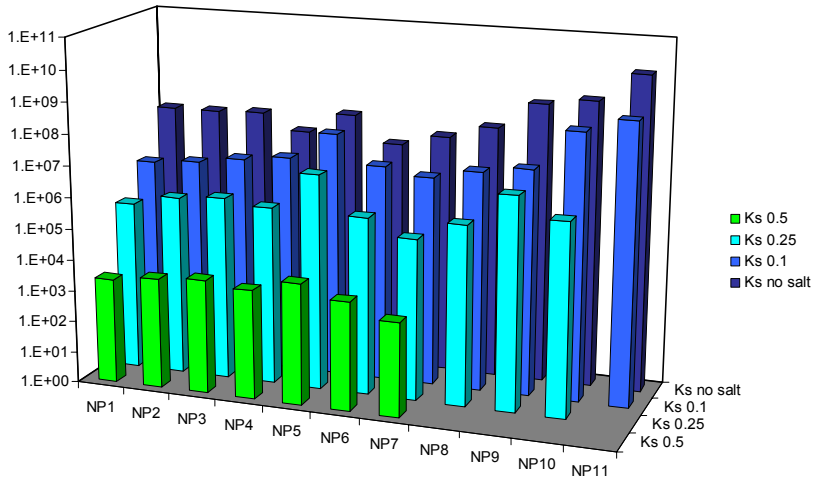

Figure 10.4. Logarithmic plot of binding constants between **NP_1-NP_{11}** and **Sw-CO_2** in the presence of different concentrations of sodium chloride.

Table 10.1 and Figure 10.4 display the results of the binding studies of **NP_1-NP_{11}** to **Sw-CO_2** in the presence of increasingly concentrated sodium chloride solutions. The binding between the negatively charged PPE and the positively charged ANPs is dependent upon the structure of the ANP and the salt concentration.

Table 10.1. Binding ratio "n" and binding constant K_a values for the complexation **NP_1-NP_{11}** with **Sw-CO_2** in PB with 0, 100, 250, 500, and 1000 mM NaCl. At higher NaCl concentrations, values could not be accurately determined for all nanoparticle-conjugated polymer constructs.

	n				$K_a * 10^{-6} (M^{-1})$			
NaCl (mM)	0	100	250	500	0	100	250	500
NP1	2.9	2.4	2.1	1.9	75	2.5	0.25	0.0022
NP2	7.3	6.8	6.4	5.9	76	3.4	0.54	0.0033
NP3	4.6	4.3	3.8	3.5	89	5.6	0.72	0.0043
NP4	3.7	3.4	3.2	2. 8	27	8.4	0.50	0.0031
NP5	5.7	5.5	5.0	4.5	130	62	7.5	0.0073
NP6	10.4	9.7	9.3	8.8	19	7.9	4.7	0.0029
NP7	12.9	12.1	11.4	10	42	4.8	0.14	0.0010
NP8	6.0	5.4	5.1	NA	110	9.7	0.55	NA
NP9	6.1	5.9	5.2	NA	780	16	6.1	NA
NP10	6.0	5.6	5.1	NA	1300	310	1.4	NA
NP11	5.7	5.5	NA	NA	10000	857	NA	NA

Increasing ionic strength screens the electrostatic interactions between ANP and PPE. In a 1 molar NaCl solution binding between PPE and ANP is weak, as the electrostatic interaction between ANP and PPE is greatly attenuated. Static quenching is interrupted by the addition of salt, but dynamic quenching should be independent of the presence of binding sites or salt concentration. At high salt concentrations we observe values of K_{sv} of around 1 x 10^3 M^{-1} for **NP_1-NP_7** while the binding constants for **NP_8-NP_{11}** are negligible. From these experiments we can conclude that the contribution of dynamic quenching to the overall quenching process is minor and that it does not influence the outcome of the binding experiments done at low salt concentrations. According to Eq. 10.2 the analysis of the binding curves gives the number of binding sites n that are available on a single nanoparticle. The aromatic nanoparticles **NP_8-NP_{11}** give values for n of around 6, i.e. 6 repeat units with 12 carboxylate functionalities are bound to one nanoparticle.

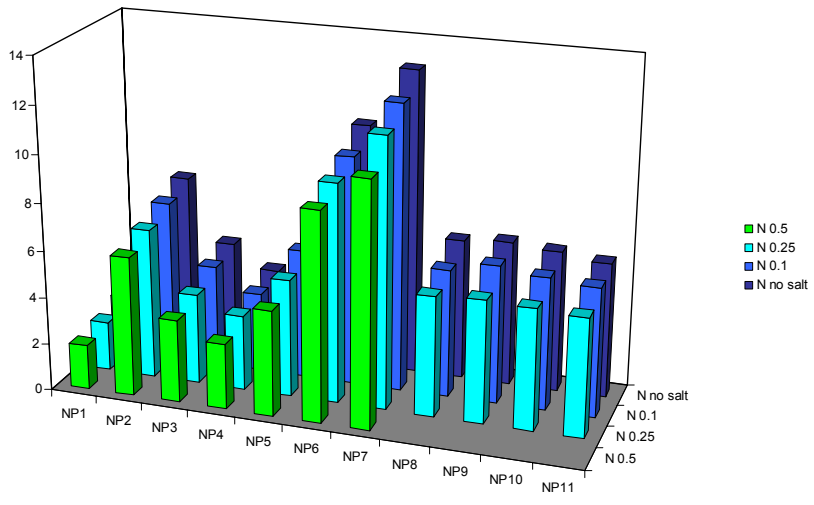

Figure 10.5. Number of binding sites n as obtained from Eq. 10.2. This value n refers to the binding sites of the ANP-PPE construct.

As we have a degree of polymerization of 12 for the PPE, this means that either several PPE molecules could interact using only one or two of their carboxylate groups, or that only one PPE chain is bound per ANP but with up to six contacts. From this model it is not possible to discern between these two scenarios. Overall, the n-values vary from 2-12, with the least hydrophobic ANPs having the least number of biding sites. Figure 10.5 depicts the obtained results.

In the absence of salt, the ANPs with aromatic ammonium species bind by far the strongest to the conjugated polymer. We rationalize this as a prevalence of π-π-interactions, i.e. the phenyl groups of the nanoparticle ligands bind strongly to the aromatic backbone of the PPE.

Although the partition coefficient *P* of a molecule alone does not provide an understanding of hydrophobic interactions of ANPs to **Sw-CO$_2$**, it does offer a means of characterizing the effect of hydrophobicity when it is combined with another parameter. Therefore, we explored the relation between logK_a and log*P* to elucidate the interaction between the hydrophobicity of the ANPs and **Sw-CO$_2$**. As shown in Figure 10.6, **NP$_{10}$** and **NP$_{11}$** that display aromatic units on their surface are the most efficient at quenching the fluorescence of the **Sw-CO$_2$**. As mentioned before, we presume that this is due to π-π-interactions between the aromatic groups on the surface of the ANP and the hydrophobic backbone of the PPE. In the case of the cyclic units, **NP$_5$** (R = cyclohexyl), **NP$_6$** (R= tert-butyl) and **NP$_7$** (R= cyclododecyl) the binding interaction in terms of logK_a is lower by orders of magnitude, and this is assumed to be the result of two factors: a) they do not have aromatic units to interact with PPE and b) they feature bulky cyclic functionalities that reduce the electrostatic

interaction with **Sw-CO_2**. However, a phenyl addition to the cyclohexane unit (**NP_8**) increases the binding interaction. In the case of **NP_1** (R= ethyl), **NP_2** (R= butyl) and **NP_3** (R= hexyl) the elongation of the aliphatic R group on the quaternary amine increases sligthly the strength of the binding. This is not the case for **NP_4** (R = decyl) where a weak binding interaction with **Sw-CO_2** is observed.

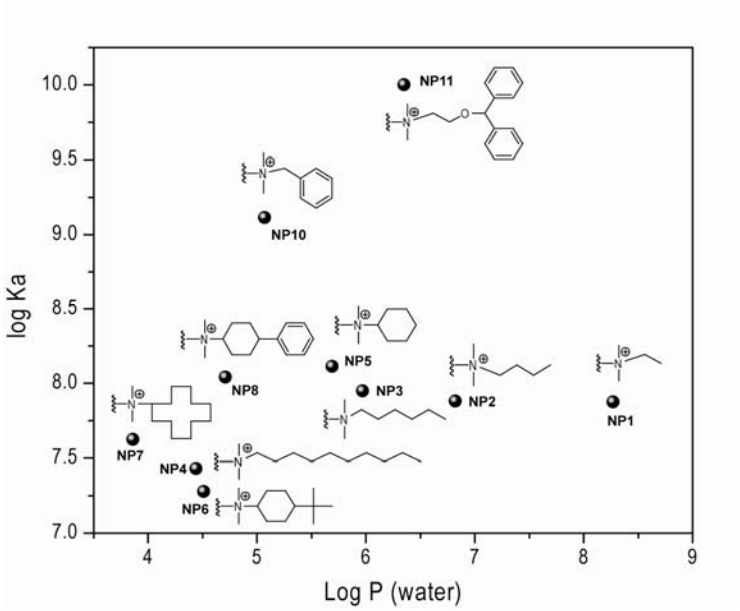

Figure 10.6. Logarithmic relation of binding constants (K_a, ANP-**SwCO_2**) and partition coefficient of **NP_1-NP_{11}** (**NP_9** is not plotted due to the force field interaction).

Surprisingly, the strongest binding ANPs (**NP_{10}** and **NP_{11}**) also display the highest sensitivity towards the addition of sodium chloride, while **NP_5** is the least sensitive to an increase in ionic strength. Conclusions that might be drawn to aid in the development of further ANP-CP constructs are: 1) Electrostatic interactions between PPE and ANP can be modulated and even turned off by an increase in ionic strength. 2) Aromatic side chains are more sensitive towards interruption of binding than aliphatic and specifically cycloaliphatic ammonium groups are. 3) Aromatic ammonium side chains display the

highest association constants and promote the interaction between PPE and ANP, presumably through aromatic stacking with the PPE backbone.

10.3 Conclusion

In conclusion, we have investigated the quenching of **Sw-CO_2** by 11 monoloayer protected, ammonium-functionalized nanoparticles (**NP_1-NP_{11}**) with varying hydrophobicity. ANPs that feature aromatic units on their surfaces are most effective in quenching the fluorescence of the PPE perhaps due to efficient edge to face interactions between the aromatic groups on the surface of the ANP and the hydrophobic backbone of the PPE in the fashion explained by Hunter and Sanders.[18] In all cases, however, increasing the ionic strength of the medium dramatically decreases the strength of the interaction between the two oppositely charged species i.e. ANP and CP.

In the aliphatic systems, an *increase* in hydrophobicity is counterbalanced by a *decrease* in the electrostatic interactions, thus it does not lead to an increase in binding between ANP and CP. In the aromatic ANPs, however, the binding constant between ANP and **Sw-CO_2** correlates well with the hydrophobicity of the aromatic tail on the ammonium group, suggesting that at low salt concentrations the contribution of the hydrophobic arenes is significant. Overall, we demonstrated that simple manipulation of the surface functionality of ANPs by varying their hydrophobicity allows for a large range of binding constants to be attained by molecular tailoring, particularly if ammonium salts with aromatic substituents are employed to stabilize the ANPs.

10.4 Experimental

Instrumentation and Materials. Swallowtail-substituted carboxylate PPE (**Sw-CO_2**) was synthesized according to published procedure.[14] Fluorescence intensity changes at 465 nm were recorded in 96-well plates (300 μL Whatman® Glass Bottom microplate) on a Molecular Devices SpectraMax M5 micro plate reader with an excitation wavelength of 405 nm. Phosphate buffer (PB), phosphate buffered saline (PBS), piperazine-1,4-bis(2-ethanesulfonic acid) (PIPES), N-2-hydroxyethylpiperazine-N'-2-ethanesulfonic acid (HEPES), and tris(hydroxymethyl)aminomethane hydrochloride (Tris-HCl) were purchased from Sigma-Aldrich. The buffers were diluted to a concentration of 5 mM and a pH of 7.2 with DI H_2O. To calculate log P, computational program Maestro 8.0 was used.

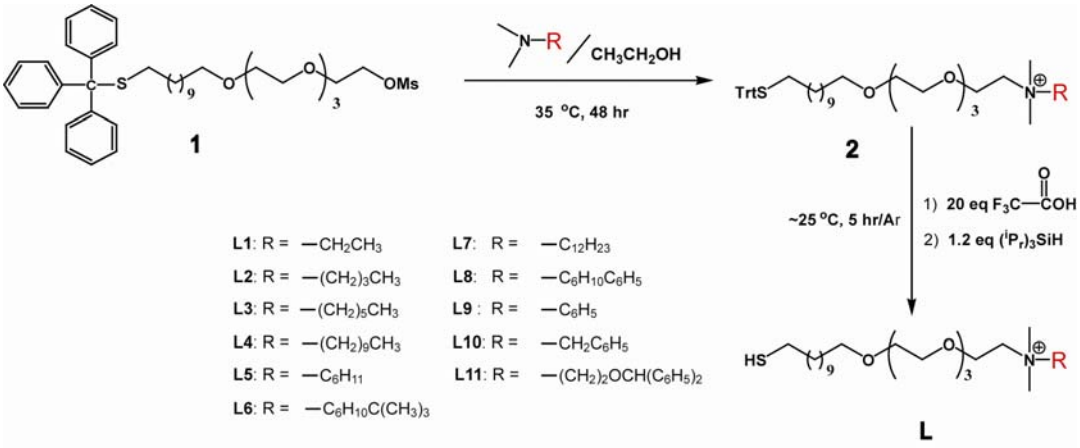

Scheme 10.2. Synthesis of Ligands[11]

General procedure: Compound **2** bearing ammonium end groups were synthesized through the reaction of 1,1,1-triphenyl-14,17,20,23-tetraoxa-2-thiapentacosan-25-yl methanesulphonate (**1**) with corresponding substituted N,N-dimethylamines during 48 h

at ~35 ^{o}C. The trityl protected thiol ligand **(2)** was dissolved in dry dichloromethane (Methylene Chloride, DCM) and an excess of trifluoroacetic acid (TFA, ~ 20 equivalents) was added. The color of the solution was turned to yellow immediately. Subsequently, triisopropylsilane (TIPS, ~ 1.2 equivalents) was added to the reaction mixture. The reaction mixture was stirred for ~5 h under Ar condition at room temperature. The solvent and most TFA and TIPS were distilled off under reduced pressure. The pale yellow residue was further dried in high vacuum. The product (**L**) formation was quantitative and their structure was confirmed by NMR. The yields were >95%.

Compound L_1: ^{1}H NMR (400MHz, $CDCl_3$, TMS): δ 3.94 (br, 2H, -CH_2N-), 3.69-3.56 (m, 14H, -CH_2O- + -OC$\underline{H}_2$-(CH_2N)-), 3.44 (t, 2H, -CH_2O-), 3.40-3.32 (m, 2H,-NCH_2-), 3.23 (s, 6H, -$(CH_3)_2$N-), 2.78 (s, 3H, -$CH_3SO^-_3$-), 2.51 (q, 2H, -CH_2S-), 1.69-1.149 (m, 4H, (SCH_2)C$\underline{H}_2$ + -C$\underline{H}_2$(CH_2O)-) , 1.44-1.24 (m, 18H, -SH + -CH_2- + -(NCH_2)C$\underline{H}_3$).

Compound L_2: ^{1}H NMR (400MHz, $CDCl_3$, TMS): δ 3.96 (br, 2H, -CH_2N-), 3.68-3.57 (m, 14H, -CH_2O- + -OC$\underline{H}_2$-(CH_2N)-), 3.49 (t, 2H, -CH_2O-), 3.39-3.33 (m, 2H,-NCH_2-), 3.17 (s, 6H, -$(CH_3)_2$N-), 2.91 (s, 3H, -$CH_3SO^-_3$-), 2.52 (q, 2H, -CH_2S-), 1.78-1.52 (m, 6H, -(NCH_2)C$\underline{H}_2$-) + (SCH_2)C$\underline{H}_2$ + -C$\underline{H}_2$(CH_2O)-) , 1.44-1.24 (m, 17H, -SH + -(NCH_2CH_2-)C$\underline{H}_2$-) + -CH_2-), 0.98 (t, 3H, - CH_3-).

Compound L_3: ^{1}H NMR (400MHz, $CDCl_3$, TMS): δ 3.95 (br, 2H, -CH_2N-), 3.68-3.56 (m, 14H, -CH_2O- + -OC$\underline{H}_2$-(CH_2N)-), 3.46 (t, 2H, -CH_2O-), 3.40-3.33 (m, 2H,-NCH_2-), 3.19 (s, 6H, -$(CH_3)_2$N-), 2.87 (s, 3H, -$CH_3SO^-_3$-), 2.52 (q, 2H, -CH_2S-), 1.76-1.53 (m, 6H, -(NCH_2)C$\underline{H}_2$-) + (SCH_2)C$\underline{H}_2$ + -C$\underline{H}_2$(CH_2O)-) , 1.41-1.22 (m, 21H, -SH + -(NCH_2CH_2-)C$\underline{H}_2$-) + -CH_2-), 0.89 (t, 3H, - CH_3-).

Compound L_4: ^{1}H NMR (400MHz, $CDCl_3$, TMS): δ 3.94 (br, 2H, -CH_2N-), 3.67-3.54 (m, 14H, -CH_2O- + -OC<u>H</u>$_2$-(CH_2N)-), 3.48 (t, 2H, -CH_2O-), 3.41-3.32 (m, 2H,-NCH_2-), 3.17 (s, 6H, -$(CH_3)_2$N-), 2.90 (s, 3H, -$CH_3SO^-_3$-), 2.51 (q, 2H, -CH_2S-), 1.78-1.52 (m, 6H, -(NCH_2)C<u>H</u>$_2$-) + (SCH_2)C<u>H</u>$_2$ + -C<u>H</u>$_2$(CH_2O)-) , 1.45-1.15 (m, 29H, -SH + -(NCH_2CH_2-)C<u>H</u>$_2$-) + -CH_2-), 0.87 (t, 3H, - CH_3-).

Compound L_5: ^{1}H NMR (400MHz, $CDCl_3$, TMS): δ3.95 (br, 2H, -CH_2N-), 3.81-3.72 (m, 1H, H_{Cyclo}), 3.69-3.53 (m, 14H, -CH_2O- + -OC<u>H</u>$_2$-(CH_2N)-), 3.49 (t, 2H, -CH_2O-), 3.11 (s, 6H, -$(CH_3)_2$N-), 2.91 (s, 3H, -$CH_3SO^-_3$-), 2.52 (q, 2H, -CH_2S-), 2.23 (d, 2H, H_{Cyclo}), 1.99 (d, 2H, H_{Cyclo}), 1.78-1.52 (m, 4H, -(SCH_2)C<u>H</u>$_2$ + -C<u>H</u>$_2$(CH_2O)-), 1.51-1.12 (m, 21H, SH + -CH2- + H_{Cyclo}).

Compound L_6: ^{1}H NMR (400MHz, $CDCl_3$, TMS): δ 3.96 (br, 2H, -CH_2N-), 3.79-3.75 (m, 1H, H_{Cyclo}), 3.66-3.57 (m, 14H, -CH_2O- + -OC<u>H</u>$_2$-(CH_2N)-), 3.46 (t, 2H, -CH_2O-), 3.12 (s, 6H, -$(CH_3)_2$N-), 2.89 (s, 3H, -$CH_3SO^-_3$-), 2.52 (q, 2H, -CH_2S-), 2.28 (d, 2H, H_{Cyclo}), 2.01 (d, 2H, H_{Cyclo}), 1.64-1.54 (m, 4H, -(SCH_2)C<u>H</u>$_2$ + -C<u>H</u>$_2$(CH_2O)-), 1.47 (q, 2H, H_{Cyclo}), 1.33 (t, ^3J = 8.0 Hz, 1H, -SH), 1.30-1.22 (m, 14H, -CH2-), 1.16 (q, 2H, H_{Cyclo}) 1.04 (td, 1H -CHC-), 0.86 (s, 9H, -$C(CH_3)_3$-).

Compound L_7: ^{1}H NMR (400MHz, $CDCl_3$, TMS): δ 3.98 (br, 2H, -CH_2N-), 3.78-3.75 (m, 1H, H_{Cyclo}), 3.64-3.55 (m, 14H, -CH_2O- + -OC<u>H</u>$_2$-(CH_2N)-), 3.46-3.42 (dt, 2H, -CH_2O-), 3.16 (s, 6H, -$(CH_3)_2$N-), 2.86 (s, 3H, -$CH_3SO^-_3$-), 2.52 (q, 2H, -CH_2S-), 1.93-1.40 (m, 26H, SCH_2)C<u>H</u>$_2$ + -C<u>H</u>$_2$(CH_2O)- + H_{Cyclo}), 1.33 (t, ^3J = 7.82 Hz, 1H, -SH), 1.29-1.24 (m, 14H, -CH2-).

Compound L_8: ^{1}H NMR (400MHz, $CDCl_3$, TMS): δ 7.4-7.2 (m, 4H, H_{Ar}), 7.17 (d, 1H, H_{Ar}), 3.95 (d and br, 2H, -CH_2N-), 3.79-3.52 (m, 14H, -CH_2O- + -OC<u>H</u>$_2$-(CH_2N)-), 3.45

(q, 2H, -CH_2O-),3.29-3.22 (m and br, 1H, H_{Cyclo}), 3.01-2.92 (m and br, 1H, H_{Cyclo}) 2.87 (s, 3H, -$CH_3SO^-_3$-), 2.81 (d and br, 6H, -$(CH_3)_2N$-), 2.52 (q, 2H, -CH_2S-), 2.39-2.26 (m, 2H, H_{Cyclo}), 2.19-2.06 (m, 2H, H_{Cyclo}), 1.96-1.84 (m, 4H, H_{Cyclo}), 1.72-1.53 (m, 4H, -$(SCH_2)C\underline{H_2}$ + -$C\underline{H_2}(CH_2O)$-), 1.42-1.1.19 (m, 15H, -SH + -CH_2-).

Compound L_9: ^{1}H NMR (400MHz, $CDCl_3$, TMS): δ 7.82 (d, 2H, H_{Ar}), 7.66-7.51 (m, 3H, H_{Ar}), 4.24 (br, 2H, -CH_2N-), 3.78 (s, 6H, -$(CH_3)_2N$-), 3.68-3.52 (m, 14H, -CH_2O- + -$OC\underline{H_2}$-(CH_2N)-), 3.47-3.36 (m, 2H, -CH_2O-), 2.87 (s, 3H, -$CH_3SO^-_3$-), 2.52 (q, 2H, -CH_2S-), 1.70-1.46 (m, 4H, -$(SCH_2)C\underline{H_2}$ + -$C\underline{H_2}(CH_2O)$-), 1.42-1.1.16 (m, 15H, -SH + -CH_2-).

Compound L_{10}: ^{1}H NMR (400MHz, $CDCl_3$, TMS): δ 8.37 (d, 1H, H_{Ar}), 7.98 (d, 1H, H_{Ar}), 7.69-7.61 (m, 3H, H_{Ar}), 7.59-7.48 (m, 1H, H_{Ar}), 4.38 (br, 2H,-NCH_2-Ar)), 3.76 (br, 2H, -CH_2N-) 3.72-3.62 (m, 14H, -CH_2O- + -$OC\underline{H_2}$-(CH_2N)-), 3.61-3.55 (m, 2H, -CH_2O-), 3.23 (s, 6H, -$(CH_3)_2N$-), 3.07 (s, 3H, -$CH_3SO^-_3$-), 2.52 (q, 2H, -CH_2S-), 1.67-1.51 (m, 4H, -$(SCH_2)C\underline{H_2}$ + -$C\underline{H_2}(CH_2O)$-), 1.35-1.21 (m, 15H, -SH + -CH_2-).

Compound L_{11}: ^{1}H NMR (400MHz, $CDCl_3$, TMS): δ 7.42 (d, 2H, H_{Ar}), 7.37-2.27 (m, 8H, H_{Ar}), 7.25-7.18 (t, 2H, H_{Ar}), 5.13 (s, 1H, H_{Ar}), 4.12 (br, 2H, -CH_2N-)), 3.96 (br, 2H, -$NC\underline{H_2}(CH_2OCAr)$, 3.64-3.51 (m, 14H, -$CH_2O$- + -$OC\underline{H_2}$-$(CH_2N)$-), 3.45 (t, 2H, -$CH_2O$-), 3.29-3.34 (m, 2H, -$CH_2OCAr$-), 3.28 (s, 6H, -$(CH_3)_2N$-), 2.86 (s, 3H, -$CH_3SO^-_3$-), 2.52 (q, 2H, -$CH_2S$-), 1.60-1.48 (m, 4H, -$(SCH_2)C\underline{H_2}$ + -$C\underline{H_2}(CH_2O)$-), 1.34-1.16 (m, 15H, -SH + -CH_2-).

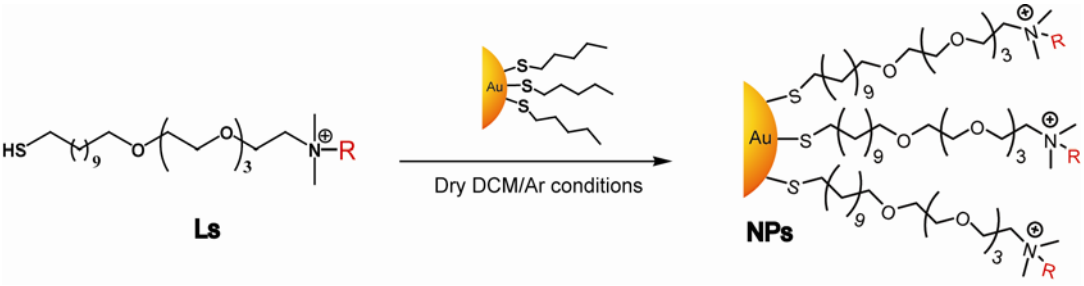

Scheme 10.3. Synthesis of cationic gold nanoparticles **(NP_1-NP_{11})**

General Procedure: 1-Pentanethiol coated gold nanoparticles (*d* = ~2 nm) were prepared according to the previously reported protocol.[9] Place-exchange reaction[19] of compound **Ls** dissolved in DCM with pentanethiol-coated gold nanoparticles (d~2 nm) was carried out for 3 days at environmental temperature. Then, DCM was evaporated under reduced pressure. The residue was dissolved in a small amount of distilled water and dialyzed (membrane MWCO = 1,000) to remove excess ligands, acetic acid and the other salts present with the nanoparticles. After dialysis, the particles were lyophilized to afford a brownish solid. The particles (**NPs**) are redispersed in water and/or ionized water (18 MΩ-cm). ^{1}H NMR spectra in D_2O showed substantial broadening of the proton signals and no free ligands were observed.

10.5 References

1. Sih, B.C.; Wolf, M.O. "Metal nanoparticle -conjugated polymer nanocomposites" *Chem. Commun* **2005**, 3375

2. Fan, C.H.; Wang, S.; Hong, J.W.; Bazan, G.C.; Plaxco, K.W.; Heeger, A.J. "Beyond superquenching: Hyper-efficient energy transfer from conjugated polymers to gold nanoparticles" *Proc. Nat. Acad. Sci.* **2003**, 100, 6297.

3. Brust, M.; Bethell, D.; Schiffrin, D.J.; Kiely, K.J. "Novel gold-dithiol nano-networks with nonmetallic electronic-properties" *Adv. Mater.* **1995**, 7, 795; Advincula, R.C. *Dalton Trans.* **2006**, 2778.

4. Stern, O.; Volmer, M. "The fading time of fluorescence"*Phys. Zeitschrift* **1919**, 20**,** 183.

5. Swager, T.M.; Zhou, Q. "Fluorescent chemosensors based on energy migration in conjugated polymers: The molecular wire approach to increased sensitivity" *J. Am. Chem. Soc.* **1995**, 117, 12593.

6. Mammen, M.; Choi, S.K.; Whitesides, G.M. "Polyvalent interactions in biological systems: Implications for design and use of multivalent ligands and inhibitors" *Angew. Chem.* **1998**, 37, 2755-2794.

7. Lee, J.S.; Seferos, D.S.; Giljohann, D.A.; Mirkin, C.A. "Thermodynamically controlled separation of polyvalent 2-nm gold nanoparticle-oligonucleotide conjugates" *J. Am. Chem. Soc.* **2008**, 130, 5430.

8. Simard, J.; Briggs, C.; Boal, A.K.; Rotello, V.M. "Formation and pH-controlled assembly of amphiphilic gold nanoparticles" *Chem. Commun.* **2000**, 1943.

9. Brust, M.; Walker, M.; Bethell, D.; Schiffrin, D.J.; Whyman, R. "Synthesis of thiol-derivatized gold nanoparticles in 2-phase liquid-liquid system" *Chem. Commun.* ***1*994**, 801.

10. Daniel, M.C.; Astruc, D. "Gold nanoparticles: Assembly, supramolecular chemistry, quantum-size-related properties, and applications toward biology, catalysis, and nanotechnology" *Chem. Rev.* **2004**, 104, 293.

11. You, C.C.; Miranda, O.R.; Gider, B.; Ghosh, P.S.; Kim, I.B.; Erdogan, B.; Krovi, S.A.; Bunz, U.H.F.; Rotello, V.M. "Detection and identification of proteins using nanoparticle-fluorescent polymer 'chemical nose' sensors" *Nature Nanotechonlogy* **2007**, 2, 318.

12. Phillips, R.L.; Miranda, O.R.; You, C.C.; Rotello, V.M., Bunz, U.H.F. "Rapid and efficient identification of bacteria using gold-nanoparticle -poly(para-phenyleneethynylene) constructs" *Angew. Chem.* **2008**, 47, 2590.

13. Brust, M.; Walker, M.; Bethell, D.; Schiffrin, D.J.; Whyman, R. "Synthesis of thiol-derivatized gold nanoparticles in a two-phase liquid-liquid system" *Chem. Commun.* **1994**, 801.

14. Kim, I.B.; Phillips, R.; Bunz, U.H.F. "Carboxylate group side-chain density modulates the pH-dependent optical properties of PPEs" *Macromolecules* **2007**, 40, 5290.

15. Bunz, U.H.F. "Poly(aryleneethynylene)s: Syntheses, properties, structures, and applications" *Chem. Rev*. **2000**, 100, 1605.

16. You, C.C.; De, M.; Han, G.; Rotello, V.M. "Tunable inhibition and denaturation of alpha-chymotrypsin with amino acid-functionalized gold nanoparticles" *J. Am. Chem. Soc*., **2005**, 127, 12873-12881.

17. Wang, J.; Wang, D.L.; Miller, E.K.; Moses, D.; Bazan, G.C.; Heeger, A.J. "Photoluminescence of Water-Soluble Conjugated Polymers: Origin of Enhanced Quenching by Charge Transfer" *Macromolecules* **2000**, 33, 5153-5158; Fan, L.J.; Zhang, Y.; Jones, W.E. "Design and Synthesis of Fluorescence "Turn-on" Chemosensors Based on Photoinduced Electron Transfer in Conjugated Polymers" *Macromolecules* **2005**, 38, 2844.

18. Hunter, C.J.; Sanders, J.K.M. "The nature of pi-pi interactions" *J. Am. Chem. Soc.* **1990**, 112, 5525.

19. Hostetler, M.J.; Templeton, A.C.; Murray, R.W. "Dynamics of place-exchange reactions on monolayer-protected gold cluster molecules" *Langmuir* **1999**, 15, 3782-3789.

CHAPTER 11

Conclusions and Future Direction

11.1 Conclusions

In this thesis, the synthesis and biological sensing applications of water soluble poly(*para*phenyleneethynylene)s (PPEs) has been presented. The PPEs are well suited for biological applications due to their ease of synthesis, exquisite sensitivity, and dramatic chromicity. Novel water soluble anionic PPEs with high fluorescence quantum yields have been synthesized and have shown great promise in both metal and biosensory applications.[1]

Encouraged by these results, sugar-substituted PPEs were synthesized and their sensitivity towards lectins and bacteria were studied. These PPEs exhibited high sensitivity for Concanavalin A (a tetrameric lectin) and induced staining and aggregation with *E. coli*.[2] During our quenching experiments with Con A, it was noted that our system deviated from the classic Stern-Volmer formalism, so a new Stern-Volmer formula had to be derived which accounted for multiple binding mechanisms.[3]

Once it was realized that PPEs exhibited strong interactions with proteins, self-assembled PPE-protein constructs were designed which possessed increased sensitivity towards Hg^{2+} ions.[4] Once the issue of sensitivity had been addressed, the next step was to see if selectivity could be achieved within these PPE-protein interactions. To test selectivity, we decided to see if we could observe molecular recognition between our PPEs and proteins on the surface of cells. Anionic PPEs were incubated with NIH 3T3 fibroblast cells and exhibited strong selectivity for the protein fibronectin. This binding

interaction occurred even in the presence of other proteins, which indicated that molecular recognition could be achieved through non-specific PPE-protein interactions.[5]

As a next step, the PPE-protein interactions were studied using an array approach. Using this approach, seventeen different proteins could be identified and quantified using only six PPEs.[6] Once the array based sensor scheme proved successful, the ability of our PPEs to detect bacteria was investigated. Anionic PPEs were incubated with cationic gold nanoparticles (ANPs), which resulted in a quenched PPE-ANP complex. Upon addition of bacteria, the polymer would be displaced from the ANP and a fluorescence recovery was observed. With the combination of three ANPs and one anionic PPE, twelve different bacteria could be accurately identified.[7]

To better understand the displacement assay, we decided to investigate the mechanism of binding which occurs between the hydrophobic nanoparticles and the conjugated polymer in order to understand the specific factors which govern fluorescence recovery. The interaction of eleven ammonium functionalized hydrophobic cationic ANPs with an anionic PPE were studied at varying PPE concentrations, buffer conditions, and salt concentrations.[8] The PPE concentration and the choice of buffer did not affect the assay, while the addition of salt greatly affected the interaction between ANP and PPE. Increasing the ionic strength of the medium dramatically decreased the strength of the binding interactions between the ANP and PPE. Overall, we were able to demonstrate that simple manipulation of the surface functionality of ANPs by varying their hydrophobicity allows for a large range of binding constants to be attained by molecular tailoring, particularly if ammonium salts with aromatic substituents are employed to stabilize the ANPs.

PPEs are fluorescent sensory materials that exhibit high sensitivities towards biological analytes and can produce rapid and efficient displacement assays with the incorporation of ANPs. With careful optimization of the assays, most of the potential drawbacks can be avoided or even utilized in the sensing scheme. The only drawback of PPEs that has not been addressed in the presented research is the interference of background fluorescence which is generated from cells and nutrient media. This is an issue that will be addressed as a future direction.

11.2 Future Direction

11.2.1 Gold Nanoparticle-PPE Constructs: Identification of Pathogens

Gold nanoparticle-PPE constructs have proven extremely successful in the detection of proteins and bacteria. However, in all of these assays, the detection and quantification of the analytes has been done in "clean" media. As a next step, the detection of proteins will be done in blood serum with the hope of identifying proteins which are associated with various diseases and the detection of bacteria will be done in contaminated water or food samples with the intention of identifying the presence of pathogenic bacteria even in the presence of non-pathogenic bacteria. With moving the displacement assays into more complicated media (e.g. serum), it may be necessary to design new polymers or nanoparticles which contain other functionalities or recognition elements. Upon optimization of these assays, the detection of other pathogens, such as viruses, should become possible.

11.2.2 Gold Nanoparticle-PPE Constructs: Understanding Their Interactions

Efforts have been made to understand the interactions that govern the ANP-PPE constructs. In these systems, changes in the hydrophobicity of the nanoparticles and salt concentrations greatly affect the binding interactions. To truly understand these interactions, new classes of nanoparticles and PPEs will have to be synthesized. Once the interactions are understood, the issue of polymer displacement in the presence of bacteria needs to be investigated which should provide information on what factors affect polymer displacement. Introduction of recognition elements to the nanoparticles (e.g. sugars) should add a degree of selectivity to the assay and should allow for the tailoring of the system to particular bacteria. This would open the door for optimization of the system to a particular bacteria and would provide a rapid assay for the detection of individual bacteria.

11.2.3 Longer Wavelength Emitting PPEs: PPE-PPV Hybrids

In the previous chapters, I have shown that PPEs with high quantum yield in water, little aggregation in aqueous solutions, and few non-specific interactions with common ions can be achieved. However, the only issue that hasn't been addressed is how to circumvent the high background fluorescence generated from cells and nutrient media due to the presence of aromatic amino acids (e.g. phenylalanine, tyrosine, and tryptophan). This issue can be avoided if the PPE's fluorescence can be red-shifted beyond its blue-green emission. In order to maximize the emission wavelengths and quantum yields, two PPEs which are near red emissive and organo-soluble were synthesized (Figure 11.1).

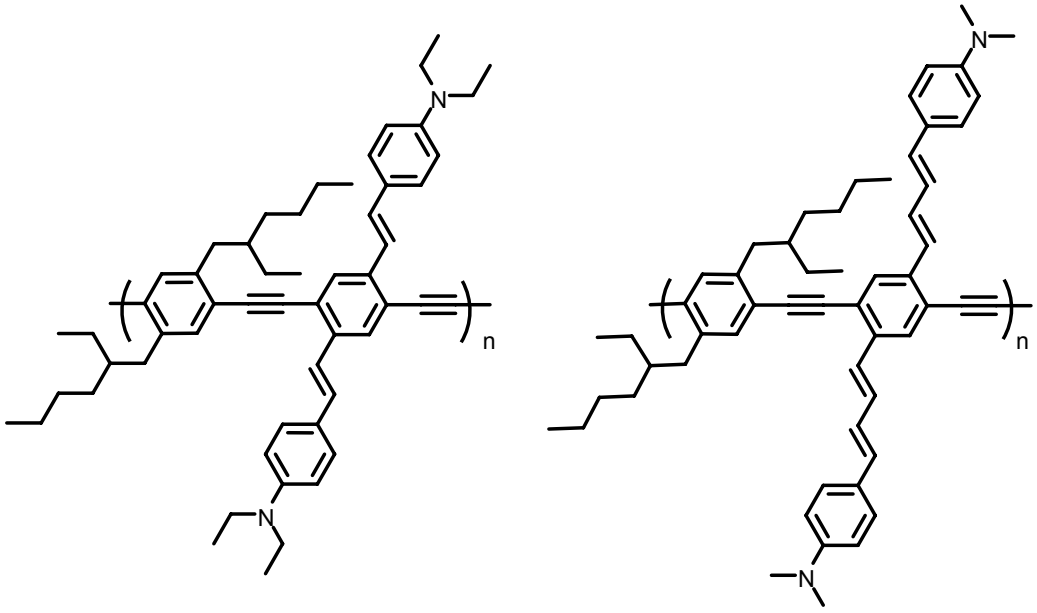

Polymer 11.1 **Polymer 11.2**

Figure 11.1. Structure of the synthesized PPE-PPV hybrids

Polymers **11.1** and **11.2** are both near red emissive with emissions of 540 nm and 550 nm, respectively. The fluorescence quantum yields of **11.1** and **11.2** in chloroform are 0.63 and 0.24 respectively. Even though **11.2** has a more red-shifted emission, polymer **11.1** has a much higher quantum yield which makes it better suited for conversion into a water-soluble PPE. To further strengthen the quantum yield and increase water solubility, carboxylate and swallowtail functionalities will be introduced into the polymer backbone (Figure 11.2).

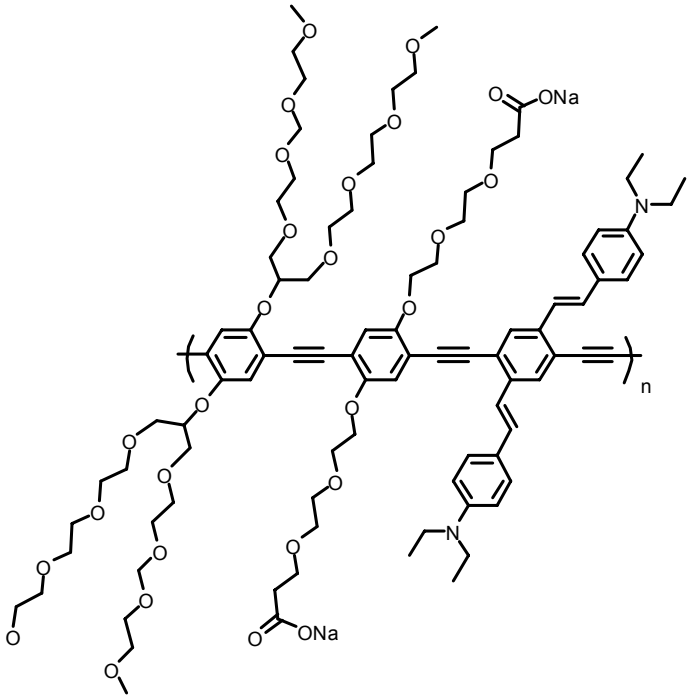

Figure 11.2. Structure of proposed water soluble PPE-PPV hybrid

With the incorporation of these two functionalities, the polymer should be completely water soluble and near red emissive. If the synthesized polymer possesses a reasonable quantum yield in water, it should be useful for future biological applications which would eliminate the issue of high background fluorescence from cells and nutrient media.

11.3 References

1. Kim, Ik-Bum; Phillips, Ronnie; Bunz, Uwe H. F. "Carboxylate group side-chain density modulates the pH-dependent optical properties of PPEs" *Macromolecules* **2007**, 40(15), 5290-5293.

2. Phillips, Ronnie L.; Kim, Ik-Bum; Carson, Bradley; Tidbeck, Bjorn; Bai, Yu; Lowary, Todd; Bunz, U.H.F. "Sugar-substituted poly(paraphenyleneethynylene)s: sensitivity enhancement towards lectins and bacteria" *Macromolecules*, accepted.

3. Phillips, Ronnie L.; Kim, Ik-bum; Tolbert, Laren; Bunz, Uwe H.F. "Fluorescence self-quenching of a mannosylated poly(p-phenyleneethynylene) induced by Concanavalin A" *J. Am. Chem. Soc.* **2008**, 130(22), 6952-6954.

4. Kim, Ik-Bum; Phillips, Ronnie; Bunz, Uwe H. F. "Forced agglutination as a tool to improve the sensory response of a carboxylated poly(p-phenyleneethynylene)" *Macromolecules* **2007**, 40(4), 814-817.

5. McRae, Reagan L.; Phillips, Ronnie L.; Kim, Ik-Bum; Bunz, Uwe H.F.; Fahrni, Christoph J. "Molecular recognition based on low-affinity polyvalent interactions: Selective binding of a carboxylated polymer to fibronectin fibrils of live fibroblast cells" *J.Am. Chem. Soc.* **2008**, 130(25), 7851-7853.

6. Miranda, Oscar R.; You, Chang-Cheng; Phillips, Ronnie; Kim, Ik-Bum; Ghosh, Partha S.; Bunz, Uwe H. F.; Rotello, Vincent M. "Array-based sensing of proteins using conjugated polymers" *J.Am. Chem. Soc*. **2007**, 129(32), 9856-9857.

7. Phillips, Ronnie L.; Miranda, Oscar; You, Chang-Cheng; Rotello, Vincent M.; Bunz, Uwe H.F. "Rapid and efficient identification of bacteria using gold-nanoparticle -poly(para-phenyleneethynylene) constructs*" Angewandte Chemie* **2007**, 47(22), 2590-2594.

8. Phillips, Ronnie L.; Miranda, Oscar; Kim, Ik-Bum; Rotello, Vince; Bunz, U.H.F. "Gold nanoparticle-PPE constructs as biomolecular material mimics: understanding the electrostatic and hydrophobic interactions" *Soft Matter*, submitted.